UC San Diego

UC San Diego Electronic Theses and Dissertations

Title

Development of synthetic glycosaminoglycan glycoconjugates and their application to manipulate cellular signaling events

Permalink

https://escholarship.org/uc/item/17s1v38t

Author

Trieger, Greg

Publication Date

2019

Peer reviewed|Thesis/dissertation

eScholarship.org Powered by the California Digital Library
University of California

UNIVERSITY OF CALIFORNIA SAN DIEGO

Development of synthetic glycosaminoglycan glycoconjugates and their application to manipulate cellular signaling events

A dissertation submitted in partial satisfaction of the
requirements for the degree of Doctor of Philosophy

in

Chemistry

by

Greg William Trieger

Committee in charge:

Professor Kamil Godula, Chair
Professor Rommie Amaro
Professor Jeff Esko
Professor Tadeusz Molinski
Professor Yitzak Tor

2019

©

Greg William Trieger, 2019

All rights reserved.

The Dissertation of Greg William Trieger is approved, and it is acceptable in quality and form for publication on microfilm and electronically:

_____

_____

_____

_____

_____

Chair

University of California San Diego

2019

DEDICATION

Throughout my life, I have benefitted immensely from the support and love of my parents, Dana Burley and Sidney Trieger. To my mother I owe my perspective, curiosities, and confidence to pursue my own ideas. To my father, I owe my work ethic, tenacity, and unrelenting desire to learn, achieve, and develop so that I may one day be of great benefit to those in need. Together, they have shown me fulfillment, love, and happiness. For this reason, I dedicate this work to them.

In addition, earning my Ph.D. would certainly have been less enjoyable (and successful) were it not for the love and support I have found in my beautiful wife, Kelsey Trieger. Every day is made more enjoyable and every task less daunting, knowing that I will return to her each evening.

EPIGRAPH

Anybody can make the simple complicated. Creativity is making the complicated simple.

— Charles Mingus

TABLE OF CONTENTS

Signature Page.....iii

Dedication.....iv

Epigraph.....v

Table of Contents.....vi

List of Figures.....xi

List of Tables.....xvi

List of Schema.....xvii

Acknowledgements.....xviii

Vita.....xxi

Abstract of the dissertation……..xxii

Chapter 1: Development of synthetic glycosaminoglycan glycoconjugates and their application to manipulate cellular signaling events.....1

1.1 General Introduction...……...1

1.2 Glycosaminoglycan structures and mechanism of action……...…….....…4

1.3 Glycosaminoglycan as targets for therapy…….....……..……...7

1.4 Challenges in glycosaminoglycan research……..……..…10

1.5 Chapter 1 References…..……..…12

Chapter 2: Glycocalyx remodeling with proteoglycan mimetics promotes neural specification in embryonic stem cells……...……15

2.1 Introduction…….……..……...15

2.2 Results and discussion…...…….…….……..……..……...…19

2.2.1 *Preparation and characterization of neoproteoglycan library.*…….…..…..…19

2.2.2 *Development and application of neoproteoglycan library to assess FGF2 binding*..21

2.2.3 *Application of neoproteoglycans to rescue neural specification in Ext1$^{-/-}$ mESC*..24

2.3 Conclusions…..…….…….……..……...…27

2.4 Materials and methods…….……30

2.4.1 *Abbreviations*……..……..…..30

2.4.2 *Materials and general procedures*…….……..……30

2.4.3 *Instrumentation*…….……..…31

2.4.4 *Procedure and characterization data for the synthesis of monomer 1*…….... 32

2.4.5 *Synthesis and characterization data for azide chain transfer agent 2*..…..…… 34

2.4.6 *General procedure and characterization data for RAFT polymerization*…..……37

2.4.7 *General procedure and characterization data for end-deprotected polymers*…..….41

2.4.8 *General procedure and characterization data for fluorophore labeling and side chain deprotection*……..……..……44

2.4.9 *General procedure for the ligation of glycans to polymer backbones*…..…..47

2.4.10 *Microarray experiments*…….……..…….62

2.4.11 *Incorporation of neoPGs onto cell surfaces*…….……..……64

2.4.12 *Determination of FGF-2 binding by fluorescence microscopy*…..…….67

2.4.13 *Differentiation procedures and data*…..……..68

2.4.14 *FGF2 stimulation*…..……72

2.5. Acknowledment……..……76

2.6 Chapter 2 references…….……..76

Chapter 3: Investigating heparan sulfate's link to adipocyte metabolism and application of synthetic glycomaterials to enhance cellular access to glucose....80

3.1 Introduction.....80

3.2 Results and discussion.....83

3.2.1 *Adipogenesis and lipid accumulation with inhibited HSPG interaction*.....83

3.2.2 *The role of HSPG interactions as they affect cellular access to glucose*.....85

3.2.3 *Metabolic impact of inhibition of HSPG interactions*.....91

3.2.4 *Wnt signaling affects cellular access to glucose*.....93

3.2.5 *Employment of HS GAG glycopolymers enhances glycolytic cellular metabolism*.....95

3.3 Conclusions.....98

3.4 Materials and methods.....100

3.4.3 *Cellular Experiments*.....101

3.4.4 *Procedure and characterization data for the synthesis of glycopolymers*.....105

3.4.5 *Collection of cellular protein and media components for analysis*.....108

3.5 Acknowledgement.....109

3.6 Chapter 3 References.....109

Chapter 4: Efficient synthesis of heparinoid bioconjugates for tailoring FGF2 activity at the stem cell–matrix interface.....112

4.1 Introduction.....112

4.2 Results and discussion.....117

4.2.1 *Preparation of reactive Heparinoid and BSA click conjugates*.....118

4.2.2 *Preparation of heparinoid-BSA conjugates*.....119

4.2.3 *Preparation and characterization of heparinoid displays on surfaces*……123

4.2.4 *Proliferation of hMSCs on heparinoid displays*……127

4.3. Materials and methods……134

4.3.1 *Materials*……134

4.3.2 *Instrumentation*……134

4.3.3 *General chemical procedures*……135

4.3.4 *Heparinoid pre-functionalization*……136

4.3.5 *BSA prefunctionalization*……140

4.3.6 *Preparation of heparinoid-BSA conjugates*……141

4.3.7 *Preparation and characterization of heparinoid displays on surfaces* ……144

4.3.8 *Proliferation of hMSCs on heparinoid displays* ……147

4.5 Appendix……150

4.6 Acknowledgement……153

4.7 Chapter 4 references……153

Chapter 5: Development and evaluation of a glycosaminoglycan microarray for the manipulation of stem cell differentiation……160

5.1 Introduction……160

5.2 Results and discussion……164

5.2.1 *Generation of microarray substrates for cell culture*……164

5.2.2 *Preparation and characterization of heparinoid displays on surfaces*……167

5.2.3 *Establishing controls for microarray analysis*……179

5.2.4. *Differentiation of* mESC *on heparinoid displays*……190

5.3 Materials and methods……200

5.3.1 *General chemistry*…..……..…….……200

5.3.2 *General instrumentation*..……...201

5.3.3 *General microarray printing*..……...……..201

5.3.4 *Preparation of cellular microarrays*..……202

5.3.5 *Preparation of glycoconjugates and AF647-FGF2*...……....212

5.3.6 *Microarray studies- analysis of protein binding and printed polymer*...……*213*

5.3.7 *Cellular microarray studies*..……...……..……214

5.4 Abbreviations……..217

5.5 References...……..……...……..……..……218

LIST OF FIGURES

Figure 1. Cell surface glycans compose the glycocalyx ……..……..…2

Figure 2. Non-template driven biosynthesis of glycans leads to complexity……...…...…4

Figure 3. Types and structures of GAGs…..……....……....5

Figure 4. Heparan sulfate controls cellular growth factor signaling…..…….....6

Figure 5. Heparin as an anticoagulant……..……....……....9

Figure 6. Neoproteoglycan design and application for glycocalyx remodeling……..…17

Figure 7. Microarray screen of neoproteoglycan library for FGF2 specificity…..……..…23

Figure 8. Glycocalyx remodeling rescued FGF2-mediated signaling in *Ext*1$^{-/-}$ mESCs……..25

Figure 9. Neural differentiation of neoPG-remodeled *Ext1*$^{-/-}$ mESCs……,……..……..27

Figure 10. ^{1}H NMR (500 MHz, $CDCl_3$) of monomer **1**…...……33

Figure 11. ^{13}C NMR (500 MHz, $CDCl_3$) of monomer **1**……..……...33

Figure 12. ^{1}H NMR (500 MHz, $CDCl_3$) of azide chain transfer agent **2**……..……35

Figure 13. ^{13}C NMR (500 MHz, $CDCl_3$) of azide chain transfer agent **2**……..……35

Figure 14. UV-Vis Spectrum of 2 (CH_2Cl_2)……....36

Figure 15. FTIR spectrum of **2**……..……..……..36

Figure 16. ^{1}H NMR (500 MHz, $CDCl_3$) of **4**....……..……...39

Figure 17. ^{1}H NMR (500 MHz, $CDCl_3$) of **8**……..……39

Figure 18. GPC spectrum for **4** and **8** (DMF, 0.2 %LiBr)../……..……..……40

Figure 19. FTIR spectrum of **4**……..……40

Figure 20. ^{1}H NMR (500 MHz, $CDCl_3$) of **5**…...…..……...…42

Figure 21. ^{1}H NMR (500 MHz, $CDCl_3$) of **9**……..……42

Figure 22. GPC (DMF, 0.2% LiBr) of **5** and **9**……..……....43

Figure 23. UV-Vis spectrum of **4** and **5**……..……...43

Figure 24. UV-Vis spectrum of **8** and **9**…….……..……44

Figure 25. ^{1}H NMR (300 MHz, D_2O) of **6**…..……..……..…46

Figure 26. ^{1}H NMR (500 MHz, D_2O) of **10**.....……46

Figure 27. ^{1}H NMR spectrum of glycerine……..…48

Figure 28. Stacked ^{1}H NMR spectra of NeoPG backbone, a diGAG ligated neoPG, and a monosaccharide ...……...……..……..49

Figure 29. neoPG ^{1}H NMR spectra for compounds **7A – 7Q, 11A, 11D, 11N** ……..…….....51

Figure 30. Cell surface incorporation of GlcNAc-6S glycopolymer (**11N**) onto cell surfaces ……...……..……...65

Figure 31. Retention of GlcNAc-6S glycopolymer (**11N**) over time ……..……..66

Figure 32. Additional microscopy images for mESC *Ext*1$^{-/-}$ cells incubated with neoPGs ….…….....…….....68

Figure 33. Fluorescence microscopy images of *Ext*1$^{-/-}$ mESCs during routine culture and after differentiation ……....……...71

Figure 34. Fluorescence microscopy images of E14TG2a wild-type mESCs during routine culture and after neural differentiation ……...72

Figure 35. Fluorescence microscopy images of E14TG2a wild-type mESCs during routine culture and after neural differentiation ..……..72

Figure 36. Wild type (E14TG2a) mESCs stimulated with 25ng/mL FGF2……73

Figure 37. NeoPG **11D** potentiates FGF2-induced Erk1/2 phosphorylation……..73

Figure 38. NeoPG **11D** potentiates FGF2-induced Erk1/2 phosphorylation……..76

Figure 39. Adipogenesis in WT, WT +heparin and Ndst1$^{-/-}$ MEFs characterized genetically and by oil red O stain ……..……83

Figure 40. Processing of lipids in WT and *Ndst1*$^{-/-}$ MEFs ……..……85

Figure 41. Inhibition of cell surface HSPG interactions during adipogenesis significantly reduces cellular access to glucose, but does not impact cellular insulin response ……87

Figure 42. Insulin stimulation WT, WT +heparin and Ndst1$^{-/-}$ adipocytes..……88

Figure 43. Glucose uptake capacity is established during adipogenesis..……89

Figure 44. Removal and addition of heparin during adipogenesis of WT MEFs …..……90

Figure 45. Metabolic impact of HSPG inhibition……92

Figure 46. Employment of Wnt activator LY2090314 and Wnt inhibitor XAV-939 impacts glucose clearance capacity ..……..……..……94

Figure 47. Titration of heparin to impact glucose uptake capacity…..……..96

Figure 48. Preparation and application of membrane-incorporating synthetic glycopolymers to favor glycolytic metabolism…..……..98

Figure 49. GPC trace of lipidated polymer backbone used for NeoPG synthesis ……105

Figure 50. ^{1}H NMR (300 MHz, D_2O) of D2A6 glycopolymer..……..……106

Figure 51. ^{1}H NMR (300 MHz, D_2O) of D2S6 glycopolymer..……..……...106

Figure 52. ^{1}H NMR (300 MHz, D_2O) of D0S0 glycopolymer……..107

Figure 53. Heparan sulfate (HS) glycosaminoglycans (GAGs) regulate FGF2 activity at the cellular boundary……..……...……112

Figure 54. Techniques for generating heparin bioconjugates……..115

Figure 55. MALDI-TOF spectra of DBCO-BSA conjugates **3** and **3-biotin**..……..……..119

Figure 56. Synthesis and characterization of heparin-BSA conjugate……..……...120

Figure 57. SEC traces of **2-hep**, **3** (DBCO BSA) and crude **hep-BSA** with unreacted **3** ……..……..121

Figure 58. Analysis of **Hep-BSA** composition based on BCA and carbazole assays...122

Figure 59. Immobilized heparinoid-BSA conjugate-protein ELISAs (FGF2, 10E4)..……123

Figure 60. FGF2 ELISA to immobilized **hep-BSA**, **hep-BSA-ra**, and **hep-BSA-ac** 124

Figure 61. Immobilization efficiency for biotinylated heparinoid-BSA conjugates.……126

Figure 62. Binding of 3G10 to immobilized heparinoid-BSA conjugates after heparinase digest..……126

Figure 63. Optimization of thymidine proliferation assay time points…...……128

Figure 64. hMSC seeding on heparinoid-BSA surfaces via microscopy…….……128

Figure 65. Heparinoid-BSA surfaces inhibit hMSC proliferation in a sulfate dependent manner ...……..……129

Figure 66. Supplemental microscopy images of calcein stained day 3 hMSCs grown upon heparinoid surfaces..……..130

Figure 67. hMSC proliferation via thymidine assay for soluble heparinoids, and PD173074 treatment..……...……...…131

Figure 68. Heparinase treatment of heparin-glycoconjugate surface…...……..131

Figure 69. Microarrayed heparinoid-BSA conjugate binding to AF647-FGF2…...……..133

Figure 70. ^{1}H NMR of **2-hep** ……..……....……137

Figure 71. ^{1}H NMR of **2-6ODSH** ……..……138

Figure 72. ^{1}H NMR of **2-2ODSH** ……..……138

Figure 73. ^{1}H NMR of **2-NDSH** ……..……...139

Figure 74. ^{1}H NMR of **2-NAcH** ……..……139

Figure 75. Validation of cloud point passivation with mESC..……..…..……...167

Figure 76. Comparison of passivation techniques..……..…..……..……...169

Figure 77. Fabrication of cellular microarrays..……..…..……..……..…..170

Figure 78. NMR spectra of hep-NHS……..…..……...…..……172

Figure 79. Heparin and hep-gel retention by AF647 FGF2 binding.……173

Figure 80. A. Polymer retention at different concentrations (1%,5%, 10%) of surface ADIBO...……..…..……..…..……..…..……..…..……..…..174

Figure 81. Comparison of ADIBO-functionalized acrylamide to unfunctionalized acrylamide hydrogel arrays.....176

Figure 82. AF647-FGF2 binding of heparinoid panel.....178

Figure 83. Binding targeted antibodies to non-heparin GAGs.....179

Figure 84. Validation of fluorescence quantification by microscopy, and selection of optimal seeding density.....182

Figure 85. Evaluation of viable Oct4-GFP mESC colonies at different seeding densities 184

Figure 86. Validation neural differentiation and ICC on array using Oct4-GFP..... 186

Figure 87. *EXT1*$^{-/-}$ mESCs neural differentiation on array.....189

Figure 88. *EXT1*$^{-/-}$ mESC differentiated on hep-gel display, Oct4 and Nestin stain 191

Figure 89. *EXT1*$^{-/-}$ mESC differentiated on hep-gel display, Rex1 and Nestin stain 192

Figure 90. *EXT1*$^{-/-}$ mESC 8 day differentiation +/- FGF4 on hep-gel display.....195

Figure 91. *EXT1*$^{-/-}$ mESC differentiation +/- FGF4 on HS glycopolymer display 196

Figure 92. ^{1}H NMR of 2-O desulfated heparin-NHS.....209

Figure 93. ^{1}H NMR of 6-O desulfated heparin-NHS 209

Figure 94. ^{1}H NMR of N-desulfated heparin-NHS 210

Figure 95. ^{1}H NMR of N-desulfated N-reacetylated heparin-NHS.....210

Figure 96. ^{1}H NMR of dermatan sulfate-NHS.....211

Figure 97. ^{1}H NMR of chondroitin sulfate AC.....211

Figure 98. ^{1}H NMR of dermatan sulfate-NHS 212

LIST OF TABLES

Table 1. Glycopolymer ligation efficiencies (LE) and valencies ……..50

Table 2. Protein and antibody concentrations used in microarrays……214

Table 3. Antibody concentrations used for ICC ……216

LIST OF SCHEMA

Scheme 1. Synthesis of neoproteoglycans ……..……20

ACKNOWLEDGEMENTS

Throughout my time as a Ph. D student, I have had the benefit of working in the Godula lab and being surrounded by many brilliant colleagues which continuously encouraged, supported, and critiqued my scientific pursuits. What is most amazing, is these same colleagues quickly became my good friends, whom I spend many evenings with talking (and not talking) about my research efforts. As such, I would like to acknowledge the ones who made my Ph. D more successful and certainly more enjoyable: Chris (Topher) Fisher, Daniel Honigfort, Matt Nattichia, Austen Michalak, Mitchell Christy, Logan Laubach, Kyle Mandla, Sean Purcell, Quint Fraumann, and Bryce Timm.

I have also had the distinct benefit of the mentorship, perspective and advice from the post-doctoral fellows I have had a chance to work with. Of particular note are Alex Smith and Mia Huang, who in my first years as a graduate student took me under their wings and initiated my journey towards a Ph.D. offering me advice I still follow to this day. Later on in my Ph.D., I had the chance to work with Steven Verespy, a good friend and a more than capable chemical biologist who has been a critical guide as I transition out of academia towards the private sector. I also would like to acknowledge Ariane Pessentheiner, who I have had the pleasure of working with in my final years of my Ph.D as I dove into increasingly biology-heavy experiments that, without her, would have been unfeasible.

One post-doctoral fellow that I wish I had gotten more time with, Yinan Wang, was an immense source of mentorship, curiosity, and fun. Although he was taken from us all far too soon, he has left a lasting impact on me as a person and as a scientist. Yinan was relentless in his work ethic and in his pursuit of fun, something that often does not go hand in hand. His work hard play harder mentality remind me both to never quit, as well as to find time for myself and my loved ones.

Most importantly, I would like to thank my PI, Kamil Godula, who has helped me to develop into the scientist and person I am today. When I joined his lab as one of the first graduate students, I wasn't sure what to expect, between an untenured professor and an unfamiliar research area, but I can whole-heartedly say I have no regrets and I am distinctly grateful for the personal mentorship I have received from Kamil. I know I would not have found it elsewhere. I also am grateful for the support and mentorship I have received from my collaborating professor, Philip Gordts.

***

Chapter 2 is a modified reprint of the material as it appears in JACS 2014, Huang M. L., Smith R. A. A., Trieger G. W. Glycocalyx Remodeling with Proteoglycan Mimetics Promotes Neural Specification in Embryonic Stem Cells. Mia Huang and Alex Smith where the primary authors on this paper, while I was responsible for the synthesis of glycopolymer back bones as well as the preparation of some of the NeoPG library, assisted by Dr. Kamil Godula and Dr. Mia Huang. I was also responsible for much of the chemical characterization of these polymers (GPC, UV-Vis) , and assisted Dr. Mia Huang

in the collection and analysis of NMRs for the NeoPG library. I was also responsible for compiling much of the chemical characterization and procedures for the supporting information. Dr. Alex Smith was responsible for the biological experiments including Erk stimulations and neural differentiations of mESCs. Dr. Mia Huang performed FACs studies, prepared and used microarrays for FGF2 binding studies.

Chapter 3 contains data which will compose an upcoming manuscript. The authors are Trieger G. W., Pressentheiner A. R., Green C. R., DeForest N., Majithia A., Metallo C. M., Godula K., Gordts P. L. S. M. The dissertation author was the primary investigator and author of this paper.

Chapter 4 is a modified reprint of the material as it appears in Bioconjugate Chemistry, 2019. Trieger G. W. VerespyIII S, Gordts P. L. S. M. Godula K. Efficient Synthesis of Heparinoid Bioconjugates for Tailoring FGF2 Activity at the Stem Cell–Matrix Interface. The dissertation author was the primary investigator and author of this paper.

VITA

2010-2013 Undergraduate Researcher, St. Mary's College of Maryland

2013 Bachelor of Arts, Chemistry, St. Mary's College of Maryland

2013-2018 Graduate Researcher, University of California San Diego

2013-2015, 2018, Teaching Assistant, University of California San Diego

2015 Master of Science, Chemistry, University of California San Diego

2019 Doctor of Philosophy, Chemistry, University of California San Diego

PUBLICATIONS

Trieger G. W., Verespy III S., Gordts P. L. S. M., Godula K. (2018) Efficient synthesis of heparinoid bioconjugates for tailoring FGF2 activity at the stem cell matrix interface. *Bioconjugate Chem.* 30, 833-840.

Huang M. L., Smith R. A. A., **Trieger G. W.**, Godula K. (2016) Glycocalyx remodeling with glycopolymer-based proteoglycan mimetics. *Methods Mol Biol., 1367*, 207-224.

Huang M. L., Smith R. A. A., **Trieger G. W.**, Godula K. (2014) Glycocalyx remodeling with proteoglycan mimetics promotes neural specification in embryonic stem cells. *J. Am. Chem. Soc, 136*, 10565-10568.

FIELDS OF STUDY

Major Fields: Chemistry and Chemical Biology

Studies in Stem Cell Biology, Glycoscience, and Bioconjugation
Professor Kamil Godula

ABSTRACT OF THE DISSERTATION

Development of synthetic glycosaminoglycan glycoconjugates and their application to manipulate cellular signaling events

by

Greg William Trieger

Doctor of Philosophy in Chemistry

University of California San Diego, 2019

Professor Kamil Godula, Chair

Growth factor signaling is a key determinant of cellular decisions ranging from stem cell fate, to metabolic behavior. As such, gaining control over these signaling events is of critical importance to the field of regenerative medicine, which is continuously seeking novel means to tailor the cellular microenvironment to direct cells towards medically advantageous outcomes. Heparan sulfate (HS) glycosaminoglycans (GAGS) are sulfated polysaccharides found on the cell surface and in the extracellular matrix which

are responsible for the engagement of growth factors as well as growth factor receptors as a means to spatiotemporally direct cell signaling events. Despite the obvious potential associated with controlling HS GAG-growth factor interactions, HS GAG-based approaches to manipulate cellular signaling has been minimal due to the complex nature of this class of sulfated polysaccharides. Sulfated GAGs like HS have a non-template driven synthesis, that is, their structure is not dictated by a genetic blue print. During assembly, the GAGs undergo a series of sulfations, isomerizations, and acetylations which give rise to their specific binding capacity, but it is this same complexity that poses a significant hurdle for synthetic or chemoenzymatic approaches geared at producing these structures for study and medical application. As a result, novel approaches must be developed to hone control over cell signaling using GAGs while circumventing the structural obstacle posed by the complexity of their structure. In this dissertation, I present a variety of accessible methods for the preparation of synthetic HS GAG glycoconjugates, and demonstrate their efficacy in several contexts. In chapter 2, I introduce a HS GAG presenting, membrane incorporating, polymer which utilizes a multivalent display of commercially available HS GAG disaccharides to exert control over stem cell fate in a structure dependent manner. In chapter 3 I reveal the role of HS GAG in the metabolic programming of adipocytes, and then apply these polymers to enhance glucose clearance capacity in adipocytes, bearing implications for the treatment of type 2 diabetes. In chapter 4, I developed a highly efficient “click” based method for the conjugation of full length GAGs to protein substrates, and applied these glycoconjugates to manipulate the growth rates of human stem cells from the extracellular matrix. Finally, in chapter 5, I apply the synthetic polymers and protein glycoconjugates to a cellular

microarray, with the goal of miniaturizing cell based assays for the high throughput study of glycomaterials.

CHAPTER 1: Development of synthetic glycosaminoglycan glycoconjugates and their application to manipulate cellular signaling events

1.1 INTRODUCTION

Glycans found at the cell surface and in the extracellular matrix (the glycocalyx) are responsible for a wide variety of recognition and signaling events between cells and other biological species including viruses, bacteria, antibodies, chemokines, receptors and growth factors. Glycan based recognition events tend to be highly specific and organized, gaining this specificity from the complex structures found within the glycocalyx.[1] Extending hundreds of nanometers from the cell membrane, the glycocalyx serves as an interface between the cell and the outside world, as all biological species are forced to make passage through this cellular canopy via a variety of mechanisms in order to perform their function (**Fig. 1)**.[2]

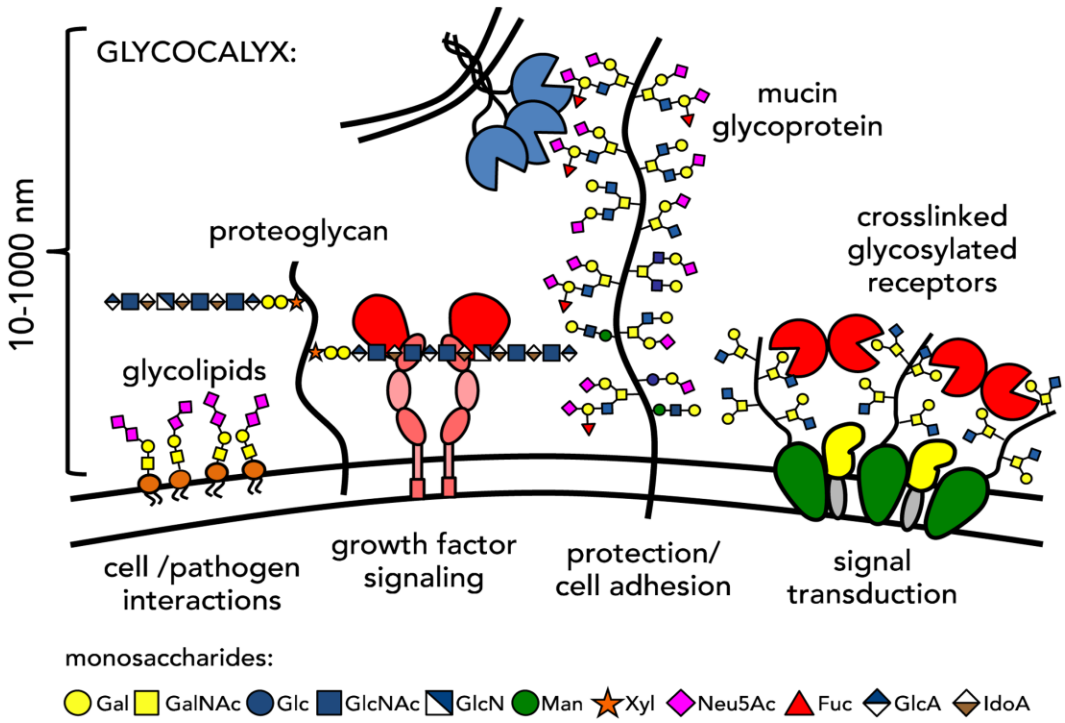

Figure 1. The cell surface is decorated with a complex variety of glycoconjugates targeted by a range of glycan-binding proteins, including receptors on pathogens, and thus serving a range of biological functions. Figure adopted from Huang and Godula, 2016, reproduced with permission.[2]

During embryogenesis, growth factors are organized into chemical gradients through interactions with cell-surface and extracellular matrix glycans that ensure spatial and temporal control over activation of associated signaling pathways and cell proliferation and differentiation giving rise to an organizationally complex functional organism. Specific to this process is a subclass of glycans known as glycosaminoglycans (GAGs), which are polysaccharide chains composed of repeating uronic acid and a hexosamine monosacchairdes *O*-linked to serine or threonine residues in protein chains through a tetrasaccharide primer (GlcA-Gal-Gal-Xyl-*O*-Ser/Thr) and chemically modified via sulfation. The composition of GAGs is determined during their biosynthesis in the

Golgi apparatus, where the GAG chains are initiated and polymerized by glycosyltransferases, which undergo further modification to epimerize glucuronic acids into iduronic acids and to introduce sulfation. This gives rise to biomolecules with high information content covering a large accessible chemical space of polysaccharide structures and associated biological activities (**Fig. 2**).[3] It is the unique sequence of modifications, sulfation in particular, that underlies the specific action of each GAG. Leveraging this class of biomolecules to manipulate signaling has far reaching implications, especially in regenerative medicine where control over cellular microenvironment and behavior, such as proliferation and differentiation, is often sought after to improve the efficacy and safety of cell-based therapies. Despite their potential for biomedical use, GAGs are difficult to study due to their compositional heterogeneity and the lack of simple and powerful methods for controlling their synthesis and activity and a limited analytical toolset to characterize their structure.

While synthetic and enzymatic methods have recently enabled new pathways toward generating chemically defined GAG oligosaccharides, the preparation of GAG polysaccharides of the size (10-500 kDa) and structural complexity of native GAGs is still out of reach of synthetic chemistry. The discrepancy of scales has created a niche for exploring synthetic nanoscale glycomaterials, which combine the precision of chemical oligosaccharide assembly with the synthesis of macromolecules that match the dimension of native glycoconjugates. This approach offers new opportunities to address the hurdle of GAG complexity and to harness the biological functions of these glycans in biomedical research.[4,5]

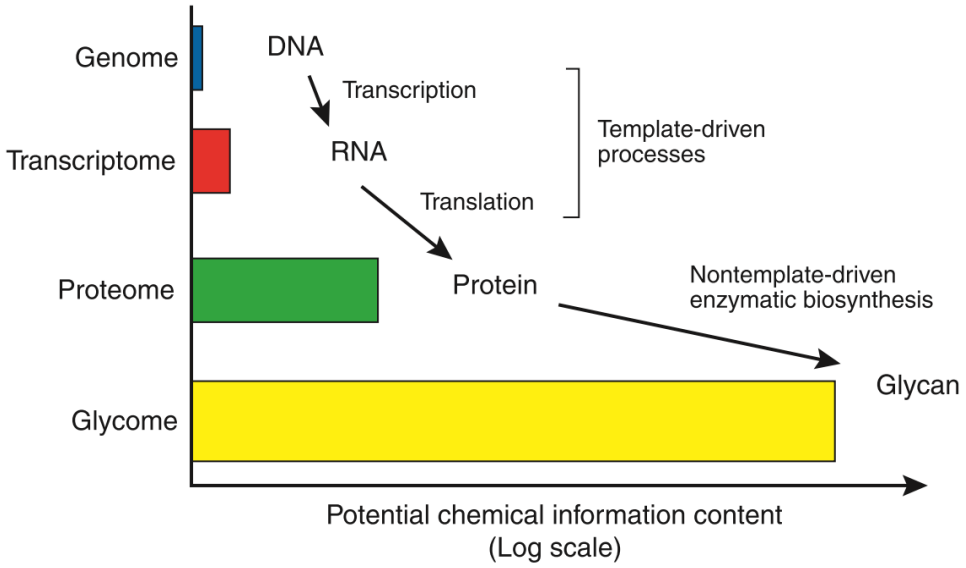

Figure 2. Template driven processes dictate transcription and translational processes, but the posttranslational modifications of proteins and glycans provide an enhanced potential for chemical information to be stored at a minimal genetic cost. Glycans represent the most diverse class of biological molecules. Figure adapted from Turnbull and Field, 2007, reproduced with permission.[3]

1.2 GAG STRUCTURE AND MECHANISM OF ACTION

GAGs are ubiquitous molecules found in all tissues of the human body, and different GAG classes are responsible for a variety of cellular functions, many of which are still being investigated and/or discovered. The function of the GAG typically relates to their structure, localization in the cellular microenvironment (i.e., associated with the cell surface or deposited into the extracellular matrix), and tissue distribution. GAGs can be classified into four main classes based on their monosaccharide content: heparan sulfate (HS), chondroitin sulfate (CS)/dermatan sulfate (DS), keratan sulfate (KS) and hyaluronic Acid (**Fig 3**).[6]

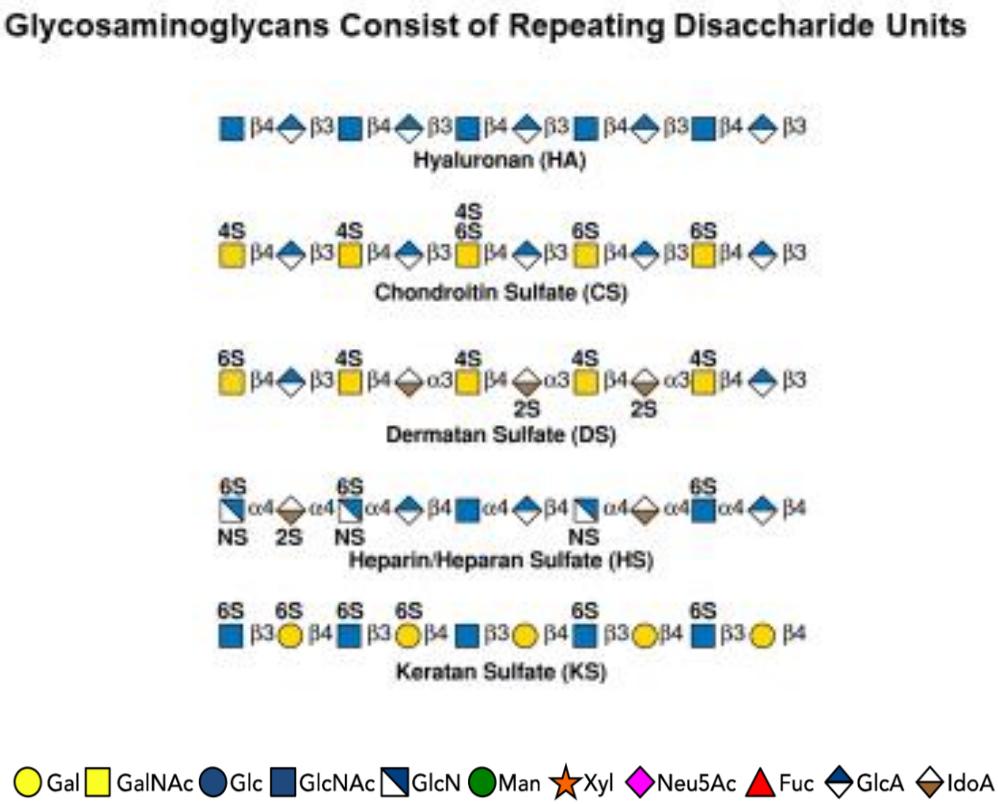

Figure 3. Classes and structure of glycosaminoglycans. Figure reproduced with permission from Essentials of Glycobiology, Chapter 17.[6]

Heparan sulfate (HS) is composed of alternating glucuronic acid (GlcA) or iduronic acid (IdoA) and *N*-acetylglucosamine (GlcNAc) residues, which can be modified with sulfates at the nitrogen atom of GlcNAc rafter deacetylation and on the C3/C6 and C2 hydroxyl groups of the GlcNAc or uronic acid residues, respectively. HS chains are found in both membrane-associated and extracellular matrix proteoglycans. The sulfation patterns in HS encode binding motifs for growth factors (GFs) and membrane-associated HS proteoglycans (PGs) are often required to form a functional signaling complex between GFs and their receptors. On the other hand, HSPG secreted or shed into the extracellular matrix (ECM) can act as depots for GFs. The reservoir can be temporally

accessed by cells through the action of secreted sulfatase or heparinase enzymes, which remove sulfate groups required for GF binding or depolymerize the GAG chains, respectively, effectively releasing the bound GFs from the ECM. [7,8]

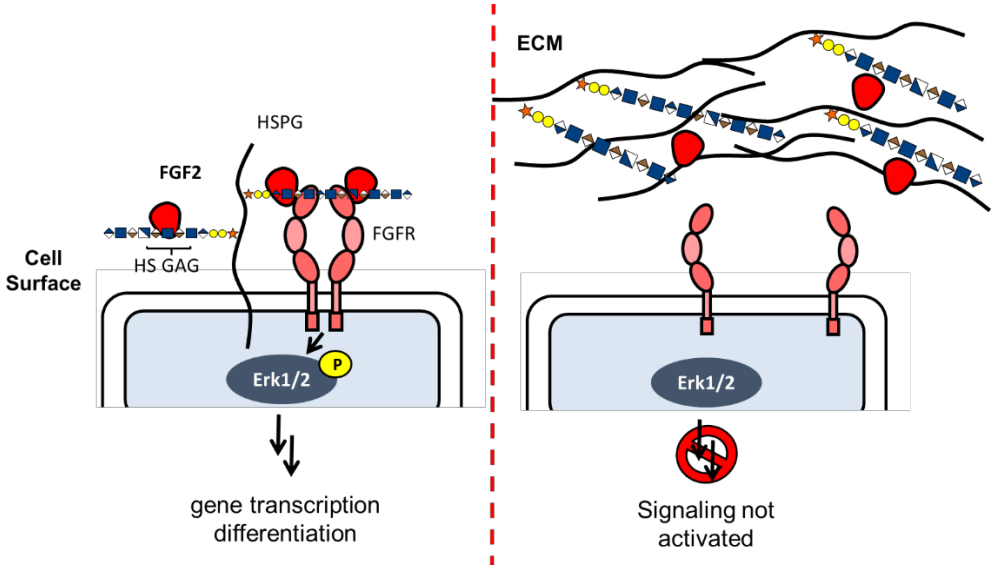

Figure 4. Heparan sulfate proteoglycan (HSPG) can assemble growth factors and their cognate receptors into active signaling complexes. This event is well studies in FGF2 signaling, which induces Erk1/2 phosphorylation and MAPK signal transduction. When HSPG is present in the extracellular matrix but inaccessible to cell surface receptors, it has a sequestration effect on growth factors like FGF2, and signaling does not occur until the growth factor is unbound from HSPG, typically via the action of secreted heparanases or sulfatases.

Chondroitin sulfate (CS) is composed of alternating GlcA and *N*-acetylgalactosamine (GalNAc) monosaccharides and modified at the C4 and/or C6 hydroxyl groups of the GalNAc residue. Epimerization of GlcA into IdoA gives rise to dermatan sulfate (DS). CS found prominently in brain and cartilage tissues has been characterized for having roles in cell division[9] and axonal growth inhibition,[10] and as an important structural material, together with HA and KS, maintaining water homeostasis and compressibility of cartilage tissues. Comparatively, CS it has been somewhat

understudied compared to HS despite having some functional overlap and structural similarities.

Keratan sulfate (KS) consists of repeating units of variably sulfated units of galactose (Gal) and GalNAc. It is richly present in corneal tissues, found at elevated levels throughout the nervous system, and is also present together with CS in the cartilage proteoglycan aggrecan. KS is evolutionarily the newest GAG, and is also considered the most poorly understood, however it has been demonstrated to contribute to cellular signaling, cytoskeletal organization, and bone formation.[11]

Hyaluronic acid (HA) is composed of alternating GlcA and GlcNAc monosaccharides. It is a unique from other GAGs in that it is not sulfated and is never attached to a protein. HA biosynthesis is localized to the plasma membrane, rather than the Golgi compartment, form which long linear HA chains are extruded directly into the ECM. HA often accounts for the majority of GAGs found in the ECM. HA influences the physical properties of tissues, providing a webbing around cells that can be decorated with other GAGs and by various proteins and signaling molecules. A growing body of literature has also provided evidence that HA is not merely a structural glycan but can participate directly in cellular signaling, for instance via the HA-receptor, CD44.[12]

1.3 GLYCOSAMINOGLYCAN AS TARGETS FOR THERAPY.

Because of the ubiquity of GAGs and their broad range of their biological functions, pursuits have been made to utilize them for therapeutic applications. CS is used as a dietary supplement recommended for the treatment of osteoarthritis, a disease

characterized mainly by the degradation cartilage, because as a principle component of cartilage it allows it to regenerate more quickly.[13] Clearly, this rationale is misleading as the digestion and metabolism leads to the breakdown of the orally introduced CS; however, some benefit may be gained by associated increase in the hexosamine biosynthesis pathway flux and elevated HA biosynthesis. Another common GAG used in the clinic is the more highly sulfated form of heparan sulfate GAG, heparin. Heparin is produced in mast cells and is the most acidic molecule in nature as a result of the high content of tri- and tetrasulfated IdoA-GlcNAc disaccharides.[6] Heparin is used as an anticoagulant, which is useful during surgeries, for blood storage, or in the prevention of embolism and stroke. At first, little was known about heparin's mechanism of action, except for the fact that it enhanced the neutralization of thrombin by plasma. While the coagulation cascade protein thrombin was one of the targets of heparin, the picture was more complicated. Heparin also bound inactivated anti-thrombin and caused a conformation change to activate it, which caused it to bind factor Xa which is then inhibited from converting prothrombin to the coagulant thrombin. [14,15]

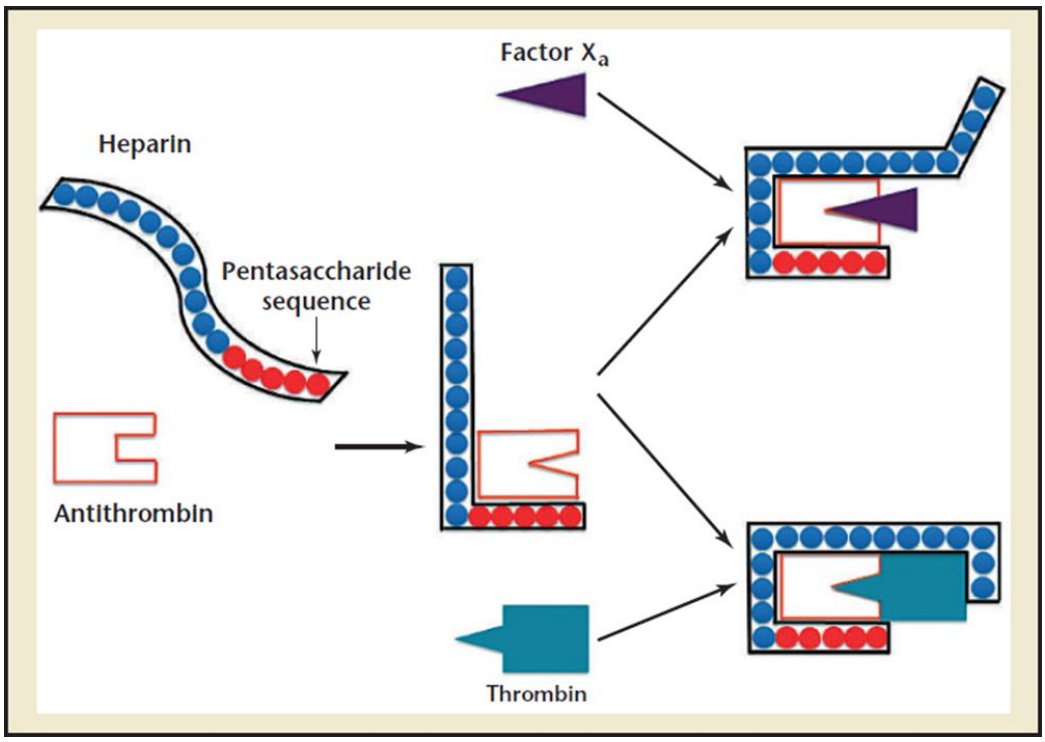

Figure 5. Heparin can bind to antithrombin to cause a conformational change which allows it to bind either factor Xa or thrombin, both of which, when bound, inhibit coagulation. When factor Xa is bound, it is unable to convert prothrombin to the coagulant thrombin.

Heparin's discovery quickly turned heparin into a clinically utilized drug, however, heparin is a heterogeneous polysaccharide with roughly 12 repeating disaccharide units of differential sulfation and has a broad binding profile which could lead to unforeseen complications in patients. As a result, researchers successfully worked to identify the minimal HS structure required for the desired AT activity, with minimal off target effects. The product drug, Fondaparinux, is a pentasaccharide with high specificity for AT with minimal off target effects and demonstrates the potency and specificity that glycan based therapeutics can and need to have in order to be considered effective and safe in the clinic.[16] Gaining a similar understanding of structure-activity relationships in GAG-GF

interactions and signaling may lead to the development of glycomaterials with utility in regenerative medicine. Unfortunately, this technological leap has not yet occurred due to the various hurdles associated with converting these complicated biopolymers into functional, target specific tools.

1.4 CHALLENGES IN GLYCOSAMINOGLYCAN RESEARCH

The compositional complexity, i.e., macromolecular size, stereochemical relationships of glycosidic bonds, and heterogeneous sulfation of GAGs, such as heparan sulfate and heparin, make their characterization using conventional analytical techniques challenging. Nonetheless, over the past 20 years, sophisticated mass spectroscopy methods utilizing electrospray ionization (ESI) and matrix assisted laser desorption ionization (MALDI-TOF) have arose enabling the characterization of small amounts of GAG harvested from tissue or cellular sources and is even able to identify important minor structures found within a cell's glycocalyx. These characterization methods, have shed light on the composition of the ECM and cell membrane of many cell types and tissues, and provided some key insights on the roles of various GAG classes.[3] Although characterization is now more feasible, production and fractionation of these biopolymers produces small quantities of heterogeneous product fractions, useful for establishing structure-activity relationships in GAG-protein interactions.[17] Further insights into their biological functions can be gained by genetic manipulation of the biosynthetic pathaways that produce GAGs.[6] Unfortunately, such manipulations have unintended effects that extend outside of the intended alteration. For instance, removal of the enzymes

responsible for *N*-sulfation of GlcNAc of heparan sulfate, *NDST1/2,* results in a reduction in 2-*O*- and 6-*O*- sulfation as well as the length of the polysaccharide chain, because other enzymes require this sulfation in order to further extent and elaborate the nascent HS structure.[18,19] As a result of the inability to effectively produce GAG structures with purity and homogeneity, a large burden has fallen on the synthetic carbohydrate chemist, who is tasked with preparing unique GAG oligosaccharides, which are commonly evaluated for growth factor and cytokine binding in microarrays. Pursuits such as these require an immense input of resources, and often fall short of their goal, as the observed binding outcomes do not always translate to biological activity in cells.[20] A parallel approach relies on chemoenzymatic synthesis of GAGs, which has seen mixed success. Recent advances in chemoenzymatic methods for GAG assembly have greatly aided these efforts.[21] Still access to sufficient amounts of synthetic GAG building blocks with diverse structures and sizes to support the development of materials for biomedical applications is limited.

While this roadblock is being addressed to make these structures widely available, creative and often unconventional solutions have been pursued by a number of research teams to demonstrate the utility GAGs for future applications. The next four chapters describe my own efforts in this area that produced a new class of semi-synthetic HS GAG-mimetic materials and their applications in different contexts of cellular differentiation. Chapter 2 describes the development of HS GAG mimetics for targeting to the plasma membrane of embryonic stem cells to regulate FGF2 signaling and neural differentiation. Chapter 3 shows that tuning the GAG composition of the cellular glycocalyx of progenitor cells can be used to alter the course of adipogenesis and the glucose uptake and

metabolism in the resulting differentiated cells. Chapter 4 introduces a new bioconjugation strategy for generating extracellular matrix GAG mimetics and their applications for regulating stem cell proliferation in tissue culture. Finally, Chapter 5 reports progress toward the integration of these new glycomaterials into high-throughput microarray platforms for the discovery of biologically active materials. Collectively, these chapters demonstrate the versatility of the GAG-mimetic materials and their broad utility in different biological applications, providing the foundation for their future development toward biomedical applications.

1.5 REFERENCES

[1] Varki, A. *Glycobiology* **2017**, 27, 3-49. Biological roles of glycans.

[2] Huang M. L., Godula K. *Glycobiology*. **2016**, 26, 797-803. Nanoscale materials for probing the biological functions of the glycocalyx.

[3] Turnbull J. E., Field R. A. *Nature Chem Bio.* **2007**, 3, 74-77. Emerging glycomics technologies.

[4] Hudak J. E., Bertozzi C. R. *Chem Biol.* **2014**, 21, 16-37. Glycotherapy: new advances inspire a reemergence of glycans in medicine.

[5] Seeberger, P. H., Cummings, R. D. *Essentials of Glycobiology, Third Edition*, **2017.** Chapter 57: Glycans in Biotechnology and the Pharmaceutical Industry.

[6]Lindahl U., Couchman J., Kimata K., Esko J. D. . *Essentials of Glycobiology*, 2nd ed.; CSHL Press: New York, **2009**. Chapter 17: Proteoglycans and sulfated glycosaminoglycans.

[7] Lin X. *Development.* **2004**, 131, 6009-6021. Functions of heparan sulfate proteoglycan in cell signaling during development.

[8] Vlodavsky, I.; Bar-Shavit, R.; Ishai-Michaeli, R.; Bashkin, P.; Fuks, Z. *Trends Biochem Sci.* **1991**, *7*, 268-271. Extracellular sequestration and release of fibroblast growth factor: a regulatory mechanism?

[9] Mizuguchi S., Uyama T., Kitagawa H., Nomura K. H., Dejima K., Gengyo-Ando K., Mitani S., Sugahara K., Nomura K. *Nature*, **2003,** 423, 443-448. Chondroitin proteoglycans are involved in cell division of *Caenorhabditis elegans*.

[10] Tully S. E., Mabon R., Gama C. I., Tsai S. M., Liu X., Hsieh-Wilson L. C.*J. Am. Chem. Soc.* **2004** 126, 25, 7736-7737. A chondroitin sulfate small molecule that stimulates neuronal growth.

[11] Caterson B., Melrose J. *Glycobiology*. **2018**, 28, 182-206. Keratan sulfate, a complex glycosaminoglycan with unique functional capability.

[12] Hascall V. C. *Journal of Biol. Chem.* **2019**, 294, 1690-1696. The journey of hyaluronan research in the Journal of Biological Chemistry.

[13] Jerosch J. *Int. J. Rheumatol*. **2011**, doi:10.1155/2011/969012. Effects of Glucosamine and Chondroitin Sulfate on Cartilage Metabolism in OA: Outlook on Other Nutrient Partners Especially Omega-3 Fatty Acids.

[14] Lee M. S., Kong *J. Cardiovasc. Med.* **2015**, 16, 189-199. Heparin: Physiology, Pharmacology, and Clinical Application

[15] Jin L., Abrahams J. P., Skinner R., Petitou M., Pike R. N., Carrell R. W. *PNAS, **1997***, 94, 14683-14688. The anticoagulant activation of antithrombin by heparin.

[16] Petitou M., van Boeckel C. A. *Angew Chem Int Ed Engl.* **2004**, 43, 3118-3133. A synthetic antithrombin III binding pentasaccharide is now a drug! What comes next?

[17] Stelling M. P., de Bento A. A., Caloba P., Vilanova E., Pavao M. S. G. *The Extracellular Matrix*, **2019**, 1952, 55-70. Methods for isolation and characterization of sulfated glycosaminoglycans from marine invertebrates.

[18] Deligny, A., Dierker T., Dagalv A., Lundequist A., Eriksson I., Nairn A. V., Moremen K. W., Merry C. L. R., Kjellen L. *Journal of Biol. Chem,* **2016**, 291, 18600-18607. NDST2 (N-Deacetylase/N-Sulfotransferase-2) Enzyme Regulates Heparan Sulfate Chain Length.

[19] Fuster M. M., Wang L., Castagnola J., Sikora L., Reddi K., Lee P. H. A., Radek K. A., Schuksz M., Bishop J. R., Gallo R. L., Sriramarao P., Esko J. D. *Journal of Cell Biology,* **2007,** 177, 539-549. Genetic alteration of endothelial heparan sulfate selectively inhibits tumor angiogenesis.

[20] Puvirajesinghe T. M., Ahmed Y. A., Powell A. K., Fernig D. G., Guimond S. E., Turnbull J. E. *Chem Biol*. **2012**, 19, 553-558. Array-based functional screening of heparin glycans.

[21] DeAngelis P. L., Liu J., Lindhardt, R. J. **Glycobiology**. **2013**, 23, 764-777. Chemoenzymatic synthesis of glycosaminoglycans: Re-creating, re-modeling and re-designing nature's longest or most complex carbohydrate chains.

CHAPTER 2: Glycocalyx remodeling with proteoglycan mimetics promotes neural specification in embryonic stem cells

2.1 INTRODUCTION

Stem Cells hold great promise in regenerative medicine due to their ability to differentiate into any cell type in the body.[1] There are many types of stem cells, which are sourced from different niches within the body and thus have a variety of intrinsic qualities linked to their source which contribute to their compatibility to combat various diseases. Currently, hematopoietic stem cells are the most commonly utilized type of stem cell, and is FDA approved for the treatment of a wide variety of cancers, most notably leukemia. Epithelial stem cells are the only other FDA approved stem cell treatment, and are typically utilized for burn victims or those with damaged corneal epithelium. Both of these cell types benefit from the ease of application of the stem cells, where epithelial transplant surfaces can be properly prepared for reception of stem cells, and hematopoietic stem cells are intravenously infused and home to the site in which they are needed as they are preprogrammed to, via a variety of recognition events.[2] Stem cells which must be locally applied to an internal degenerated area encounter a host of complications associated with controlling the fate of the transplanted stem cells. Diseased organs which would benefit from stem cells do not possess a nurturing or instructive environment for the differentiating stem cells, which need to clear and replace damaged tissue. The application of stem cells to an injury site without proper control over their fate typically results in teratomas.[3]

Stem cell differentiation requires a delicate balance of external cues that instruct the formation of organismal complexity. This orchestration occurs within a stem cell niche,

where biochemical, mechanical, and biophysical cues guide the stem cell towards its proper fate.[3] A potent director of cellular fate are growth factors (GFs), which activate key signaling pathways involved in gene regulation. As such, a great effort has been directed in pursuit of controlling growth factor signaling as a means to remotely control the fate of stem cells.[4] Signaling typically occurs when a growth factor reaches a cell surface receptor, at which point a signaling complex is formed followed by a phosphorylation event indicating the activation of a signaling cascade. However, in order for the signaling growth factor to reach the receptor, it often requires guidance and receptor-complex assembly provided from extracellular matrix proteins known as proteoglycans, which make up the glycocalyx of the cell.[5,6] Proteoglycans gain their activity through sulfated polysaccharides called glycosaminoglycans (GAGs) which are appended to the core protein backbone. The sulfation patterns of GAGs are believed to be responsible for proteoglycan activity, and allows for a broad range of affinities for different target proteins.[7] In mouse embryonic stem cells (mESCs), PGs with heparan sulfate (HS) GAGs composed of alternating units of variously sulfated glucosamine and uronic acid orchestrate the formation of complexes between fibroblast growth factors (FGFs) and their receptors, FGFRs (Figure 6A).[8] Subsequent phosphorylation of the *Ext*racellular Signal-regulated Kinases 1 and 2 (Erk1/2) and downstream signaling events that ensue result in differentiation of mESCs into neural precursor cells (NPCs).[9] In mESCs lacking exostosin 1 (*Ext*1), an enzyme responsible for the biosynthesis of HS, FGFs fail to form functional complexes with FGFRs leading to cell arrest in an embryonic state (Figure 6A).[9c,10] Harnessing glycocalyx interactions to regulate GF signaling may elucidate a novel approach for the guidance of stem cells toward a target fate.

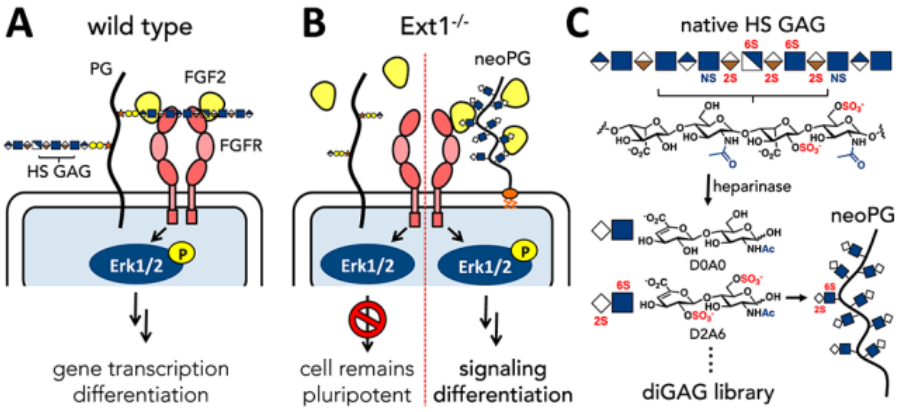

Figure 6. A) Glycocalyx remodeling strategy for influencing stem cell specification. HSPGs are required for FGF signaling during development. B) Synthetic neoproteoglycans (neoPGs) are introduced to surfaces of ESCs deficient in HS biosynthesis to rescue FGF signalingand enable differentiation. C) Glycan building blocks derived from native HS serve as growth factor recognition elements for neoPGs.

Herein, we report a cell-surface engineering strategy that targets GAG-mediated growth factor signaling to influence stem cell specification. Glycocalyx remodeling has emerged as a powerful strategy for introducing specific glycan epitopes to the cell surface, where they can mediate a range of biological processes. This can be achieved through manipulation of metabolic pathways responsible for glycan biosynthesis,[11] enzymatic degradation,[12] genetic knockout methods,[13] covalent grafting of glycans to surface proteins,[14] or through passive insertion of lipid-functionalized glycoconjugates into the cell membrane.[15] The latter approach is particularly appealing, as it has minimal impact on existing membrane structures and as a functional material, can be directly applied to target cells. For instance, elegant studies by Bertozzi and co-workers using synthetic lipid functionalized glycopolymers have revealed the roles of various glycocalyx components in receptor oligomerization and immunomodulation.[16] More recently, lipid-terminated chondroitin sulfate GAGs from natural sources were introduced onto rat

cortical neurons, where they enhanced nerve growth factor-mediated signaling and promoted neural outgrowth.[17] Unfortunately, native HS is highly structurally heterogeneous and not amenable to the targeting of specific growth factor interactions. The synthesis of uniform HS polysaccharides poses a significant challenge, whereas shorter HS oligomers that are more synthetically manageable typically exhibit limited biological activity despite possessing the requisite sulfation pattern. Short oligomers are not without their use though, and are typically utilized for microarray binding studies to determine binding criteria for target proteins without requiring them to be of sufficient length to enable signaling.[18] Additionally, this shortcoming can be remedied by taking advantage of multivalency effects, in which many low affinity interactions culminate into high affinity binding of the molecule.[19] Seeberger and co-workers first demonstrated that dendrimers functionalized with synthetic HS hexasaccharides were able to potentiate Erk1/2 signaling,, while the hexasacharride alone at the same concentration had no effect on signaling.[20] A major breakthrough followed when Hsieh-Wilson and her co-workers showed that soluble linear polymers decorated with synthetic GAG disaccharides were able to inhibit neural outgrowth and alter chemokine activity.[21] Inspired by this minimalistic approach, we designed a strategy for generating mimetics of HSPGs neoproteoglycans or neoPGs that completely obviates the need for GAG synthesis by utilizing commercially available disaccharides of sourced from heparinase digests (Figure 6c). We then demonstrate the utility of the approach by rescuing MAPK signaling and resultant neural differentiation in mESC cells lacking HS (*Ext1*$^{-/-}$). Moreover, we are confident this strategy can be adopted as a novel tool to study glycocalyx interactions and gain mechanistic insights into newly discovered GAG dependent cellular events

2.2 RESULTS AND DISCUSSION

2.2.1 *Preparation and characterization of neoproteoglycan library*

The glycopolymer backbone was designed with three functional components: an anchoring motif which could be either an azide for click chemistry or a lipid for passive membrane insertion, a fluorescent label to for detection, and most importantly, pendant N-methylaminooxy groups, which are reactive toward the hemiacetal functionality of a reducing glycan. Ligated to the N-methylaminooxy groups are GAG disaccharides (diGAGs) generated by depolymerization of HS by bacterial heparinases and available in pure form from commercial sources.[22] We first prepared a 17 member azide-NeoPG library to be applied to a microarray platform we developed to identify neoPG candidates with specificity toward FGF2. This way, only sub milligram quantities of material is required during this preliminary screening process. The binders of FGF2 are then selected and resynthesized as lipidated polymers which can be introduced into the glycocalyx of *Ext*1$^{-/-}$ mESCs to promote their differentiation into NPCs via rescued FGF2 signaling.

First, we prepared a key polymer intermediate 6 primed for diGAG conjugation and terminated with an azido group for covalent immobilization on cyclooctyne-coated glass via the strain-promoted azide-alkyne cycloaddition (Scheme 1).[23] Trimethylsilyl chloride and phenol to give the desired intermediate 6.

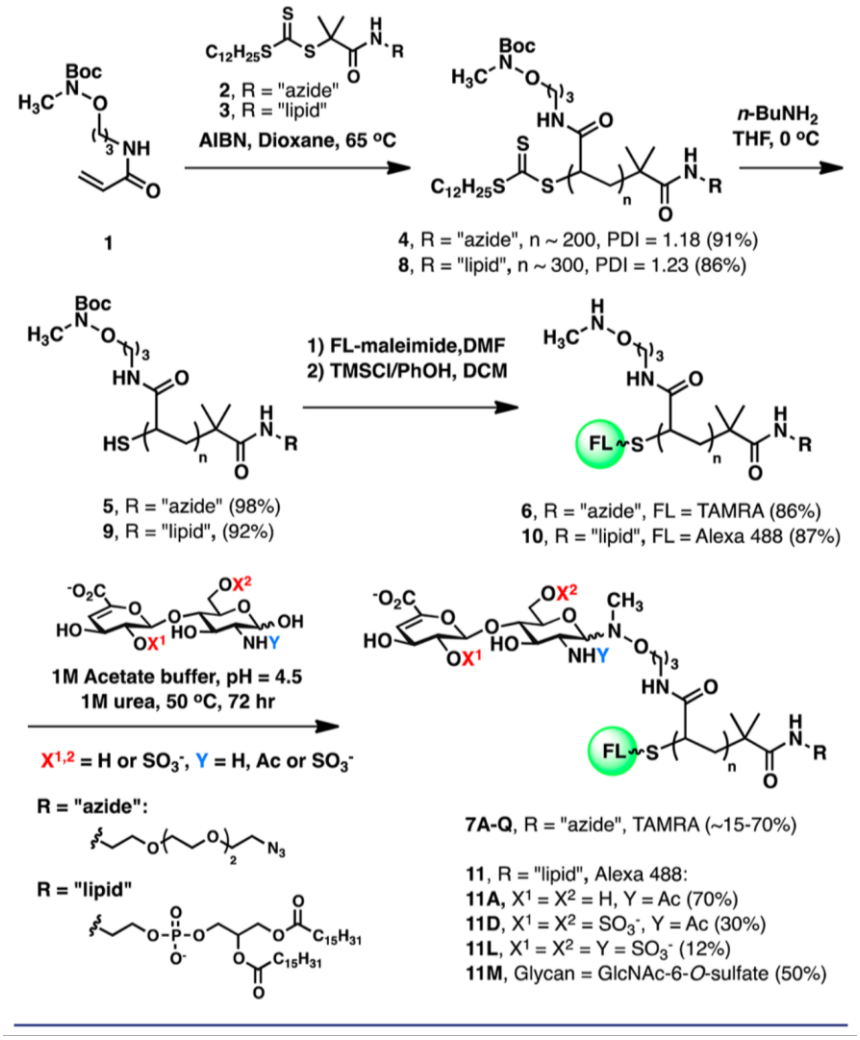

Scheme 1. Synthesis of neoproteoglycans.

Conjugation of diGAGs as well as several glucosamine derivatives to polymer 6 proceeded smoothly under acidic conditions (1 M acetate buffer, pH = 4.5) at 50 °C to afford a library of neoPG structures 7A-Q (Figure 7). Using 1H NMR analysis, we established the extent of incorporation for the individual glycans (Table 1). Not surprisingly, we observed a decrease in glycan incorporation with increasing negative charge. Typical ligation efficiencies ranged from ~50%-70% for nonsulfated glycans to

~15% for the trisulfated diGAG, D2S619 (Table 1). Nonetheless, we anticipated that even the lowest ligation efficiency should provide sufficient valency (~30diGAGs) to support FGF2 binding.

2.2.2 *Development and application of neoproteoglycan library to assess FGF2 binding*

Azido-terminated neoPGs 7A-Q were microarrayed on cyclooctyne-functionalized glass and evaluated for binding of FGF2. Only a subset of our neoPG structures effectively engaged FGF2 (Figure 7). We observed that 2-O-sulfation on the uronic acid residue was required for FGF2 binding with additional affinity derived from 6-O-sulfation of the glucosamine unit, consistent with known FGF2 specificities for GAG motifs.6 Neither neoPG 7A carrying the nonsulfated diGAG (D0A0) nor neoPG 7N decorated with N-acetylglucosamine-6-O-sulfate (GlcNAc-6S) showed any appreciable binding of the growth factor, indicating a requirement for both the disaccharide motif and a specific sulfation pattern for recognition (Figure 7). FGF2 binding across the entire library was abolished in the presence of soluble heparin (1 μg/mL), further confirming that FGF2 binding to neoPGs was glycan specific (Figure 7). Normalizing the fluorescence intensities of Alexa Fluor 647 used for the detection of FGF2 in the microarray to the TAMRA signal associated with the underlying glycopolymers provided a semi-quantitative means to rank the neoPGs according to their relative affinity toward FGF2 (Figure 7), however the relative valency of neoPG isn't considered using this approach so conclusions on structure-affinity relationships can't be definitively drawn. Regardless, the best FGF2 binding NeoPG that emerged from our screen was neoPG 7D carrying the 2,6-O-disulfated diGAG, D2A6 (Figure 7). It should be mentioned that has been

demonstrated by us and others that in native heparin and heparan sulfate, N-sulfation significantly enhances FGF2 binding activity, but this trend was not consistent among the library.[24] We believe it is possible that multivalent interactions or the unsaturated bond found within the uronic acid diGAGs may compensate for the lack of N sulfation or somehow reduce its role in FGF2 binding.

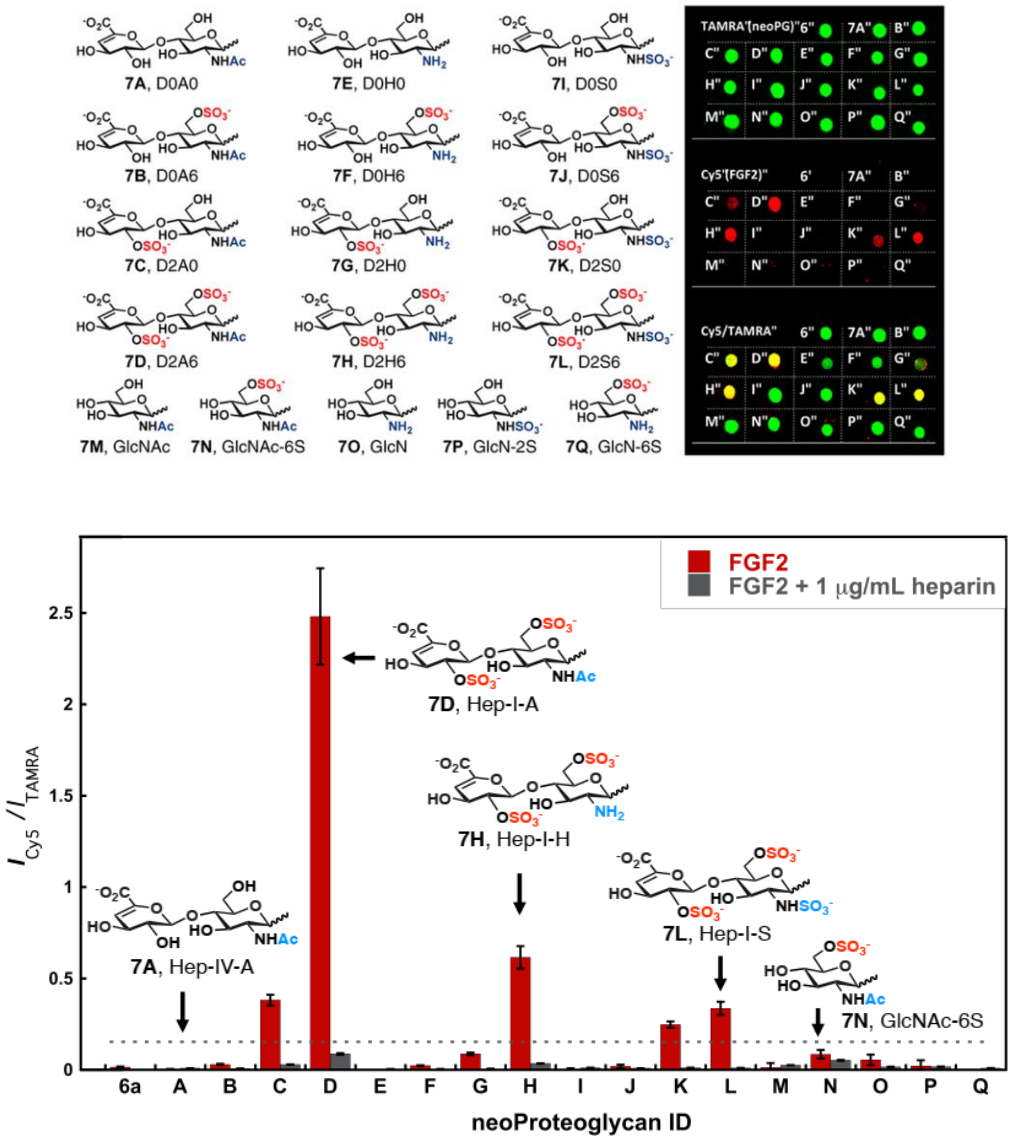

Figure 7. Microarray screen of a library of TAMRA-labeled neoPGs representing most naturally occurring HS sulfation motifs identified neoPGs with specificity for FGF2.

2.2.3 *Application of neoproteoglycans to rescue neural specification in Ext1$^{-/-}$ mESC*

To evaluate whether the ability of neoPGs to bind FGF2 established in our microarray screen can be recapitulated on the surface of mESCs, we synthesized analogs of neoPGs 7A, D, and N functionalized with a phospholipid tail for membrane insertion and an Alexa Fluor 488 (AF488) tag for imaging (neoPGs 11, Scheme 1).

Incubation of *Ext*1$^{-/-}$ mESCs in solutions of neoPGs 11 in base media at 37 °C for 1 h led to a successful introduction of the polymers to the cell surface (Figure 7A). The amount of neoPG delivered to the cell surface is proportional to the polymer concentration in the media and the incubation time, offering control over the extent of cell surface remodeling (for optimization of these variables for neoPG 11N, see Figure 26). The degree of remodeling by the different neoPGs was assessed by fluorescence microscopy (Figure 2.3A). Interestingly, the nonsulfated neoPG 11A exhibited higher levels of membrane incorporation relative to 11D and 11N, presumably due to its lower overall negative charge. To sustain differentiation, the neoPGs need to remain active on the cell surface for a period of several hours.[9b] To establish the membrane residence time for our polymers, we cultured *Ext*1$^{-/-}$ mESCs remodeled with neoPG 11D and monitored its clearance from the cell surface using an antiAF488 antibody. Satisfyingly, >50% of the neoPG still remained localized to the cell surface after 8 h (Figure 22).

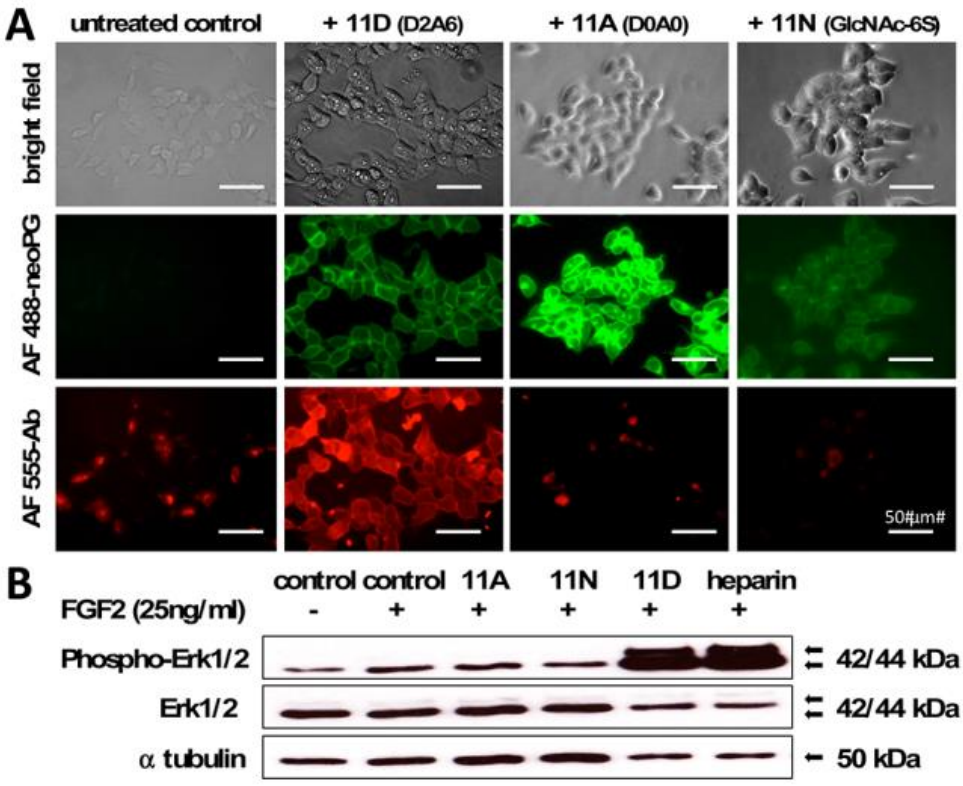

Figure 8. A) Glycocalyx remodeling rescued FGF2-mediated signaling in *Ext*1$^{-/-}$ mESCs. NeoPGs 11A, D, and N (1 µM) inserted into membranes of *Ext*1$^{-/-}$ mESCs (green) and promoted FGF2 binding according to the structure of their glycans (red). B) FGFs binding neoPG 11D enhanced Erk1/2 phosphorylation.

In agreement with our microarray data, we observed enhanced FGF2 binding to *Ext*1$^{-/-}$ mESCs remodeled with neoPG 11D carrying the sulfated diGAG, D2A6, while 11A and N, which have undetectable affinity for FGF2, failed to recruit the growth factor to the cell surface (Figure 8A). To determine whether enhanced FGF2 binding also translated into induction of Erk1/2 phosphorylation required to initiate differentiation, we conducted a growth factor stimulation assay. *Ext*1$^{-/-}$mESCs remodeled with neoPGs 11 were stimulated with exogenous FGF2 for 15 min. Changes in phosphorylation were assessed by Western blot analysis of protein isolated from cell lysates. As expected, induction of

Erk1/2 signaling was observed only for neoPG 11D (Figure 8B) or in the presence of soluble heparin as reported previously.[10]

To assess whether neoPGs can induce neural specification in *Ext*1$^{-/-}$ mESCs, we performed differentiation in monolayer culture.[25] Concordant with previous work, *Ext*1$^{-/-}$ mESCs failed to undergo neural specification after 6 days, as evidenced by expression of the pluripotency marker, Oct4. Gratifyingly, mESCs remodeled with neoPG 11D, which promotes FGF2 recruitment to the cells' surface and stimulates the associated Erk1/2 signaling, successfully exited from their pluripotent state and formed characteristic nestin-positive neural rosettes with decreased Oct4 expression (Fig 9A). In comparison, neoPGs 11A and N, which do not engage FGF2, had no effect on differentiation and colonies expressing high levels of Oct4 similar to those in untreated *Ext*1$^{-/-}$ mESCs remained abundant (Figure 10). A dose-dependent reduction in the number of neural rosettes was observable upon decreasing the surface density of 11D (Figure 10f), which correlated with increased Oct4 expression as well as attenuated Erk1/2 phosphorylation in our stimulation. It should be noted that addition of soluble heparin at 5 μg/mL to the culture medium also rescued neural differentiation in *Ext*1$^{-/-}$ mESCs (Figure 9E). However, titers of heparin need to be established to prevent sequestering of FGF2 away from the cell surface and introduced continuously over a period of at least 4 days.4d This contrasts with the ability of neoPG 11D to sustain neural specification in *Ext*1$^{-/-}$ mESCs after only one initial treatment prior to differentiation. These results demonstrate the power of glycocalyx engineering as a strategy to influence cellular responses that ultimately determine the outcome of stem cell differentiation. We anticipate that this technology, powered by the ease of neoPG synthesis and the versatility of the microarray platform,

can be rapidly extended to differentiation of other cell types, including therapeutically useful human pluripotent cells.

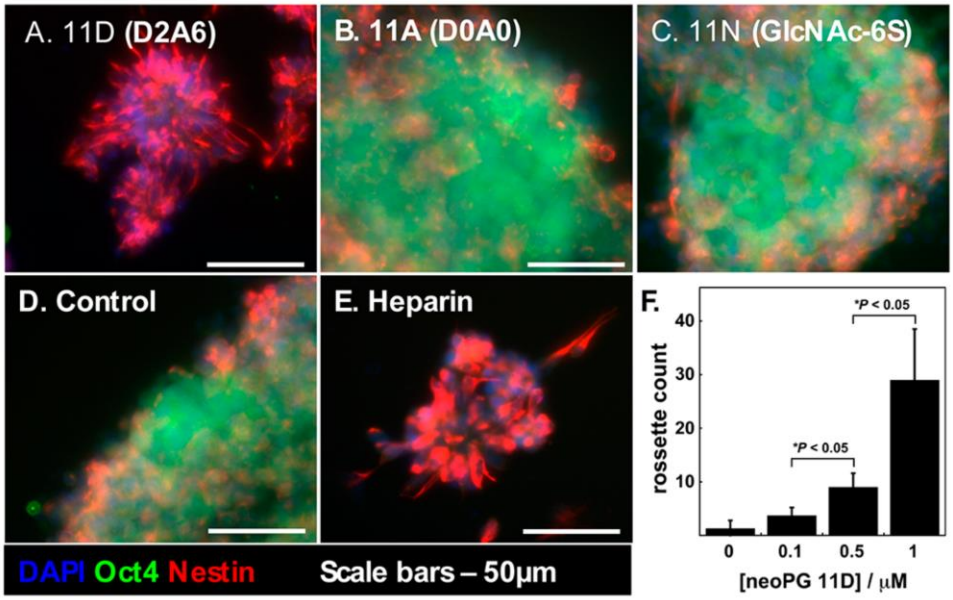

Figure 9. A) Neural differentiation of neoPG-remodeled *Ext*1$^{-/-}$ mESCs. NeoPG 11D with affinity toward FGF2 promoted differentiation into neural rosettes (A), while cells remodeled with neoPGs 11A and N (B and C) or left untreated (D) retained their embryonic characteristics. Soluble heparin also promoted differentiation (E). The ability to produce rosettes improved in cells treated at increasing concentrations of neoPG 11D (F).

2.3 CONCLUSIONS:

The development of the NeoPGs in the Godula lab has allowed for their broad application as glycocalyx remodeling tools in a variety of contexts, and have consistently delivered novel insights into GAG dependent signaling events. Notably, Matt Naticchia demonstrated that these materials can be applied for the remodeling of 3D stem cell aggregates known as embryoid bodies, which have enhance complexity and enable more

efficient differentiation towards mesodermal lineages. The remodeling of *Ext*1$^{-/-}$ mESCs with the same D2A6 bearing polymer enhanced BMP4 signaling and allowed cells to efficiently exit pluripotency and commit to a mesodermal lineage. Now, partnered with Logan Laubach, they are developing a method to spatially pattern NeoPG throughout the EB by modulating polymer length to tune penetration, unlocking new applications for these glycomaterials to establish signaling gradients in 3D. In chapter 3, I demonstrate a novel application of the neoPGs, using them not to rescue differentiation per se, but rather to enhance a specific and previously unidentified, HS-dependent-signaling event responsible for the metabolic programming of differentiating preadipocytes. Interestingly, soluble heparin was only able to inhibit the phenotype I was observing regardless of concentration, while the membrane incorporating neoPGs provided the only means to enhance the signaling event, and highlighting the utility of these materials from both a basic research perspective as well as therapeutics. Without access to sophisticated materials capable of restoring or enhancing HS-GAGs on a cell surface, we would not have discovered that enhancement of a healthy metabolic profile were possible via GAG based therapies.

The main drawback of NeoPGs is that they can't reliably be used to identify structural requirements for binding events between native HS GAGs and their typical binding partners. As pointed out earlier, the diGAG which bound FGF2 the strongest, D2A6, bears a sulfation pattern that typically has reduced FGF2 binding in full length heparin relative to the N-sulfated D2S6 diGAG motif found in heparin. Additionally, it seems that this disaccharide is promiscuous as well, as it was also determined to be the most effective binder of FGF2 and BMP4, despite them having unique GAG binding

preferences. [24,26] In order to make the NeoPG more capable of providing structural insights to binding events, the GAG must be extended to more biologically relevant lengths and valency should be controlled for. However, because the N-methylaminooxy moeity already suffers from low ligation efficiencies for highly sulfated disacharrides, it is clear the ligation strategy must be adjusted if we hope to include longer heparan sulfate GAGs. In chapter 4 I demonstrate an approach that hinges on the more reliable CuAAC “click” chemistry to overcome the steric barriers of preparing a multivalent heparin glycoconjugate , and this click approach has been applied to the next generation NeoPG backbone. In an effort led by Daniel Honigfort, multivalent polymers are being functionalized with azides to react with alkynes appended to prefunctionalized full length heparin and HS GAGs. These exciting materials will represent natural proteoglycans more faithfully than other polymers currently demonstrated in the literature, and can even be derivitized with full length HS isolated from various cell lines expressing different structural forms of HS. I am confident these materials will be utilized for a broad variety of studies, and will serve as both an approach for the manipulation of cellular signaling as well as a tool for gaining structure-function relationships for a variety of binding partners.

2.4 MATERIALS AND METHODS

2.4.1 Abbreviations

Abbreviations

AIBN = azobisisobutyronitrile
Boc = ditertbutyldicarbonate
BSA = bovine serum albumin
DCM = dichloromethane
DIPEA = N, N-diisopropylethylamine
DMF = N, N-dimethylformamide
DP = degree of polymerization
Et_3N = triethylamine
EtOAC = ethyl acetate
FBS = fetal bovine serum
FGF2 = fibroblast growth factor 2
TAMRA = tetramethylrhodamine
THF = tetrahydrofuran
TMSCl = tritmethylsilyl chloride
PDI = polydispersity index
PhOH = phenol
M_n = number average molecular weight
M_w = weight average molecular weight
NeoPG = synthetic neoproteoglycan

2.4.2 Materials and General Procedures

All chemicals, unless stated otherwise, were purchased from Sigma Aldrich. Purchased starting materials were used as received unless otherwise noted. Glycans were purchased from Iduron (Manchester, UK), V-labs (Covington, LA) or Carbosynth (San Diego, CA). Glycosaminoglycan nomenclature used here is decribed in Lawrence et al.[271] Anhydrous dioxane was generated via filtration through basic alumina. Polymers were isolated by gel filtration on Sephadex G-25 columns (PD-10, GE Healthcare). Epoxide-coated glass substrates were purchased from Thermo Fisher. Fluorophores were purchased from Life Technologies (Carlsbad, CA.) Reaction progress was checked by analytical thin-layer chromatography (TLC, Merck silica gel 60 F-254 plates) monitored either with UV illumination, or by staining with iodine or ninhydrin. Solvent compositions are reported on a volume/volume (v/v) basic unless otherwise noted.

2.4.3 Instrumentation

Column chromatography was performed on a Biotage Isolaera One automated flash chromatography system. Nuclear magnetic resonance (NMR) spectra were collected on either a Bruker 300 MHz or Jeol 500 MHz NMR spectrometer. Spectra was recorded in $CDCl_3$ or D_2O solutions at 293K and are reported in parts per million (ppm) on the δ scale relative to the residual solvent as an internal standard (for ^1H NMR: $CDCl_3$ = 7.26 ppm, D_2O = 4.79 ppm, for ^{13}C NMR: $CDCl_3$ = 77.0 ppm). Data are reported as follows: chemical shift, multiplicty (s = singlet, d = doublet, dd = doublet of doublets, t = triplet, q = quartet, br = broad, m = multiplet), coupling constants (Hz), and integration. Size exclusion chromatography was performed on a Hitachi Chromaster system equipped with an RI detector and a 5 □m, mixed bed, 7.8 mm I.D. x 30 cm TSKgel column (Tosoh Bioscience). Polymers were analyzed using an isocratic method with a flow rate of 0.7 mL/min in DMF (0.2% LiBr, 70 °C). Infrared spectrophotometry data for compound **2** was collected on a Perkin Elmer Spectrum Two FTIR Spectrophometer and data for compound **4** with a Perkin Elmer Paragon 500 FTIR. UV-Vis spectra were collected with a quartz cuvette using a ThermoScientific Nanodrop2000c spectrophotometer. HRMS (high resolution mass spectrometry) analysis was acquired via an Agilent 6230 ESI-TOFMS in positive ion mode.

*2.4.4 Procedure and characterization data for the synthesis of monomer **1***

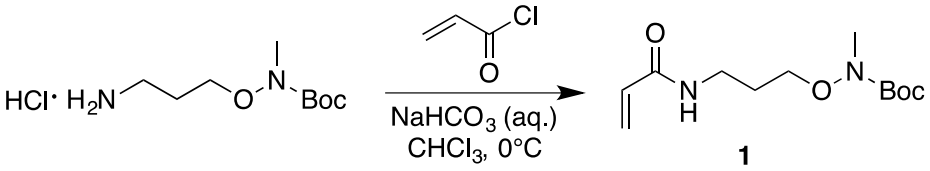

Synthesis of (1). A round bottom flask was charged with *N*-(3-aminopropoxy), *N*-methyl-carbamic acid, 1,1-dimethylester hydrochloride[28] (9.0 g, 0.037 mol, 1.0 eq). Chloroform (95 mL) was then added, followed by cooling to 0 °C, and the addition of $NaHCO_3$ (9.4 g, 0.112 mmol, 3.0 eq) in water (95 mL). The reaction mixture was cooled and freshly distilled acryloyl chloride was added drop wise over 30 min. After this time, the reaction was complete by TLC. The layers were separated, and the aqueous layer extracted (3x) with $CHCl_3$. The combined organic layers were washed with a saturated aqueous solution of $NaHCO_3$ (1x), H_2O (2x), brine (1x), dried with $MgSO_4$, and concentrated (without heating) to give a clear liquid (10 g, quant.). 1H NMR (500 MHz, CDCl3) δ (ppm): 7.63 (br s, 1H), 6.28 (dd, 1H, J = 17 Hz, J = 2Hz), 6.11 (dd, 1H, J = 17 Hz, J = 10 Hz), 5.56 (dd, 1H, J = 10 Hz, J = 2 Hz), 3.91 (t, J = 6 Hz, 2H),3.50 (m, 2H), 3.09 (s, 3H), 1.78 (dd, 2H, J = 10 Hz, J = 2 Hz), 1.47 (s, 9H). 13C NMR (125 MHz, CDCl3): δ (ppm): 165.6, 156.9, 131.6, 125.5, 81.9, 72.4, 36.9, 28.3, 26.9. Calculated C12H22N2O4, 258.16, [M+Na]+: 281.15. HRMS m/z found: 281.1470.

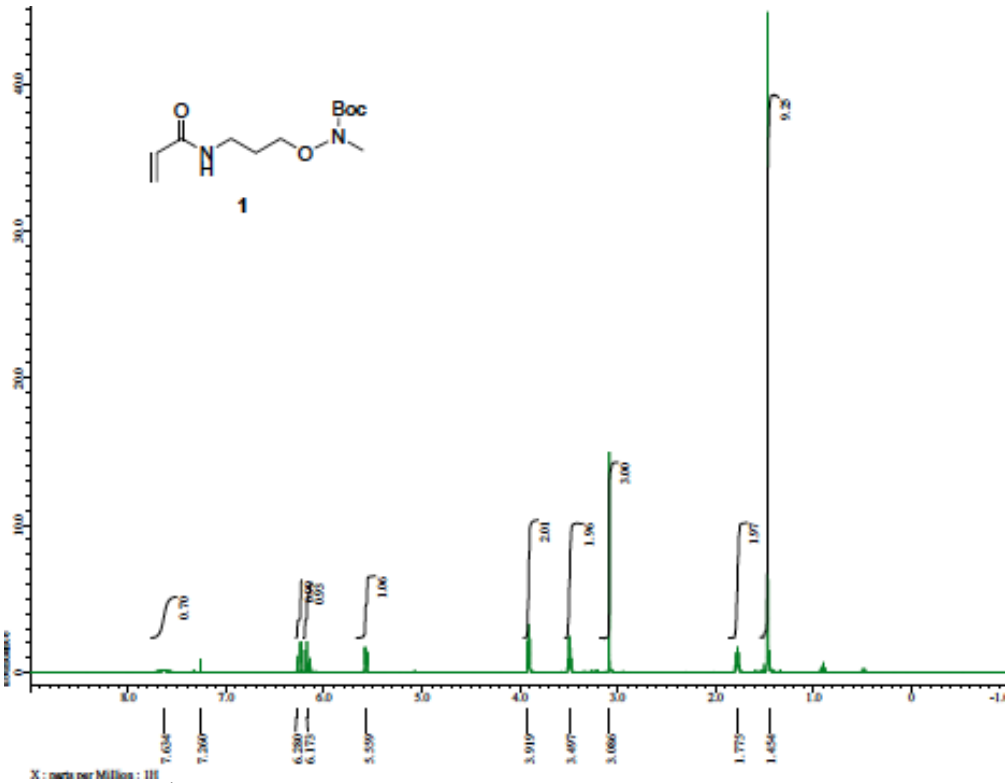

Figure 10. ^{1}H NMR (500 MHz, $CDCl_3$) of monomer **(1)**

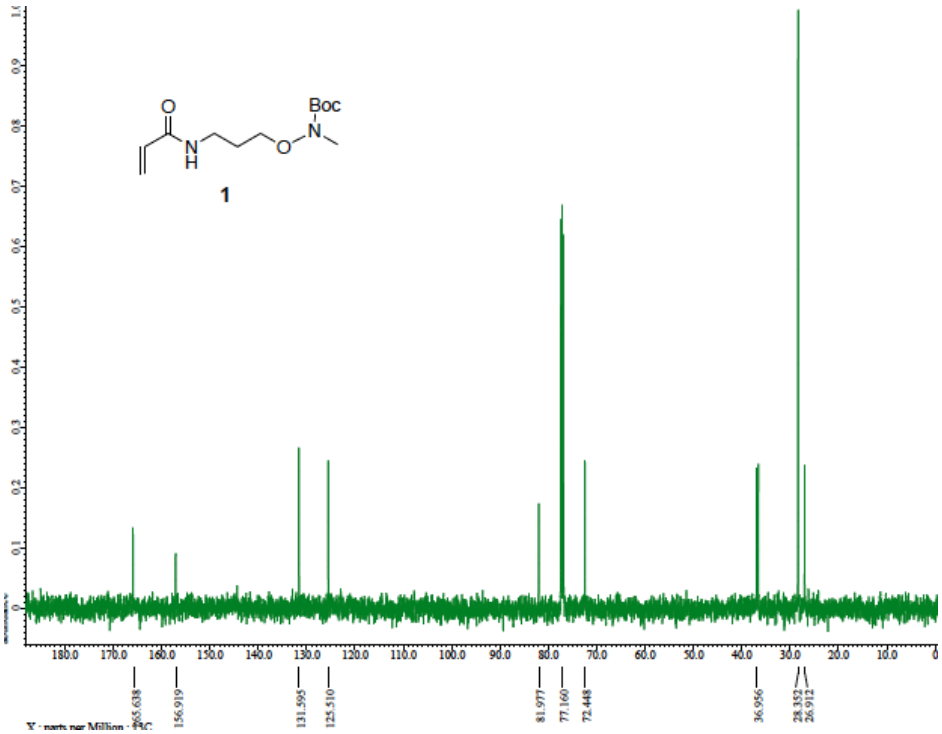

Figure 11. ^{13}C NMR (125 MHz, $CDCl_3$) of monomer **(1)**

*2.4.5 Synthesis and Characterization data for azide chain transfer agent **2***

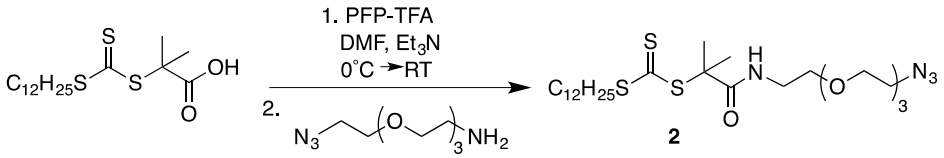

Synthesis of (2). A flame-dried Schlenk flask was charged with S-dodecyl-S'-(α, α-dimethylaceticacid) trithiocarbonate3 (1.38 g, 3.78 mmol, 1.0 eq) and anhydrous DMF (19 mL) was added. Upon cooling to 0 °C, triethylamine (1.32 mL, 9.46 mmol, 2.5 eq) and pentafluorophenyl-trifluoroacetate (PFP-TFA, 718 µL, 4.16 mmol, 1.1 eq) was added. After 1 hour at 0 °C, 11-azido-3,6,9-triundecan-1-amine (826 µL, 4.16 mmol, 1.1 eq) was added. After 2 hours, the reaction was complete by TLC. The reaction mixture was then partitioned between 1 N HCl and Et2O. The organic layer was washed 1 N HCl (1x), H2O (2x), brine (1x), dried with MgSO4, concentrated, and chromatographed (10 to 80% EtOAc/hexanes) to give 1.83 g of 2 (3.24 mmol) as a yellow solid (86%). 1H NMR (500 MHz, CDCl3) δ (ppm): 6.87 (m, 1H), 3.67 (m, 6H), 3.62-3.60 (m, 2H), 3.56-3.54 (m, 2H), 3.51-3.48 (m, 2H), 3.42-3.38 (m, 4H), 3.25 (t, 2H, J = 7 Hz), 1.68 (s, 6H), 1.40-1.25 (m, 19H), 0.87 (m, 3H). 13C NMR (125 MHz, CDCl3): δ (ppm): 220.1, 172.4, 70.7, 70.6, 70.3, 70.1, 69.6, 57.1, 50.6, 39.8, 36.7, 31.9, 29.6, 29.4, 29.3, 29.1, 28.9, 27.7, 25.8, 22.7, 14.1. Calculated C25H48N4O4S3, 564.28, [M+Na]+:587.27. HRMS found: 587.2727. UV–Vis absorbance at 310 nm (CH2Cl2, 23 µM) = 0.321, ε = 13, 956 M-1 cm-1. IR (cm-1): 2927, 2859, 2252, 1662, 1513, 1463, 1381, 1218, 1097, 901, 773, 727, 645.

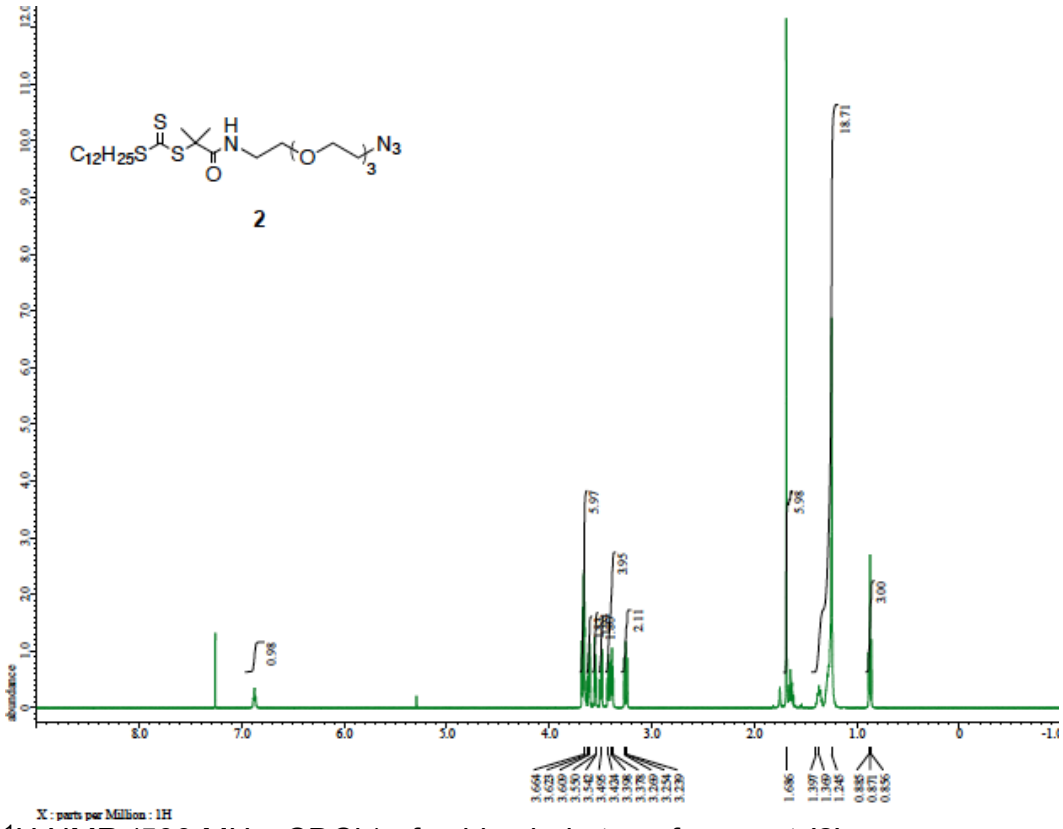

Figure 12. ^{1}H NMR (500 MHz, $CDCl_3$) of azide chain transfer agent **(2).**

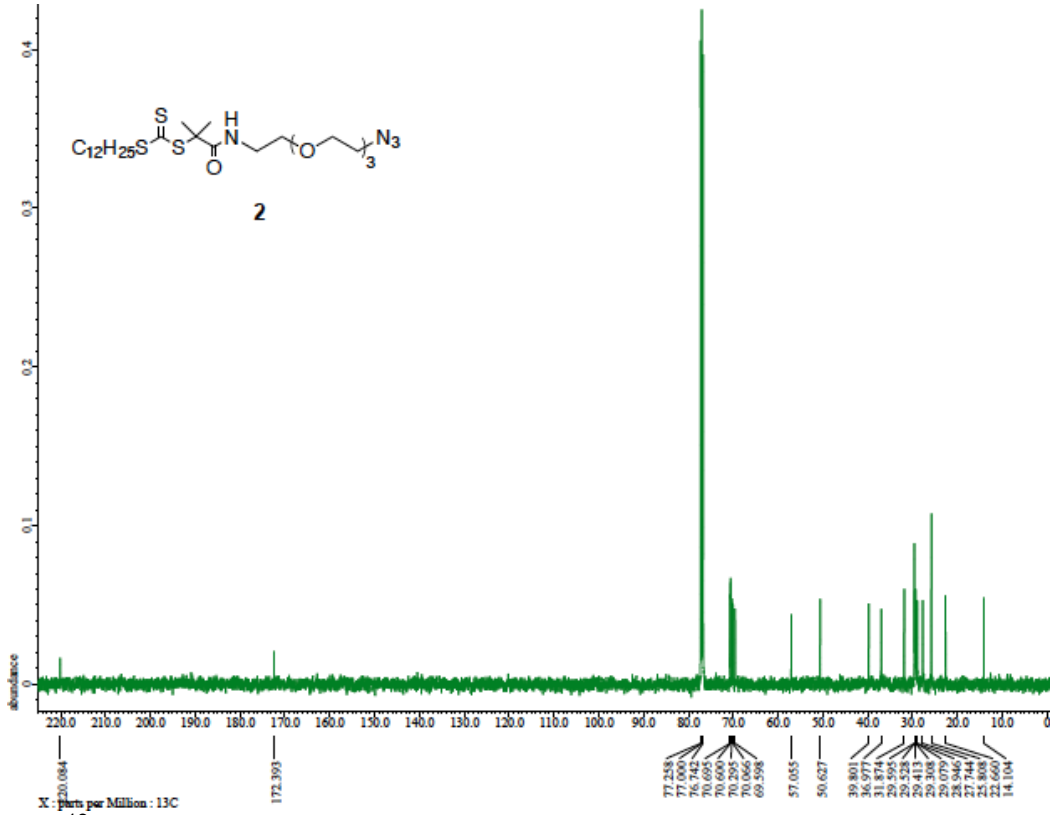

Figure 13. ^{13}C NMR (125 MHz, $CDCl_3$) of azide chain transfer agent **(2).**

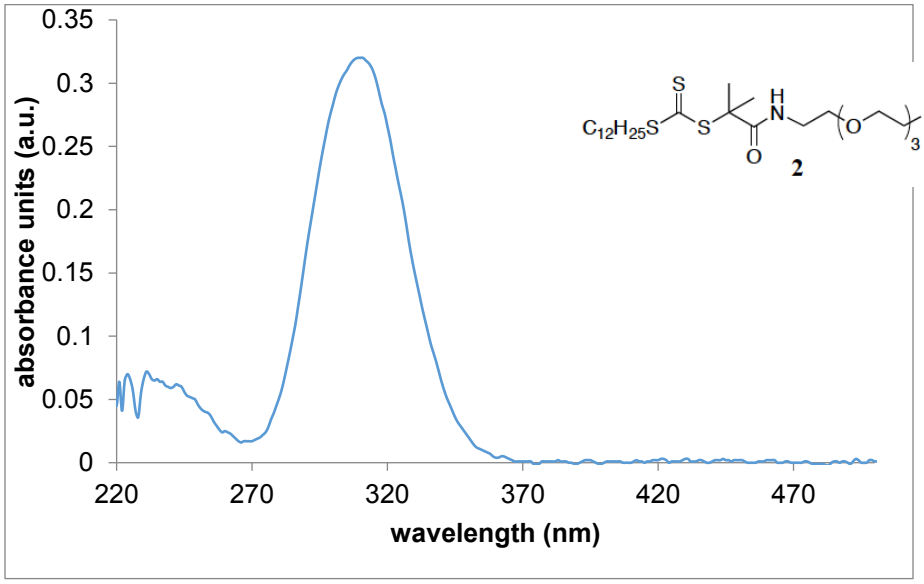

Figure 14. UV-Vis Spectrum of **2** (CH_2Cl_2, 23 μM).

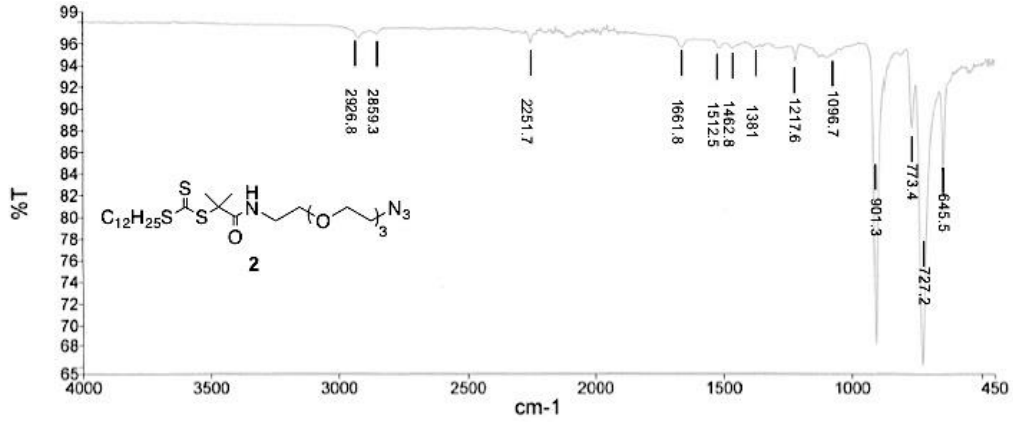

Figure 15. FTIR Spectrum of **2**.

2.4.6 General procedure and characterization data for RAFT polymerization

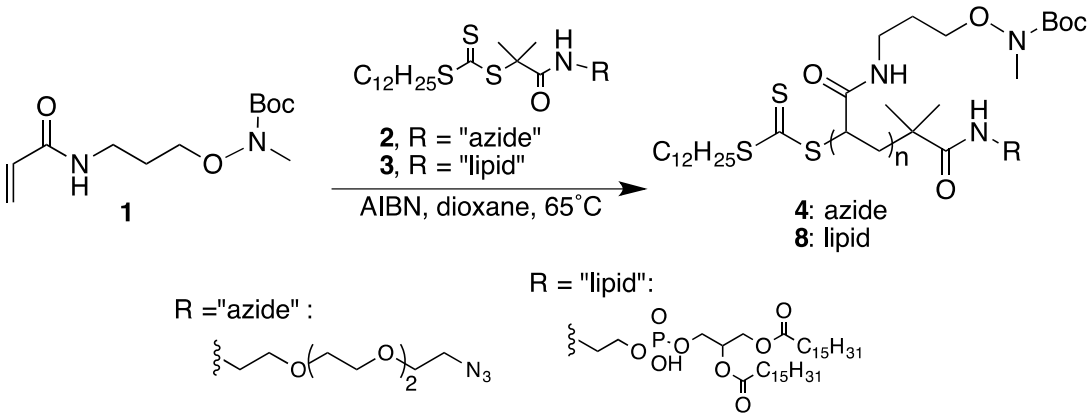

General procedure for the RAFT polymerization[29] of *tert*-butyl (3-acrylamidopropoxy)methyl carbamate monomer (1): A flame-dried Schlenk flask (10 mL) equipped with a magnetic stirring bar was charged with **2** (6.2 mg, 11 μmol, 0.50 mol% with respect to **1**), AIBN (0.2 mg, 1.10 μmol, 0.05 mol% with respect to **1**, delivered as 100 μL of a 0.109 mM solution in anhydrous dioxane, monomer **1** (570.2 mg, 2.2 mmol), and anhydrous dioxane (443.3 mg). The flask was equipped with a rubber septum and filled with N_2. The yellow solution was thoroughly degassed by three freeze-pump-thaw cycles. The flask was then allowed to warm to room temperature and then immersed into an oil bath preheated to 65 °C. After 12 hours, the viscous reaction mixture was then diluted in ether and precipitated into excess hexanes with vigorous stirring. The solid residue was then re-dissolved into ether, and precipitated again in hexanes. This was repeated once more. The faintly yellow polymer was then concentrated from $CHCl_3$ three times to remove residual hexanes and dried under vacuum overnight to yield **4** as a pale yellow solid (524 mg, 90.5%). GPC (DMF, 0.2% LiBr): M_w = 47.3 kDa, M_n = 40.1 kDa, PDI = 1.18, DP ≈ 200. ^{1}H NMR ($CDCl_3$, 500 MHz) δ (ppm): 3.90-3.65 (bs, 2H), 3.35-2.80 (bm, 5H), 1.80-1.05 (bm, 16H). UV–Vis absorbance at 310 nm of **4** (CH_2Cl_2, 23 μM) = 0.303.

IR (cm^{-1}): 4197, 3676, 3054, 2987, 2306, 1696, 1654, 1560, 1420, 1369, 1266, 1155, 896, 738, 705.

Lipid-terminated polymer **8** was synthesized using the same molar ratio of AIBN chain transfer agent **3**,[30] however a 300:1 ratio of monomer to chain transfer agent was used to achieve the desired degree of polymerization. Using this procedure, polymer **8** was synthesized (455 mg, 86.0% yield). GPC (DMF, 0.2% LiBr): M_w = 78.5 kDa, M_n = 63.9 kDa, PDI =1.23, DP ≈ 300. ^{1}H NMR ($CDCl_3$, 500 MHz) δ (ppm): 3.90-3.65 (bs. 2H), 3.35-2.80 (bm, 5H), 1.80-1.05 (bm, 17H). UV–Vis absorbance at 310 nm (CH_2Cl_2, 23 μM) = 0.125.

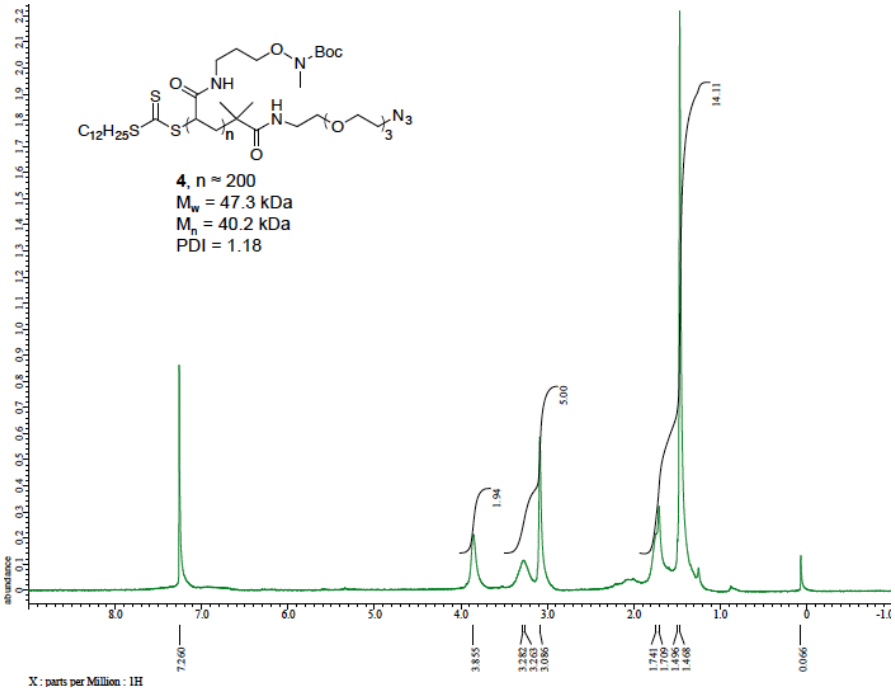

Figure 16. ^{1}H NMR (500 MHz, $CDCl_3$) of **4.**

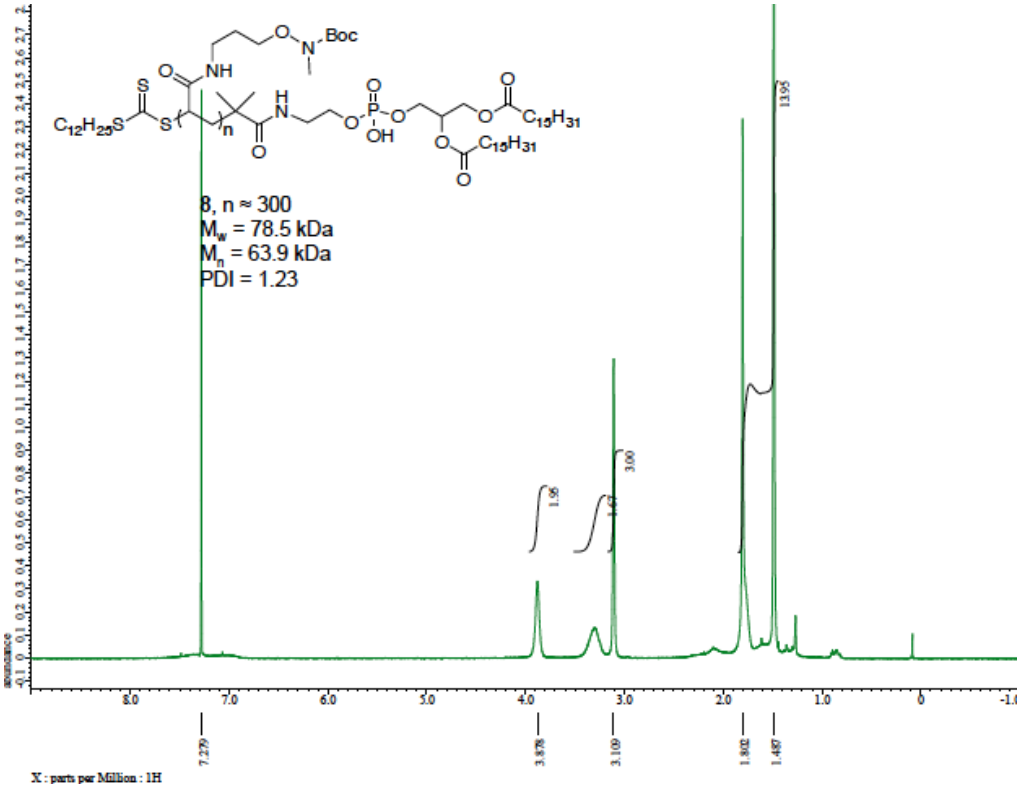

Figure 17. ^{1}H NMR (500 MHz, $CDCl_3$) of **8**.

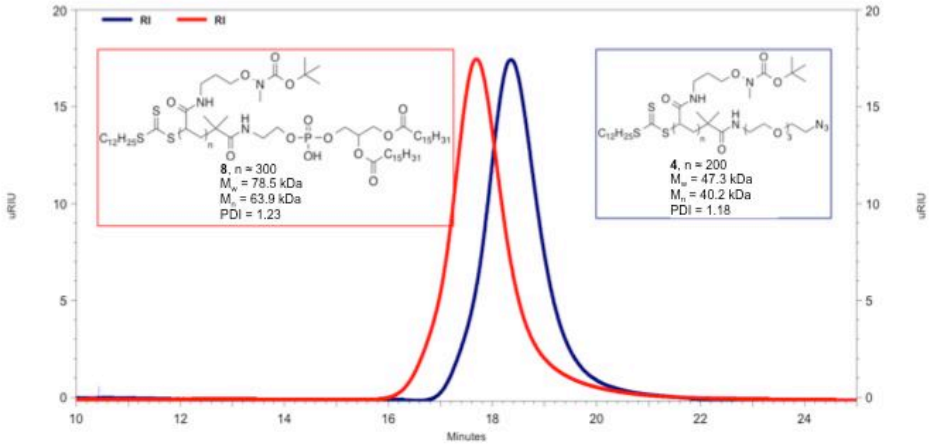

Figure 18. GPC spectrum for **4** and **8** (DMF, 0.2 % LiBr).

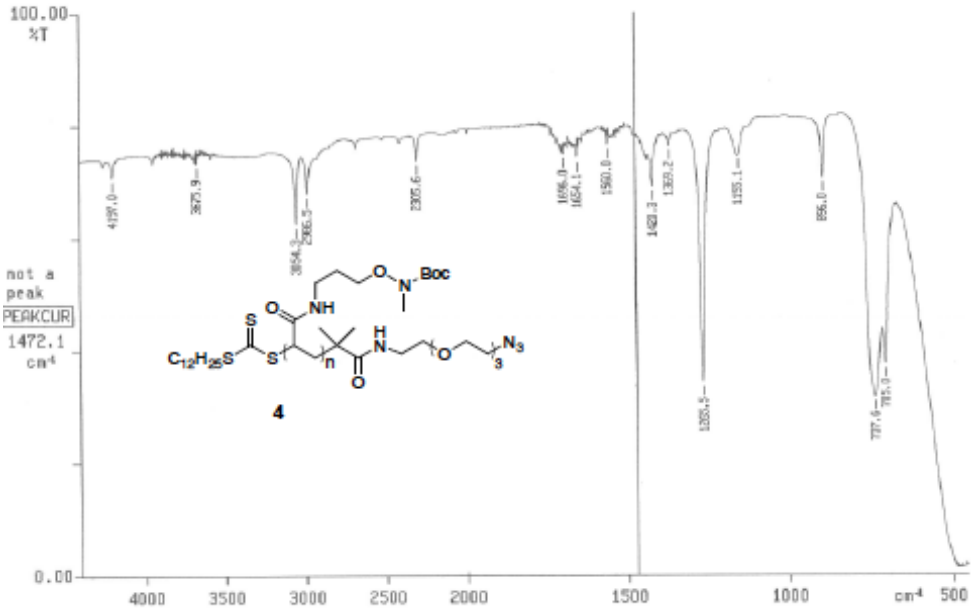

Figure 19. FTIR spectrum of **4**.

2.4.7 General procedure and characterization data for end-deprotected polymers

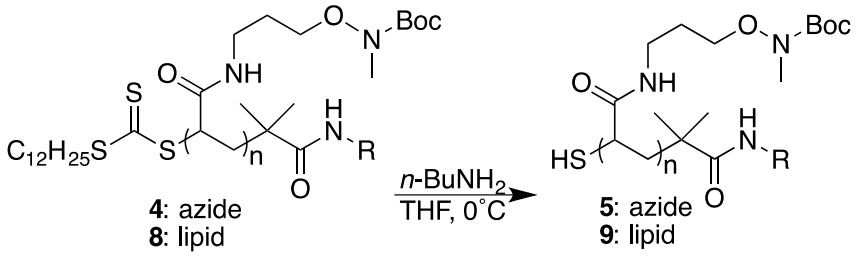

General procedure for the synthesis of end-deprotected polymers. A Schlenk flask (10 mL) equipped with a magnetic stir bar was charged with **4** (171.1 mg, 3.44 μM) and 1.71 mL of a degassed 20 mM *n*-butylamine solution in THF. The Schlenk flask was submerged in an ice bath and allowed to react for 2 hours. The reaction mixture was then diluted in ether and precipitated into excess hexanes with vigorous stirring. The precipitation was performed three times. The polymer was concentrated from $CHCl_3$ three times to remove residual hexanes and dried under vacuum overnight to give polymer **5** (98% yield) as a white solid. ^{1}H NMR ($CDCl_3$, 500 MHz) δ (ppm): 3.85 (bs, 2H), 3.27-3.08 (bm, 5H), 2.13-1.46 (bm, 15H). UV-Vis absorbance at 310 nm (CH_2Cl_2, 23 μM) = 0.111. GPC (DMF, 0.2% LiBr): M_w = 49.2 kDa, M_n = 39.3 kDa, PDI = 1.25, DP ≈ 200.

Polymer **9** was prepared from **8** as described above for **5** to yield 92% of a white solid. ^{1}H NMR ($CDCl_3$, 500 MHz) δ (ppm): 3.79 (bs, 2H), 3.21-3.02 (bm, 5H), 1.66-1.18 (bm, 15H). UV-VIS absorbance at 310 nm (CH_2Cl_2 , 23 μM): 0.054. GPC (DMF, 0.2% LiBr): M_w = 47.3 kDa, M_n = 40.2 kDa, PDI = 1.18, DP ≈ 300).

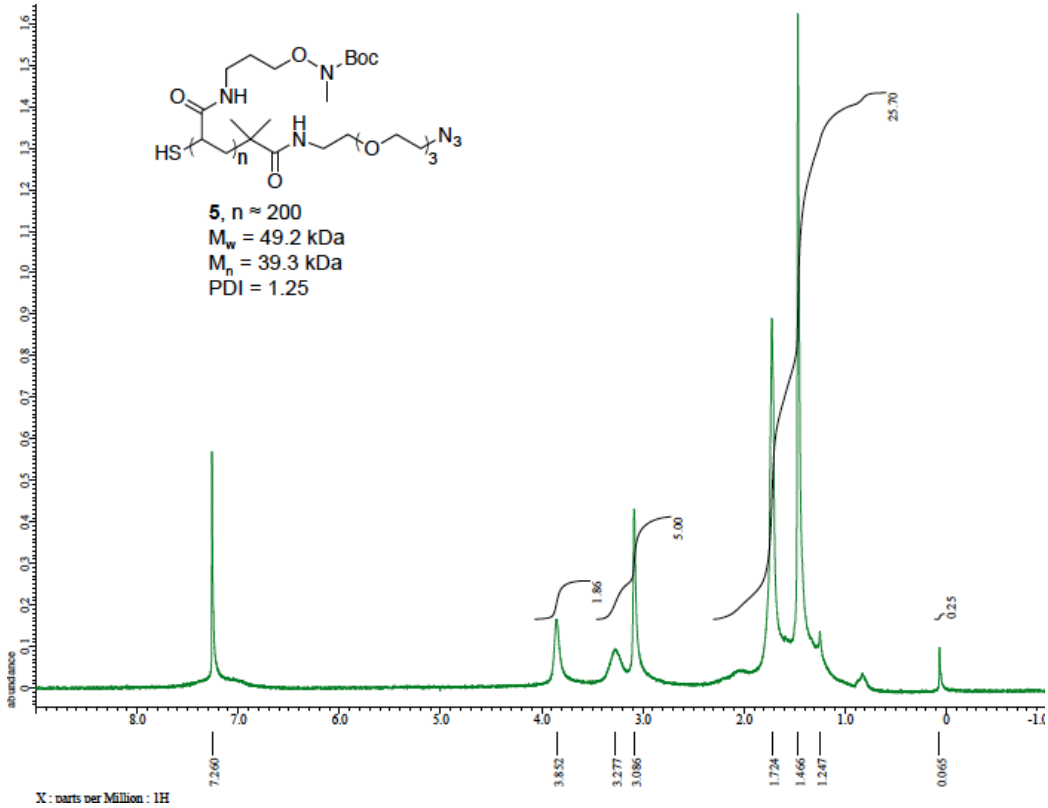

Figure 20. ^{1}H NMR (500 MHz, $CDCl_3$) of **5.**

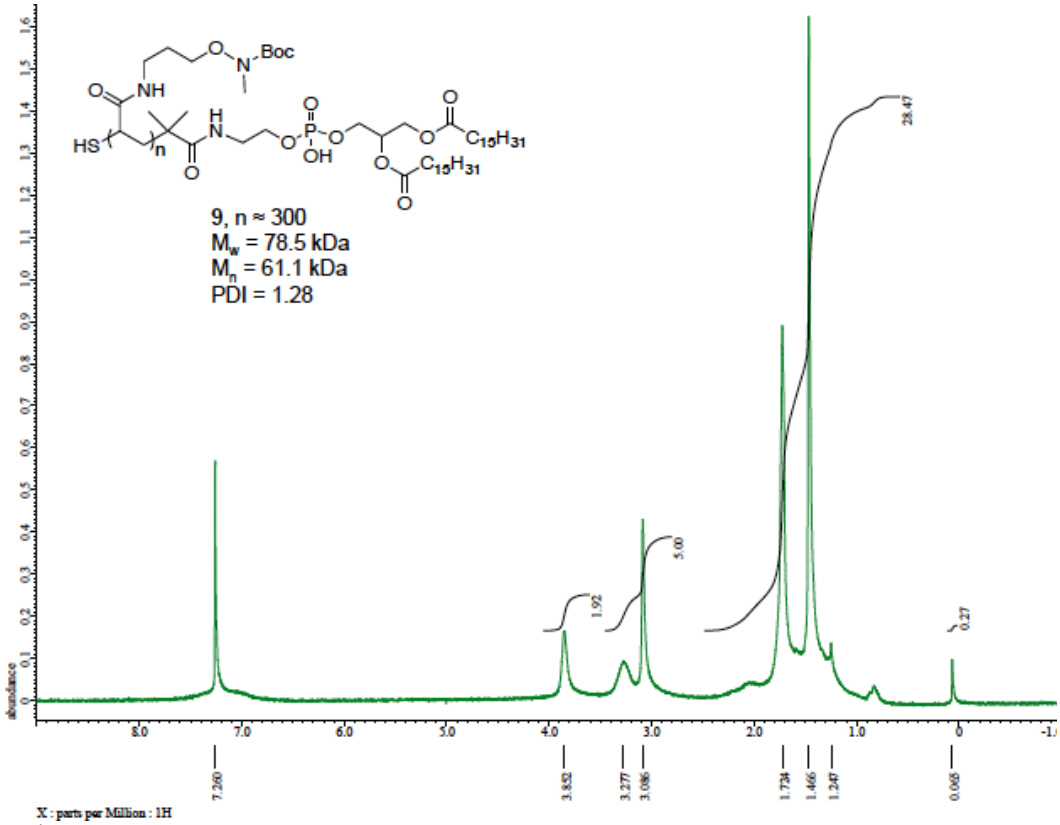

Figure 21. ^{1}H NMR (500 MHz, $CDCl_3$) of **9.**

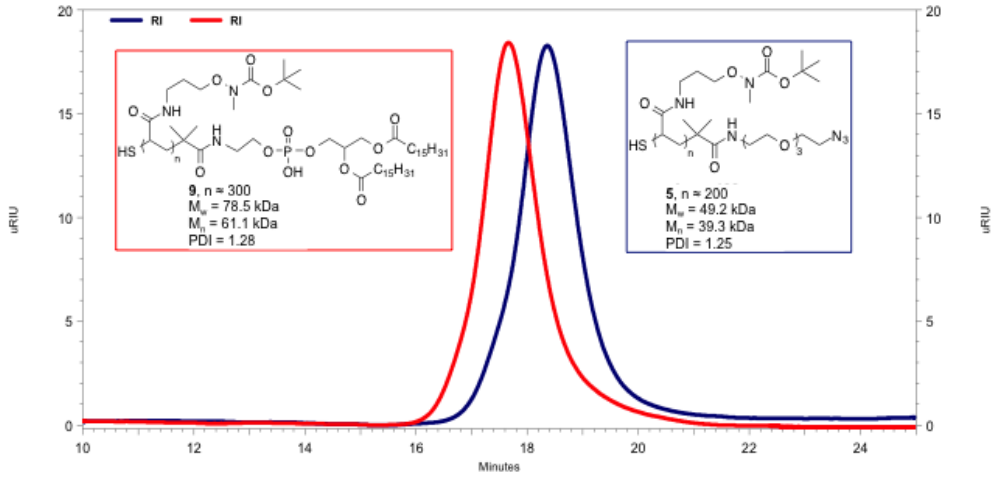

Figure 22. GPC spectrum (DMF, 0.2% LiBr) of **5** and **9.**

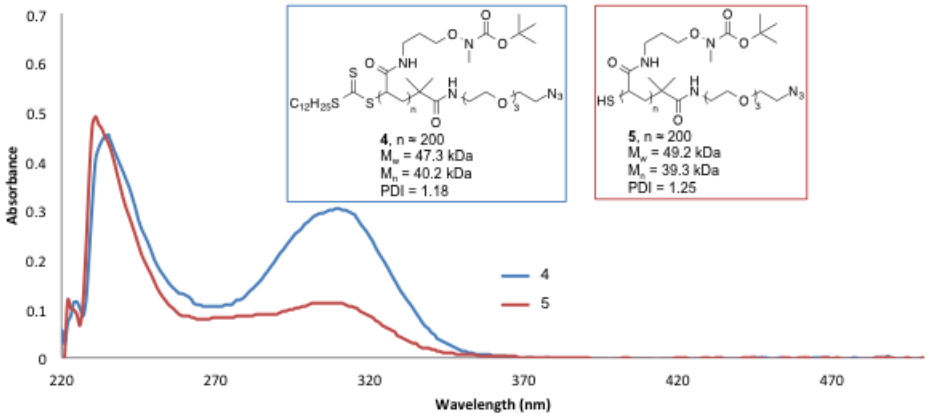

Figure 23. UV-VIS spectrum of **4** and **5**.

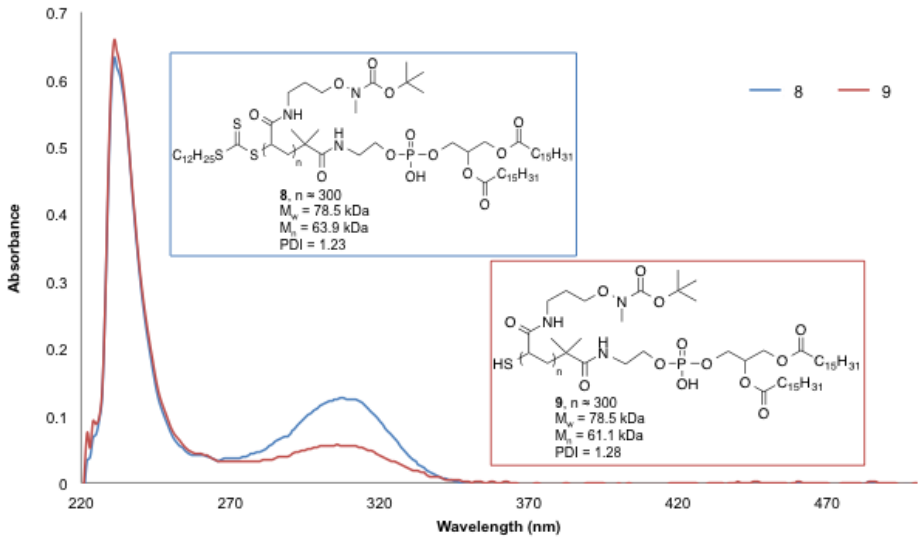

Figure 24. UV-Vis spectrum of **8** and **9.**

2.4.8 General procedure and characterization data for fluorophore labeling and side chain deprotection

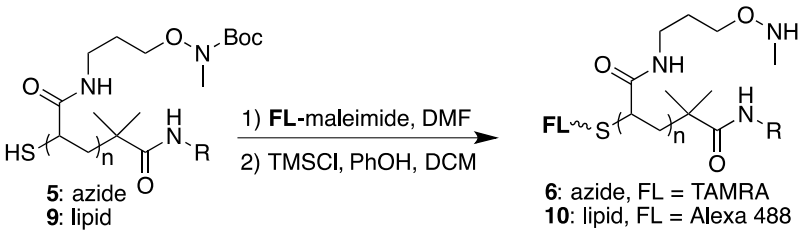

General procedure for the synthesis of fluorophore-labeled polymers and subsequent side chain deprotection. A vial (4 mL) equipped with a magnetic stirring bar, was charged with polymer **5** (6.35 mg) and dissolved in 81.2 µL of a 2 mM TAMRA C_5-maleimide (1.3 eq) solution in DMF. Following degassing by three freeze-pump-thaw cycles, the reaction mixture was stirred overnight in dark. The reaction mixture was then diluted with ether and precipitated in excess hexanes. The solution was centrifuged (1000 xg, 3 min) and solvent was replaced with fresh hexanes and resubmitted to centrifugation.

The precipitation procedure was repeated once more. The polymer was then concentrated from $CHCl_3$ three times to remove residual hexanes and dried under vacuum. Side-chain deprotection was conducted using previously published procedures.[31] To the labeled polymer intermediate, was added 500 µL of a freshly prepared solution of TMS-Cl (1M) and phenol (3M) in anhydrous DCM. The resulting solution was stirred for 2 hours. The polymer is then precipitated by ether and isolated by centrifugation (1000 xg, 3 min), washed 3x with ether using a PD-10 column and lyophilized to afford polymer **6**. ^{1}H NMR (D_2O, 300 MHz) δ (ppm)**:** 3.94 (bs, 2H) 3.13 (bs, 2H), 2.82 (bs, 3H), 1.75 (6H, bm). UV-Vis spectrophotometry was used to determine labeling efficiencies: **6**, (TAMRA, λ_{max}: 512) = 50%;

Polymer **9** was converted into AF488-labeled **10** as described above for polymer **6**. ^{1}H NMR (D_2O, 300 MHz) δ (ppm)**:** 3.94 (bs, 2H) 3.13 (bs, 2H), 2.82 (bs, 3H), 1.75 (6H, bm).

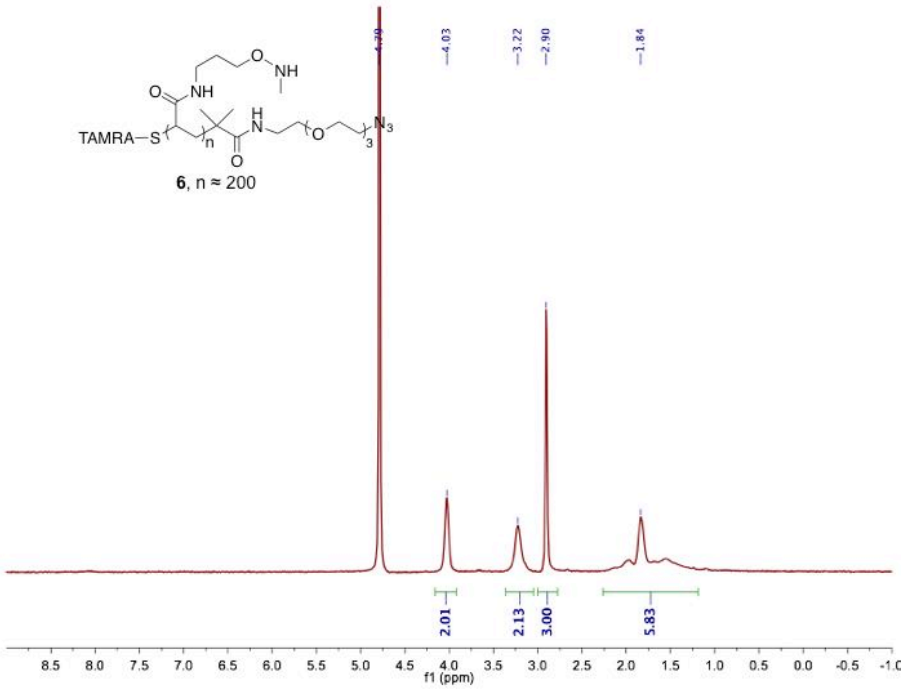

Figure 25. ^{1}H NMR (300 MHz, D_2O) of **6**.

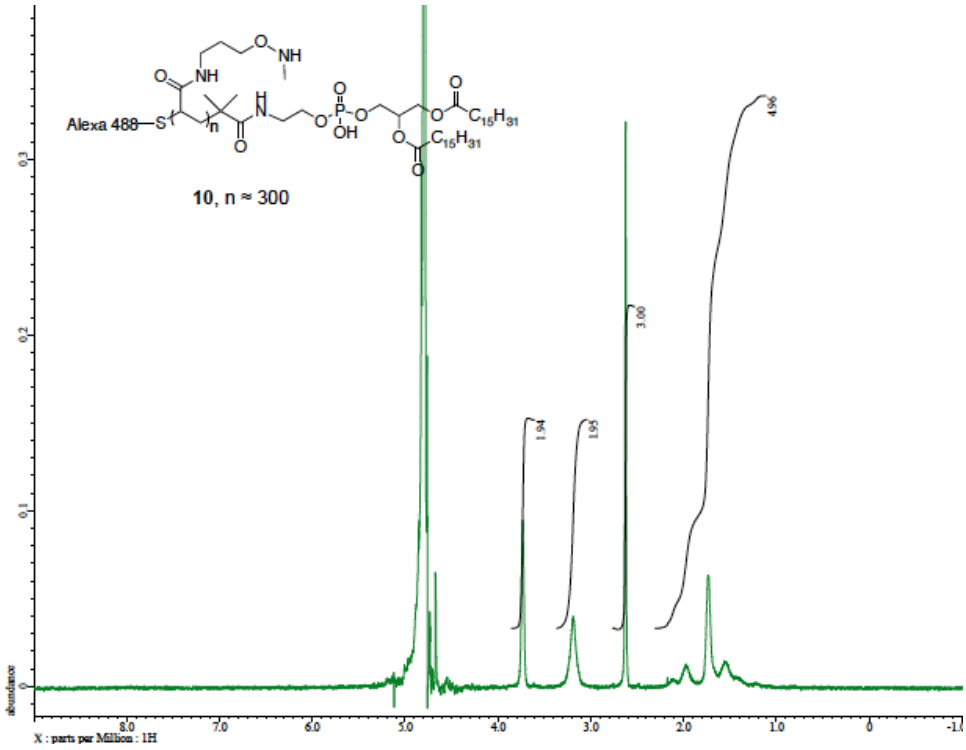

Figure 26. ^{1}H NMR (500 MHz, D_2O) of **10**.

2.4.9 General procedure for the ligation of glycans to polymer backbones

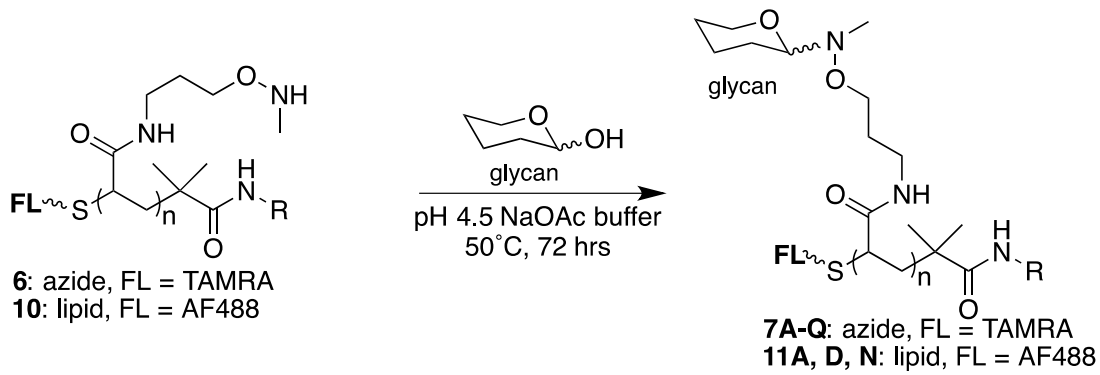

6: azide, FL = TAMRA
10: lipid, FL = AF488

7A-Q: azide, FL = TAMRA
11A, D, N: lipid, FL = AF488

General procedure for glycopolymer (7 or 11) synthesis. A PCR tube containing polymer **6**, along with 1.1 eq of glycan was dissolved in sodium acetate buffer (1 M NaOAc, 1 M urea, pH 4.5) to form a 200 mM (by side chain) solution. Following reaction in a thermocycler at 50˚C for 72 hours, the mixture was submitted to an Amicon Ultra Centrifugal Filter (pre-washed with Milli-Q water twice by spin dialysis, 10K MWCO, Millipore), and spin dialyzed (6000 xg, 10 min.) four times using a deuterated phosphate buffered saline solution (100 mM phosphate, 150 mM NaCl, pD 7.4), discarding the flow through and filling to 500 µL each time. Then, the spin column was inverted into a clean centrifuge tube and a solution of **6** was collected via centrifugation (300 xg, 4 min) and analyzed by ^{1}H NMR.

Notes on glycopolymer ^{1}H NMR analysis:

During library synthesis, a glycerine contaminant arising from spin filtration (using Amicon 10K MWCO filters) was detected via ^{1}H NMR (below, glycerine in D_2O).[32] This purification step has now been improved by pre-rinsing the filters overnight with Milli-Q water prior to use. Filters can also be washed with 0.1 M NaOH as indicated in instructions to remove this peak. Residual acetate from the ligation buffer (*s*, δ 1.88 ppm) was also detected.

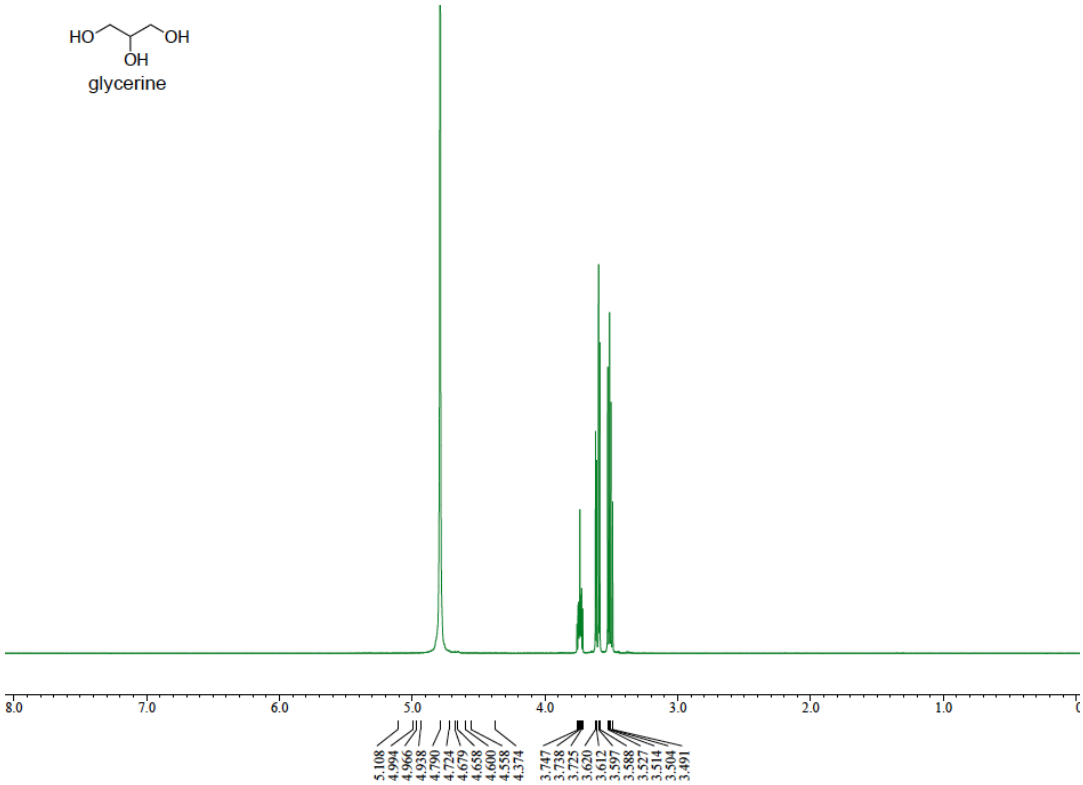

Figure 27. ^{1}H NMR spectrum of glycerine (500 MHz, D_2O).

Analysis of glycan ligation efficiencies via ^{1}H NMR:

For diGAGs containing α,β-unsaturated uronic acids (e.g. **11A**, middle spectrum), ligation efficiency (LE) was determined by integrating the glycan olefin signal (H_q, δ5.8 ppm) relative to the polymer backbone methyl protons (H_a, δ2.4-2.8 ppm). For monosaccharides such as GlcNAc-6S (e.g. **11N**, bottom spectrum) which lack a unique isolated signal in the 5.8 ppm range, LE was determined by subtracting polymer backbone protons (see top spectrum) from the total integration in the region δ2.5-4.5 ppm, and dividing the difference by the number of glycan protons.

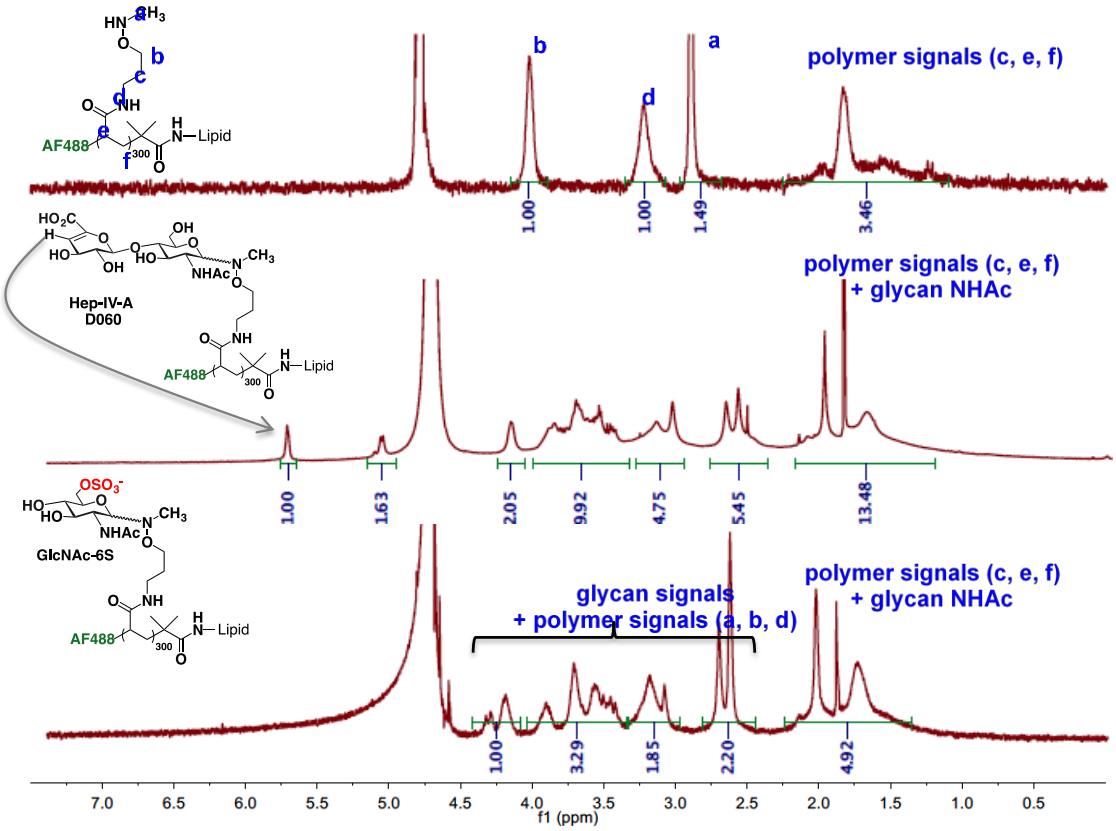

Figure 28. Stacked NMR spectra of the neoPG polymer backbone (top), a neoPG composed of a diGAG (**11A**, middle), and a monosaccharide (**11N**, bottom).

Table 1. Glycopolymer ligation efficiencies (LE) and valencies.

polymer	glycan	LE, %	valency
7A	**D0A0** Hep-IV-A	33	63
7B	**D0A6** Hep-II-A	47	89
7C	**D2A0** Hep-III-A	38	72
7D	**D2A6** Hep-I-A	56	106
7E	**D0H0** Hep-IV-H	38	72
7F	**D0H6** Hep-II-H	50	95
7G	**D2H0** Hep-III-H	34	65
7H	**D2H6** Hep-I-H	15	29
7I	**D0S0** Hep-IV-S	14	27
7J	**D0S6** Hep-II-S	17	32
7K	**D2S0** Hep-III-S	18	34
7L	**D2S6** Hep-I-S	14	27
7M	GlcNAc	56	106
7N	GlcNAc-6S	68	129
7O	GlcN	44	84
7P	GlcN-2S	21	40
7Q	GlcN-6S	17	32
11A	**D0A0** Hep-IV-A	62	190
11D	**D2A6** Hep-I-A	50	150
11N	GlcNAc-6S	50	150

Figure 29. ^{1}H NMR spectrum glycopolymer library described in table 1 **7A-7Q,** and **11A,11D and 11N (**500 MHz, deuterated phosphate buffer pD 7.4).

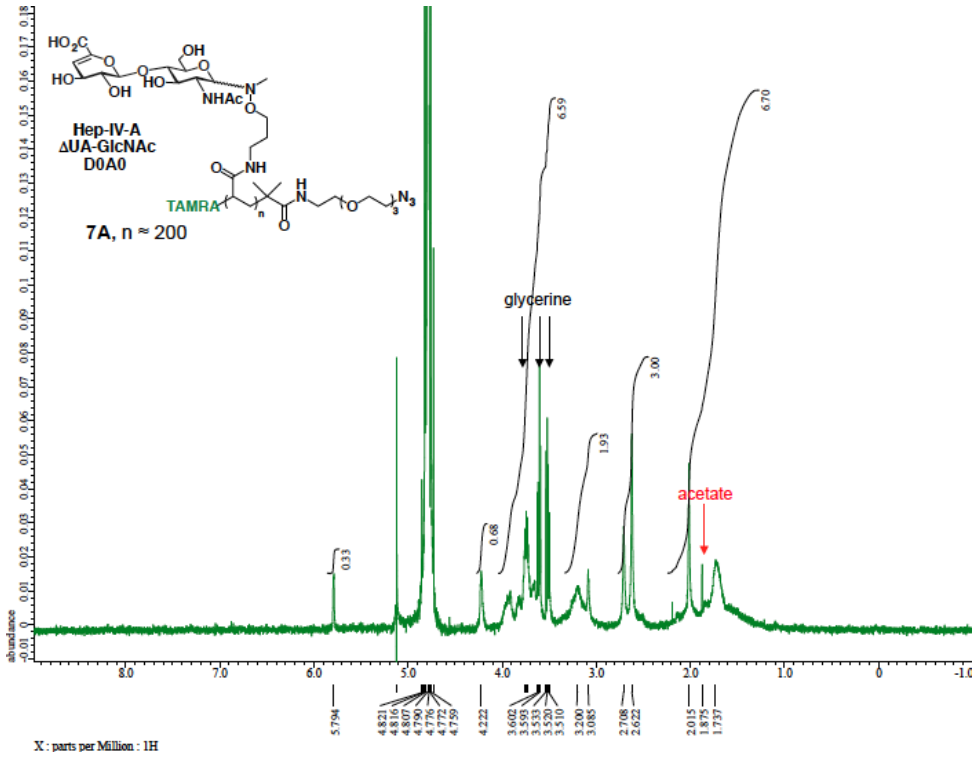
Hep-IV-A
ΔUA-GlcNAc
D0A0
TAMRA
7A, n ≈ 200
glycerine
acetate
6.59
6.70
3.00
1.93
0.68
0.33
X : parts per Million : 1H

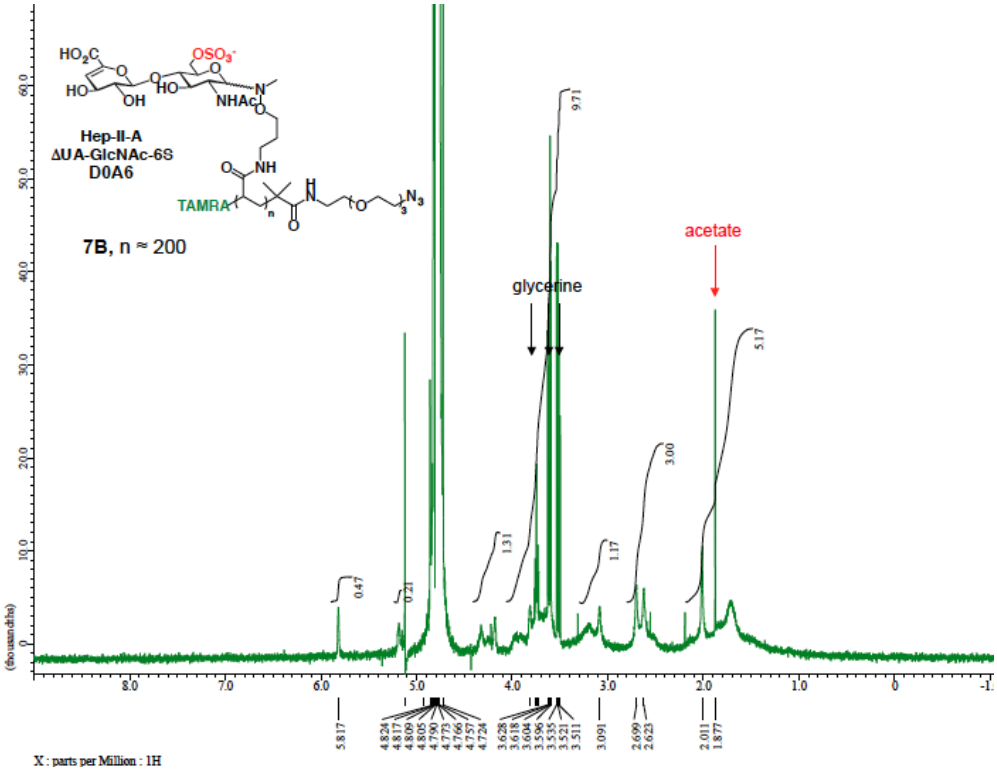
Hep-II-A
ΔUA-GlcNAc-6S
D0A6
TAMRA
7B, n ≈ 200
glycerine
acetate
9.71
5.17
3.00
1.31
1.17
0.47
0.21
X : parts per Million : 1H

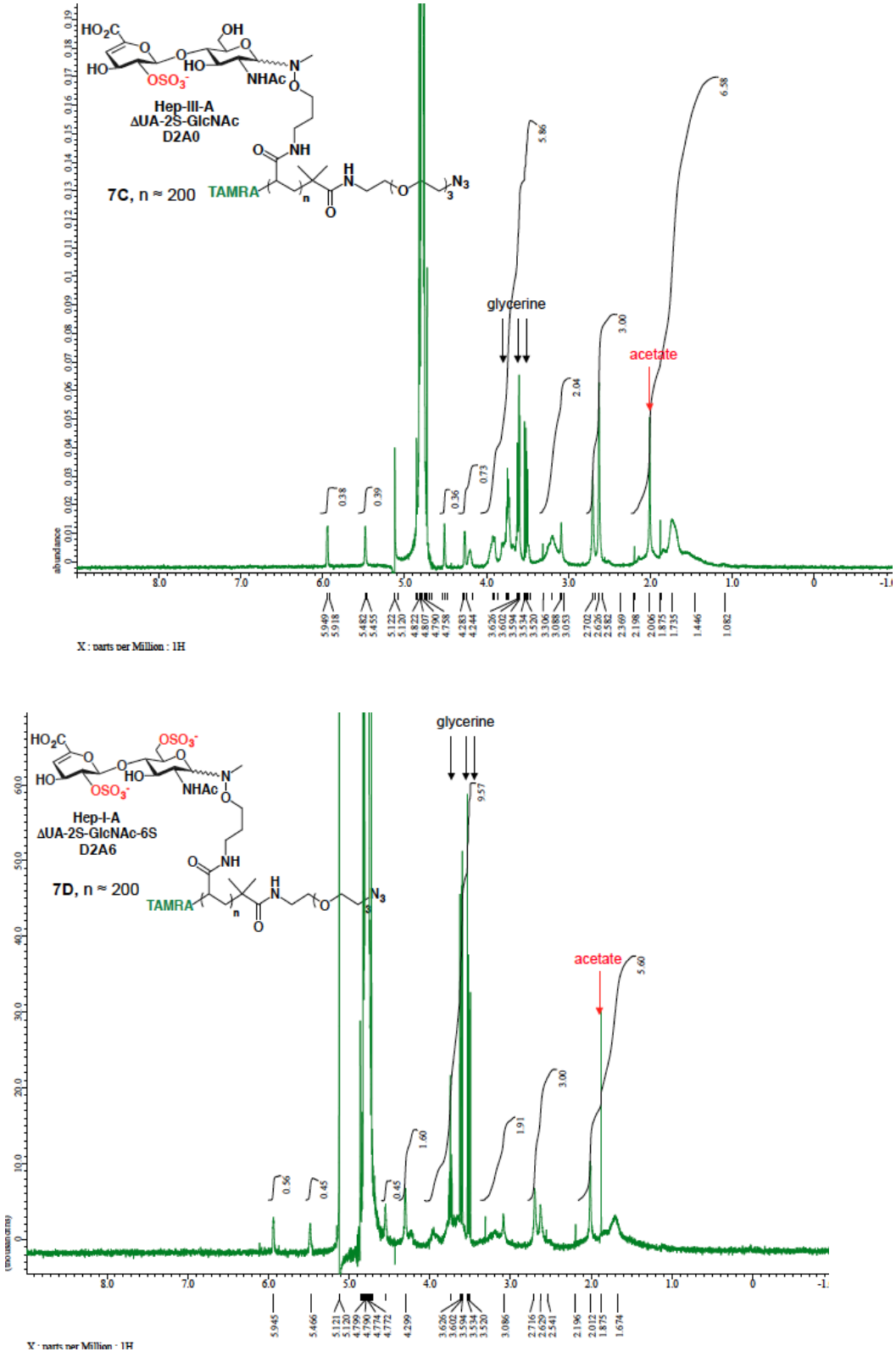

Figure 29. ^{1}H NMR spectrum continued

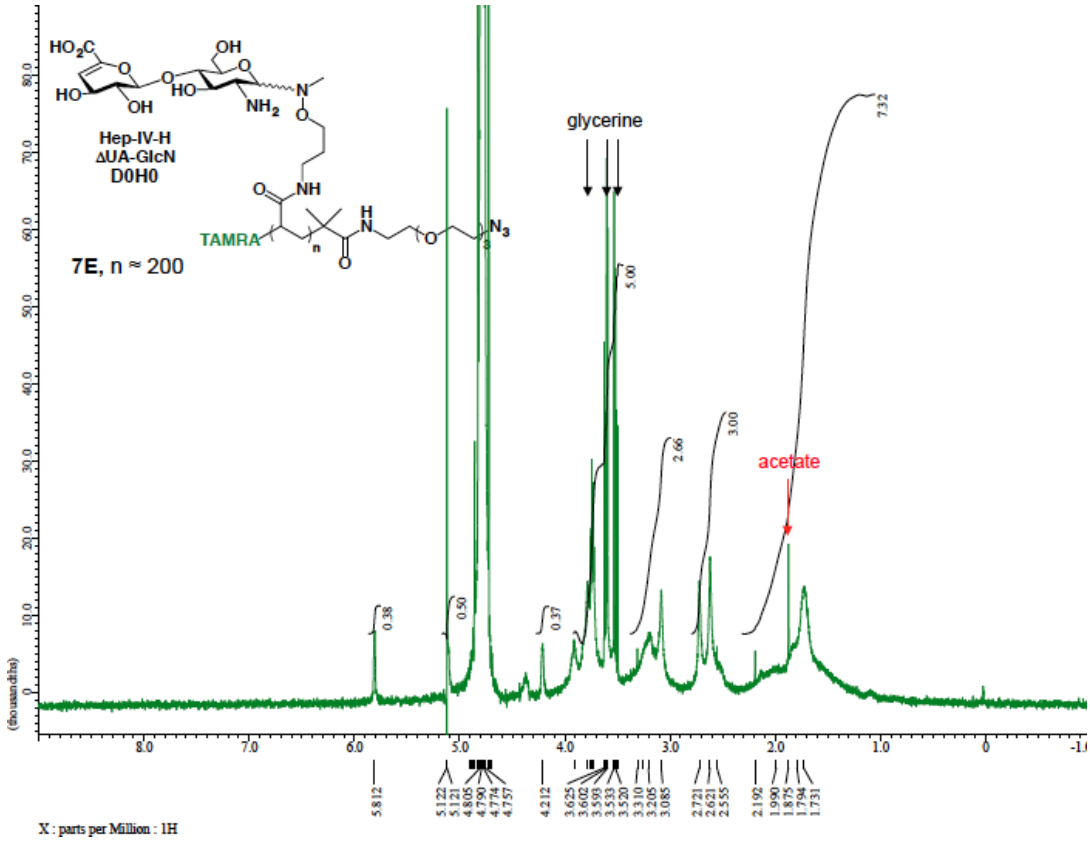

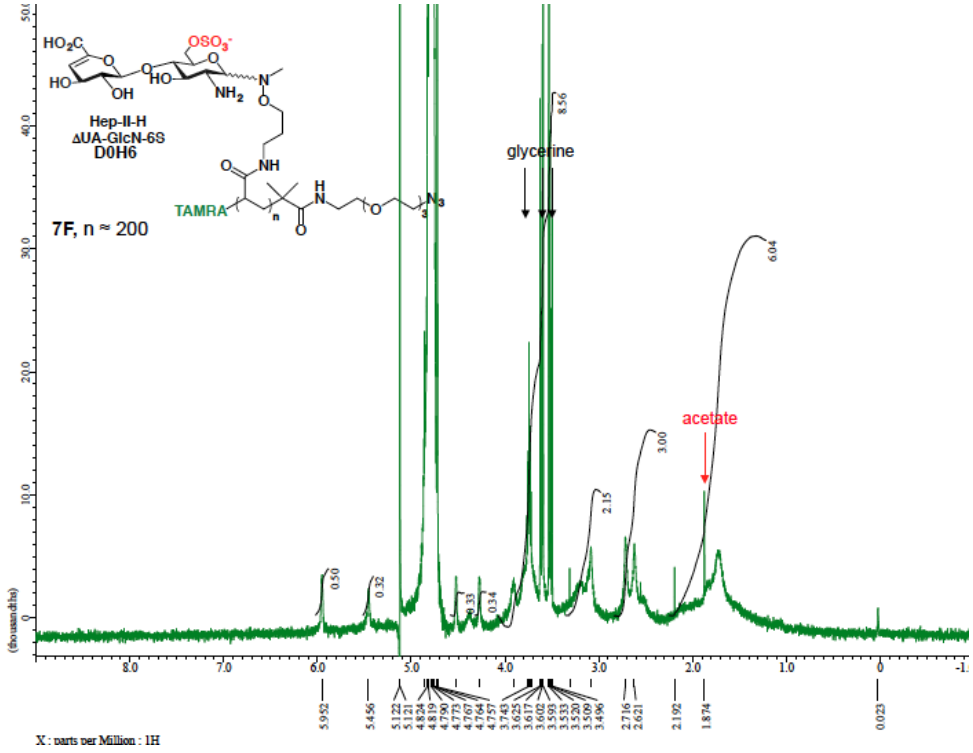

Figure 29. ^{1}H NMR spectrum continued

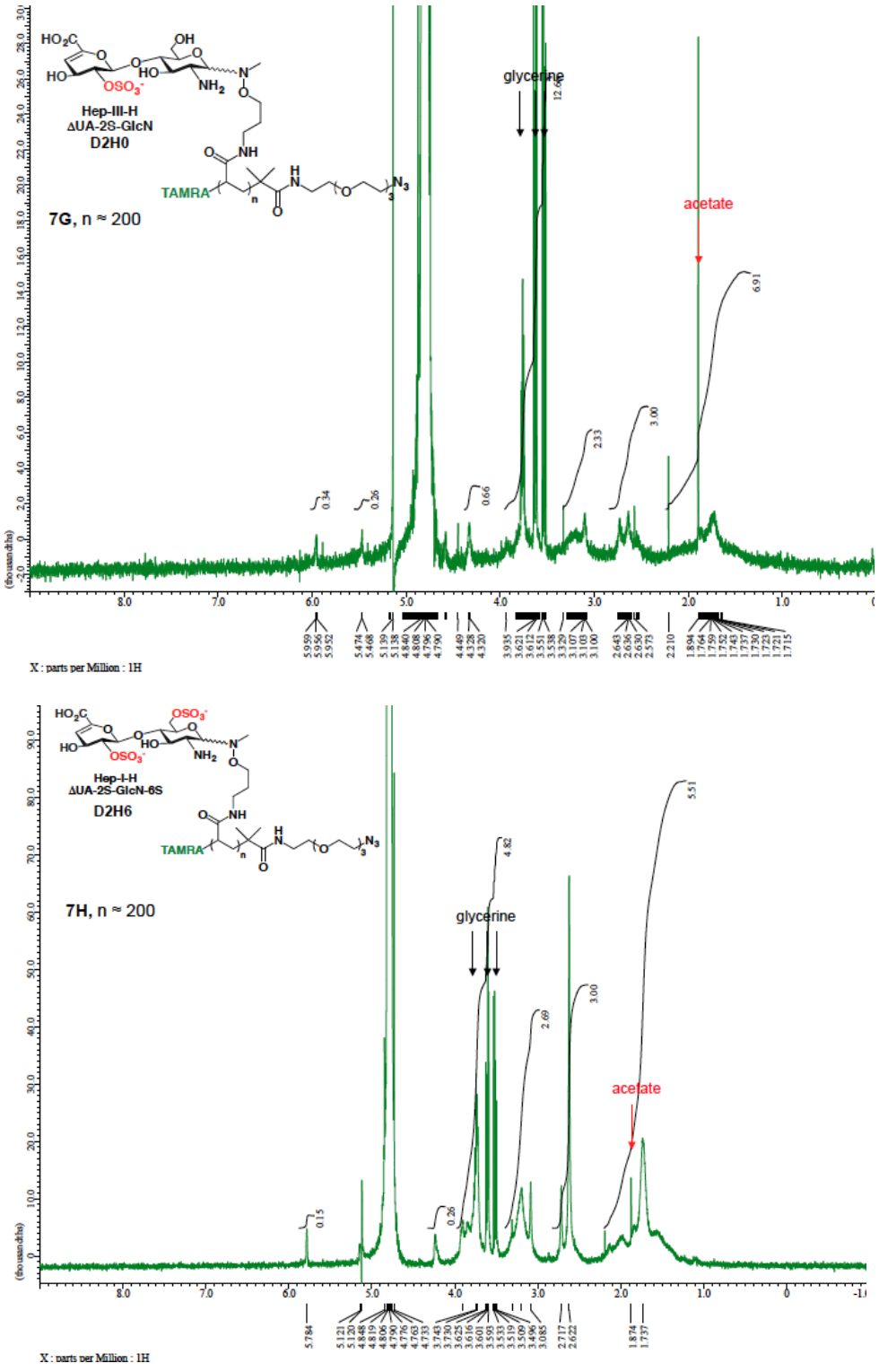

Figure 29. ^{1}H NMR spectrum continued

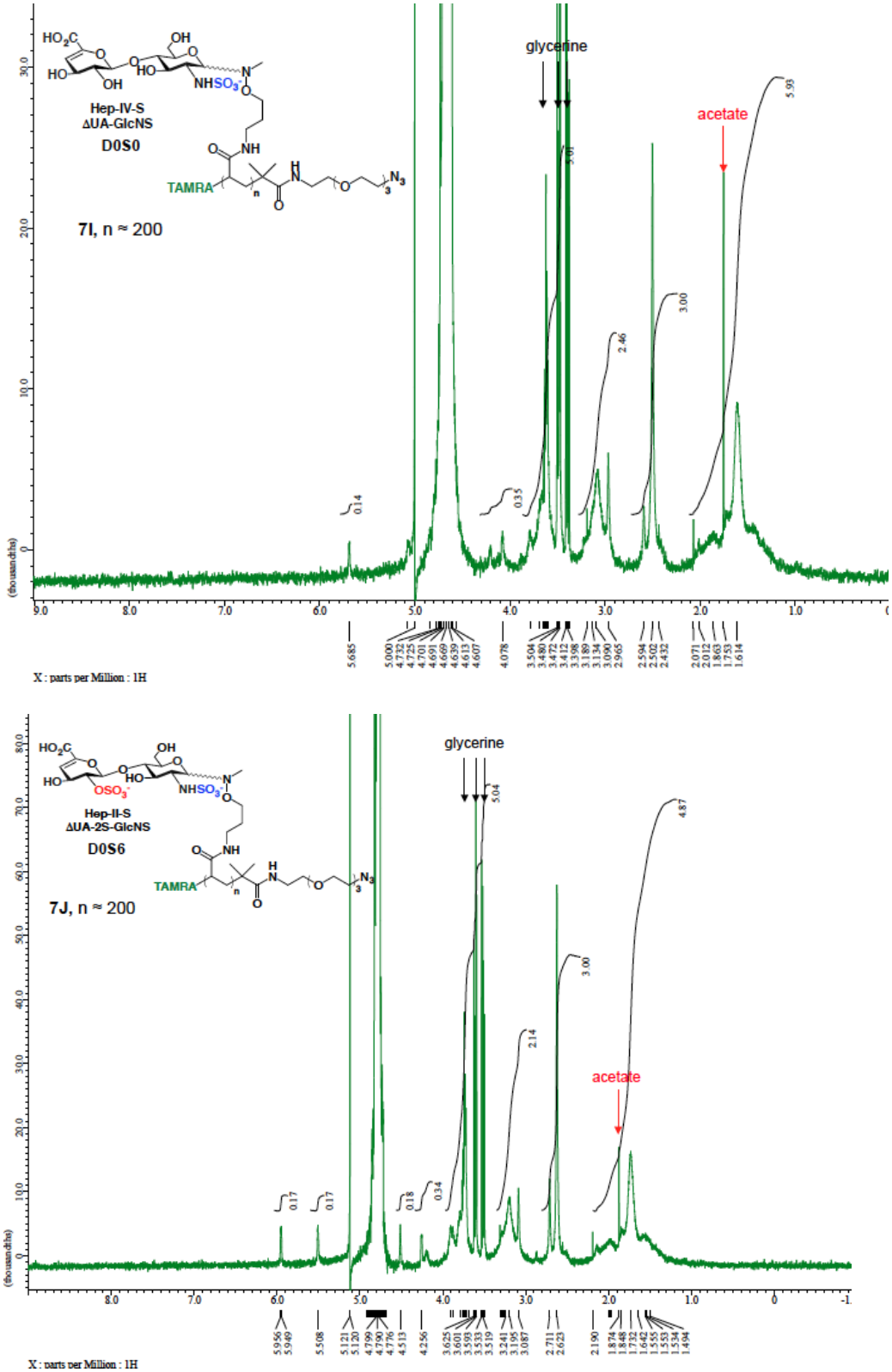

Figure 29. ^{1}H NMR spectrum continued

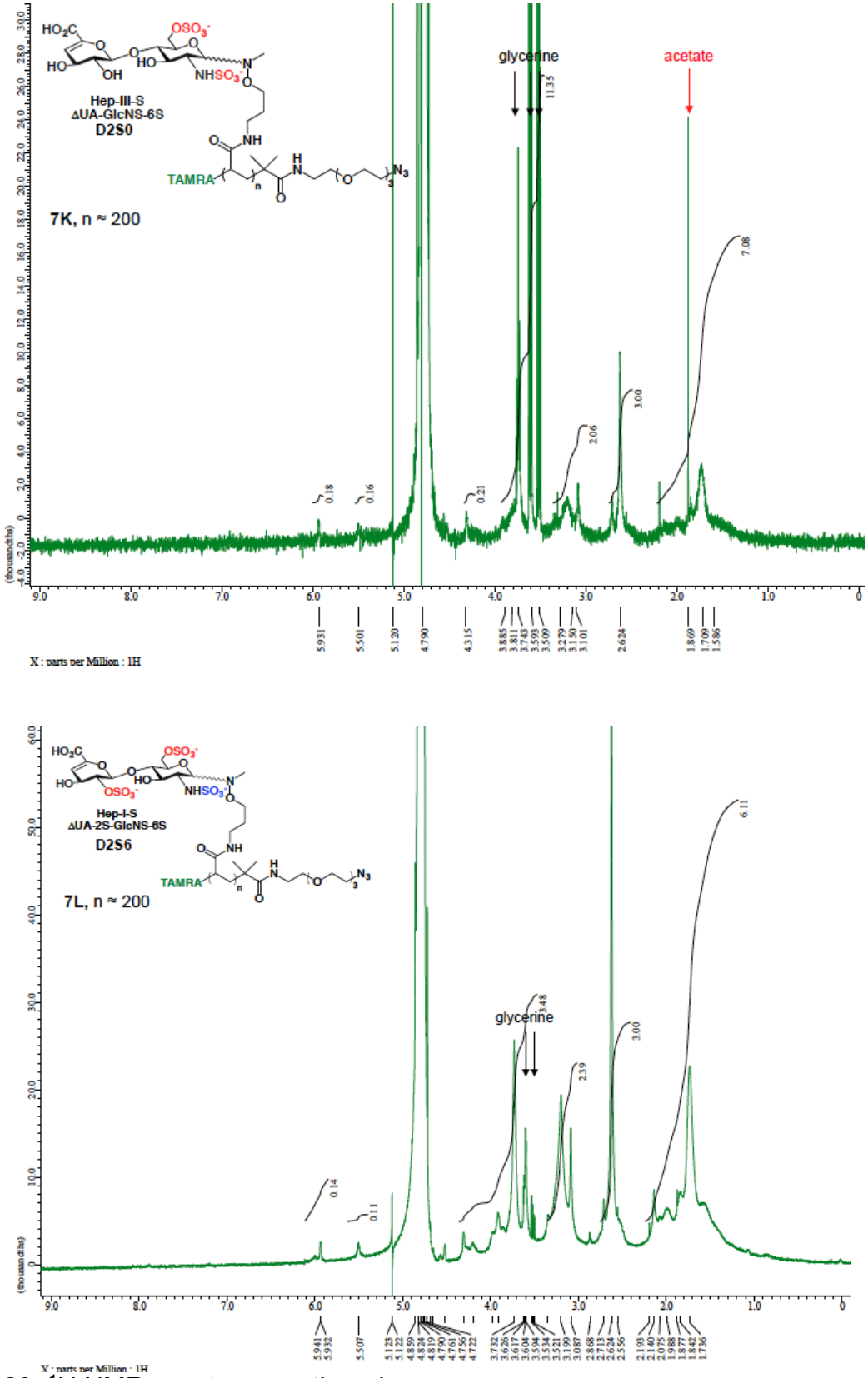

Figure 29. ^{1}H NMR spectrum continued

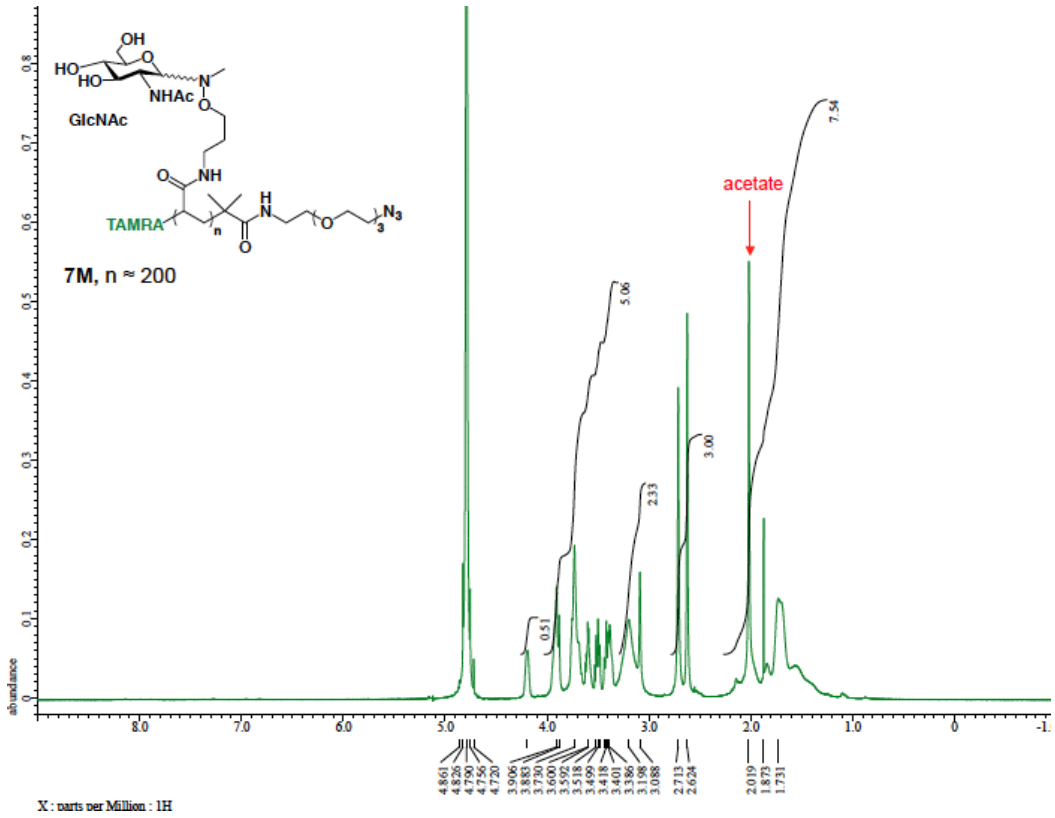

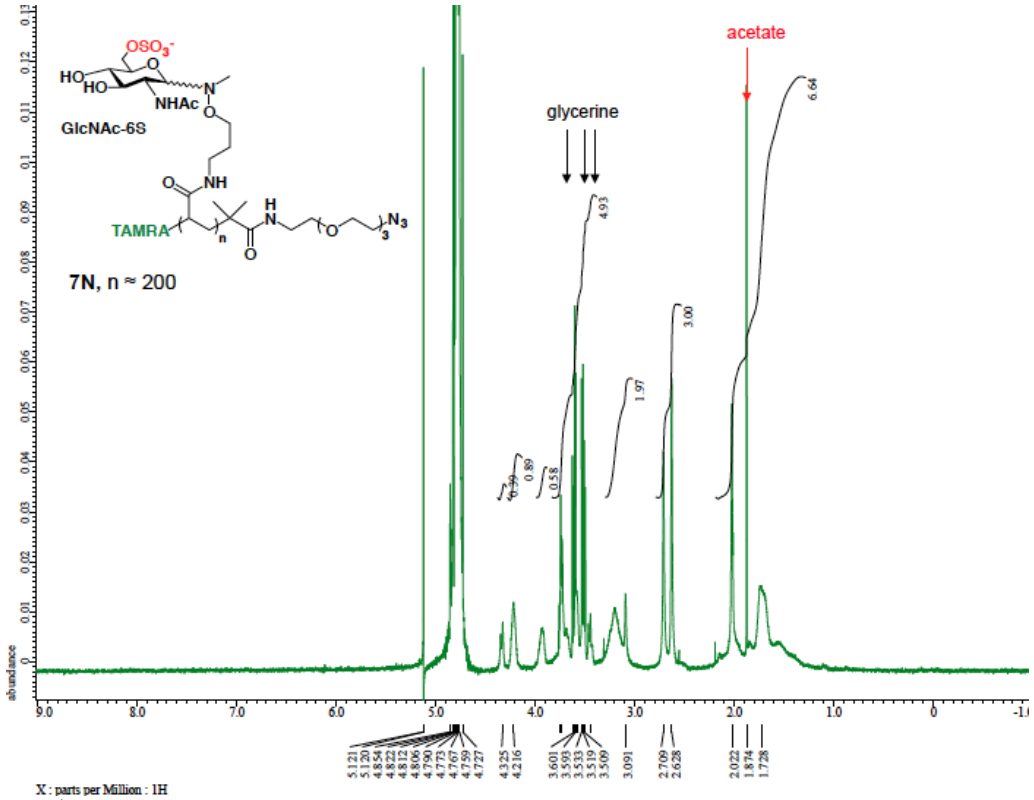

Figure 29. ^{1}H NMR spectrum continued

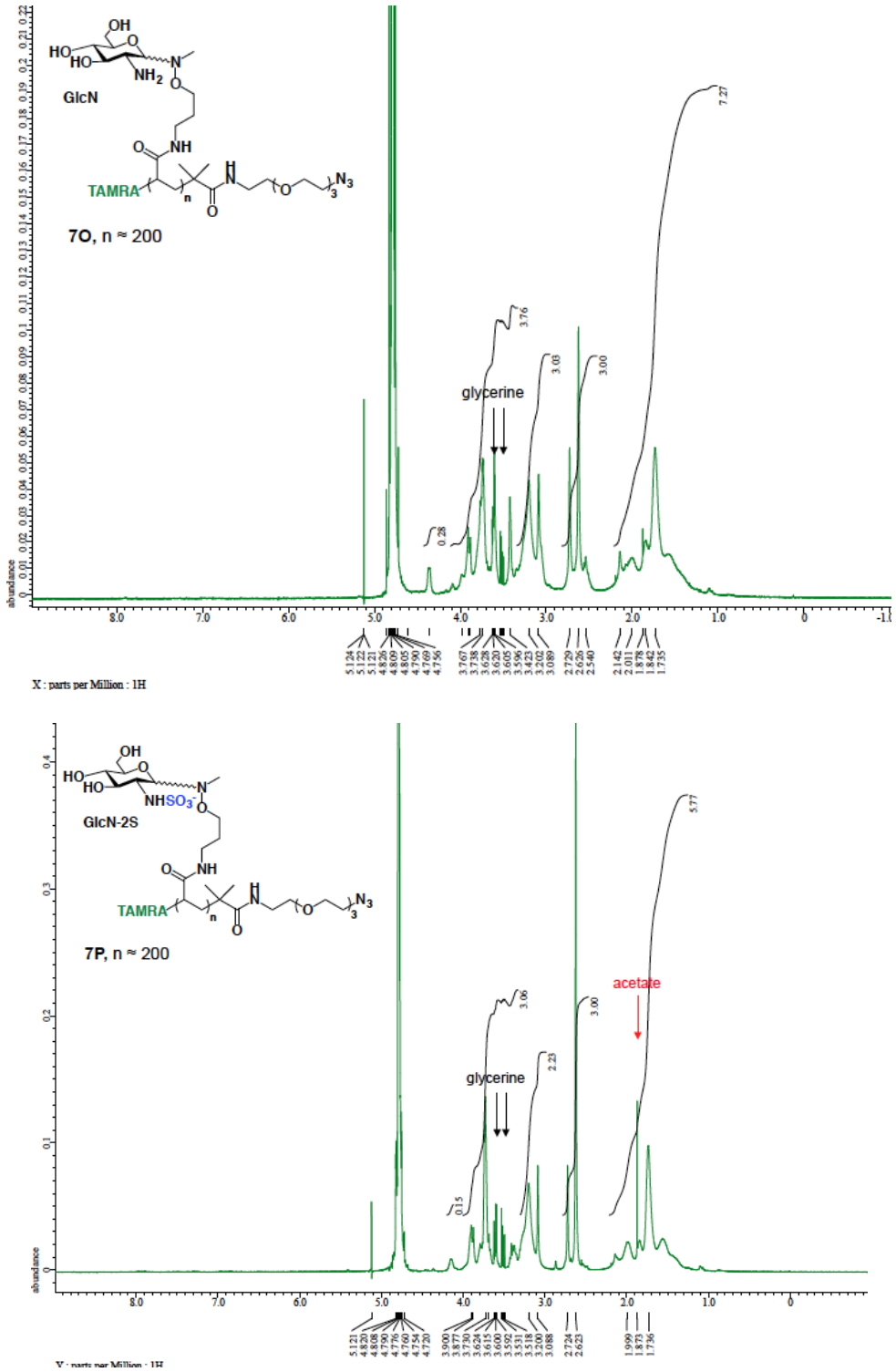

Figure 29. ^{1}H NMR spectrum continued

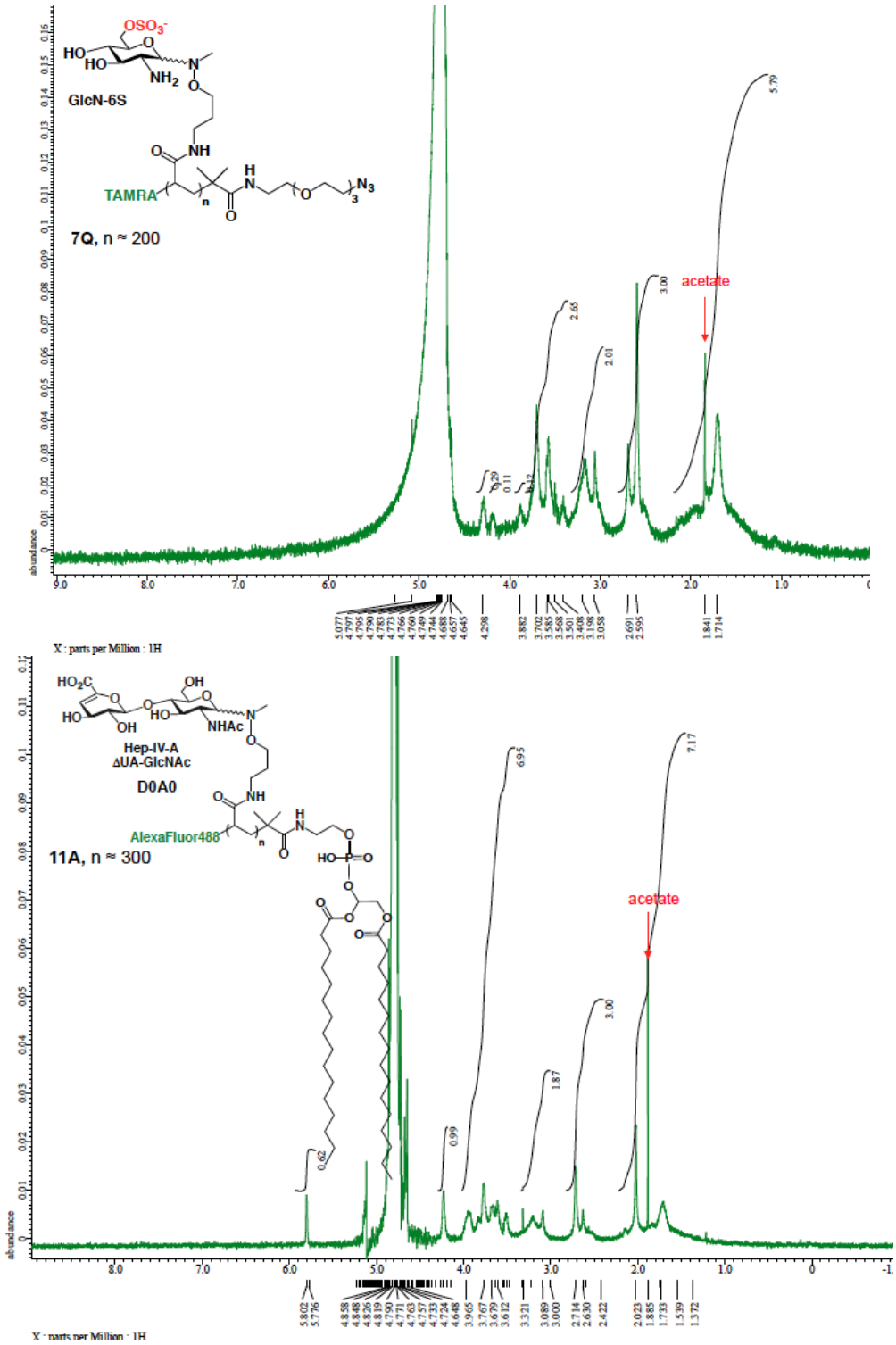

Figure 29. ^{1}H NMR spectrum continued

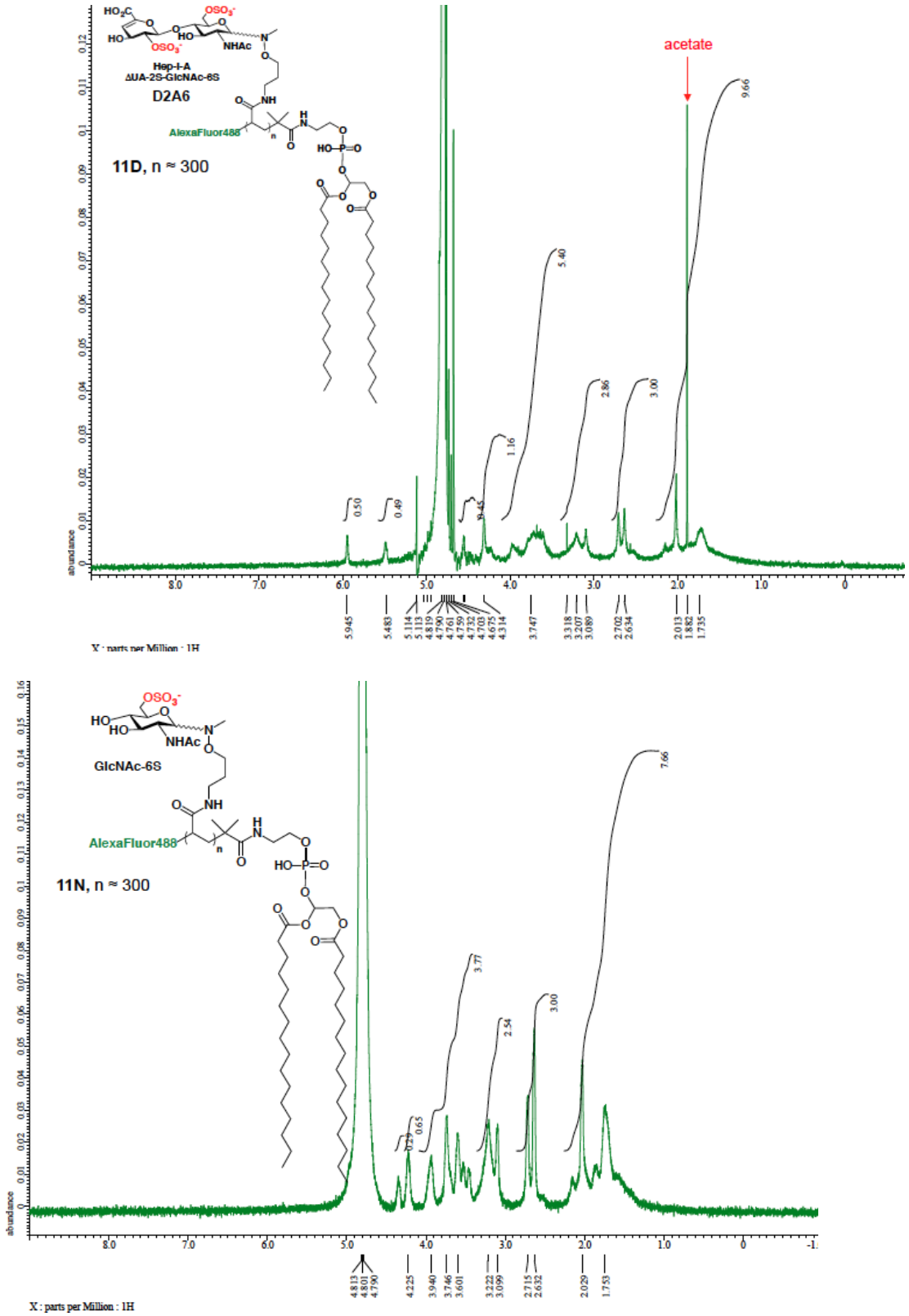

Figure 29. ^{1}H NMR spectrum continued

2.4.10 Microarray experiments

General microarray experiments. Microarrays were fabricated on epoxide-coated glass substrates using a GIX Microplotter Desktop (Sonoplot Inc., Middleton, WI) fluid dispensing system, which uses controlled ultrasonics to enable noncontact printing. Microarrays were analyzed on Axon GenePix 4000B microarray scanner (Molecular Devices). Proteins and antibodies were used as received unless otherwise indicated. Stock solutions of proteins and antibodies were prepared according to manufacturer's instructions. For microarray experiments, all water used was doubly-distilled from a Milli-Q purification system (Millipore). PBS solutions were prepared from a 20X PBS pH 7.5 stock solution (Amresco), and titrated if necessary to the desired pH. Unless otherwise noted, PBS solutions are pH 7.4. Recombinant human fibroblast growth factor-basic was purchased from Gibco (Cat. # PHG0264), heparin sodium was purchased from Acros Organics (Cat. #411212500), mouse anti-FGF2 monocloncal antibody, clone bFM-1 was obtained from Millipore (Cat. # 05-117), and goat-a-mouse IgG, Cy5 was purchased from GE Healthcare (Cat. # PA45009V).

Procedure for microarray printing. Epoxy slides (Thermo Fisher) were rinsed with water and incubated overnight at room temperature with a 1 mM solution of dibenzocyclooctyne-amine[33] and 10 mM DIPEA in DMF (anhyd).[34] The slides were then removed, sonicated in methanol 2 x 15 min., rinsed with water, centrifuged at 500 rpm for 5 min to "spin-dry", and stored at 4°C until use. Prior to printing, the slides were passivated with 0.1% BSA/PBS for 30 min, rinsed with water, and spin-dried. The azide-neoPGs (7**A**

– **Q**) were printed on cyclooctyne-functionalized slides at 80-85% relative humidity (10 mM glycopolymer in 0.005% Tween, pH 7.4, filtered through a 0.22 μm membrane). Each glycopolymer was spotted in triplicate, and each slide contained 16 full neoPG library subarrays. The slides were briefly humidified over a 80°C water bath and snap-dried over a dry 80°C glass surface for uniform spot morphologies. The printed slides were allowed to react overnight at 4°C in dark. Following a quick rinse with water, the slides were spin-dried, plunged in 0.1% Triton X/PBS for 2 min, followed by additional rocking or 15 min to remove unbound polymers. The slide was then washed twice in PBS for 10 min with rocking, rinsed with water, and spin-dried. The array was blocked with 1% BSA, 0.1% Tween/PBS for 30 min rinsed with water, and spin-dried, prior to use.

NeoPG microarray screening for selective FGF2 binders. Hydrophobic boundaries were manually drawn around each sub-array (Invitrogen PAP pen). Solutions of FGF2 (100 nM, 90 min.,), anti-FGF2 (90 min.), and goat Cy5-a-mouse (90 min.) antibodies were then sequentially incubated with the array at 4°C, following four washes with 1% BSA, 0.1% Tween, PBS pH 7.4 in between each step. Incubations with heparin were conducted with 100 nM of FGF2 and 1 □g/mL heparin, pre-incubated for 15 min. Following all incubations, the slide was washed 2 x 15 min in PBS, rinsed with water, spin-dried, and scanned.

2.4.11 Incorporation of neoPGs onto cell surfaces

General Biology Procedures: Unless otherwise stated, reagents were purchased from Gibco. The mESC wild-type E14TG2a and *Ext*1$^{-/-}$ cell lines[3] were a gift from Cathy Merry (Manchester, UK). Both cell lines were maintained in Knockout Dulbecco's modified Eagle's medium (KO-DMEM, Gibco, Cat. #10829-018) supplemented with 10% (v/v) FBS, 1% (v/v) L-glutamine (1% of a 200X solution, (Gibco, Cat. #25030-081), 1% (v/v) NEAA, 0.1% (v/v) 2-mercaptoethanol (Gibco, Cat. #21985-023), and LIF (Millipore ESGRO, 1000 U/mL). Heparin was obtained from Acros Organics (Cat. #411212500). BSA fraction V was obtained from Gemini Bio Products, catalogue #700-110. For normal passaging, cells were detached and seeded onto tissue-culture plates pre-treated with 0.1% gelatin (Sigma) in PBS solutions for at least ten minutes. For detachment, cells were incubated with trypsin or cell dissociation solution (Sigma). For flow cytometry experiments, a BD FACSCalibur flow cytometer equipped with BD FACSStation was used, and data was analyzed using FlowJo (TreeStar) using 10, 000 events during collection. For microscopy experiment, ProLong Gold antifade reagent with DAPI was used to visualize nuclei (Cell Signalling Technology, catalogue #8961). Images were captured using a Zeiss Axio fluorescence microscope and analyzed using Zen Blue 2012 software.

neoPG incorporation assay. A (60-80%) confluent T-75 flask of mESC *Ext*1$^{-/-}$ cells was trypsinsized and re-suspended to 1 x 10^6 cells/mL. A 1 mL cell suspension as then used to seed each well of a twelve-well plate, previously coated with 0.1% gelatin/DPBS (10 min, RT). Following incubation overnight at 37 °C, 5% CO_2, the plates were washed with

1 mL DPBS, and incubated with 0.5 mL of a neoPG solution in serum-free KO-DMEM at RT for desired times. Following incubation, the cells were washed twice with DPBS, and detached using cell dissociation media (1 mL). The cells were then harvested into a microtube, centrifuged at 300 xg for 4 min, washed twice with DPBS, and fixed with 4% paraformaldehyde/DPBS for 30-60 min on ice. The cells were then washed twice and resuspended in 0.1% BSA/DPBS for flow cytometry analysis. Assay was repeated in triplicate at least twice.

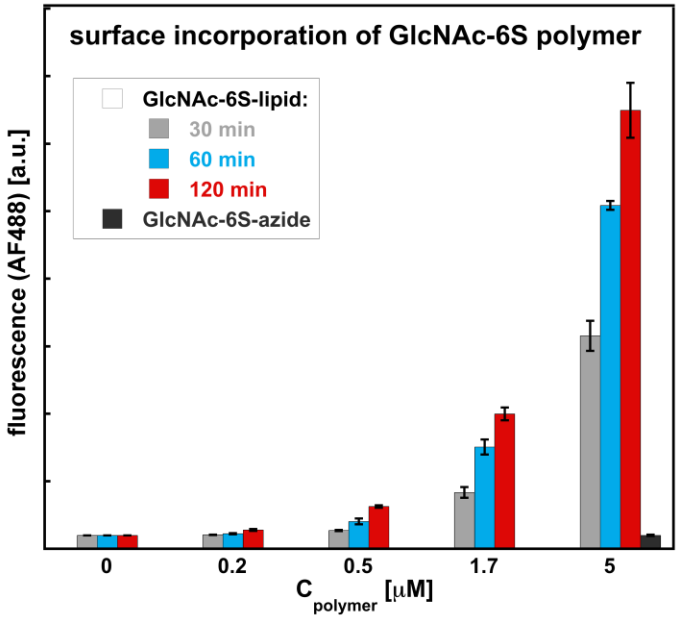

Figure 30. Cell surface incorporation of GlcNAc-6S polymer (**11N**) onto mESC *Ext*1$^{-/-}$ cell surfaces is dependent on polymer concentrations and incubation times.

Cell surface incorporation assay. A (60-80%) confluent T-75 flask of mESC *Ext*1$^{-/-}$ cells was trypsinsized and re-suspended to 1 x 10^6 cells/mL. A 1 mL cell suspension as then used to seed each well of a twelve-well plate, previously coated with 0.1% gelatin/DPBS (10 min, RT). Following incubation overnight at 37 °C, 5% CO_2, the plates were washed

with 1 mL DPBS, and incubated with 0.5 mL of a neoPG solution in serum-free KO-DMEM at RT. Following incubation for desired periods of time, the cells were washed twice with DPBS, and incubated with fresh complete medium for desired periods of time at 37°C, 5% CO_2. The cells were then washed twice with DPBS, detached, and fixed as above. The fixed cells were then stained with rabbit anti-AlexaFluor488 (Molecular Probes Cat. #A11094, 1:1000 in 0.1% BSA/PBS) and goat-PE-Cy5.5-anti-rabbit (Molecular Probes Cat. # L43018). Each antibody was incubated on ice for 30 min. with periodic agitation. The cells were centrifuged and washed as above between each staining step, and re-suspended in 0.1% BSA/PBS for flow cytometry analysis.

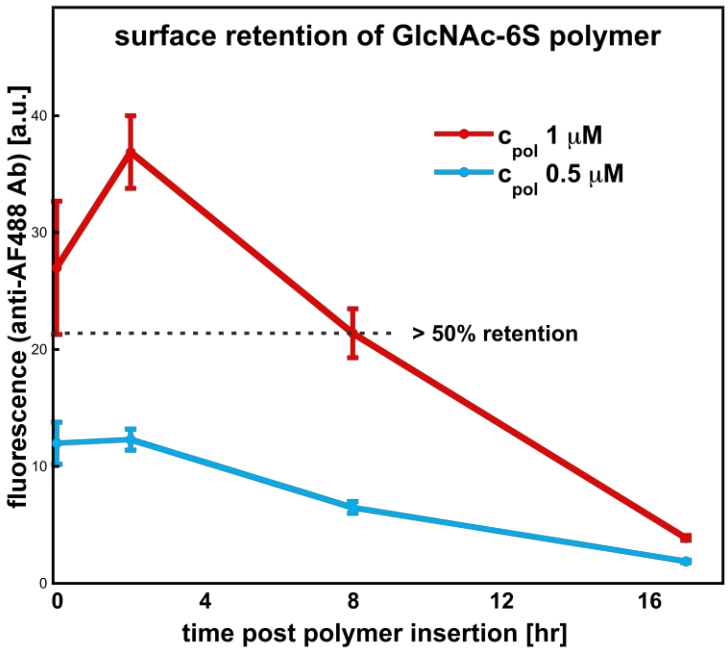

Figure 31. Retention of GlcNAc-6S neoPG (**11N**) incubated at different polymer concentrations (c_{pol}) on mESC *Ext1*$^{-/-}$ cell surfaces. Eight hours after polymer insertion, greater than 50% of the polymers are retained on the cell surface.

2.4.12 *Determination of FGF-2 binding by fluorescence microscopy*

FGF2 binding assay via microscopy. Following seeding overnight at 37°C and 5% CO_2 onto gelatin-coated 24-well plates, cells were washed twice with DPBS and incubated with or without glycopolymer solutions (3.4 □M solutions in KO-DMEM) for 1 hour at 37°C, 5% CO_2. The solution was then removed, and the adherent cells were washed twice with DPBS, and fixed with 4% PFA/PBS for 1 hour at 4°C. The fixed cells were then washed twice with DPBS, blocked with 2% BSA/PBS for 1 hour at 4°C, and incubated with 450 nM FGF2 in 2% BSA/PBS for 1 hour at 4°C. Immunostaining was performed with rabbit anti-fibroblast growth factor (Sigma Aldrich F3393, 1:200), and AlexaFluor555 anti-rabbit antibody (1:1000, Molecular Probes).

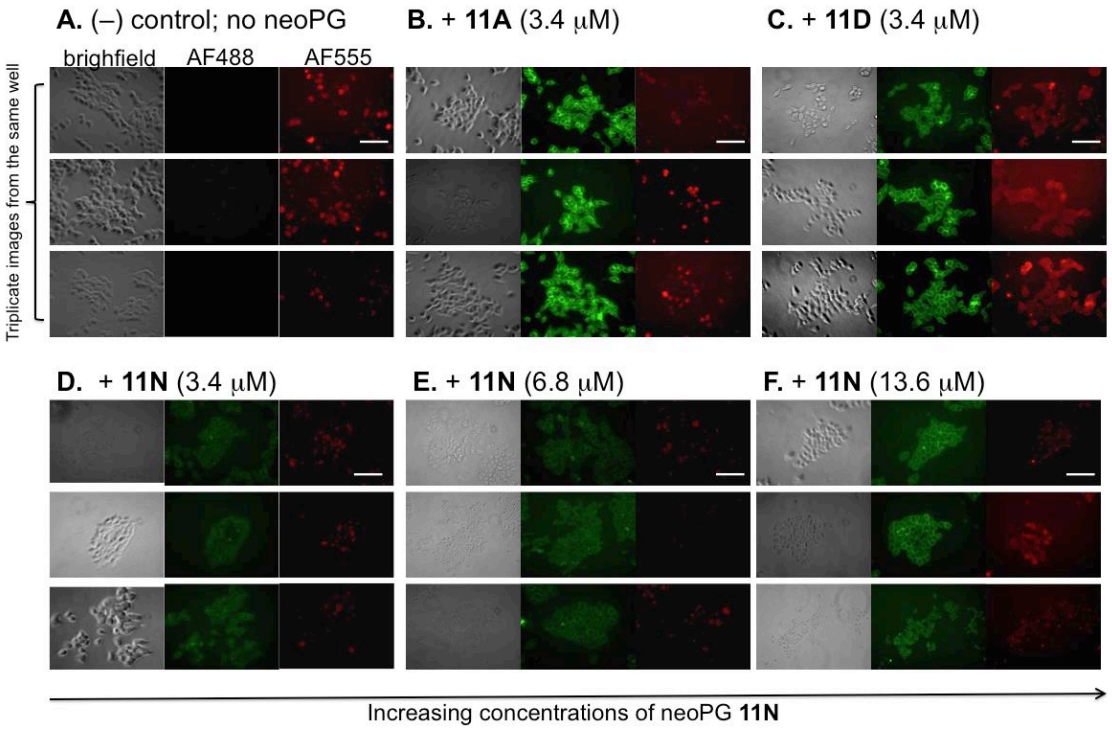

Figure 32. Microscopy Images at 40X magnification unless otherwise indicated (from left to right, brightfield, Alexa 488 channel, and Alexa 555 channel) collected for mESC *Ext*1$^{-/-}$ cells incubated without (A) or with 3.4 □M of neoPGs **11A** (B), neoPG **11D** (C), or **11N** (D). Following neoPG incubation, cells were fixed, incubated with FGF-2 (450 nM), and immunostained with rabbit anti-FGF2 (1:500), and anti-mouse AF555 (1:1000). Some variation in neoPG incorporation (green signal) is observed among the different neoPGs, with the least negatively charged polymer **11A**, exhibiting the greatest fluorescence signal (B). Nevertheless, cells incubated with **11D** (C) display robust binding to FGF-2 (red channel) compared to cells incubated with **11A** (**A**) or **11N** (C), which display background fluorescence similar to cells incubated with the primary and secondary antibody alone (A). Background fluorescence arising from the primary antibody was observed despite washes and signal optimization, and appears as small punctate red spots that do not cover the entire cell surface. A dose-dependent increase in green fluorescence is observed upon incubation of increasing concentrations of neoPG **11N** (6.8 □M, E and 13.6 □M, F), without increases in FGF2-binding (red fluorescence).

2.4.13 *Differentiation procedures and data*

Neural differentiation. For neural differentiation, E14TG2a or *Ext*1$^{-/-}$ mESCs were plated in gelatinised 24-well plates (Corning, Cat. #3527) at a density of 0.8 x 10^4 cells per cm^2

in mESC growth medium. The following day (day 0), medium was replaced with N2B27 medium, a 1:1 mixture of DMEM/ Ham's F12 (Gibco, Cat. #11330-032) and Neurobasal medium (Gibco Cat. #21103-049), 0.5x N2 supplement (Gibco, Cat. #17502-048), 0.5x B27 supplement (Gibco, Cat. #17504-044), 50 µg/mL BSA fraction V, 500 µM L-glutamine, 55 µM 2-mercaptoethanol, 100 units/mL penicillin and 100 µg/mL streptomycin (Gibco). Additionally, heparin was added at 5 µg/mL to + heparin conditions. Medium was replaced every one to two days as required. Cells were fixed at day six with 4% (w/v) paraformaldehyde for ten minutes at room temperature for subsequent analysis via immunocytochemistry.

For neoPG incubations (day 0), neoPGs were diluted to 1 µM using a 1:1 mixture of DMEM/ Ham's F12 and Neurobasal medium. mESC growth medium was removed and cell monolayers washed three times with PBS. *Ext*1$^{-/-}$ mESCs were incubated with either **11A**, **11D**, **11N**, or medium alone for 1 hour at 37 °C, 5% CO_2. The neoPG solutions were removed, cell monolayers washed three times with PBS and N2B27 medium was added. ProLong Gold antifade reagent with DAPI was added to stained cells to visualize nuclei and incubated for three hours at room temperature. Representative images of triplicate experiments were captured.

Immunocytochemistry and fluorescence microscopy. Fixed cells were blocked and permeabilized for one hour at room temperature using block solution (2% (v/v) goat serum, 1 mg/mL BSA, 0.1% (v/v) Triton-X100 in PBS). Primary and secondary antibody incubations were performed for one hour at room temperature. Primary antibodies against

Nestin (1:250, Millipore, cat #MAB353) and Oct3/4 (1:100, Santa Cruz Biotechnology, Cat. #sc-25401) were used. Anti-mouse AlexaFluor555 (1:1000, Cell Signalling Technology, Cat. # 4409) and anti-rabbit AlexaFluor488 (1:1000, Cell Signalling Technology, Cat. #4412) secondary antibodies were used. ProLong Gold antifade reagent with was added to stained cells to visualize nuclei and incubated for three hours at room temperature. Representative images of triplicate experiments were captured.

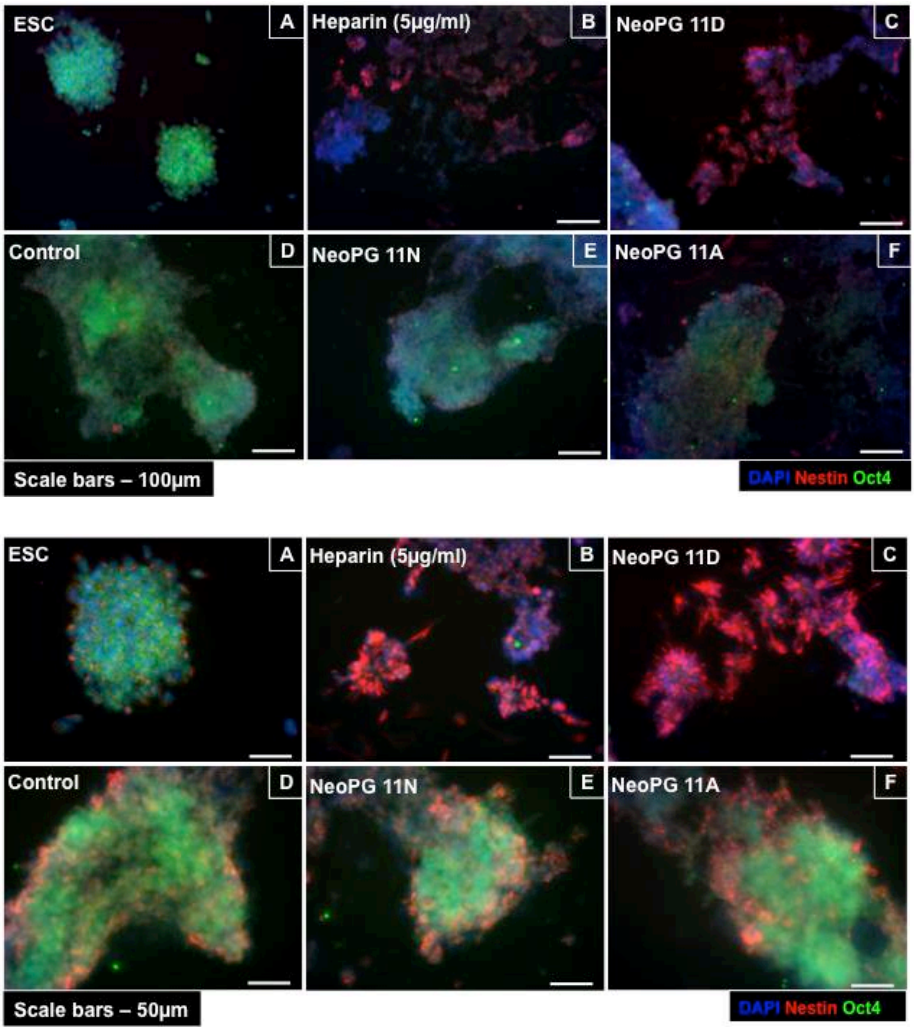

Figure 33. *Ext*1$^{-/-}$ mESCs during routine culture (A) and after six days of neural differentiation (B-F). ESCs (A) express high levels of Oct4 and low levels of nestin, whereas cells treated with soluble heparin (B) and neoPG **11D** (C) lose Oct4 expression and form nestin positive rosettes. Control (D), neoPG **11N** (E) and neoPG **11A** (F) all retain high levels of Oct4 low levels of nestin. 20x magnification (top) and 40x magnification (bottom).

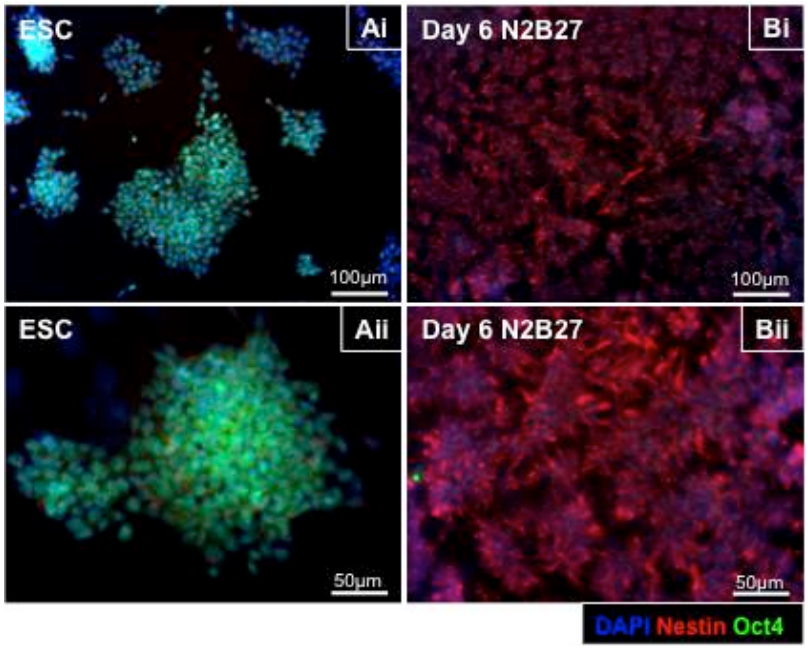

Figure 34. Neural differentiation of wild type (E14TG2a) mESCs. Wild type mESCs retain high levels of Oct4 during routine culture (Ai-ii). After six days after neural differentiation (Bi-ii) wild type ESCs lose Oct4 expression and express high levels of nestin in a characteristic rosette formation.

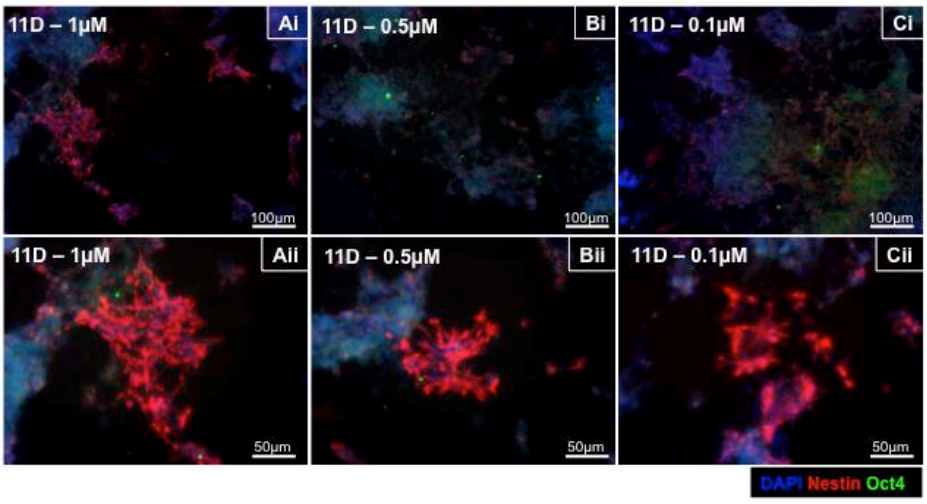

Figure 35. Neural differentiation of wild type (E14TG2a) mESCs. Wild type mESCs retain high levels of Oct4 during routine culture (Ai-ii). After six days after neural differentiation (Bi-ii) wild type ESCs lose Oct4 expression.

2.4.14 *FGF2 stimulation*

FGF2 stimulation. E14TG2a or *Ext*1$^{-/-}$ mESCs were plated in gelatinised 6-well plates (Corning, Cat. #3506) at a density of 1 x 10^5 cells per cm^2 in mESC growth medium. Cells were then serum starved overnight in mESC growth medium without FBS. Stimulation was performed by adding 25 ng/mL recombinant human basic FGF (Cell Signalling Technology, Cat. #8910) in KO-DMEM (Gibco, Cat. #10829-018) with or without 5 µg/mL heparin (Acros Organics, Cat. #411212500) to cell monolayers for 15 minutes at 37°C, 5% CO_2. Protein was extracted using 1x cell lysis buffer (Cell Signalling Technology, Cat. #9803) with 1x protease inhibitor cocktail (Cell Signalling Technology, Cat. #5872) and 1 mM PMSF (Cell Signalling Technology, Cat. #8553).

For neoPG incubations, neoPGs were diluted to 1 µM using KO-DMEM medium. Serum free mESC growth medium was removed and cell monolayers washed three times with PBS. *Ext*1$^{-/-}$ mESCs were incubated with either GlcNAc-6S (**11N**), HepIVA (**11A**), HepIA (**11D**), or medium alone for 1 hour at 37 ^{o}C, 5% CO_2. NeoPG solutions were removed, cell monolayers washed three times with PBS and 25 ng/ml recombinant human basic FGF in KO-DMEM with or without 5 µg/mL heparin was added.

Western blotting. 5 µg of total protein was resolved on 10% SDS-PAGE gels and transferred to immobilon-FL 0.45 µm PVDF membranes (Millipore, Cat. #IPFL00010). Membranes were blocked in 5% (w/v) BSA in tris-buffered saline with 0.1% (v/v) Tween-

20 (TBST) for 1 hour at room temperature. Primary antibody incubations were performed overnight at 4 °C using anti-phospho-Erk1/2 (1:4000, Cell Signalling Technology, Cat. #4370), anti-total Erk1/2 (1:6000, Cell Signalling Technology, Cat. #4695) or anti alpha-tubulin (1:10,000, Abcam, cat #ab7750) in 5% BSA/TBST. Membranes were washed 3x with TBST then incubated with HRP-conjugated secondary antibodies anti-rabbit HRP (1:7500, Cell Signalling Technology, Cat. #7074) or anti-mouse HRP (1:7500, Cell Signalling Technology, Cat. #7076) for 1 hour at room temperature. Membranes were washed 3x with TBST and developed using Luminata forte HRP detection reagent (Millipore, Cat. #WBLUF0100) and ECL Hyperfilm (GE healthcare, Cat. #28-9068-35).

For sequential antibody staining, membranes were stripped of primary and secondary antibodies using Restore PLUS Western blot stripping buffer (Thermo scientific, Cat. #46430) for 15 min. at room temperature. Membranes were washed 3x with TBST and blocked with 5% BSA in TBST for 1 hour at room temperature before subsequent antibody staining. Densitometry was performed using ImageJ analysis software (National Institute of Health), phospho-Erk1/2 and total Erk1/2 levels were normalized to alpha-tubulin levels, then phospho-Erk1/2 levels were normalized to total-Erk1/2 levels.

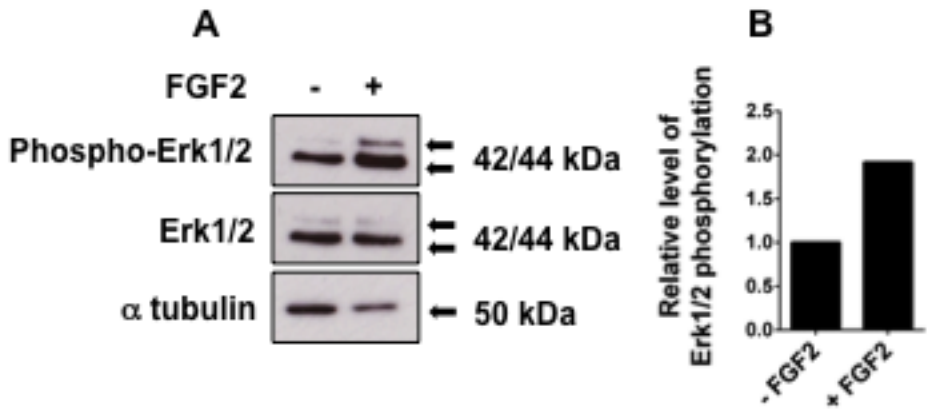

Figure 36. Wild type (E14TG2a) mESCs stimulated with 25ng/mL FGF2. Western blotting (A) and subsequent analysis via densitometry (B) indicated that phosphorylation of Erk1/2 in increased wild type mESCs stimulated with FGF2.

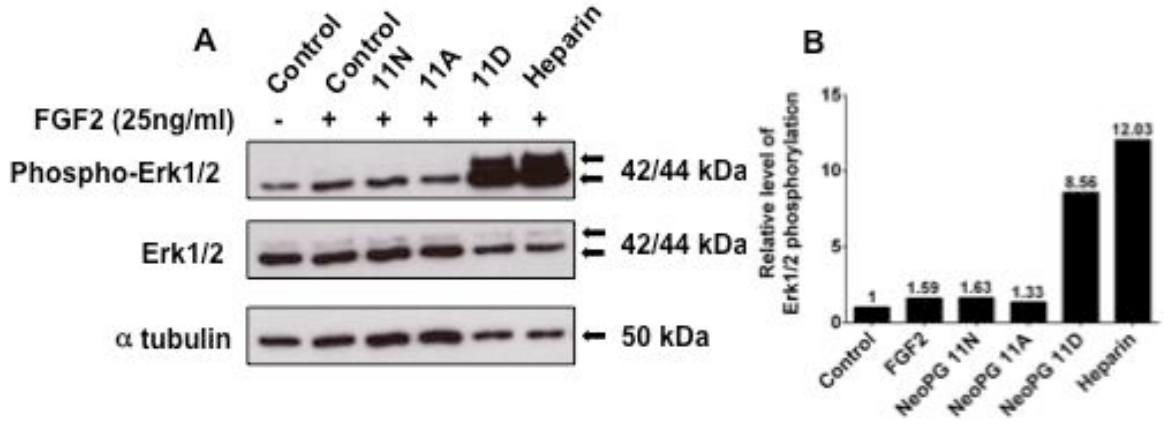

Figure 37: NeoPG **11D** potentiates FGF2-induced Erk1/2 phosphorylation. Western blotting (A) and subsequent analysis of duplicate experiments via densitometry (B) reveal that *Ext*1$^{-/-}$ mESCs remodelled with neoPG 11D display an increased sensitivity to FGF2 treatment.

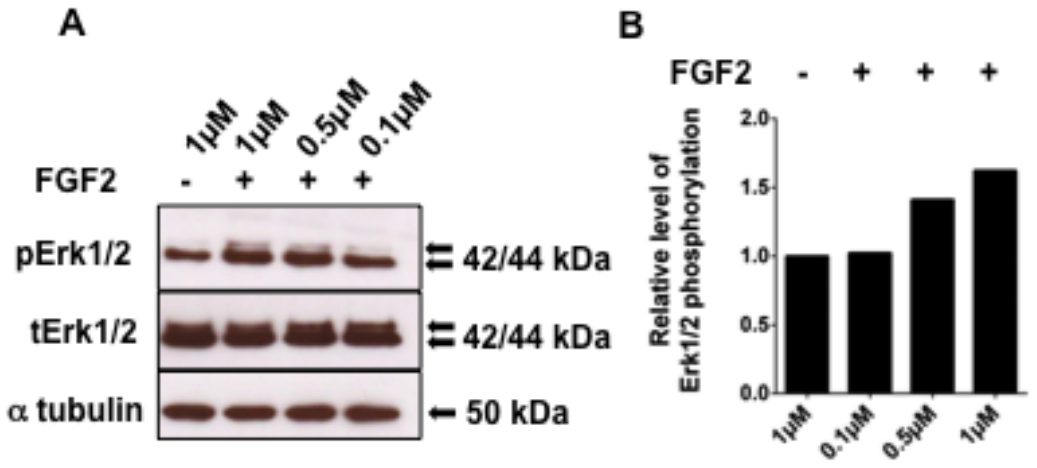

Figure 38: NeoPG **11D** potentiates FGF2-induced Erk1/2 phosphorylation in a dose-dependent manner. Western blotting (A) and subsequent analysis via densitometry (B) reveal Erk1/2 phosphorylation in *Ext*1$^{-/-}$ mESCs decreases when remodelled with lower concentrations of neoPG **11D.**

2.5 ACKNOWLEDGEMENT

Chapter 2 is a modified reprint of the material as it appears in JACS 2014, Huang M. L., Smith R. A. A., Trieger G. W. Glycocalyx Remodeling with Proteoglycan Mimetics Promotes Neural Specification in Embryonic Stem Cells. Mia Huang and Alex Smith where the primary authors on this paper, while I was responsible for the synthesis of glycopolymer back bones as well as the preparation of some of the NeoPG library, assisted by Dr. Kamil Godula and Dr. Mia Huang. I was also responsible for much of the chemical characterization of these polymers (GPC, UV-Vis) , and assisted Dr. Mia Huang in the collection and analysis of NMRs for the NeoPG library. I was also responsible for compiling much of the chemical characterization and procedures for the supporting information. Dr. Alex Smith was responsible for the biological experiments including Erk stimulations and neural differentiations of mESCs. Dr. Mia Huang performed FACs studies, prepared and used microarrays for FGF2 binding studies.

2.6 REFERENCES

[1] Sipp D., Caulfield T., Kaye J. Blackburn C., Chan S., De Luca M., Kent A., McCabe C., Munsie M, Sleeboom-Faulkner M., Sugarman J., Van szimmeren E., Zarzeczny, Sajo J. E. J. *Sci. Transl. Med.* **2017**, 9, 426.

[2] De Luca M., Aiuti A.,Cossu A., Parmar M., Pellegrini G. Robey P. G. *Nat Cell Bio.* **2019**, 21, 801–811.

[3] Hwang N. S., Varghese S., Elisseeff J. *Adv Drug Deliv Rev*. **2008,** 60(2): 199–214.

[4]Eshghi S., Schaffer D. V. *Stembook,* Cambridge (MA): Harvard Stem Cell Institute, **2008**.

[5] Varki, A.; Freeze, H. H.; Vacquier, V. D. *Essentials of Glycobiology*, 2nd ed.; CSHL Press: New York, **2009**; pp 531-6.

[6] (a) Xu, D.; Esko, J. D. *Annu. Rev. Biochem*. **2014**, 83, 17.1-17.29. (b) Gallagher, J. T. *J. Clin. Invest*. **2001**, 108, 357-61. (c) Smith, R. A. A.; Meade, K.; Pickford, C. E.; Holley, R. J.; Merry, C. L. R. *Biochem. Soc. Trans*. **2011**, 39, 383-7.

[7] (a) Kreuger, J.; Spillmann, D.; Li, J. P.; Lindahl, U. *J. Chem. Biol*. **2006**, 174, 323-7. (b) Turnbull, J. E.; Fernig, D. G.; Ke, Y.; Wilkinson, M. C.; Gallagher, J. T. *J. Biol. Chem.* **1992**, 267, 10337-41.

[8] Yayon, A.; Klagsbrun, M.; Esko, J. D.; Leder, P.; Ornitz, D. M. *Cell* **1991**, 64, 841-8.

[9] (a) Kunath, T.; Saba-El-Leil, M. K.; Almousailleakh, M.; Wray, J.; Meloche, S.; Smith, A. *Development* **2007**, 134, 2895-902. (b) Stavridis, M. P.; Lunn, J. S.; Collins, B. J.; Storey, K. G. *Development* **2007**, 134, 2889-94. (c) Johnson, C. E.; Ward, C. M.; Wilson, V.; van Kuppevelt, T. H.; Esko, J. D.; Smith, A.; Gallagher, J. T.; Merry, C. L. R. *Stem Cells* **2007**, 25, 1913-23. (d) Pickford, C. E.; Holley, R. J.; Rushton, G.; Stavridis, M.; Ward, C. M.; Merry, C. L. R. *Stem Cells* **2011,** 29, 629-40.

[10] Kraushaar, D. C.; Yamaguchi, Y.; Wang, L. *J. Biol. Chem*. **2010**, 285, 5907-16.

[11] (a) Rillahan, C. D.; Antonopoulos, A.; Lefort, C. T.; Sonon, R.;Azadi, P.; Ley, K.; Dell, A.; Haslam, S. M.; Paulson, J. C. *Nat. Chem.Biol*. **2012**, 8, 661-8. (b) Mahal, L. K.; Yaerma, K. J.; Bertozzi, C. R. *Science* **1997**, 276, 1125-8. (c) Xie, R.; Hong, S.; Feng, L.; Rong, J.; Chen, X. *J. Am. Chem. Soc*. **2012**, 134, 9914-7.

[12] Sullivan W. J., Mulle P. J., Schmid E., Flores A., Momcilovic M., Sharpley M. S., Jelinek D., Whiteley A. E., Maxwell M. B., Wilde B. R., Banerjee M. A., Coller H. A. Christofk H. R. *Cell* **2018**, 175, 117 –13.

[13] Kraushaar D. C., Wang L. *J Biol Chem*. **2010** 285(8), 5907–5916.

[14] Sackstein, R.; Merzaban, J. S.; Cain, D. W.; Dagia, N. M.; Spencer, J. A.; Lin, C. P.; Wohlgemuth, R. *Nat. Med*. **2008**, 14, 181-7.

[15] (a) Frame, T.; Carroll, T.; Korchagina, E.; Bovin, N.; Henry, S. *Transfusion* **2007**, 47, 876-882. (b) Wikstrom, M.; Xie, J.; Bogdanov, M.; Mileykovskaya, E.; Heacock, P.; Wieslander, A.; Dowhan, W. *J. Biol. Chem*. **2004**, 279, 10484-93. (c) Rabuka, D.; Forstner, M. B.; Groves, J. T.; Bertozzi, C. R. *J. Am. Chem. Soc*. **2008,** 130, 5947-53.

[16] a) Belardi, B.; O'Donoghue, G. P.; Smith, A. W.; Groves, J. T.; Bertozzi, C. R. *J. Am. Chem. Soc.* **2012,** 134, 9549-52. (b) Hudak, J. E.; Canham, S. M.; Bertozzi, C. R. *Nat. Chem. Biol*. **2014**, 10, 69-75.

[17] Pulsipher, A.; Griffin, M. E.; Stone, S. E.; Brown, J. M.; HsiehWilson, L. C. *J. Am. Chem. Soc.* **2014**, 136, 6794-7.

[18] (a) Noti, C.; Seeberger, P. H. *Chem. Biol*. **2005**, 12, 731-56. (b) Arungundram, S.; Al-Mafraji, K.; Asong, J.; Leach, F. E.; Amster, I. J.; Venot, A.; Turnbull, J. E.; Boon, G.-J. *J. Am. Chem. Soc*. **2009**, 131, 17394-405. (c) DeAngelis, P. L.; Liu, J.; Linhardt, R. J. *Glycobiology* **2013**, 23, 764-77.

[19] Mammen, M.; Choi, S.-K.; Whitesides, G. M. Angew. *Chem., Int. Ed*. **1998**, 37, 2754-94.

[20] De Paz, J. L.; Noti, C.; Böhm, F.; Werner, S.; Seeberger, P. H. *Chem. Biol*. **2007**, 14, 879-87.

[21] (a) Rawat, M.; Gama, C. I.; Matson, J. B.; Hsieh-Wilson, L. C. *J. Am. Chem. Soc*. **2008**, 130, 2959-61. (b) Shen, G. J.; Oh, Y. I.; Chang, S.-K.; Hsieh-Wilson, L. C*. J. Am. Chem. Soc*. **2013**, 135, 10898-901.

[22] Peri, F.; Dumy, P.; Mutter, M. *Tetrahedron* **1998**, 54, 12269-78.

[23] Jewett, J. C.; Bertozzi, C. R. *Chem. Soc. Rev*. **2010**, 39, 1272-9.

[24] (a) Zong C., Venot A., Lu X. W. L., Xiao W., Wilkes J. L., Salanga C. L., Hande T. M., Wang L., Wolfert M. A., Boons G-J., *J. Am. Chem. Soc.* **2017**, 139, 9534-9543 (B) C. Noti, Dr. J. L. de Paz, Dr. L. Polito P. H. Seeberger *Chem. Eur. J.* **2006**, 12, 8664 – 8686. (C) Shipp, E L., Hseih-Wilson L. C. *Chemistry & Biology*14, 195–208, (D) Trieger G. W., Verespy S, Gordts, P L. S. M., Godula K. *Bioconjugate Chem*. **2019**, 30, 833−840

[25] Ying, Q. L.; Stavridis, M.; Griffiths, D.; Li, M.; Smith, A. *Nat.Biotechnol*. **2003**, 21, 183-6.

[26] Smith R. A. A., Murali S., Rai B., Lu X., Lim Z. X. H. Lee J. J. L, Nurcombe V., Cool S. M. *Biomaterials* **2018**, 184, 41-55.

[27] Lawrence, R.; Lu, H.; Rosenberg, R. D.; Esko, J. D.; Zhang, L. *Nature Methods* **2008**, *5*, 291-2.

[28] Carrasco, M. R.; Alvarado, C. I.; Dasher, S. T.; Wong, A. J; Wong, M. A. *J. Org. Chem.* **2010**, 75, 5757–9.

[29] Chiefari, J.; Chong, Y. K.; Ercole, F.; Krstina, J.; Jeffery, J.; Le, T. P. T.; Mayadunne, R. T. A.; Meijs, G. F.; Moad, C. L.; Moad, G.; Rizzardo, E.; Thang, S. H. *Macromolecules* **1998**, 31, 559-62.

[30] Godula, K; Umbel, M. L.; Rabuka, D.; Botyanszki, Z.; Bertozzi, C.; Parthasarathy, R. *J. Am. Chem. Soc.* **2009** 131, 10263-8.
Kaiser, E.; Picart, F.; Kubiak, T.; Tam, J. P.; Merrifield, R. B. *J. Org. Chem.*, **1993**, 58, 5167-75.

[32] McDowall, L. and Stenzel, M. H. *Polym. Chem.* **2014**, 5, 1772-1781.

[33] Ning, X.; Guo, J.; Wolfert, M. A., Boons, G. J. *Angew. Chem. Int. Ed.* **2008**, 47, 2253-5.

[34] Kuzmin, A.; Poloukhtine, A.; Wolfert, M. A.; Popik, V. V. *Bioconj. Chem*. **2010**, 21, 2076-85.

CHAPTER 3: Investigating heparan sulfate's link to adipocyte metabolism and application of synthetic glycomaterials to enhance cellular access to glucose

3.1 INTRODUCTION

Obesity has become a global pandemic of increasing severity due to the popularity and increase availability of a western style diet. This trend has resulted in the onset of a variety of metabolic diseases, highlighting a need for novel treatment avenues to combat this deadly trend. Caused by excess caloric intake and reduced energy expenditure, obesity is characterized by the excessive accumulation of body fat in subcutaneous and visceral adipose deposits throughout the body leading to a variety of severe medical ailments. Commonly, the constant influx of nutrients results in elevated blood sugar (hyperglycemia) requiring insulin to be constantly secreted from the beta cells of pancreatic islets in an effort to reduce the hyperglycemic state by inducing glucose uptake from adipose tissue. Overtime, the adipose tissue becomes desensitized to insulin due to persistent signaling and requires increasing amounts insulin to be secreted to elicit the required glucose clearance response. Ultimately, this leads to the exacerbation and failure of the beta cells, marking the onset of type 2 diabetes (T2D). T2D puts patients at high risk for complications including neuropathy, retinopathy, cardiovascular disease and stroke, greatly reducing the quality of life for those afflicted.[1]

As a result, T2D has been a prominent focus of medical research related to its treatment, prevention, and reversal.

A human genetic screen identified the heparan sulfate proteoglycan (HSPG) glypican 4 (GPC4) as an adipokine secreted in the circulation that directly correlated with insulin resistance, impaired glucose uptake, and high body mass index (BMI), making it

a positive correlator for those afflicted with or at risk for T2D.[2] In healthy patients, GPC4 functions as an adipokine by regulating insulin signaling through a yet unidentified interaction with the insulin receptor as well as by inducing differentiation of adipocytes. While in overweight patients GPC4 seems to be shed from the surface of adipose cells it remains remain unclear and relatively unexplored how this is taking place.[3] Multiple studies have shown that genetic knockout of the protein core of GPC4 results in an overall reduction in adipogenesis, which manifests both genetically as well as through reduced: cellular access to glucose, insulin sensitivity, and lipid accumulation, indicating its essentiality to adipogenesis.[4]

Structurally, GPC4 is a GPI-anchored HSPG which is composed of a core protein with several heparan sulfate (HS) glycosaminoglycan (GAG) chains extending from the protein core.[5] These HS chains are composed of repeating units of an uronic acid and glucosamine, which are enzymatically sulfated and isomerized at various positions throughout the extended polysaccharide. It is through sulfation and isomerization that HS chains are able to exhibit high specificity for binding a variety of proteins.[6] HSPGs have been minimally studied in the context of adipogenesis, but have been extensively characterized for binding and internalization of proteins involved in lipoprotein metabolism, such as lipoprotein lipase as well as apolipoproteins (apo) on triglyceride-rich lipoproteins such as apoA-V, apoB and apoE.[7] In fact, it is unclear if the GPC4 protein core or the HS chains are involved in the binding of insulin receptors and enhancement of differentiation through growth factor interactions. Previous studies in preadipocytes lacking either another HSPG, Syndecan-1 or the HS biosynthetic enzyme *N*-acetylglucosamine *N*-deacetylase-N-sulfotransferase 1 (Ndst1) have shown that lack of

either results in lack of lipid droplet formation possibly via decreased endocytosis of triglyceride-rich lipoproteins.[8]

In this study we aimed to clarify the relative contribution of HS GAGs on various aspects of adipogenesis and adipocyte functions including insulin perception, lipid accumulation, and glucose clearance. We used a genetic approach by inactivation of an HS biosynthetic enzyme *Ndst1* (*Ndst1*$^{-/-}$) in murine preadipocytes as well as a chemical approaches by administering heparin, a highly sulfated form of HS, and synthetic membrane anchored HSPG-mimetic glycopolymers.[9] Using these tools we identified that HSPGs are responsible for establishing glucose clearance capacity in differentiating adipocytes, and inhibition of these HSPG interactions early in differentiation results in a reduced ability to clear glucose while not impacting adipogenesis or insulin perception. Further investigation revealed that HSPG control a cellular metabolic transition away from anaerobic respiration in favor of oxidative phosphorylation during adipogenesis, which attribute the lack of lipid droplets as lipids are primarily utilized as an energy source. Importantly the HSPG-mimetic glycopolymers were capable of not only restoring normal glucose metabolism in *Ndst1*$^{-/-}$ adipocytes, they were able to significantly enhance glucose uptake in WT adipocytes in a sulfation dependent manner, demonstrating a tunable, materials based approach for the manipulation of glucose sensitivity in cells, bearing immediate implications for the treatment of people with T2D and/or hyperglycemia.

3.2 RESULTS AND DISCUSSION

3.2.1 Adipogenesis and lipid accumulation with inhibited HSPG interactions

Our investigation began with an evaluation of adipogenesis in mouse embryonic fibroblasts (MEFs) which either lacked the sulfotransferase *Ndst1* or were treated with a high concentration of heparin in the media throughout the differentiation protocol. In agreement with previous studies from the Orlando lab, soluble heparin was capable of inhibiting lipid accumulation in the differentiating cells, presumably through cell surface HSPG's reduced access to lipid particles such as VLDL in the serum-containing media.[8] Cells lacking normally sulfated HSPG due to the deletion of *Ndst1* were also unable to accumulate lipids (**Fig 39A,B**). The lack of lipid accumulation was not due to a lack of cellular growth (**Fig 39C**), nor as a result of an incomplete differentiation, as critical adipogenic markers typically behaved similarly regardless of HSPG inhibition via genetic or chemical means (**Fig. 39 D-G)**.

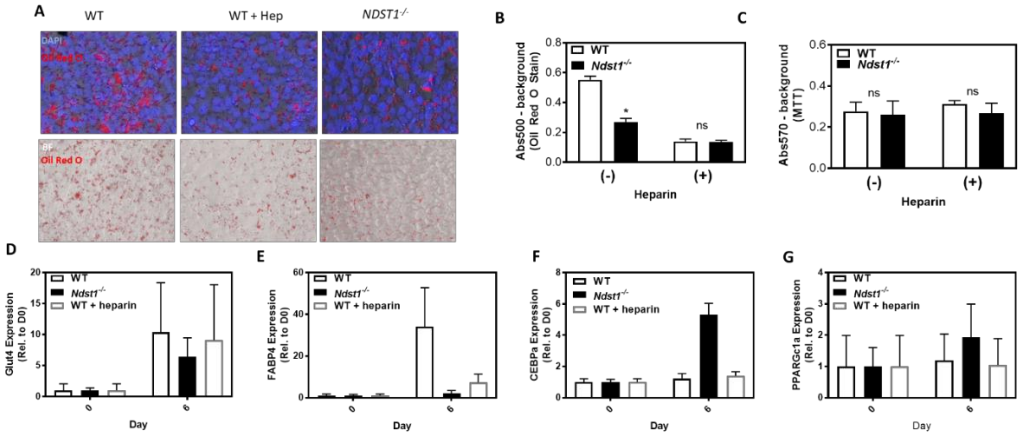

Figure 39. Adipogenesis in WT and Ndst1$^{-/-}$ MEFs. A. Oil Red O stain of differentiated WT, WT + heparin, and Ndst1$^{-/-}$ MEF. Nuclei visualized with DAPI. B. Quantified Oil red stain performed by elution of stain. C) MTT assay of WT and Ndst1$^{-/-}$ MEFs +/- heparin. D-F). mRNA expression of adipogenesis markers relative to day 0 expression levels: D) Glut4, E) FABP4, F) CEBPa, G) PPARGc1a.

Next we investigated VLDL binding as the potential cause of the reduced lipid accumulation (**Fig 40A)**. We did not see a significant reduction in VLDL binding capacity between HSPG inhibited (*Ndst1*$^{-/-}$) cells and wild type MEFs, suggesting that differences in lipid accumulation was occurring through an alternative mechanism. On the other hand, lipoprotein lipase (LPL), a HSPG binding protein that is responsible for the extracellular releasing fatty acids from triglycerides, had reduced binding to the cell surface of cells treated with exogenous heparin or those that lacked Ndst1 (**Fig 40B**). While the effect is significant, the implication is likely not, because little to no LPL protein is expressed during and after *in vitro* differentiation of MEFs, and thus likely plays a minimal role in the uptake of lipids in our model. Additionally, when we differentiated WT MEFs and assessed acute fatty acid uptake using radiolabeled ^{3}[H]-palmitate, we found that the WT + heparin cells actually internalize fatty acids significantly more than the WT control cells, and that *Ndst1*$^{-/-}$ cells had an equal ability to internalize palmitate (**Fig 41C**). Considering these data, one begins to question whether other mechanisms are responsible for the reduced lipid accumulation in HS deficient/inactive adipocytes.

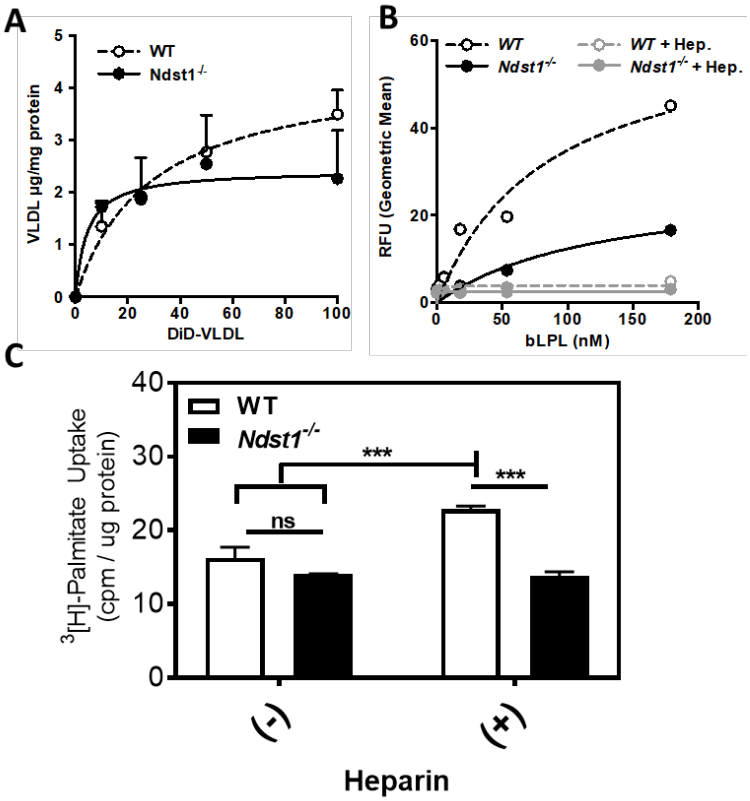

Figure 40. Processing of lipids in WT and *Ndst1*$^{-/-}$ MEFs. A. VLDL binding is not significantly impacted by the *Ndst1* knock-out. B. LPL binding is reduced in *Ndst1*$^{-/-}$ cells. Treatment with heparin blocks all interaction with LPL. C. 3[H]-palmitate uptake in day 6 differentiated MEFs. Palmitic acid is taken up significantly more in heparin treated WT cells compared to WT cells. Heparin treatment during differentiation has no effect on *Ndst1*$^{-/-}$ cells' ability to internalize palmitate.

3.2.2 The role of HSPG interactions as they affect cellular access to glucose

In an attempt to clarify the conceptually conflicting data between fatty acid uptake and lipid accumulation, we turned our focus towards adipocytes' access to glucose when HS interactions are inhibited through genetic and chemical means. Glucose clearance is one of the primary functions of adipocytes, typically in response to insulin via the glucose transporter Glut4. We reasoned that the potential discrepancy between lipid accumulation

and access to fatty acids could be a product of reduced conversion of glucose into fatty acids or reduced glycolysis in the cell, causing cells to favor fatty acid oxidation as the primary energy producing pathway. To test this hypothesis, WT and *Ndst1*$^{-/-}$ MEFs were differentiated to day 6 in the presence or absence of exogenous heparin, and on day 6 the adipocytes were treated with radioactive 2-deoxy-glucose and the extent of its accumulation was determined as a measure for glucose uptake (**Fig. 42**). Inactivation of cell surface HSPG interaction led to a robust reduction in cellular glucose uptake, regardless of the mode of HSPG inhibition. Addition of heparin did not have additive effects in the case of *Ndst1*$^{-/-}$ cells, consistent with the lipid accumulation studies detailed in **Fig. 39**. Additionally, when insulin stimulation was performed prior to 2-deoxy glucose uptake, the same relative glucose uptake enhancement was observed regardless of HSPG inhibition (**Fig. 41A-C**), indicating an equal sensitivity to insulin. When we tested if heparin treatment impacted glucose uptake capacity in primary preadipocytes isolated from murine subcutaneous adipose tissue and differentiated into adipocytes, we again observed a reduced glucose uptake capacity in heparin treated cells (**Fig 41D**).

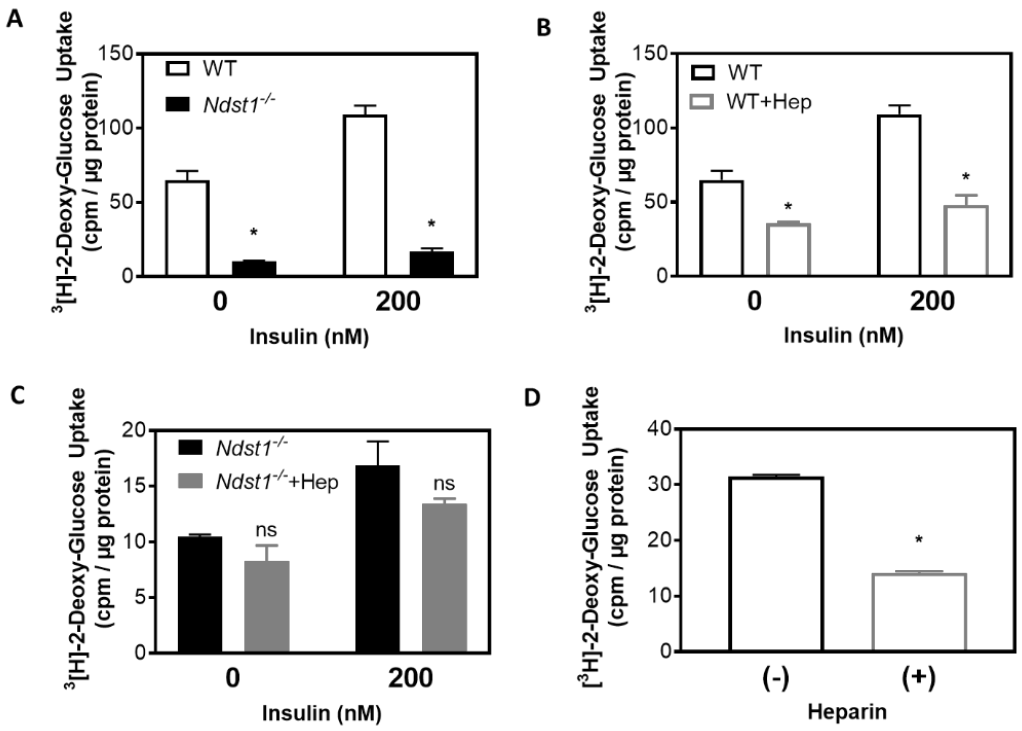

Figure 41. Inhibition of cell surface HSPG interactions during adipogenesis significantly reduces cellular access to glucose, but does not impact cellular insulin response. A) *Ndst1*$^{-/-}$ cells have a significantly reduced glucose uptake potential relative to WT adipocytes. B) Heparin treatment (100 µg/mL) reduces glucose uptake potential relative to WT adipocytes. C) Heparin treatment does not further reduce *Ndst1*$^{-/-}$ adipocytes ability to access glucose. D) Subcutaneous white adipose tissue precursor cells differentiated into adipocytes in the presence of heparin exhibit a reduced ability to access glucose. E) Insulin stimulation of day 6 differentiated MEF cells shows that regardless of HSPG inhibition, cells still differentiate into insulin responsive adipocytes.

To further demonstrate that insulin response was not impacted by inhibition of HSPG interactions, we performed insulin stimulations on differentiated adipocytes. As the glucose uptake data suggests in **Fig. 41** the adipocytes, regardless of HSPG interaction inhibition, were equally responsive to insulin stimulation **(Fig. 42)**.

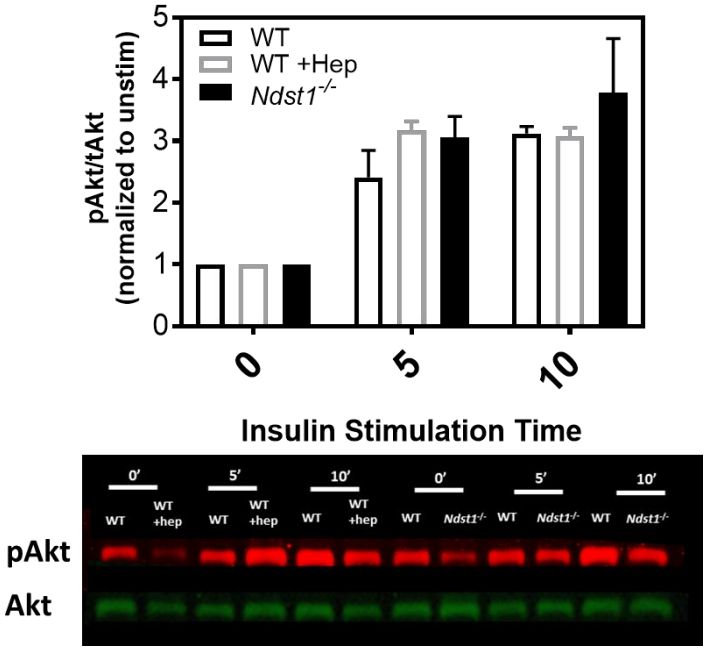

Figure 42. Insulin stimulation (20nM, 30 min) of day 6 adipocytes leads to an equal response (phosphorylation of Akt) regardless of HSPG interaction.

Fascinated to find that HSPG has a direct impact on glucose sensitivity, we set out to determine at what point during differentiation is HSPG responsible for establishing glucose sensitivity. We first determined that acute heparin treatment during the ^{3}[H]-2-deoxy-glucose uptake assay did not elicit any reduced glucose uptake potential in differentiated MEF cells (**Fig. 41**). We also confirmed that the absence of functional cell surface HSPG did not impact glucose uptake potential by treatment of differentiated adipocytes with heparinase, which removes and digests heparan sulfate GAG, followed by a ^{3}[H]-2-deoxy-glucose uptake assay (**Fig**. **43**) . We next wanted to determine if the deletion of *Ndst1* could impact glucose uptake in undifferentiated cells, and tested this in three different cell lines with this deletion (A375 (human skin), Hep3B (human hepatoma), and MEFs), finding that the deletion had no significant effect in any of the cell lines (**Fig**

44). Aware that the glucose clearance capabilities of adipocytes are established during differentiation, and convinced that inhibition of cell surface HSPG interactions plays no role in the physical uptake of glucose, we set out to determine the window in which glucose sensitivity can be affected in differentiating cells.

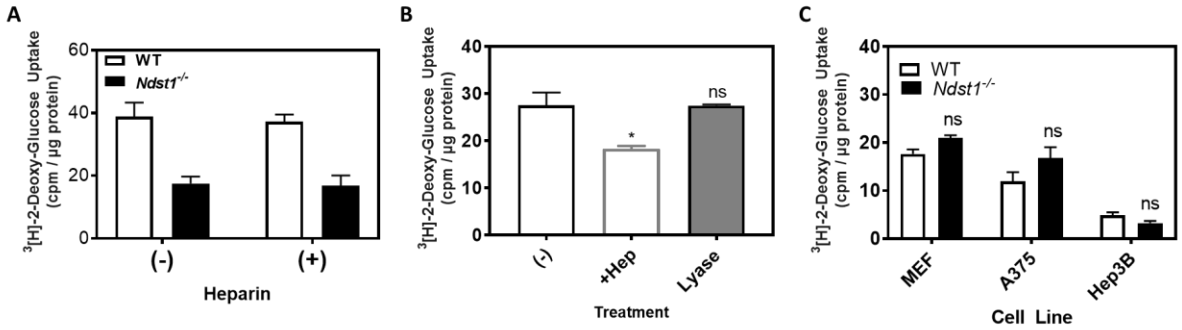

Figure 43. Inhibition of HSPG interactions must occur during adipogenesis to cause a reduced glucose uptake potential A) MEF cells differentiated to day 6 were treated with 100µg/mL heparin during 10 minute ^{3}[H]-2-deoxy-glucose uptake period. ^{3}[H]-2-deoxy-glucose uptake was unaffected. B) MEF cells differentiated to day 6 were treated with Hep lyase I-III for 30 minutes prior to ^{3}[H]-2-deoxy-glucose uptake period. ^{3}[H]-2-deoxy-glucose uptake was unaffected by digest. C) MEFs, A375 (human skin), and Hep3B (human hepatoma) cells with and without *Ndst1*$^{-/-}$ mutation have no significant difference in their ability to uptake ^{3}[H]-2-deoxy-glucose.

To hone in on the time frame during differentiation responsible for the establishment of glucose sensitivity, we used a two pronged approach of both adding in heparin at different points during the 6 day differentiation to WT MEFs, as well as by removing heparin from heparin treated WT cells throughout differentiation. By analyzing glucose sensitivity on day 6 of the differentiated cells, we can identify both when heparin becomes effective, as well as when heparin is no longer effective (**Fig. 44**). By initially treating cells with heparin bearing media, then removing it after different durations, we

were able to determine that treatment up to day 3 is required to impact glucose uptake. Interestingly, longer treatment with heparin exhibited no effect on the glucose uptake potential of the adipocytes(**Fig. 44A**). When heparin was added to differentiation media increasingly late in the differentiation program, we were again able to identify that treatment on day 3 is critical for the HSPG dependent establishment of glucose uptake potential (**Fig**. **44B**). Addition of heparin on day 4 and beyond had no impact on the adipocytes ability to uptake glucose. Together, these data suggest that a HSPG-dependent signaling event must be occurring around day 3 of adipogenesis which establishes an adipocyte's glucose uptake potential.

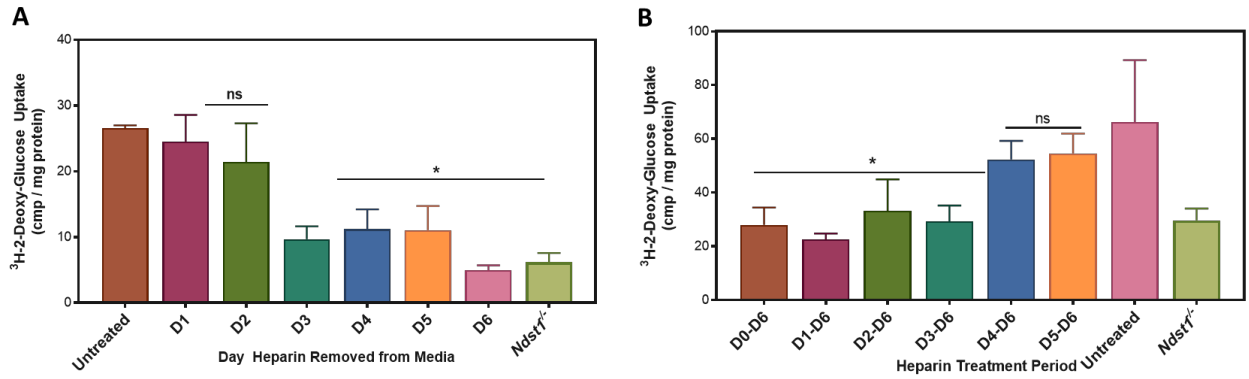

Figure 44. Removal and addition of heparin during adipogenesis of WT MEFs to determine time frame in which heparin impacts glucose uptake potential. All measurements of glucose uptake taken on the final day of differentiation, day 6. A) Heparin Removal: All conditions except untreated and Ndst1$^{-/-}$ cells were initially placed in heparin bearing (100µg/mL) media, and on the indicated day, heparin-bearing media was replaced with heparin-free differentiation media. Glucose uptake potential was significantly reduced if cells were treated up to day 3 and beyond. B) Heparin Addition: All conditions except D0-D6 begin with no heparin in the media. Heparin is added to the differentiation media increasingly late in the differentiation to observe when heparin can no longer impact glucose uptake potential. Glucose uptake potential could only be impacted if heparin treatment begins no later than day 3 of differentiation.

3.2.3 Metabolic impact of inhibition of HSPG interactions

To gain a greater understanding of the impact of inhibiting cell surface HSPG-dependent signaling events in differentiating adipocytes, we compared the metabolic profiles of HSPG inhibited cells to uninhibited WT adipocytes. One striking difference between the untreated WT cells and the HSPG inhibited cells (Both *Ndst1*$^{-/-}$ and WT+ exogenous heparin), is the difference in media coloration. Cellular media is typically pink due to the indicator, phenol red, which becomes increasingly yellow as media acidity rises due to secreted lactic acid, the by-product of glycolysis (**Fig. 45**). HSPG inhibited conditions typically did not induce a discoloration of the pink media, and thus we measured the input and output of glycolysis (glucose and lactic acid respectively), in the media of differentiated adipocytes. Predictably, the untreated WT cells had a far higher concentration of the glycolysis-byproduct lactic acid than the HSPG inhibited cells, while these inhibited cells had a far greater concentration of glucose in the media, indicating a lack of glycolysis (**45B, C**). Considering the reduced reliance on glycolysis for energy among HSPG inhibited cells, we suspected that these cells maybe utilizing oxidative phosphorylation of fats for energy to a greater relative extent compared to control cells. By treating day 8 differentiated adipocytes with isotopically labeled [U-$13C_{16}$] palmitate for 6 hours, we were able to utilize mass spectroscopy to determine the amount of [U-$13C_{16}$] palmitate taken in by cells relative to total palmitate levels, as well as to trace the metabolites sourced from metabolized [U-$13C_{16}$] palmitate (**Fig 45 D-F)**. In agreement with our hypothesis and previous data, the HSPG inhibited cells had an overall greater population of [U-$13C_{16}$] palmitate relative to overall palmitate levels, and the [U-$13C_{16}$] palmitate was utilized significantly more for the generation of metabolites associated with

the citric acid (TCA) cycle, indicating a greater dependence on fats for energy via oxidative phosphorylation among adipocytes which differentiated with inhibited HSPG signaling. This observation corroborates the idea that the reduced amount of fat droplets observed in HSPG inhibited cells versus control comes as a result of the utilization of these fats for energy, and not necessarily a significantly reduced ability for adipocytes to access fats from their environment.

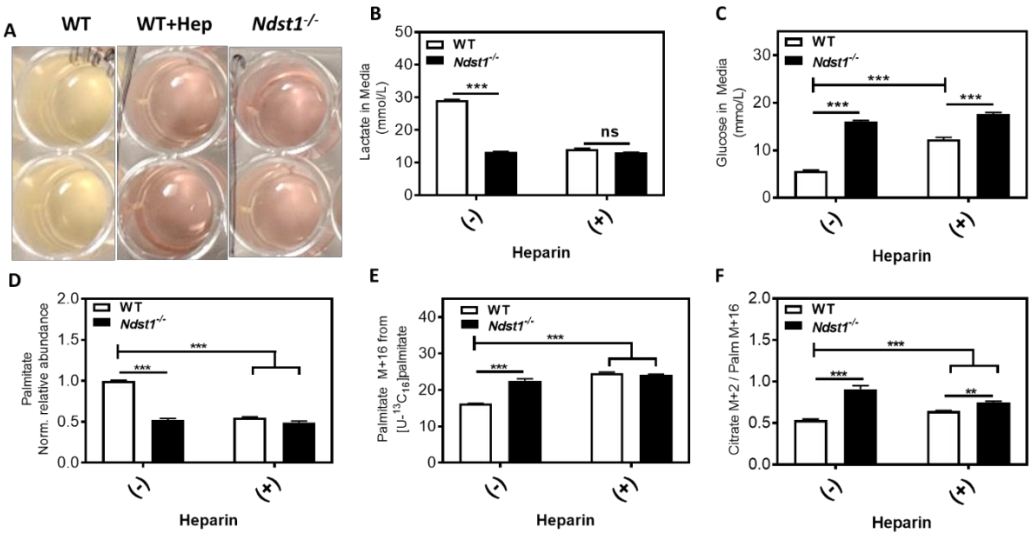

Figure 45. Metabolic impact of HSPG inhibition. A) WT cells produce a greater amount of lactate than *Ndst1*$^{-/-}$ adipocytes, which can be observed by the coloration of the phenol red indicator. B) YSI measurement of lactate in spent media collected on the final day (day 6) of adipogenesis. Fresh media has a concentration of 1.5 mmol/L. C) YSI measurement of glucose in spent media collected on the final day (day 6) of adipogenesis. Fresh media has a concentration of 19 mmol/L. D) Palmitate abundance relative to control WT cells measured using mass spectroscopy, indicating total intracellular palmitate is higher in WT control cells. E) Intracellular [U-13C_{16}] palmitate levels indicate that HSPG inhibited conditions internalize more palmitate than control WT cells. F) Tracing of [U-13C_{16}] palmitate metabolism indicates that palmitate is being converted to citrate more in HSPG inhibited cells than control WT cells, indicating the HSPG inhibited cells are utilizing fatty acids for energy to a greater extent than control cells.

3.2.4 Wnt signaling affects cellular access to glucose

Wnt signaling exerts control over many aspects of cellular metabolism, having roles both inhibiting and inducing adipogenesis depending on the signal context and Wnt protein. Wnt signaling is also effected by HSPG interactions, however the various receptors, coreceptors, and ligands involved in this signaling have not been thoroughly studied in this context. Recently however, It has been shown that Syndecan-1, a cell surface HSPG, interacts with the Wnt coreceptor Frizzled to enhance canonical Wnt paracrine and autocrine signaling.[10,11] Canonical Wnt signaling is initiated by Wnt10a, Wnt5a, or Wnt3a among others, which interact with cell surface lipoprotein-receptor-related protein 5/6 (LRP 5/6) –Frizzled complexes, ultimately preventing the formation of an β-catenin degradation complex which marks intracellular β-catenin for ubiquination. When β-catenin is allowed to accumulate, it is translocated to the nucleus where it binds to the lymphoid-enhancer-binding factor/T-cell specific transcription factor (LEF/TCF) family of transcription factors, which activate Wnt target genes. This activation leads to a reduction of adipogenesis in favor of other lineages, such as osteogenesis. In non-canonical signaling, which can be initiated via Wnt5b, adipogenesis is induced through the inhibition of intracellular canonical Wnt signaling factors.[12,13] Unfortunately, the impact of Wnt signaling (both canonical and non-canonical) is broad in scope and may have unclear impacts on cell fate. Specifically, while canonical Wnt signaling does not favor adipogenesis, it is intimately involved establishing the metabolic profile of cells; and is both directly and indirectly linked to increasing flux through glycoclysis, resulting in the utilization of glucose and glutamine for biosynthetic processes and the production of lactate.[14] To better understand the relevance of Wnt signaling to our HS inhibited

adipocytes, we utilized small molecule Wnt effectors to observe if inhibition or enhancement of Wnt signaling during adipogenesis could lead to the manipulation of glucose clearance capacity, potentially not via the manipulation of adipogenic fate but instead through the manipulation of the metabolic programs Wnt signaling is tied to. We titrated two drugs with opposite effects: LY2090314 which activates Wnt signaling via stabilization of Axin, which is part of an intracellular complex which degrades β-catenin in canonical Wnt signaling, and XAV-939 which destabilizes Axin, allowing for the reduction of canonical Wnt signaling by inhibiting the accumulation of β-catenin (**Fig. 46**).

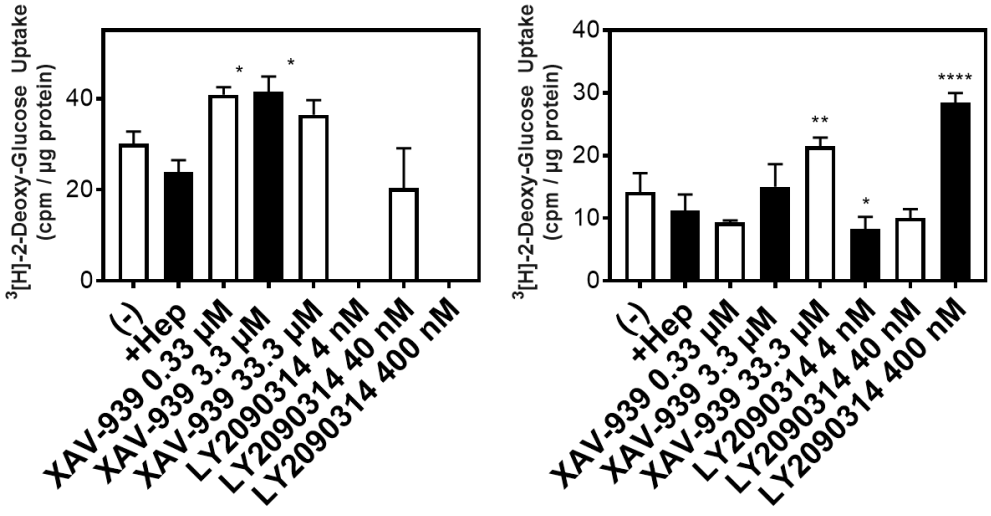

Figure 46. Employment of Wnt activator LY2090314 and Wnt inhibitor XAV-939 impacts glucose clearance capacity. A) In wild type cells, the Wnt inhibitor XAV-939 causes an enhancement of glucose clearance at 0.33 and 3.33 µM, while the Wnt enhancer LY2090314 has little effect. LY2090314 did cause cell monolayers to lift off from cell culture plate, resulting in loss of 4 and 400 nM conditions. B) *Ndst1*$^{-/-}$ cells treated with the Wnt inhibitor XAV-939 results in a slight enhancement in glucose uptake potential, and exerts a trend suggesting a dose response is being achieved. The Wnt signaling enhancer, LY2090314 had a significant ability to enhance glucose clearance capacity in *Ndst1*$^{-/-}$ cells.

Application of Wnt inhibitor XAV-939 lead to enhancement of glucose uptake capacity in both WT and *Ndst1*$^{-/-}$ cells, suggesting that canonical Wnt signaling has a negative impact on glucose uptake potential, although it is unclear if this comes from a reduction in adipogenesis or an enhancement in the cells reliance on glycolysis, or both. When the Wnt activator LY2090314 was applied to cells, there was little effect, except for at the highest concentration of treated *Ndst1*$^{-/-}$ which led to a two-fold enhancement in glucose uptake compared to untreated *Ndst1*$^{-/-}$ cells. Interestingly, this drug did appear to cause noticeable hyper-proliferation in WT cells, which caused the adipose cell monolayer to detach from cell culture plates, preventing their analysis at 4 nM and 400 nM. Taken together, this data begins to suggest the hypothesis that Wnt signaling is at the heart of the metabolic shift from anaerobic respiration to oxidative phosphorylation observed when cellular HSPG interactions are inhibited.

3.2.5 Employment of HS GAG glycopolymers enhances glycolytic cellular metabolism.

Targeted manipulation of cellular glucose uptake capacity has immediate applications in the treatment of diabetes and other hyperglycemic conditions. Considering that HSPG-Wnt-receptor interactions have been demonstrated to enhance Wnt signaling, we investigated if heparin could be used to enhance rather than reduce Wnt signaling. However, when we titrated exogenous heparin treatment from milligram/mL to nanogram/mL concentrations, we were unable positively impact glucose uptake potential in WT or *Ndst1*$^{-/-}$ (**Fig.** 47)

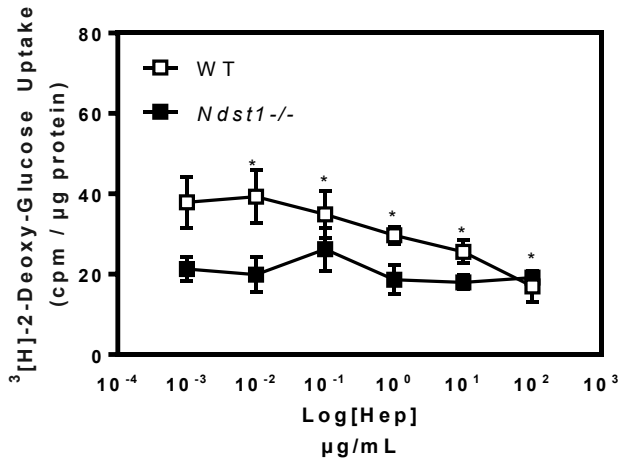

Figure 47. Titration of heparin between 1 ng/mL to 100 µg/mL does not lead to enhancement or rescue of glucose uptake potential when treated throughout differentiation in either WT or *Ndst1*$^{-/-}$ cells.

The inability to enhance this metabolic phenotype using soluble heparin suggested that the HSPG-dependent signaling event which dictates the metabolic programing of the cell may need to occur from cell surface anchored HS GAG, as has been previously observed in a handful of HSPG dependent cellular events.[15,16] Our lab has developed synthetic, HSPG mimetic glycopolymers capable of passively inserting into cellular membranes via a lipid anchor to enhance or rescue HSPG dependent cellular events.[9] These polymers gain their function via the HSPG disaccharides which decorate the length of the polymer, relying on multivalent interactions to compensate for the short GAG fragment length. Each polymer is functionalized with a single type of disaccharide so that the presented structure can be directly linked to the cellular response (**Figure 3.48A)**. By applying these polymers daily for only 1 hour a day, during the identified treatment window (day 0 – day 3) **(Fig 44)**, we were able to restore glucose sensitivity to day 6 *Ndst1*$^{-/-}$ adipocytes beyond WT levels in a dose and sulfation dependent manner (**Fig 48B**).

Excitingly, when we applied these same glycopolymers to differentiating WT cells, we were again able to dose and sulfation dependently enhance glucose uptake potential. (**Fig 3.48C**). When we assessed the media contents of the day 6 *Ndst1*$^{-/-}$ adipocytes from the same glycocalyx remodeling experiment, we found that the lactate production and glucose consumption were also affected in a dose and sulfation dependent manner, with the most effective treatments resulting in the greatest amount of glycolytic metabolic behavior (**Fig 3.48D,E**).

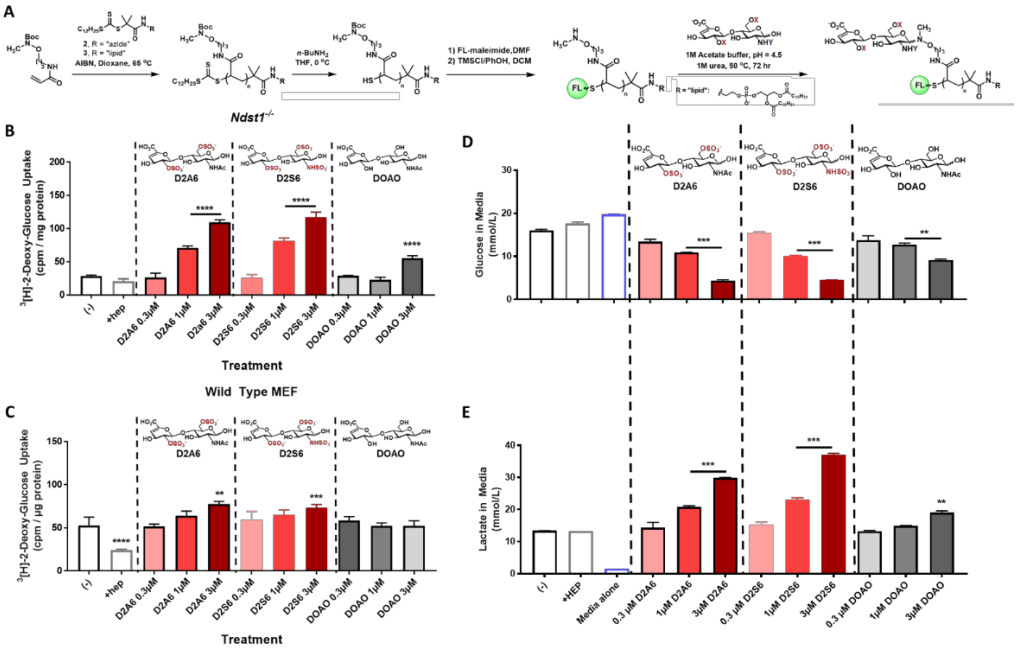

Figure 48. Preparation and application of membrane-incorporating synthetic glycopolymers capable of enhancing glucose uptake on day 6 in differentiated WT and *Ndst1*$^{-/-}$ MEFs A) Polymers are prepared via AIBN initiated RAFT polymerization of Boc-protected N-methlyaminooxypropylacrylamide monomer in the presence of an DPPE-terminated chain transfer agent, resulting in low dispersity polymer (1.19) with n=130 repeating units. The trithiocarbonate group can be removed post-polymerization, and the remaining thiol is conjugated to the fluorophore Alexafluor 488. The fluorescent polymer is then Boc-deprotected using timethylsilyl chloride and phenol to reveal the N-methylaminooxy group, which ligates to the reducing end of GAGs. In the final step of the polymer synthesis, HS GAG disaccharides are ligated to the polymer backbone under acidic conditions. B, C) WT and *Ndst1*$^{-/-}$ cells are treated with glycopolymer for one hour at 37 °C on day 0-3. Sulfated glycopolymers D2A6 and D2S6 are able to dose dependently enhance glucose uptake on day 6, as assessed via a ^{3}[H]-2-deoxy-glucose uptake assay. C,D) The media of treated Ndst1$^{-/-}$ cells was assessed for glucose and lactate concentration using YSI 2900. Cells treated with sulfated glycopolymers show a dose response in terms of the increased utilization of glucose (lowered media concentration) and increased production of the glycolysis product lactate.

3.3 CONCLUSIONS

This work demonstrates and characterizes HSPG's role in establishing the metabolic program for differentiating adipocytes. Within the first four days of *in vitro*

adipogenesis, HSPG-dependent signaling induces the adipocyte to fuel biosynthesis and energy production via anaerobic respiration (glycolysis), while in the absence of HSPG, oxidative phosphorylation is favored. HSPG does not appear to be heavily involved in the process of adipogenesis aside from this critical signaling event, which we suspect comes from Wnt signaling because of its ties to metabolic programming. Indeed, when employed small molecule Wnt effectors, glucose metabolism was readily manipulated, although the details of this signaling event are yet to be revealed. Further study will surely be required to shed light on the details of this event in terms of the mechanism in which HSPG interacts with Wnt proteins and associated surface receptors, as well as to understand the intracellular outcome of this activated signaling. Additional study must also be performed to understand if Wnt activators which induce a glycolytic metabolic profile are simultaneously inhibiting adipogenesis, which could complicate the observations presented in **Fig. 39.** Regardless of the details of the mechanism, we were delighted to find that glycocalyx remodeling using sulfated glycopolymers was capable not only of restoring glucose uptake capacity in *Ndst*$^{-/-}$ cells, but also of enhancing WT cells glucose uptake capacity. Manipulation of cellular glucose sensitivity using a materials-based approach is a novel prospect which bears exciting implications for the treatment of glucose insensitive patients suffering from T2D or hyperglycemia.

\

3.4 MATERIALS AND METHODS

General Biology: MEF cells were grown in monolayer culture in tissue culture treated T25 flasks at 37 °C, 5% CO2. Cells were maintained in DMEM +glucose, +L glutamine with 10% fetal bovine serum. Cells were passaged every 3 days at a ratio of 1:10 after dissociation with 0.25% trypsin-EDTA at 37 °C, 5% CO2, which was neutralized with an equal volume of growth medium. Cells were washed with PBS after the removal of old media. Statistical analysis was performed using Prism software. Error bars refer to standard deviation from the mean and p values were calculated using a one-way ANOVA, $p^* < 0.05$, $p^{***} < 0.001$.

General Chemistry: All chemicals, unless stated otherwise, were purchased from Sigma Aldrich. Purchased starting materials were used as received unless otherwise noted. Glycans were purchased from Iduron (Manchester, UK), V-labs (Covington, LA) or Carbosynth (San Diego, CA). Glycosaminoglycan nomenclature used here is decribed in Lawrence et al.[171] Anhydrous dioxane was generated via filtration through basic alumina. Polymers were isolated by gel filtration on Sephadex G-25 columns (PD-10, GE Healthcare). Nuclear magnetic resonance (NMR) spectra were collected on a Bruker 300MHz NMR spectrometer. Spectra are reported in parts per million (ppm) on the δ scale relative to the residual solvent as an internal standard. Size exclusion chromatography (SEC) was performed on a Hitachi Chromaster system equipped with an RI detector and an 8μm, mixed bed, 300 x 7.5 mm cm PL aquagel-OH mixed medium column.

3.4.3 Cellular Experiments

Oil Red O Assay: MEFs differentiated to day 6 into adipocytes in a 24 well plate are washed twice with PBS, then fixed in 4% paraformaldehyde for 10 minutes. The cells are then washed twice with PBS and once with MilliQ water before being then incubated for 1 minute in 60% isopropanol. Then, the oil red working solution is placed on the cells for 8 minutes. The working solution is prepared from an Oil Red O stock solution consisting of 0.5 g Oil Red O in 100 mL isopropanol which has been heated to 56 °C until the Oil Red O has dissolved. The working solution is prepared by taking 30 mL of stock solution and adding to 20 mL distilled water. The mixture must stand for at least 10 minutes then be filtered before use. After the 8 minute incubation, cells are incubated in 50% isopropanol for 1 minute, followed by another 1 minute incubation in 10 % isopropanol, then MilliQ water, followed by tap water. After each of these 1 minute incubations, the fixed, stained cells are placed in MQ water and imaged. The water is removed, and the wells are allowed to dry. The stain can then be eluted in 200µL 100% isopropanol over a 10 minuted incubation period. The eluted stain is then placed into a 96 well plate, and absorbance is measured at 500 nm.

MTT Assay: MEFs differentiated to day 6 into adipocytes in a 24 well plate, and on day 6 cells are treated with 50 µL of the Cytoselect MTT assay preformulated reagent, which is added directly to media. The cells are incubated in this mixture for 4 hours as violet precipitates form. The cells are then treated with 500µL of the supplied detergent solution for 2 hours, and wells are agitated with pipetting to enhance the dissolution of the precipitate. The detergent with dissolved precipitate is then moved to a fresh 24 well plate and absorbance is measured at 570 nm.

^{3}[H]-2-Deoxy-Glucose Uptake Assay Cells are washed twice with PBS, and placed into DMEM with 2 mg/mL BSA for two hours. Then, if cells are to be insulin stimulated, they are treated with 200 nM insulin for 30 minutes at 37 °C in freshly prepared transport solution consisting of 137 mM NaCl, 1.2 mM MgSO4, 1.2 mM KH2PO4, 4.7 mM KCl, 2.5 mM CaCl2, and 20 mM HEPES with a pH of 7.3. The insulin solution is then removed and the cells are washed twice with transport solution before radioactive transport solution is added, which consists of .25μCi/well of ^{3}[H]-2-deoxy-glucose and 0.025 mM 2-deoxy-glucose. After a 10 minute incubation in the radioactive transport solution, it is removed and the , the glucose uptake is halted by addition of ice cold PBS. The cold PBS is removed and each well is washed twice with PBS. Then, lysis buffer consisting of 0.1 M NaOH and 0.1% w/v sodium dodecyl sulfate, is added to each well. The radioactive lysate was transferred to a scintillation vial containing 5 mL of Ultima Gold liquid scintillation fluid and analyzed using a liquid Scintillation counter.

Palmitate Tracer Study: MEF cells on day 8 of adipogenesis were incubated for 6h in 100uM [U-$^{13}C_{16}$]Palmitate. The media contained 10% delipidated FBS and 5% (v/v) of a BSA-conjugated [U-$^{13}C_{16}$]Palmitate stock. To make the stock, briefly, 100mM [U-$^{13}C_{16}$]Palmitic acid was dissolved in ethanol at 50C. A solution of 4.4% essentially FA-free BSA (Sigma) in PBS was warmed to 37 °C. A 50:1 mixture BSA:Palmitate solution was made and incubated at 37 °C for 1-2 hours before aliquoting and freezing in glass tubes. The stock contains a 3:1 FA:BSA ratio. After incubation, cells are lysed on ice and prepared for GC-MS analysis, as previously reported.[18]

^{14}C-Palmitate Uptake Assay: Cells are washed twice with PBS, and placed into DMEM with 2 mg/mL BSA for two hours. During this time, 14C-palmitic acid is complexed with BSA at a molar ratio of 1:1 for 30 minutes. After the cells have been starved for 2 hours, the cells washed twice with PBS and incubated in radioactive transport solution (see 2-deoxyglucose uptake assay for contents of transport solution) with 1 µCi/well ^{14}C-palmitic acid:BSA for 10 minutes. After a 10 minute incubation in the radioactive transport solution, it is removed and the glucose uptake is halted by addition of ice cold PBS. The cold PBS is removed and each well is washed twice with PBS. Then, lysis buffer consisting of 0.1 M NaOH and 0.1% w/v sodium dodecyl sulfate, is added to each well. The radioactive lysate was transferred to a scintillation vial containing 5 mL of Ultima Gold liquid scintillation fluid and analyzed using a liquid Scintillation counter.

Adipogenesis: Cells are seeded into a 24 well plate at a density of 30,000 cells/cm^2. Cells are allowed to grow to confluence for 48 hours, at which point the media is switched to differentiation media (day 0). Differentiation media consists of 0.1 µM dexamethasone, 450 µM 3-isobutyl-1-methylxanthine, 2 µM insulin, and 1 µM rosiglitazone in DMEM with 10% FBS. On day 3, cells are washed with PBS and treated with insulin media, which consists of 2 µM insulin, and 1 µM rosiglitazone in DMEM with 10% FBS.

Heparin Addition Experiment: Cells are subjected to typical six day differentiation protocol. All conditions except untreated and Ndst1$^{-/-}$ cells were initially placed in heparin bearing (100µg/mL) media, and on the indicated day, heparin-bearing media was

replaced with heparin-free differentiation media. On day 6 of the differentiation, glucose uptake is measured using a ^{3}[H]-2-deoxy-glucose uptake assay.

Heparin Withdrawal Experiment: Cells are subjected to typical six day differentiation protocol. All conditions except D0-D6 begin with no heparin in the media. Heparin is added to the differentiation media on the indicated day, and heparin treatment continues until day 6 once it has begun. On day 6 of the differentiation, glucose uptake is measured using a ^{3}[H]-2-deoxy-glucose uptake assay.

Insulin Stimulation: MEFs differentiated to day 6 into adipocytes in a 24 well plate in the presence or absence of exogenous heparin (100 µg/mL), and on day 6 cells are washed with PBS and serum starved for 2 hours in DMEM with 2 mg/mL BSA. After 2 hours, each well is stimulated with insulin at a final concentration of 10 nM, with the insulin delivered directly to the serum free media as a 10 µL aliquot. The plate in then place into an incubator at 37 °C for the indicated amount of time. After stimulation, the entire 24 well plate is placed on ice, and the wells are washed with ice cold PBS twice. Then, 100µL RIPA buffer with protease inhibitor (PIC) and phosphostop is added to each well. The cell lysate is collected into an eppendorf, placed on ice for 30 minutes, and then centrifuged at 14,000 xg at 4 °C for 15 minutes. The supernatant is then transferred to a fresh tube and protein concentration is determined using a BCA assay.

3.4.4 Procedure and characterization data for the synthesis of glycopolymers

Synthesis and characterization of Glycopolymers See chapter 2 materials and methods section.[9] The lipidated polymer backbone has a molecular weight of 41,238 g/mol and was synthesized to a degree of polymerization of n=160, with dispersity of 1.19.

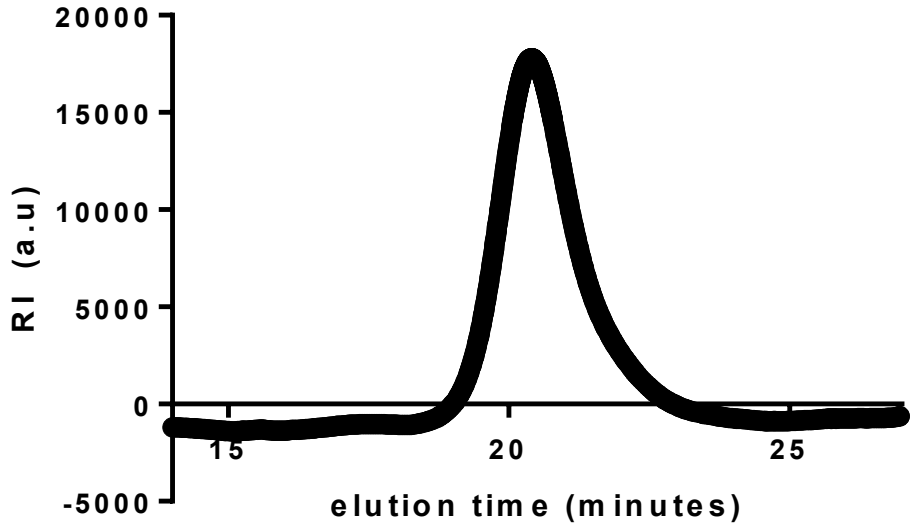

Figure 49 GPC trace of lipidated polymer backbone used for NeoPG synthesis. Number average molecular weight= 41,238 n= 160, dispersity= 1.19.

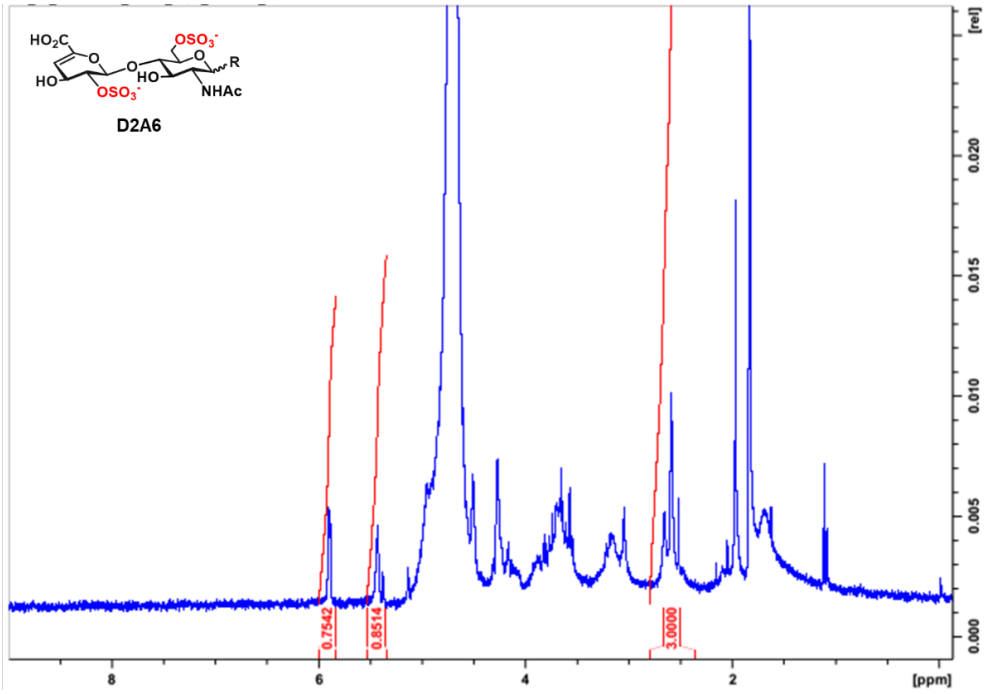

Figure 50 ^{1}H NMR (300 MHz, D_2O) of D2A6 glycopolymer with 75% ligation efficiency of D2A6 to polymer side chains.

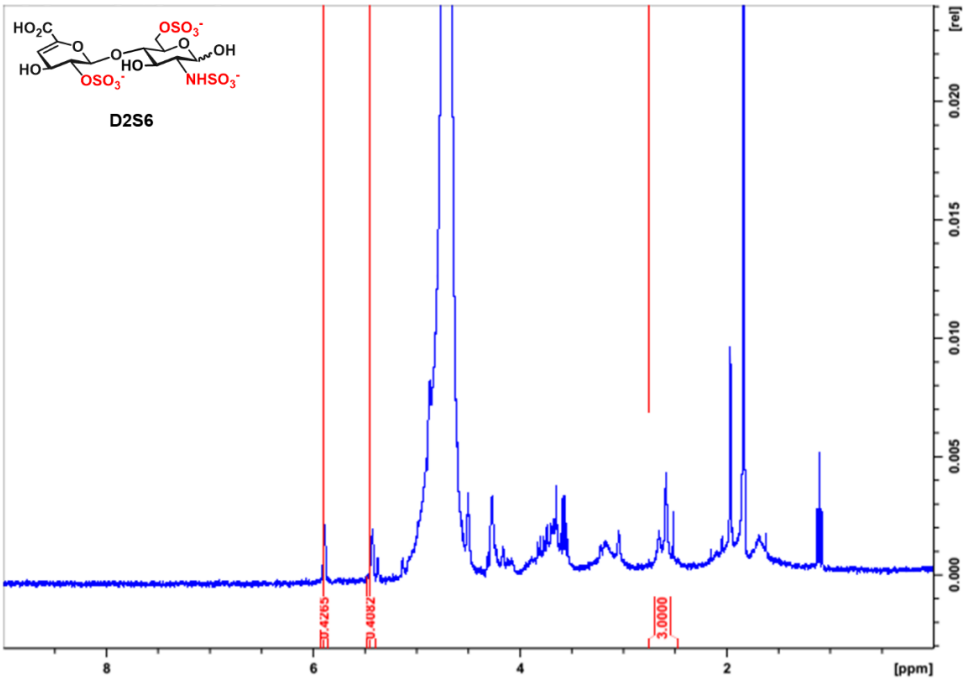

Figure 51 ^{1}H NMR (300 MHz, D_2O) of D2S6 glycopolymer with 43% ligation efficiency of D2A6 to polymer side chains.

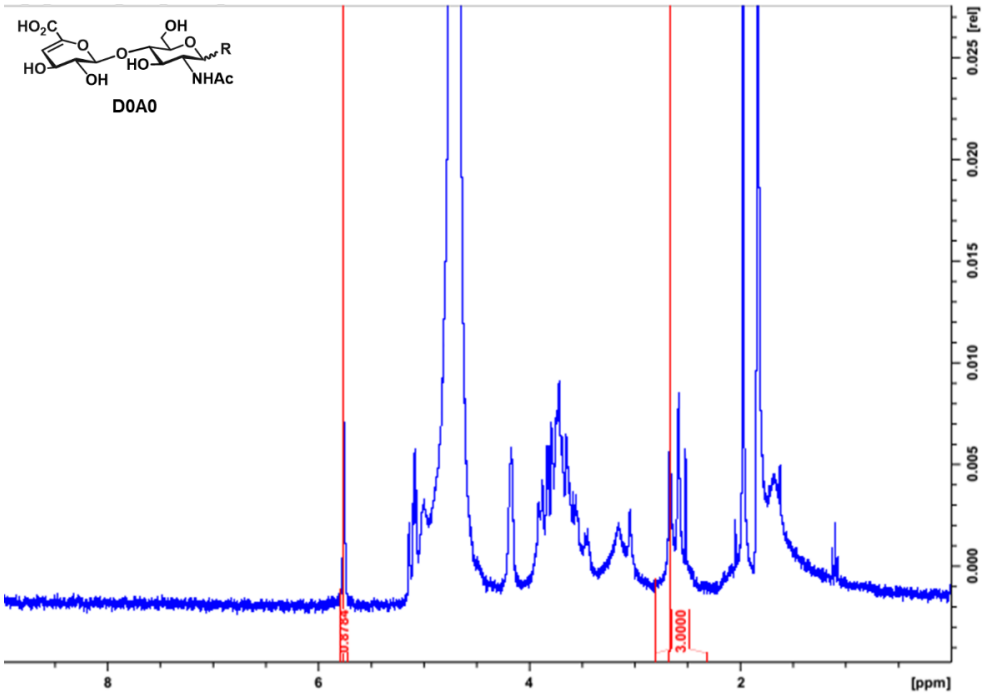

Figure 52 ^{1}H NMR (300 MHz, D_2O) of D0S0 glycopolymer with 88% ligation efficiency of D2A6 to polymer side chains.

Glycocalyx Remodeling: Cells are subjected to typical differentiation protocol. On day 0, day 1, day 2 and day 3, media is removed, wells are washed with PBS, and a 200µL solution of DMEM with glycopolymer is placed in each well and incubated for 1 hour at 37 °C. After the incubation, the solution is removed, the cells are washed once with PBS, and media is replaced. On day 6, the impact of the glycocalyx remodeling is measured using a ^{3}[H]-2-deoxy-glucose uptake assay as well as with YSI measurements of glucose and lactate in the spent media.

3.4.5 Collection of cellular protein and media components for analysis

Western Blot Analysis: Cells were lysed using RIPA buffer, and protein was quanitified using a BCA assay. Protein was analyzed by SDS-PAGE on 4–12% Bis-Tris gradient gels (NuPage; Invitrogen) with an equal amount of protein loading. Proteins were visualized after transfer to Immobilon-FL PVDF membrane (Millipore). Membranes were blocked with Odyssey blocking buffer (LI-COR Biosciences) for 30 min and incubated overnight at 4°C with respective antibodies. Goat, mouse, and rabbit antibodies were incubated with secondary Odyssey IR dye antibodies (1:14,000) and visualized with an Odyssey IR imaging system (LI-COR Biosciences).

Media Analysis of Glucose and Lactate by YSI 2900: MEFs are differentiated to day 6 into adipocytes in a 24 well plate, and on day 6 500µL of media is collected from each well in an Eppendorf tube and immediately frozen in liquid nitrogen. Once all samples are collected, the frozen samples are thawed on ice and filtered through an Amicon ultra 3000 molecular weight cut-off centrifugal filter at 4 °C. Then, the filtrate is analyzed using a YSI 2900, where the sample is loaded into two wells of a 96 well plate, 200µL media per well. The samples are then analyzed for lactate and glucose concentration.

Membrane isolation: Membrane isolation was performed according to previously published procedures[19]. Breifly, Cells from 10-cm dishes were washed with ice-cold PBS, then scraped in 1 mL hypotonic lysis medium (HLM) containing 50 mM HEPES, 50 mM sucrose, 1 mM EDTA, 100 mM NaCl and 1 x PIC and were lysed using a Dounce

homogenizer (~50 strokes). Lysates were centrifuged at 5000 g, 4 °C for 10 min. The supernatant was centrifuged at 100,000 g, 4 °C for 30 min. The resulting supernatant represented the cytosolic fraction; membrane pellets were resuspended in RIPA buffer with 1 x PIC for Western blotting.

3.5 ACKNOWLEDMENT

Chapter 3 contains data which will compose an upcoming manuscript. The authors are Trieger G. W., Pressentheiner A. R., Green C. R., DeForest N., Majithia A., Metallo C. M., Godula K., Gordts P. L. S. M. The dissertation author was the primary investigator and author of this paper.

3.6 REFERENCES

[1] Olokoba, A. B.,Olusegun, A. O., Olokoba, L. B. *Oman Med J.* **2012**, 27, 269-273. Type 2 diabetes mellitus: a review of current trends.

[2] Gesta S, Blüher M, Yamamoto Y, Norris, A. W., Berndt J., Kralisch S., Boucher J., Lewis C. Kahn C. R. *Proc Natl Acad Sci*. **2006**, 103, 6676 – 6681. Evidence for a role of developmental genes in the origin of obesity and body fat distribution.

[3] Li K., Xu X., Hu W., Li M., Yang M., Wang Y., Luo Y., Zhang X., Liu H., Li L., Yang G. Acta Diabetol, **2014**, 51, 981-990. Glypican-4 is increased in human subjects with impaired glucose tolerance and decreased in patients with newly diagnosed type 2 diabetes.

[4] Ussar S., Bezy O., Bluher M., Kahn C. R. *Diabetes*, **2012**, 61, 2289-2298. Glypican-4 enhances insulin signaling via interaction with the insulin receptor and serves as a novel adipokine.

[5] Filmus J., Capurro M., Rast J. *Genome Biol.* **2008,** 9, 224-230. Glypicans.

[6] Lindahl U., Couchman J., Kimata K., Esko J. D. . *Essentials of Glycobiology,* 2nd ed.; CSHL Press: New York, **2009**. Chapter 17: proteoglycans and sulfated glycosaminoglycans.

[7] Gordts P. L. S. M., Esko J. D. *Matrix Biology*, **2018**, 71-72, 262-282. The heparan sulfate proteoglycan grip on hyperlipidemia and atherosclerosis.

[8] Wilsie L. C., Gonzales A. M., Orlando R. A., *Lipids Health Dis.* **2006**, 5, 23-37. Syndecan-1 mediates internalization of apoE-VLDL through a low density lipoprotein receptor-related protein (LRP)-independent, non-clathrin-mediated pathway.

[9] Huang M. L., Smtih R. A. A., Trieger G. W., Godula, K. *J. Am. Chem. Soc.* **2014**, 136, 10565-10568. Glycocalyx remodeling with proteoglycan mimetics promotes neural specification in embryonic stem cells.

[10] Alexander C. M., Reichsman F., Hinkes M. T., Lincecum J., Becker, K. A., Cumberledge S., Bernfield M. *Nat Genet.* **2000**, 25, 329-332. Syndecan-1 is required for Wnt-1-induced mammary tumorigenesis in mice.

[11] Rem Z., vanAndel H., de Lau W., Hartholt R. B., Maurice M. M., Clevers H., Kersten M. J., Spaargaren M., Pals S. T. *Blood,* **2018**, 131, 982-994

[12] Kanazawa A., Tsukada S., Kamiyama M., Yanagimoto T., Makajima M., Maeda S. *Biochem Biphys Res Commun.,* **2005**, 330, 505-510. Wnt5b partially inhibits canonical Wnt/beta-catenin signaling pathway and promotes adipogenesis in 3T3-L1 preadipocytes.

[13] Christodoulides C., Lagathu C., Jaswinder S. K., Vidal-Puig A. *Cell*, **2009**, 1, 16-24. Adipogenesis and WNT signaling.

[14] Sethi, J. K., Vidal-Puig A. *Biochem J.* **2010**, 427, 1-17. Wnt signalling and the control of cellular metabolism.

[15] Wallace B. G. *J. Neurosci*. **1990**, 10, 3576-3582. Inhibition of agrin-induced acetylcholine-receptor aggregation by heparin, heparan sulfate, and other polyanions.

[16] Huang M. L., Tota E. M., Lucas T. M., Godula K. *ACS Chem Neurosci*. **2018**, 9, 3086-3093. Influencing early stages of neuromuscular junction formation through glycocalyx engineering.

[17] Lawrence, R.; Lu, H.; Rosenberg, R. D.; Esko, J. D.; Zhang, L. *Nature Methods* **2008**, *5*, 291-2.

[18] Wallace M., Green C. R., Roberts L. S., Lee Y. M., McCarville J. L., Sanchez-Gurmaches J., Meurs N., Gengatharan J. M., Hover J. D., Phillips S. A., Ciaraldi T. P., Guertin D. A., Cabrales P., Ayres J. S., Nomura D. K., Loomba R., Metallo C.M. *Nat*

Chem Biol. **2018**, 14, 1021-1031. Enzyme promiscuity drives branched-chain fatty acid synthesis in adipose tissues.

[19] Xia W., Pessentheiner A. R., Hofer D. C., Amor M., Schreiber R., Schoiswohl G., Eichmann T. O., Walenta E., Itariu B., Prager G., Hackl H., Stulnig T., Kratky D., Rülicke T., and Bogner-Strauss J. G. *Cell Reports*, **2018**, 23, 1948-1961. Loss of ABHD15 impairs the anti-lipolytic action of insulin by altering PDE3B stability and contributes to insulin resistance.

CHAPTER 4: Efficient synthesis of heparinoid bioconjugates for tailoring FGF2 activity at the stem cell–matrix interface

4.1 INTRODUCTION

The regulation of growth factor (GF) associated cellular proliferation and differentiation continues to be the focus of intense research in the areas of tissue engineering and regenerative medicine.[1] Integral to these efforts is the development of new biomaterials capable of delivery and tuning of GF activity in the cellular context.[2] The functions of GFs are influenced by the extracellular matrix (ECM) microenvironment, which is abundant in sulfated glycosaminoglycan (GAG) polysaccharides, such as heparan sulfate (HS), attached to core polypeptide backbones of proteoglycans (PGs). HS is a polymer composed of disaccharide repeat units of glucosamine and uronic acid modified by sulfate groups on specific nitrogen and oxygen atoms, which provide high-affinity binding sites for various GFs and modulate their activity (**Fig. 53**).[3] While the arrangement of sulfation patterns in HS provides a molecular basis for affinity and selectivity in GF binding, the distribution of these molecules across the cell-matrix interface determines whether a GF signaling event will be promoted or attenuated (**Fig. 53**). In the cellular glycocalyx, cell surface PG-associated HS promotes GF interactions with membrane receptors; however, when shed and deposited into the ECM, HS can sequester GFs away from the cell surface and downregulate signaling (**Fig. 53**).[4] Consequently, HS offers a useful, tunable element for controlling GF-mediated signaling, provided that its influence on cellular activity is properly considered in the context of their presentation within the cellular microenvironment.[5,6]

While approaches for tailoring GAG-GF interactions directly within the cellular glycocalyx have begun to emerge,[7,8,9] more commonly GAGs are integrated into biomaterials for ECM engineering applications.[6] Heparin, a highly sulfated analog of HS with affinity for a broad spectrum of GFs, has been a popular choice for a functional component in biomaterials for GF delivery and release.[6,10,11,12] The biological activities of heparin (**hep**) can be modulated through selective chemical de-sulfation[13] at the C6 hydroxyl of glucosamine (**6ODSH**), C2 hydroxyl of iduronic acid (**2ODSH**), or at the C2 nitrogen atom of glucosamine (**NDSH**, **Fig. 53**). Reacetylation of the free amine groups in **NDSH**, which still contains 2-*O*- and 6-*O*- sulfates, then gives rise to the heparin analog, **NAcH** (**Fig. 53**). The removal of sulfates from heparin alters the ability of the resulting heparinoids to engage GFs. For instance, the binding of the fibroblast growth factor 2 (FGF2) decreases in the following order: **hep** > **6ODSH > 2ODSH >> NDSH ~ NAcH**.[14] Therefore, these polysaccharides are well-suited as components for biomaterials to control FGF2 activity and the associated cell mitogenicity and proliferation.

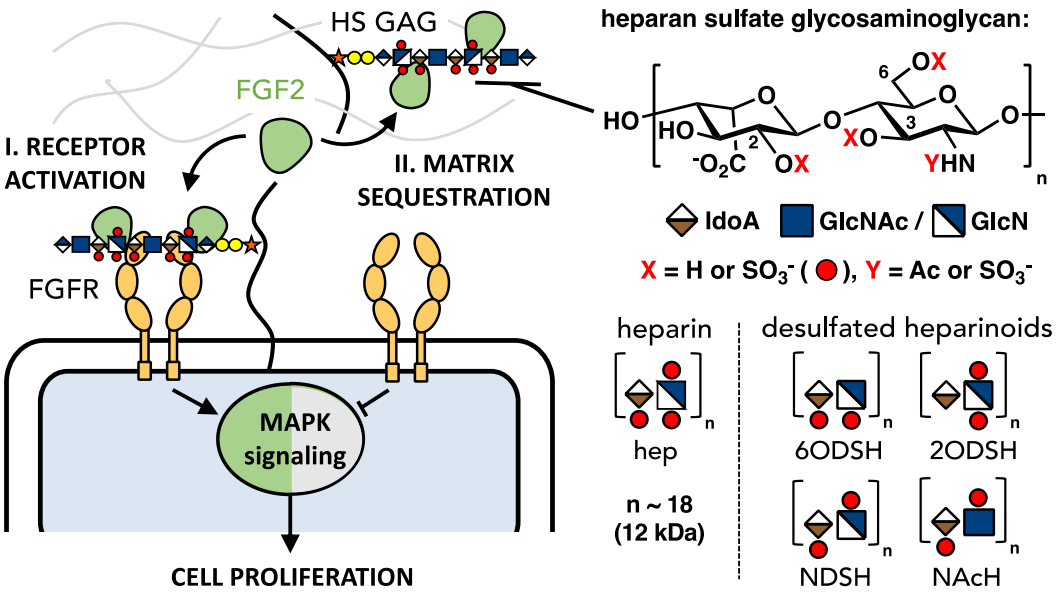

Figure 53. Heparan sulfate (HS) glycosaminoglycans (GAGs) regulate FGF2 activity at the cellular boundary. Cell surface HS facilitates the activation of FGF receptors (FGFRs) and promotes cell proliferation. Extracellular matrix (ECM) HS sequesters FGF2 away from the cell surface and inhibits proliferation. Selective chemical desulfation of heparin, a highly sulfated HS, yields heparinoids with distinct FGF2 binding profiles.

a behavior.[15,16,17,18,19] The most commonly used strategy for covalent incorporation of GAGs into biomaterials makes use of the preponderance of carboxylic acid groups or, to a lesser extent, amino groups released by chemical *N*-desulfation along the polysaccharide chain, which are both suitable for conjugation via amide bond formation (**Fig 54**).[20, 21,22] The high frequency of these reactive side chain groups limits control over the number and location of covalent modifications with individual polysaccharide molecules and may obscure sulfated regions required for HS bioactivity. Alternatively, amino acid residues that remain at the reducing ends of GAGs released from proteoglycans by peptidase treatment can be modified selectively under mild conditions using amide coupling conditions;[23] however, GAGs are often subjected to β-elimination

to remove the peptide fragments and expose the glycan reducing end, thus limiting the generality of this approach. The unique reactivity of the reducing end offers an opportunity for single regiospecific chain functionalization outside of the sulfated regions via reductive amination (**Fig 54**)[24,25] or ligation with α-heteroatom nucleophiles, such as oximes or hydrazides.[20] Due to the requirement for large amounts of polysaccharides for their coupling to other macromolecules, these methods are often not amenable to the conjugation of scarcely available GAGs.

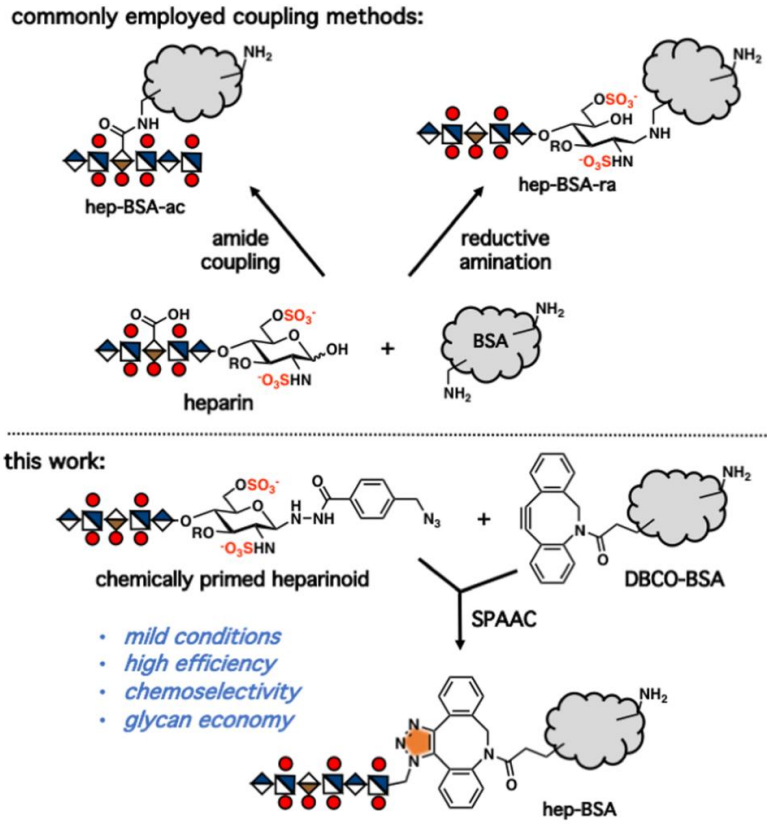

Figure 54. Common techniques for generating heparin bioconjugates include crosslinking of solvent exposed lysine residues on proteins (e.g., BSA) with either pendant carboxylic acid groups along the polysaccharide chain (amide coupling) or through its reducing end (reductive amination). The strain-promoted alkyne-azide cycloaddition (SPAAC) between chemically primed heparinoids and cyclooctyne-modified proteins offers a highly efficient chemoselective alternative to the existing methods.

In order to remedy the issues of GAG presentation and glycan economy posed by the currently used conjugation techniques, we turned our sights towards the use of “click” chemistries. Bioorthogonal chemical ligation strategies, such as the copper-catalyzed[26] or strain-promoted[27] alkyne-azide cycloaddition (CuAAC and SPAAC, respectively) between alkynes and organic azides, exhibit fast kinetic profiles that allow for the efficient joining of biomacromolecules,[28,29] including GAGs,[30,31,32,33] under physiological conditions. A mild chemoselective strategy for covalently linking GAGs to proteins would expand the utility of these biologically important molecules in ECM engineering, as large comprehensive libraries of structurally well-defined GAG oligo- and polysaccharides are becoming increasingly available through chemoenzymatic synthesis[34] and glycosylation engineering.[35,36,37] Here, we report an efficient method for the ligation of variously sulfated heparinoids to protein carriers using a SPAAC-based conjugation strategy (Fig 54). We demonstrate the utility of the resulting bioconjugates as ECM proteoglycan models capable of controlling FGF2 activity and human mesenchymal stem cell (hMSC) proliferation in culture according to their patterns of sulfation.

4.2 RESULTS AND DISCUSSION

4.2.1 Preparation of reactive Heparinoid and BSA click conjugates

We initiated our study by identifying conditions under which a hydrazide ligation to the reducing ends of HS chains could serve as an efficient chemo- and regioselective method for the formation of heparinoid-protein conjugates. The direct coupling of heparinoids to macromolecules chemically modified to present hydrazide groups generally suffers from low efficiency.[20] Under equilibrium, the formation of the hydrazide adduct is disfavored by the low concentration of the reactive aldehyde form of the polysaccharide reducing end as well as by the size of the two macromolecular coupling partners, which is exacerbated by the high negative charge density of HS. We reasoned that the conjugation process would be more effective if it were accomplished in two steps by first priming the GAG chain reducing end with a small azide-containing handle followed by coupling to cyclooctyne-modified proteins via the rapid and irreversible SPAAC reaction.

Using heparin (Mw ~ 12kDa) as a model for HS GAGs, we first optimized the chain-end pre-functionalization step (Fig 55A). Priming of heparin was achieved by heating the polysaccharide with 4-azidomethyl benzhydrazide[38] (**1**, 6.5 equiv.) at 50 °C for 72 hrs under acidic conditions (1:1 acetate buffer/DMSO, pH = 5.5). After neutralization, the heparin derivative was purified by dialysis against water to remove unreacted linker **1**, salts, and the DMSO co-solvent. ^{1}H-NMR analysis of the purified heparin product **2-hep** in D_2O clearly indicated the presence of a new broad signal at ~ 7.5 ppm corresponding to the aromatic protons of the 4-azidomethyl benzhydrazide end group (Fig 54); however, the low abundance of the end modification NMR signals with respect to those of the heparin polysaccharide chain made accurate determination of the reaction efficiency

difficult. The reaction conditions were also effective for introducing the azidomethyl benzhydrazone handle into commercially available **6ODSH**, **2ODSH**, **NDSH**, and **NAcH** heparin derivatives derived by chemical desulfation of the parent heparin polysaccharide (Fig. 70-Fig 74).

4.2.2 *Preparation of heparinoid-BSA conjugates*

Having derived chemically primed heparinoids **2**, we next evaluated the SPAAC conjugation of the azide-terminated heparin (**2-hep**) to bovine serum albumin (BSA), a model protein carrier, modified with complementary cyclooctyne functionality (Fig 56). We chose BSA based on its previously demonstrated suitability for generation of synthetic neoglyconjugates.[39,40,41] The treatment of BSA with dibenzocyclooctyne-PEG_4-*N*-hydroxysuccinimidyl ester (DBCO-PEG_4-NHS, 8 equiv.) in sodium bicarbonate buffer (100 mM, pH = 8.0) overnight resulted in covalent functionalization of solvent exposed lysine side chains in BSA. MALDI analysis of the resulting DBCO-BSA conjugate **3** indicated the introduction of ~ 6 DBCO residues per BSA molecule (Fig 8B). The DBCO-BSA conjugate **3** can be further treated with NHS-biotin (21 equiv.) in bicarbonate buffer (100 mM, pH = 8.0) overnight to incorporate biotin handles for quantification in downstream applications (**3-biotin**, ~ 19 biotins per BSA by MALDI, Fig 55).

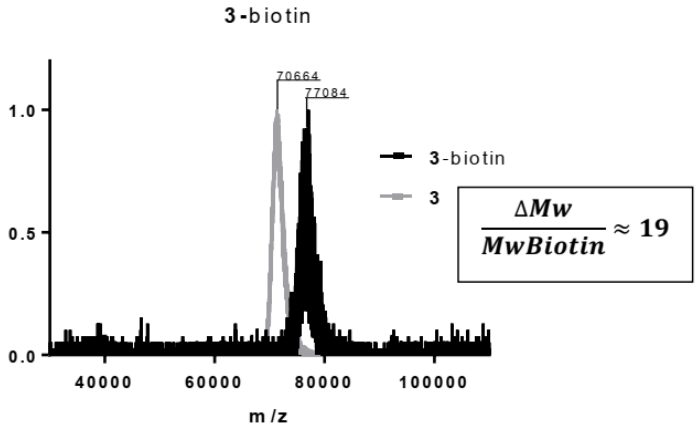

Figure 55. MALDI-TOF spectra of DBCO-BSA conjugates **3** and **3-biotin.**

The appropriately functionalized azide-heparin (**2-hep**) and DBCO-BSA (**3**) coupling partners could now be joined together to generate the desired heparin-BSA conjugate. The two components (0.5 μM, 1 equiv. of **2-hep** per DBCO residues in **3**) were allowed to react in PBS at ambient temperature for 48 hrs. The crude heparin-BSA (**hep-BSA**) adduct was purified by spin-dialysis (25kDa MWCO) and ion-exchange to remove unreacted **2-hep** and **3**, respectively, and analyzed by size exclusion chromatography (SEC, **Fig. 56**, **Fig. 57**). Composition analysis of the purified neoglycoprotein product using carbazole and BCA assays revealed that the reaction proceeded to completion. This garnered BSA molecules decorated with ~ 6 pendant heparin chains, matching the number of reactive cyclooctyne residues in **3** (**Fig. 58**). The remaining desulfated heparinoids **2** were subjected to the optimized coupling conditions to yield the desired panel of heparinoid-BSA conjugates (**6ODSH-**, **2ODSH-**, **NDSH-**, and **NAcH-BSA**, Fig 4.3C). For biological experiments (*vide infra*), only partial purification of the crude bioconjugates by spin-filtration (25kDa MWCO) was required to eliminate the

contributions of unreacted heparinoids **2**, thus limiting the need for laborious isolation sequences and large quantities of expensive or scarce GAG materials.

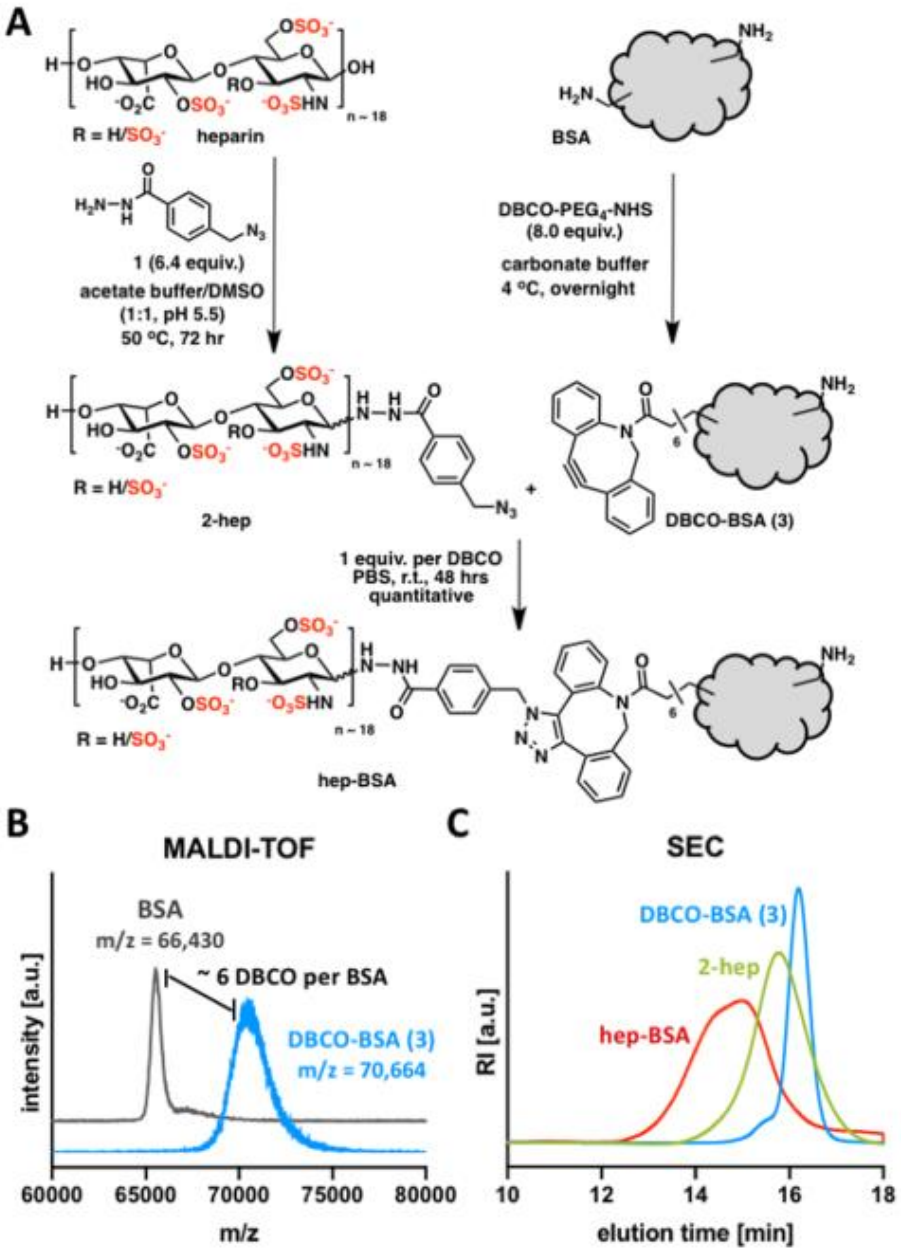

Figure 56. Synthesis and characterization of heparin-BSA conjugate (hep-BSA). A) Hep-BSA synthesis via a reducing end priming with azidomethyl benzhydrazide (1) followed by SPAAC reaction between the resulting azido-heparin (2-hep) and DBCO-BSA (3). B) MALDI analysis of 3 indicated ~ 6 DBCO groups per BSA molecule. C) SEC traces for 3 (blue), 2-hep (green) and purified hep-BSA (red).

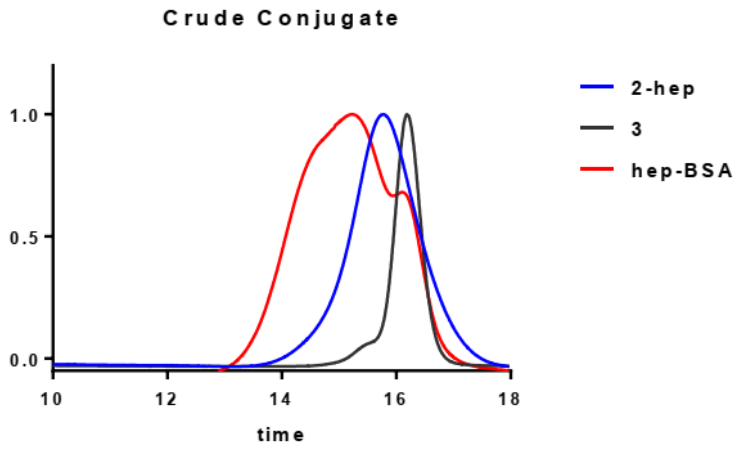

Figure 57. SEC traces of **2-hep, 3** (DBCO BSA) and crude **hep-BSA** with unreacted **3.**

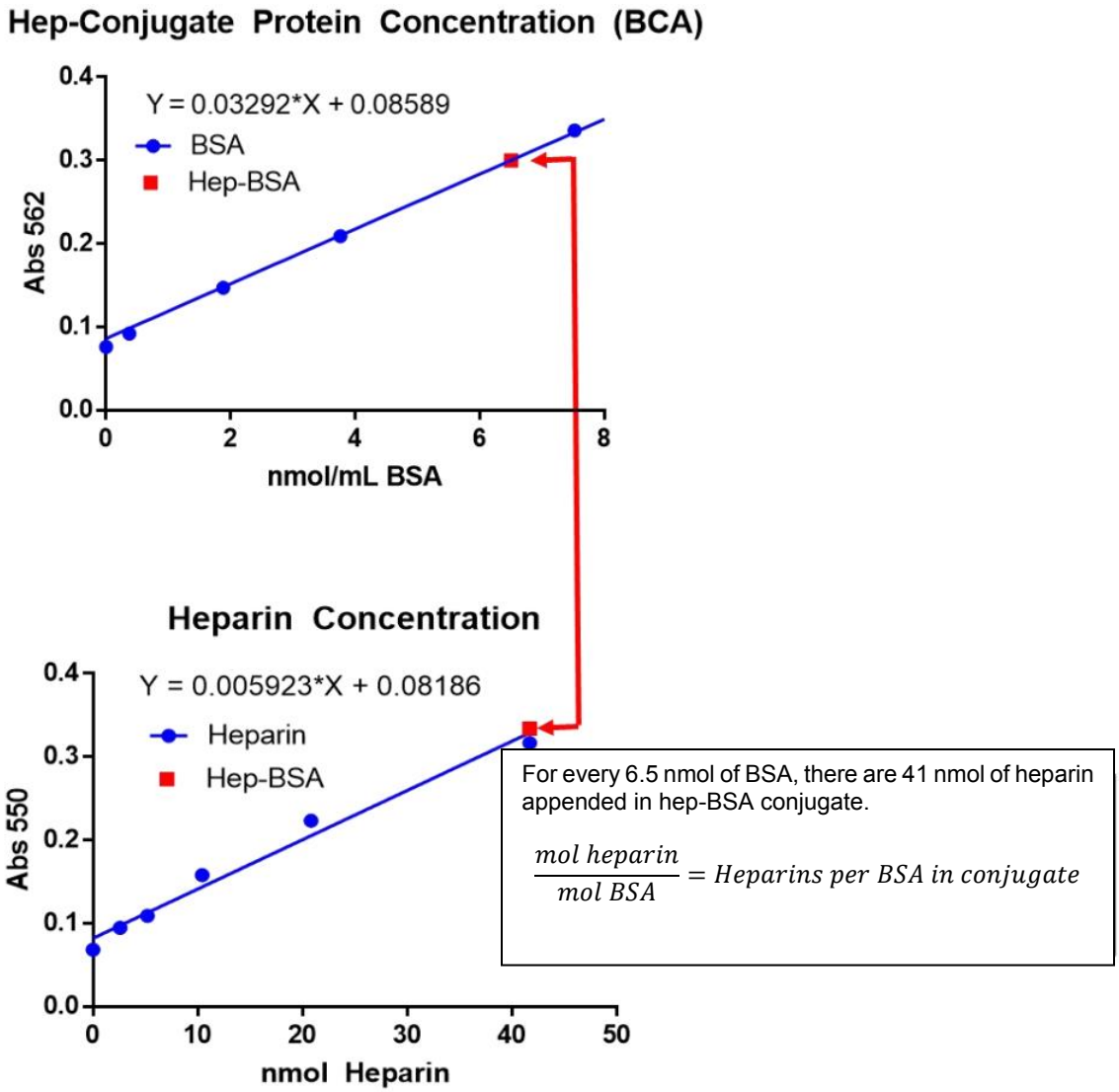

Figure 58. Analysis of **Hep-BSA** composition based on BCA and carbazole assays.

4.2.3 Preparation and characterization of heparinoid displays on surfaces

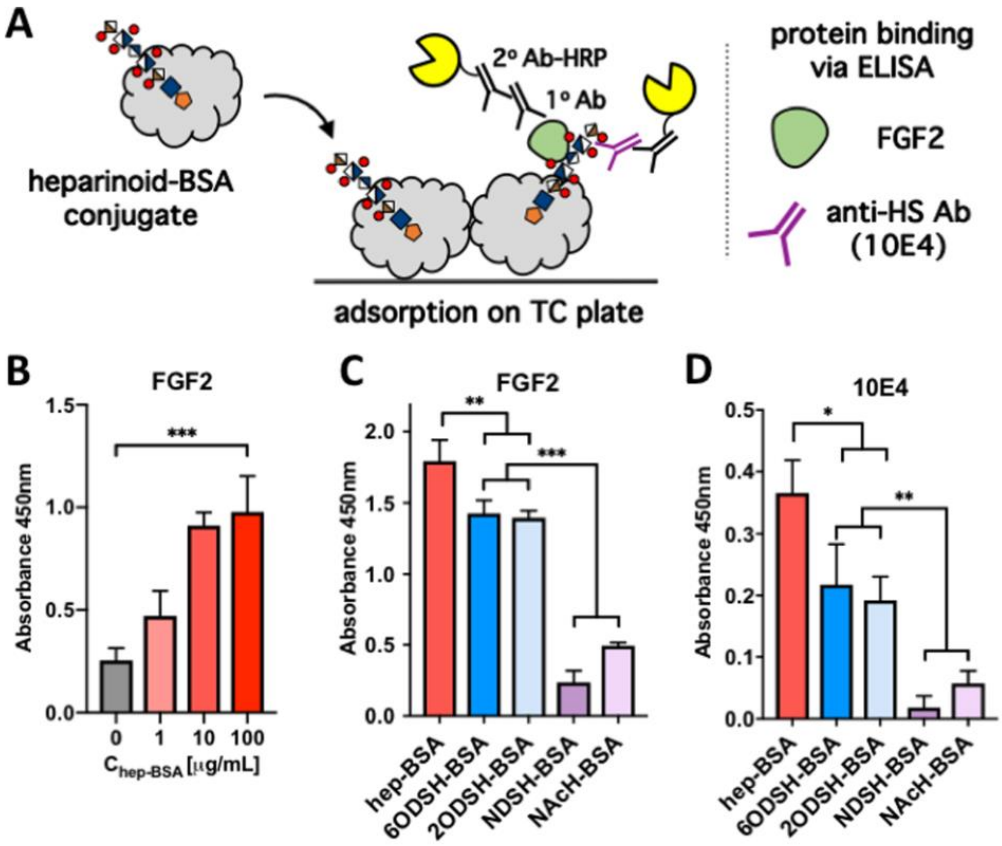

Figure 59. Immobilized heparinoid-BSA conjugates are recognized by proteins based on their sulfate composition. A) The conjugates were adsorbed on polystyrene tissue culture (TC) plates and evaluated for the binding of FGF2 (10 nM) and the anti-HS antibody, 10E4 (1:1000 dilution), using ELISA. B) Maximum FGF2 binding was observed for hep-BSA immobilized at 100 μg/mL concentration. C) and D) Removal of 6-*O*-, 2-*O*- and *N*-sulfation in immobilized heparinoid-BSA conjugates (100 μg/mL) led to increasing loss of FGF2 and 10E4 binding. (ANOVA, Tukey's multiple comparisons test; $p^* < 0.05$, $p^{***} < 0.001$).

I envisioned that the new heparinoid-BSA conjugates could serve as ECM components for controlling the proliferation of hMSCs in culture by sequestering the proliferative signal, FGF2, away from its cell surface receptors. To test the ability of the

conjugates to capture FGF2, I first immobilized **hep-BSA** at increasing concentration (1, 10, and 100 μg/mL based on BSA) on tissue culture-treated polystyrene 96 well plates. Using an ELISA format, the resulting heparin-BSA displays were probed with FGF2 (10 nM) and detected using a primary anti-FGF2 antibody followed by a secondary antibody-HRP conjugate in the presence of chromogenic reagent, TMB (Fig 4.7A). The immobilized **hep-BSA** captured FGF2 at all surface densities, reaching signal saturation in wells threated with 100 μg/mL of the conjugate (Fig 4.7B). Importantly, cross-examination of the SPAAC derived **hep-BSA** against heparin conjugates prepared using standard NHS-promoted amide coupling[42] (**hep-BSA-ac**) and reductive amination[43] (**hep-BSA-ra**) procedures revealed similar FGF2-binding ability for all three compounds (Fig 60).

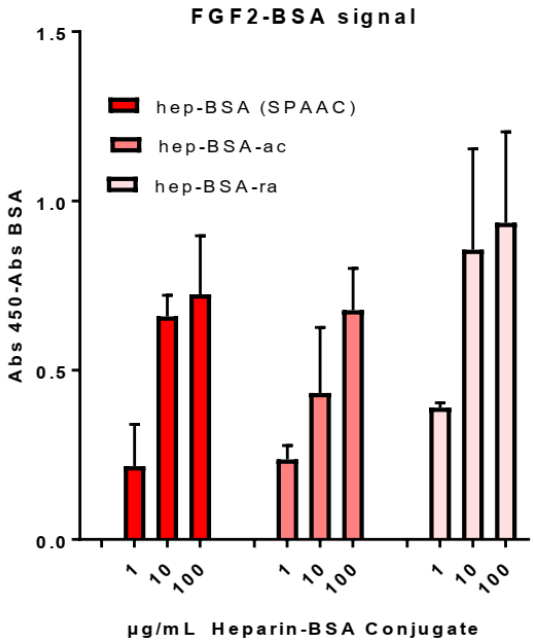

Figure 60. Binding of 10 nm FGF2 to immobilized **hep-BSA, hep-BSA-ra,** and **hep-BSA-ac**

To assess FGF2 capture in response to altered sulfation patterns, the differentially sulfated heparinoid-BSA conjugates were immobilized (100 μg/mL) and analyzed using ELISA (Fig 61). In line with previous observations,[14] the 6-*O*- and 2-*O*-desulfated heparinoid conjugates (**6ODSH-**and **2ODSH-BSA**) showed decreased FGF2 binding compared to **hep-BSA**, while the *N*-desulfated analogs (**NDSH-** and **NAcH-BSA**) exhibited minimal avidity for the growth factor. It should be noted that the **2ODSH-BSA** conjugate retained surprisingly high FGF2 binding capacity, which may, presumably, be attributed to the relatively high overall sulfation level of the parent heparin compared to HS, in which the loss of 2-*O*-sufation ablates FGF2 binding.[14] The anti-HS antibody, 10E4, which recognizes predominantly *N*-sulfated HS GAGs also detected the immobilized heparinoid conjugates according to their composition (Fig 62), further confirming the sulfation pattern-dependent bioactivity of the materials. To ensure that the differential FGF2 and 10E4 binding reflected the unique heparinoid composition rather than unequal neoglycoconjugate immobilization, we employed a two-point assay using biotinylated heparinoid-BSA conjugates in conjunction with heparinase digest and glycan stub detection. ELISA analysis of the arrayed glycoconjugates with streptavidin-HRP revealed equal surface density of BSA (Fig 61). The conjugates were then treated with heparinase to depolymerize the GAG component. ELISA quantification using an anti-HS stub antibody, 3G10, indicated equal distribution of the remaining heparinoid fragments bound to the immobilized BSA (Fig 62). Collectively, these assays confirm uniform surface adsorption for all heparinoid-BSA conjugates, regardless of their level of sulfation and overall charge density.

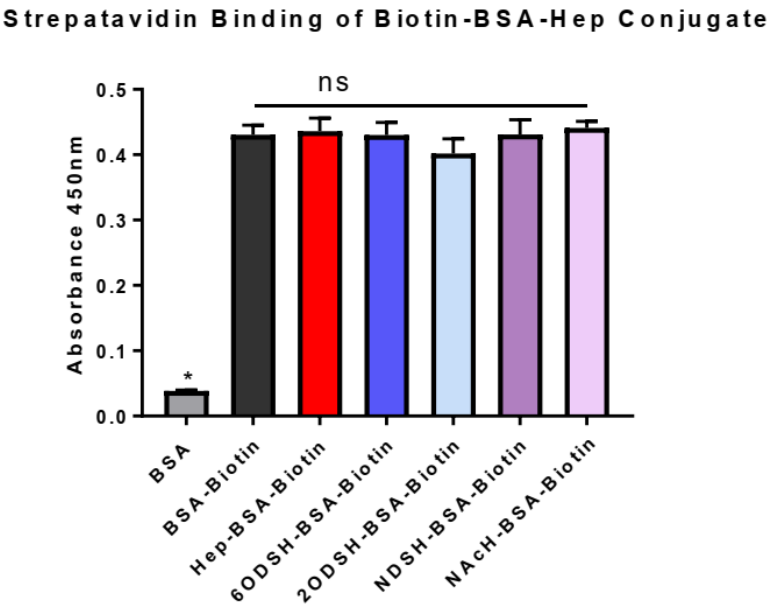

Figure 61. Immobilization efficiency for biotinylated heparinoid-BSA conjugates

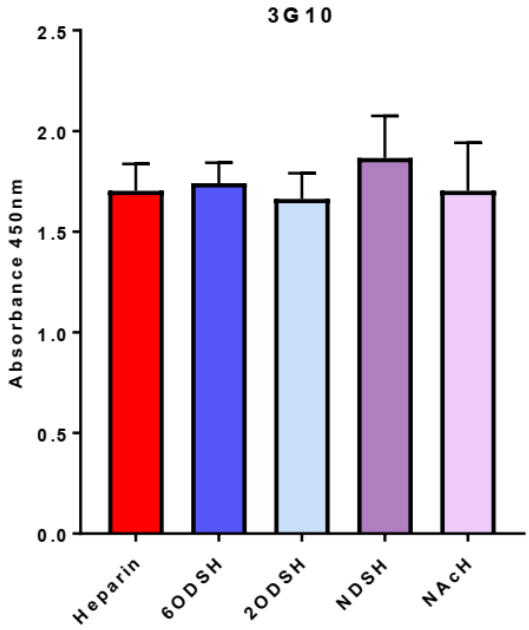

Figure 62. Binding of 3G10 to immobilized heparinoid-BSA conjugates after heparinase digest.

4.2.4 Proliferation of hMSCs on heparinoid displays

HS GAGs deposited into the ECM by cells provide binding sites for a variety of GFs. There, they can serve a dual role as a depot for concentrating GF activity or as a local sink sequestering these biochemical cues away from cell surface receptors.[3] To assess the ability of the newly generated heparinoid-BSA conjugates to function as ECM proteoglycan models, we tested their effects on FGF2-mediated hMSC proliferation *in vitro* (Fig 4.13). In this assay, hMSCs were seeded in 24 well tissue culture plates coated with heparinoid-BSA conjugates (100 μg/mL). The cells were allowed to proliferate for 3 days and proliferation rates were assessed by microscopy assisted cell counting (Days 0-3, Fig 64, Fig 65, Fig 66,) and by the incorporation of radioactive [^{3}H]-thymidine into newly synthesized DNA (Day 3, Fig 4.63, Fig 64C, Fig 65, Fig 66). While the glycoconjugate composition had no effect on hMSC seeding and adhesion compared to control BSA-coated wells (Day 0, Fig 63), we observed significant attenuation of cell proliferation concurring with the ability of the immobilized heparinoid conjugates to capture FGF2 (Figs 63 and 64). Accordingly, **hep-BSA** coating exhibited maximal proliferation inhibition (~ 2-fold, Fig 64), followed by **6ODSH-** and **2ODSH-BSA** conjugates, while **NDSH-** and **NAcH-BSA** conjugates showed no appreciable effect on cell proliferation compared to BSA-treated surfaces. Supplementation of the culture medium with soluble heparin (100 μg/mL) or the FGFR kinase inhibitor, PD173074 (10 nM), inhibited hMSC proliferation to a similar extent as immobilized **hep-BSA** (Fig 67). Heparinase treatment of the immobilized **hep-BSA** conjugate to remove the GAG component fully restored hMSC proliferation (Fig 4.68). These control conditions

provided support for the conclusion that proliferation inhibition on heparinoid surfaces resulted from the attenuation of FGF2 activity.

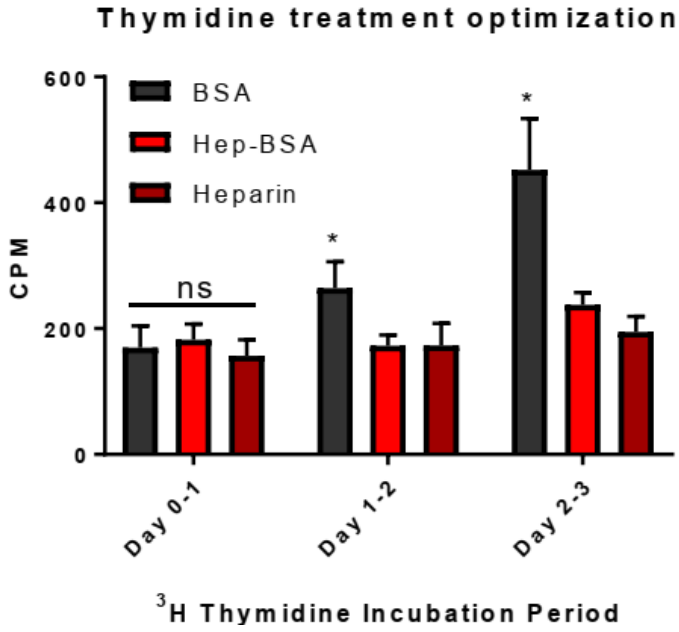

Figure 63. Optimization of thymidine proliferation assay time points.

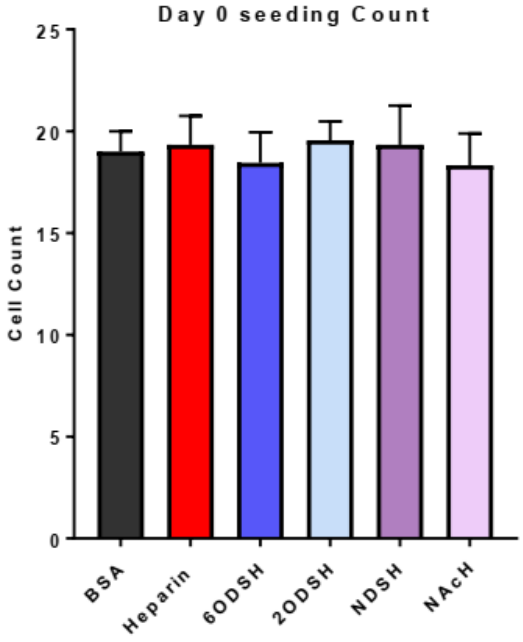

Figure 64. hMSC seeding on heparinoid-BSA surfaces via microscopy

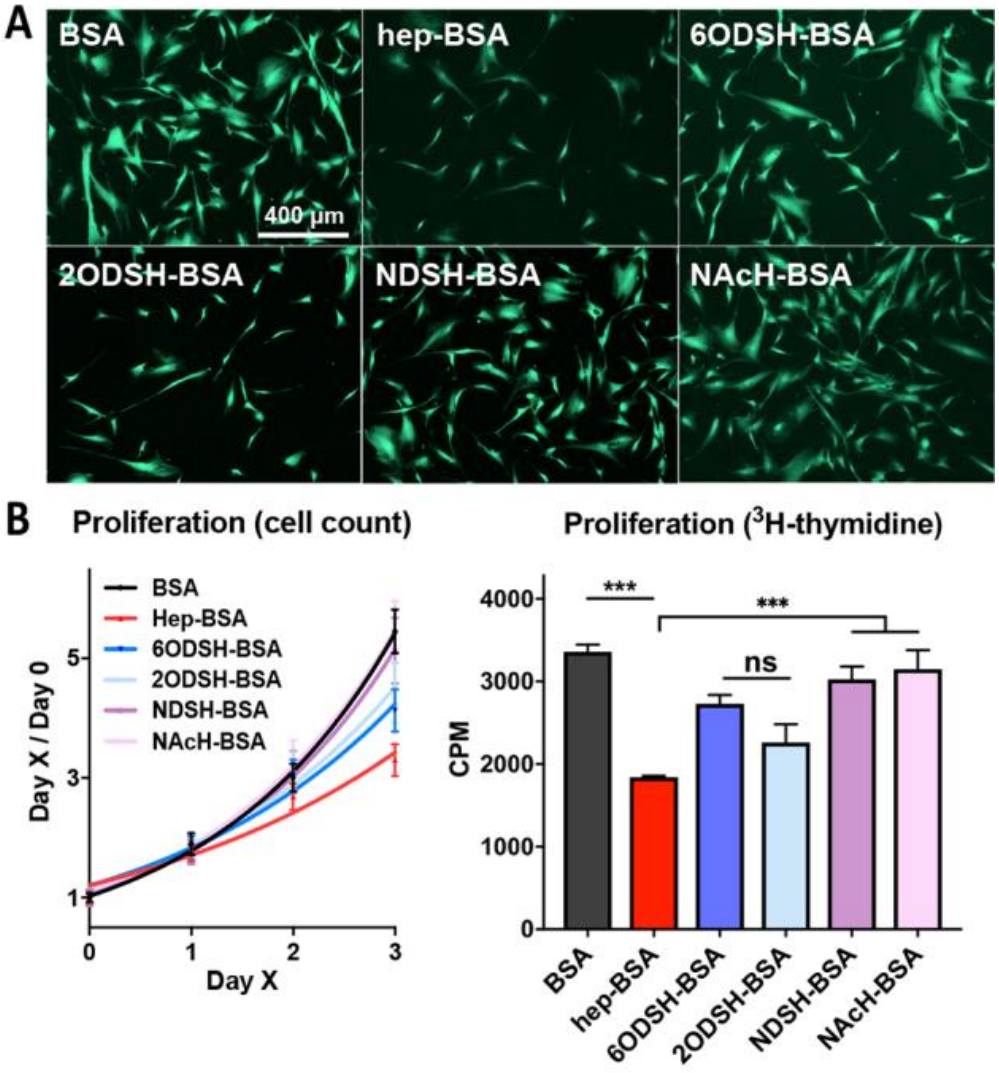

Figure 65. Immobilized heparinoid-BSA conjugates inhibit hMSC proliferation based on their sulfation pattern and capacity to bind FGF2. A) Fluorescent micrographs of calcein-stained (1 µM) hMSCs cultured on heparinoid-BSA conjugates (Day 3). B) Cell counts for hMSCs (Day0-Day3). C) Uptake of ^{3}H-thymidine (0.5 µCi) by hMSCs during Day 3 of culture on immobilized heparinoid-BSA conjugates. (ANOVA, Tukey's multiple comparisons test; $p^{*} < 0.05$, $p^{***} < 0.001$).

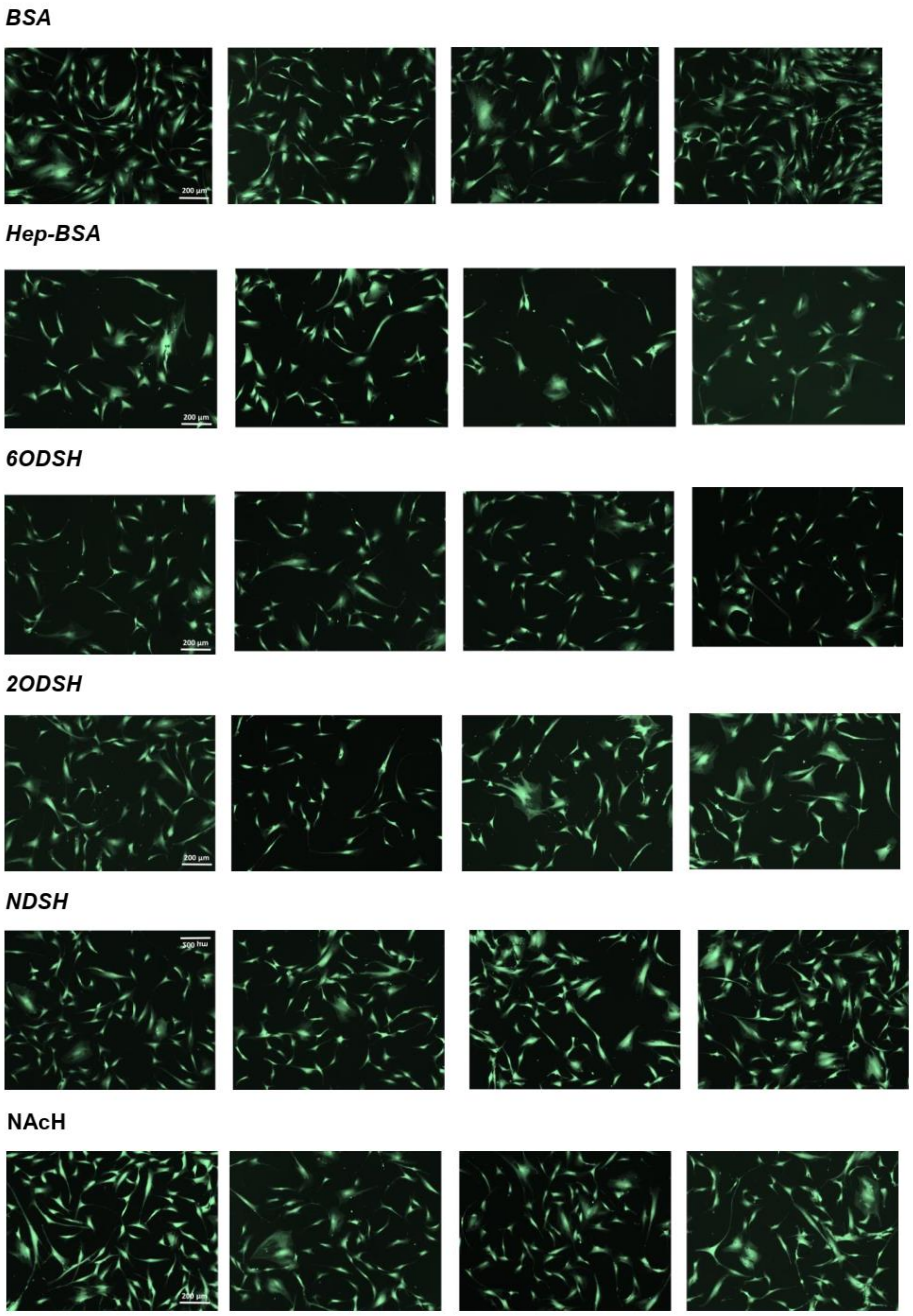

Figure 66. Supplemental fluorescent micrographs of calcein-stained (1 μM) hMSCs cultured on heparinoid-BSA conjugates (Day 3). (supplementary for figure **4.13)**

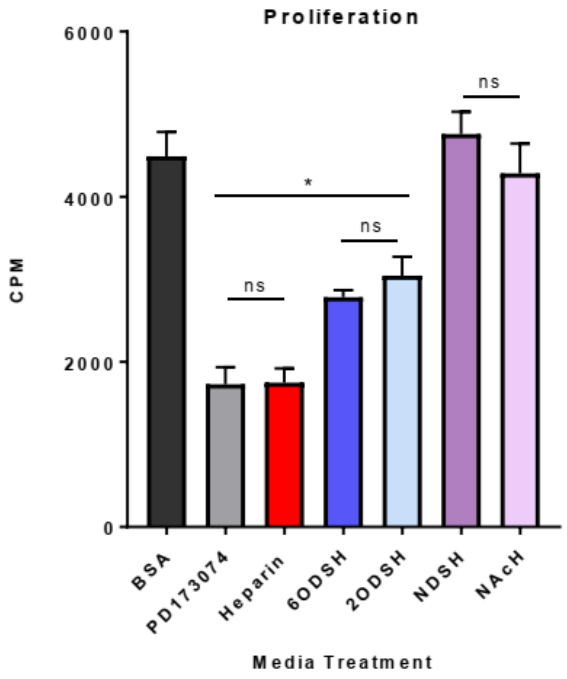

Figure 67. hMSC proliferation via thymidine assay using soluble heparinoids and the FGFR1 inhibitor PD173074, assesed on day 3.

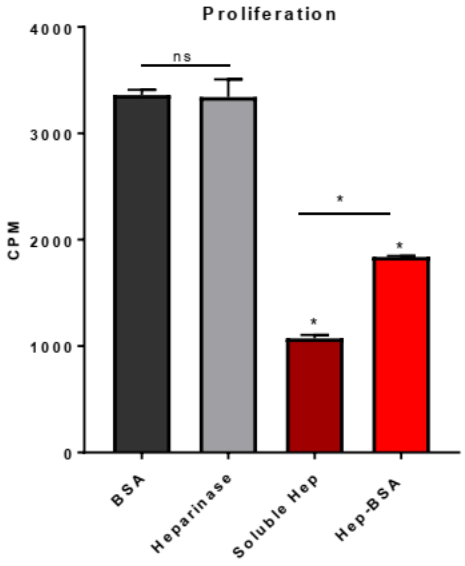

Figure 68. Heparinase treatment of heparin-glycoconjugate surface prior to seeding cells results in a loss of inhibitory proliferation effect. Heparin-BSA coated culture plate was treated with heparinase, and proliferation was assessed on day 3 of hMSC growth on the treated surface.

These findings need to be brought into context with prior observations reporting on enhanced proliferation of hMSC produced with heparin-coated chitosan surfaces,[22] heparin-functionalized PEG hydrogels,[17] or with surfaces modified with HS-binding peptides.[12] In these studies, the positive effects on cell proliferation were postulated to arise from improved cell adhesion and spreading on the substrates in the presence of heparin or HS and the ability of the glycans to concentrate exogenous FGF2 from the growth media. In contrast, the present study evaluated the ability of the heparinoid conjugates to influence hMSC proliferation by acting as localized sink for FGF2 present in the cell culture medium (~ 30-50 ng/L) while exhibiting similar cell adhesion properties (Fig 65 and Fig 64). Given the dual role of ECM HS to act as both a sink and a depot for GFs, we anticipate that the bioactivity of the heparinoid-BSA conjugates will be context-dependent and determined by the concentration of GFs in media relative to the binding capacity of the immobilized glycoconjugates.

In conclusion, we have developed an efficient method for generating and presenting heparinoid-protein conjugates. The neoglycoproteins were prepared using a two-step process, in which the reducing ends of HS GAG polysaccharides were pre-functionalized with reactive azide handles via a chemoselective hydrazide ligation for a subsequent coupling to cyclooctyne modified BSA. When adsorbed on the surface of polystyrene tissue culture plates, the conjugates provided extracellular environments with capacity to bind and sequester FGF2 according to the sulfation patterns of their pendant glycans and downregulate stem cell proliferation. The mild bioconjugation conditions and glycan economy make this method well suited for expanding the diversity of the

neoglycoconjugates with respect to both the protein and glycan components, including GAGs derived in small quantities from biological samples. Current efforts in the lab lead by Logan Laubach have made progress in adapting this two-step click conjugation strategy for microarray applications (**Fig 69**). Because the strategy enables conjugation of sparingly small quantities of GAG, Logan has begun to isolate GAGs from mouse organs, derivitizing them with a click handle, and conjugating these GAG derivitives to BSA in order to profile differential growth factor binding characteristics of GAGs found throughout the body.

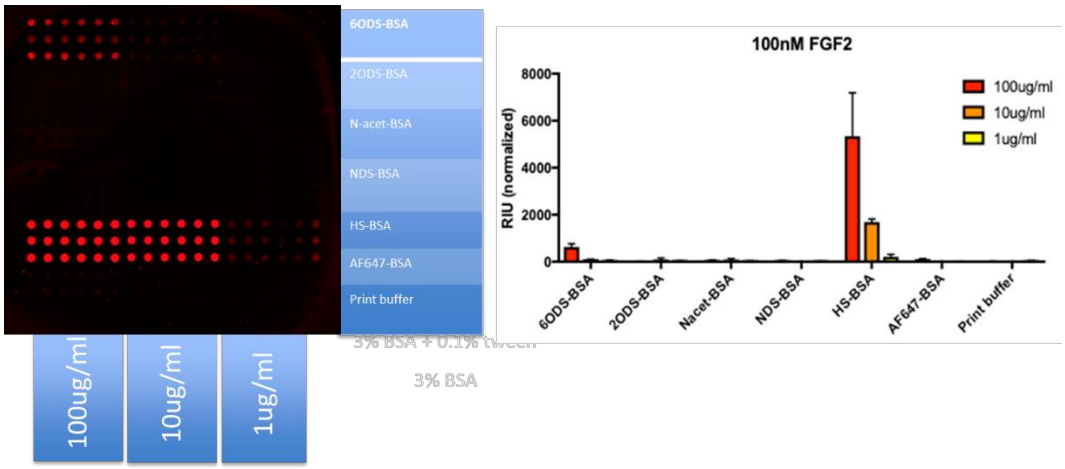

Figure 69. Heparinoid-BSA conjugates arrayed at 100 µg/mL, 10 µg/mL, and 1 µg/mL using microarray printer. Each condition is printed in 3x6 pattern (n=18). FGF2 binding was measured using a AF647-FGF2 conjugate. AF647 labeled BSA was not successfully labeled.

4.3 MATERIALS AND METHODS

4.3.1 Materials

All chemicals, unless stated otherwise, were purchased from Sigma Aldrich and used as received. A complete list of biological reagents and materials is provided in Table S1. Heparin and desulfated heparinoids were purchased from Iduron (Manchester, UK). The chemically desulfated heparinoids used in this study originated from the unmodified heparin. The disaccharide analysis of the heparin and desulfated heparins was provided Iduron and is in the appendix. The major (> 75%) unit of heparin is the trisulfated disaccharide, IdoA(2S)-GlcNS(6S). Chemical desulfation resulted in 6ODSH (~ 90% reduction in 6-*O*-sulfates and ~ 25% loss of 2-*O*-sulfates), 2ODSH (~95% reduction in 2-*O*-sulfates), NDSH and NAcH (~ 90% reduction in *N*-sulfate).

4.3.2 Instrumentation

Nuclear magnetic resonance (NMR) spectra were collected on a Bruker 300MHz NMR spectrometer. Spectra are reported in parts per million (ppm) on the δ scale relative to the residual solvent as an internal standard. Size exclusion chromatography (SEC) was performed on a Hitachi Chromaster system equipped with an RI detector and an 8μm, mixed bed, 300 x 7.5 mm cm PL aquagel-OH mixed medium column. 96-well plate assays (ELISA, carbazole) were analyzed using a Varioskan LUX multimode microplate reader. Matrix-assisted laser desorption ionization coupled with time of flight (MALDI-TOF) analysis was acquired via a Bruker Biflex IV MALDI-TOFMS in positive ion mode using sinapinic acid matrix. Bright field and fluorescence microscopy images were taken using

ZEISS Axio Observer microscope. Radioactive thymidine assays were analyzed using a Beckman Coulter LS6500 Liquid Scintillation Counter.

4.3.3 General chemical procedures

All chemicals, unless stated otherwise, were purchased from Sigma Aldrich. Purchased starting materials were used as received unless otherwise noted. Azidomethyl benzhydrazide linker (1) was prepared according to a published procedure. Heparin and desulfated heparinoids were purchased from Iduron (Manchester, UK). The selectively chemically desulfated heparinoids originated from the unmodified heparin used in this study. The distributors of the heparin reported the average molecular weight of the parent heparin approximately 12,000 g/mol, but stated the heparin they prepare has a wide range of molecular weights, and do not have a polydispersity data for the polymer. The disaccharide analysis of the heparin and desulfated heparins are depicted in the spectra (appendix) Briefly, the major (greater than 75%) disaccharide unit of heparin is the trisulfated IdoA(2S)-GlcNS(6S). The extent of desulfation of the heparinoids are as follows: 6ODSH: approximately 90% reduction in 6-O-sulphates and 25% loss of 2-O-sulphates, 2ODSH: approximately 95% reduction in 2-O-sulphates, NDSH and NAcH: approximately 92% reduction in N-sulphates. The progress of reactions was monitored by analytical thin-layer chromatography (TLC, Merck silica gel 60 F-254 plates) using detection via UV illumination, or by staining with iodine or ninhydrin. Solvent compositions are reported on a volume/volume (v/v) basis unless otherwise noted.

4.3.4 Heparinoid pre-functionalization

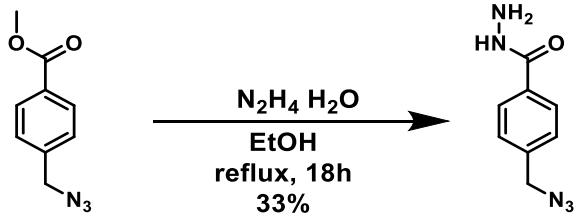

1

Synthesis of (4-(azidomethyl)benzhydrazide) (1).[1] In a 100 mL round-bottom flask equipped with a stir bar charged with 4-(azidomethyl)benzoate (1.66 g, 8.73 mmol) was added ethanol (30 mL). Aqueous hydrazine hydrate (35 %, 2.4 mL, 27 mmol, 3 equiv.) was added to the suspension and the flask was equipped with a Findenser. The reaction mixture was refluxed for 18 hr in an oil bath and monitored by TLC (5% MeOH in DCM, Rf_{prod} = 0.38). After this time, the reaction was cooled to RT and concentrated under reduced pressure to give a colorless oil. The residue was placed on high-vacuum and a white residue formed. The residue was dissolved in a hot mixture of ethanol and ethyl acetate (2:1, 6 mL) and allowed to slowly crystallize, first at RT, then at -20C. The small colorless crystals were filtered and collected and washed with water to afford 1 (0.55 g, 33%), which was stored at -20C in the dark until use. 1H NMR (300 MHz, DMSO-d6): 9.80 (s, 1H), 7.85 (d, J = 8.3 Hz, 2H), 7.44 (d, J = 8.3 Hz, 2H), 4.52 (s, 2H), 4.50 (s, 2H); 13C NMR (75 MHz, DMSO-d6): 165.8, 139.1, 133.5, 128.7(2), 127.8(2), 53.6. HRMS m/z calculated for C8H10N5O1 [M+H]+ 192.0885, found [M+H]+ 192.0881.

Synthesis of end-functionalized heparinoids 2. In a PCR tube, heparin (6.0 mg, 0.5 μmol) was dissolved in sodium acetate buffer (100 mM, 53.4 μL, pH 5.5) containing

aniline (100 mM). In a separate PCR tube, 4-(azidomethyl)benzhydrazide (6.0 mg, 31.4 µmol, 6.4 equiv.) was dissolved in DMSO (30.0 µL) and added to the heparin solution. The PCR tube containing the final mixture was then capped, placed into a thermocycler set to 50 °C and heated for 72 hrs. After this time, the reaction mixture was diluted with PBS (~ 7.0 mL) and dialyzed in SnakeSkin dialysis tubing (3.5 kDa MWCO) against MQ water for 48 hrs, replacing the MQ water after 24 hrs. The dialyzed product was lyophilized to afford the end-chain modified heparin product, **2-hep** (6.0 mg, quatitative recovery). Heparinoids **2** were prepared and purified using an identical procedure.

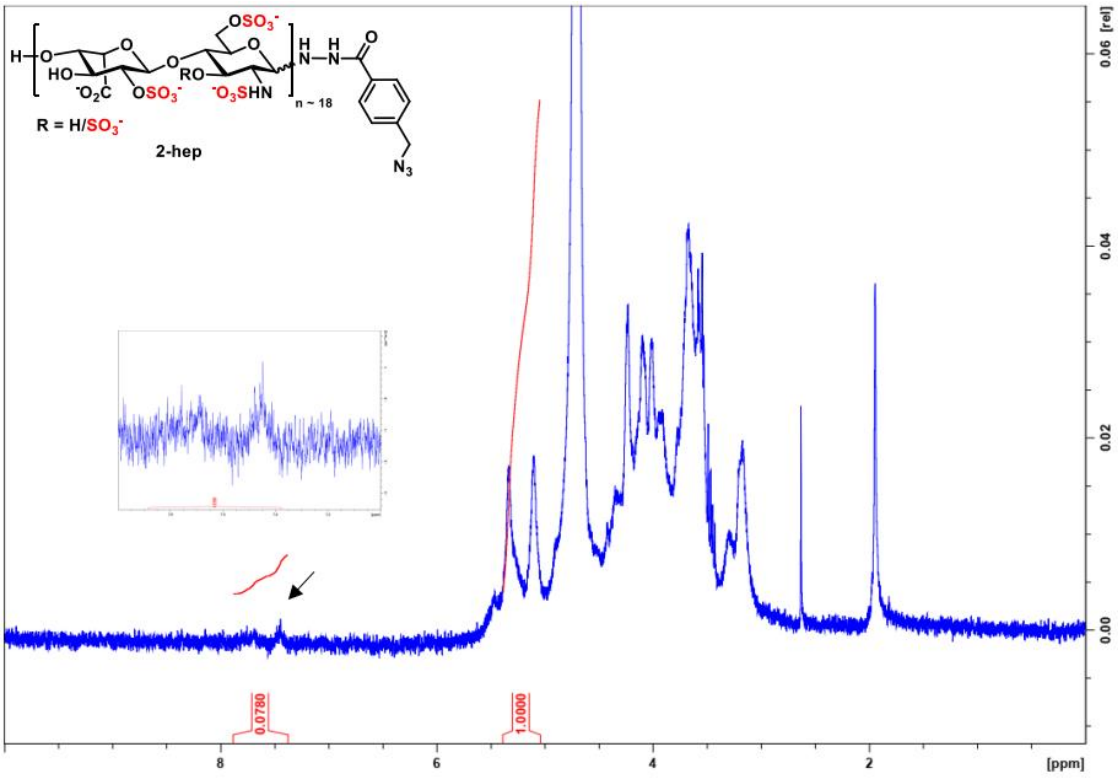

Figure 470. ^{1}H NMR of **2-hep**

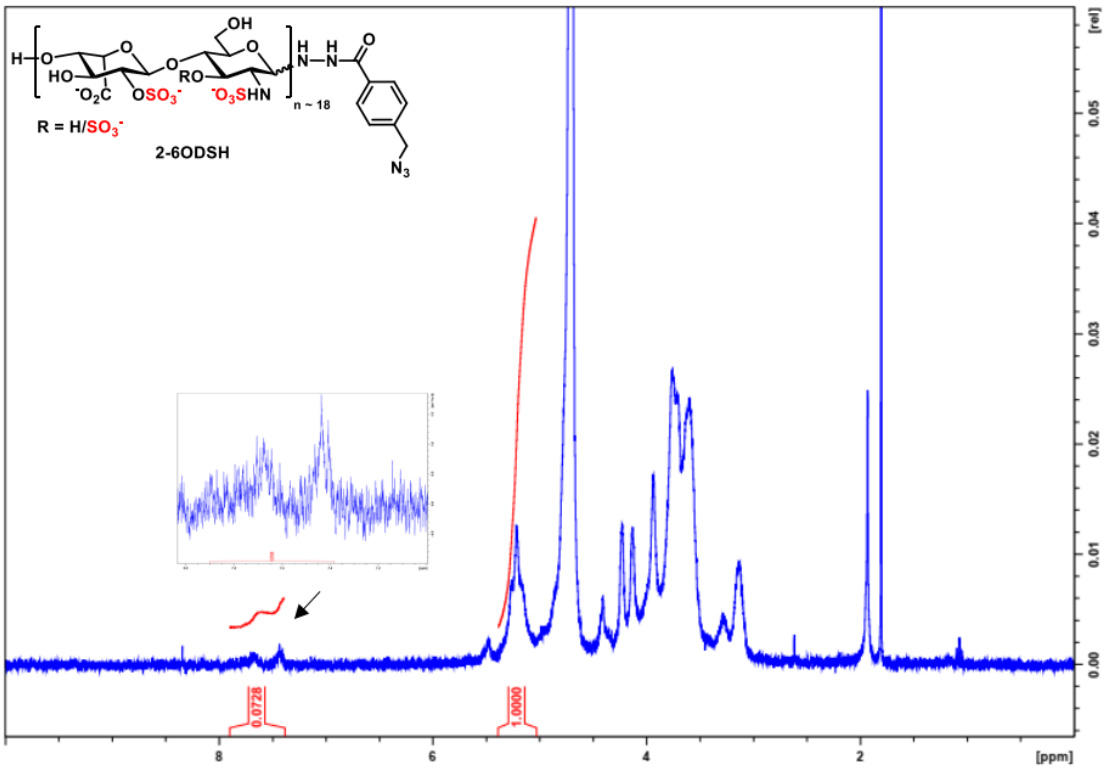

Figure 71. ^{1}H NMR of **2-6ODSH**

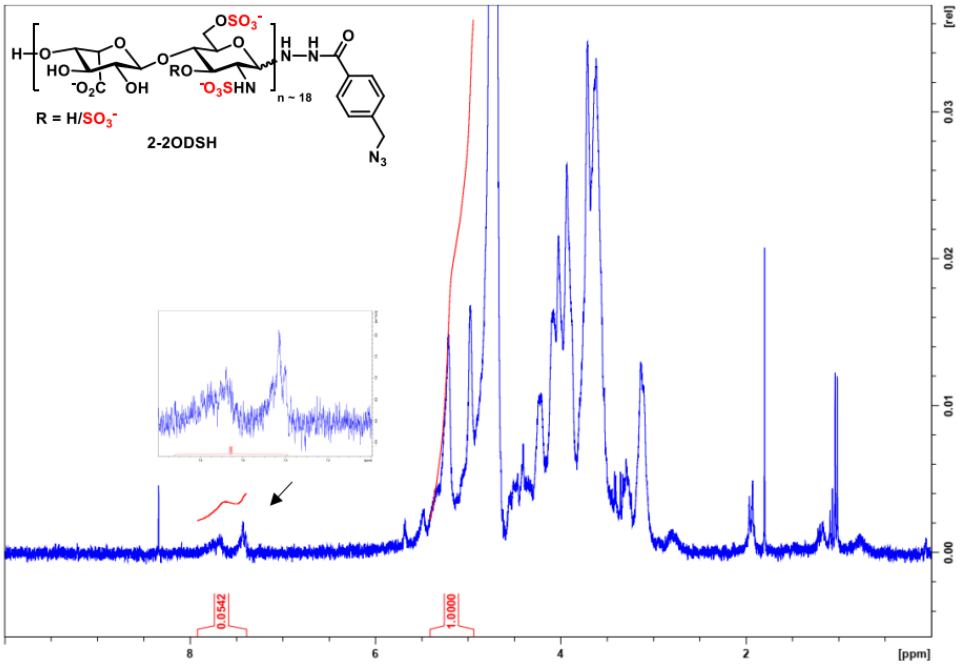

Figure 72. ^{1}H NMR of **2-2ODSH**

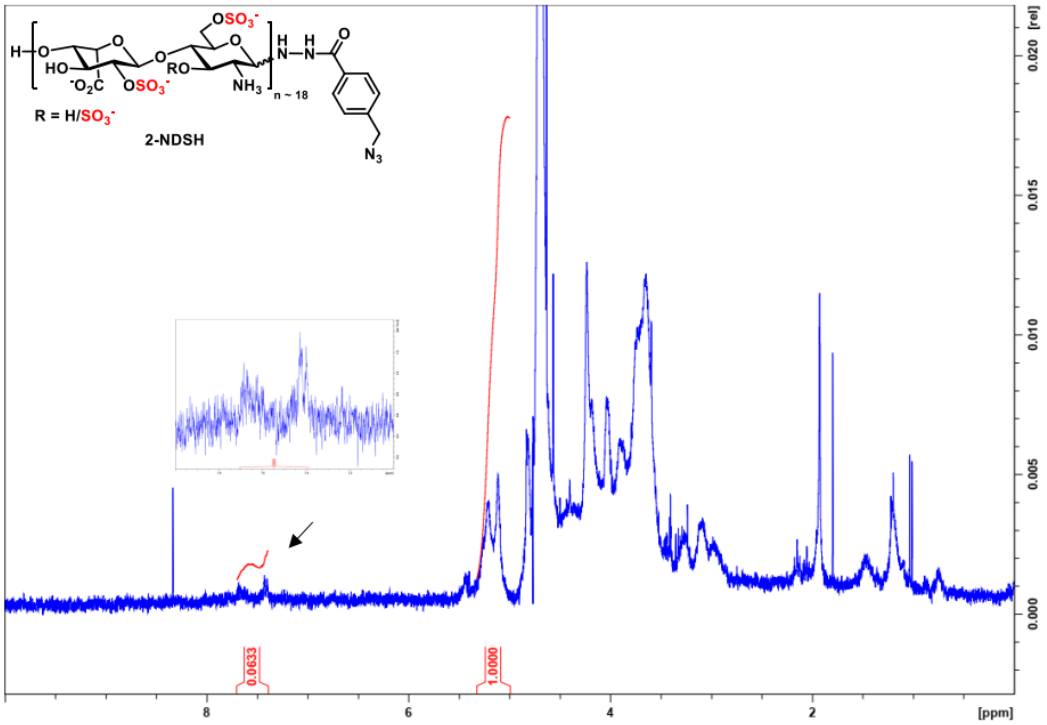

Figure 73. ^{1}H NMR of **2-NDSH**

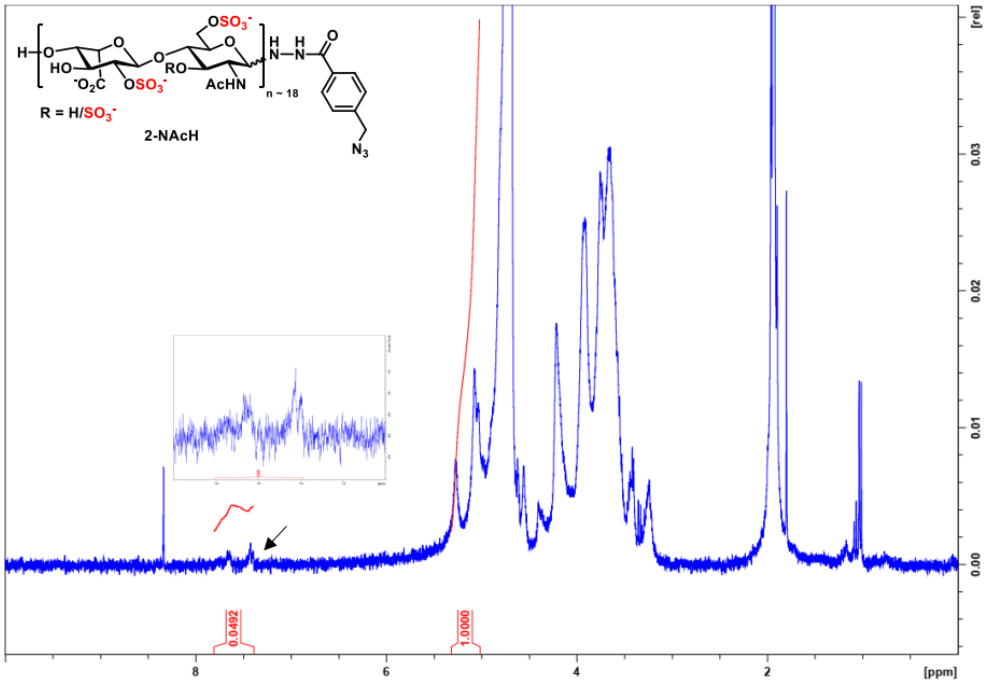

Figure 74. ^{1}H NMR of **2-NAcH**

4.3.5 BSA pre-functionalization

Synthesis of DBCO-BSA conjugate 3. In a 1.5 mL microcentrifuge tube, BSA (10.0 mg) was dissolved in sodium bicarbonate buffer (100 mM, 1.0 mL, pH= 8.3). A solution of dibenzocyclooctyne-PEG4-N-hydroxysuccinimidyl ester in DMSO (10.0 mg/mL, 78.0 µL, 8.0 equiv.) was added and the reaction was stirred at 4 °C overnight. After this time, the reaction mixture was transferred into dialysis tubing (25 kDa MWCO) and dialyzed against MQ water for 48 hrs, replacing water after 24 hrs. The dialyzed DBCO-BSA product **3** was lyophilized to afford white solid (11.0 mg, 94% mass recovery). The product **3** was analyzed by MALDI-TOF (m/z = 70,803) indicating the addition of an average of ~ 6 DBCO modifications per molecule of BSA.

Synthesis of biotinylated DBCO-BSA conjugate (3-biotin). To a solution of DBCO-BSA conjugate **3** (10.0 mg) in sodium bicarbonate buffer (100 mM, 1.0 mL) a DMF solution of NHS-Biotin (10 mg/mL, 100.0 µL) is added. The resulting mixture was stirred overnight. After this time, the conjugate was diluted with 7 mL of PBS and transferred into dialysis tubing (25 kDa MWCO) and dialyzed against MQ water for 48 hours, replacing water after 24 hours. The dialyzed dibenzocyclooctyne-BSA (DBCO-BSA) product **3** was lyophilized to afford white solid (10.0 mg, 100% mass recovery). The product **3-biotin** was analyzed by MALDI-TOF (m/z =77,084), indicating the addition of an average of ~ 19 biotin modifications per molecule of **3**.

4.3.6 Preparation of heparinoid-BSA conjugates

Synthesis of heparin-BSA conjugate via amide coupling (**hep-BSA-ac**)[44]. Following a previously published procedure, HEPES buffer (100 mM, 15.0 mL, pH 7.4) was first prepared. Then, heparin (4.0 mg, 0.3 µmol) was dissolved in 200.0 µL the stock solution and stirred overnight at 4 °C to afford heparin NHS-ester. The activated NHS ester solution was diluted to a total volume of 2.5 mL using in MQ water, loaded onto a PD-10 column, and eluted with 2.5 mL MQ water. The solution was lyophilized to afford intermediate heparin NHS-ester (4.0 mg, 100% mass recovery), 3.3 mgs of which which was dissolved in a PBS solution containing BSA (10.0 mg/mL, 300.0 µL). The reaction was allowed to proceed overnight and the resulting heparin-BSA conjugate (**hep-BSA-ac**) was placed in dialysis tubing (25kDa MWCO) and purified by dialysis against MQ water over 48 hours, replacing water after 24 hours. The resulting solution was lyophilized to afford purified **hep-BSA-ac** as a white solid (6.3 mg, 100% mass recovery based on BSA).

Synthesis of heparin-BSA conjugate via reductive amination (hep-BSA-ra)[45]: Following a previously published procedure, a 1.5 mL microfuge tube was charged with heparin (10.0 mg) dissolved in sodium phosphate buffer (0.2 M, 400.0 µL, pH = 8.0), followed by a solution of BSA (2.0 mg/mL, 200.0 µL) and $NaCNBH_4$ (2.0 mg/mL, 200.0 µL) in sodium phosphate buffer (0.2 M, pH = 8.0). The resulting mixture was stirred at 37 °C for 48 hrs. After this time, the reaction was diluted with an aqueous solution of NaCl (1.5 M, 3.2 mL) and purified using an amicon ultra centrifugal filter unit (30 kDa MWCO).

Upon loading 4 mL of the dilute sample, the filter was spun at 13,000 x g for 15 minutes. The retentate was diluted with more NaCl solution and spun again at 13,000 x g for 15 minutes. This procedure was repeated twice more. The resulting concentrated sample was diluted to a final volume of 2.5 mL with MQ water, loaded onto a PD-10 desalting column, and eluted with an additional 2.5 mL of MQ water. The eluted product was collected and lyophilized to give the **hep-BSA-ra** conjugate as white solid (0.7mg, 100% mass recovery based on BSA).

Heparin-/heparinoid-BSA conjugation via SPAAC. To a 1.5 mL microcentrifuge tube charged with azide end-prefunctionalized heparin **2-hep** (6.0 mg, 0.5 μmol) was added a solution of DBCO-BSA conjugate **3** in PBS (10.0 mg/mL, 600.0 μL, 1 equiv. per DBCO). The reaction was allowed to proceed at RT for 48 hrs. After this time, the conjugate was diluted to a total volume of 4 mL with aqueous solution of NaCl (1.5 M) and spin-dialized (30 kDa MWCO, 4,000 x g, 20 min). This was repeated a second time with the NaCl solution and 4 more times with MQ water. After this treatment, all unconjugated heparin was removed leaving behind **hep-BSA** with some amount of unreacted DBCO-BSA conjugate **3**, as evidenced by SEC analysis (57). The product was lyophilized to afford a white solid **hep-BSA** conjugate (11.0 mg, quantitative mass recovery by BSA), which was used directly for biological experiments or purified further for compositional analysis by size exclusion and ion exchange chromatography to remove **3**. Heparinoid-BSA conjugates were synthesized using an identical procedure.

Synthesis of biotinylated heparin- and heparinoid-BSA conjugates via SPAAC (hep-, 6ODSH-, 2ODSH-, NAcH-, and NDSH-BSA-biotin). In an 1.5 mL microcentrifuge tube,

azide end-functionalized heparin or heparinoids (2, 6.0 mg) were dissolved in a solution of biotinylated DBCO-BSA (3-biotin) in PBS (10.0 mg/mL, 600μL) and the resulting solution was allowed to react at ambient temperature for 48 hours. After this time, the mixture was diluted with an aqueous NaCl solution (4.0 mL, 1.5 M) and spin-filtered (30 kDa MWCO, 4,000 x g, 20 minutes). This was repeated a second time with NaCl solution, and then 4 times with MQ water. The resulting material, free of heparin or heparinoids (2) but still containing some unreacted 3-biotin, was used directly without further purification in subsequent protein binding and biological assays.

Determination of BSA concentration via the BCA assay: Protein concentration of **hep-BSA** was determined using the Bradford BCA assays according to a standard protocol. A series of BSA calibration standards in MQ water was prepared at a 0-30 nmol/mL concentration range and aliquoted (13.0 μL) into a 96 well plate in triplicate. After size exclusion, ion exchange chromatography, and lyophilization, a solution of the purified **hep-BSA** was prepared at an unknown concentration and was aliquoted (10.0 μL) and added the 96 well plate in triplicate. Reagent A and Reagent B of the kit are combined at a ratio of 1:50 (A: B) to a total volume of 10.0 mL and added to the BSA standards and **hep-BSA** samples in the 96 well plate. The plate was heated at 37 °C for 30 minutes before the solutions were analyzed for absorbance at 562 nm using a plate reader. A standard calibration curve was generated. Using the linear regression produced from the calibration curve, the concentration of BSA in the purified **hep-BSA** sample was determined to be 41 nmol/mL.

Determination of heparinoid concentration via the carbazole assay.[46] Safety note: This procedure involves heating of concentrated acid in a 96 well plate and thus should be performed inside of a fume hood with extreme caution being taken when manipulating the plate when acid is in wells. Aliquots of heparin standard solutions in MQ water (50 µL) at concentrations of 42 nm/mL, 21 nm/mL, 10.5 nm/mL, 5.3 nm/ mL, 2.6 nm/mL. and an aliquot of purified **hep-BSA** conjugate (c_{BSA} = 6.5 nM, 50.0 µL) were transferred into a 96 well plate. A solution of sodium tetraborate decahydrate (25 mM, 200.0 µL) in concentrated sulfuric acid (18 M) was added to each well and the plate was placed into an oven preheated to 100 °C for 10 minutes. After that time, the plate was removed from the oven and allowed to cool to RT for 15 minutes, followed by the addition of a carbazole solution in absolute ethanol (1.25 mg/mL, 50.0 µL) to each well. The plate was returned to the oven and heated to 100 °C for 10 minutes. After cooling to RT, absorbance was measured at 550 nm. The heparin concentration in the purified **hep-BSA** conjugate sample was calculated using the equation for the linear regression of the standard curve. The ratio of heparin and BSA concentrations in the purified **hep-BSA**, indicated an average of ~ 6 heparin chains per molecule of BSA.

4.3.7. Preparation and characterization of heparinoid displays on surfaces

Surface immobilization of heparinoid-BSA conjugates. A 1.0 mg/mL heparinoid-BSA conjugate solution in PBS was filtered through a 0.22 µm sterile filter and 50.0 µL of the solution was added per well of a 24 well plate. The solution was spread using the back of a p200 pipette tip to fully cover the well surface. The plate was dried and further sterilized

overnight under UV irradiation. The plate was then washed 3 times with PBS. before being used for cellular experiments. When immobilizing conjugates in a 96 well plate for ELISA, wells were treated with 13 µL/well of a heparinoid-BSA conjugate in PBS. The plate was centrifuged at 70 x g for 3 minutes to spread the solution evenly within the well. The coated 96 well plate was left at RT to dry overnight. The plate was washed six times using 200 µL PBS with 2 minutes of rocking per wash prior to use. Both 24 and 96 well plates were composed of the same tissue culture treated plastic.

FGF2 binding assay. The wells of a 96 well plate were coated with heparinoid-BSA conjugates as described above. After blocking with 2% BSA solution in PBS for 1 hr at RT, the blocking solution was removed and the wells were incubated with a solution of FGF2 (10nM) in 1% BSA/PBS for 1 hr at RT. After incubation, the wells were washed 6 times with 200 µL PBS containing 0.1% v/v Tween 20 with rocking for 2 min per wash. The wells were washed again 6 times with 200 µL PBS with rocking for 2 min per wash. To the washed wells, was added a solution of primary anti-FGF2 antibody in 1% BSA/PBS (1:1000 dilution). After 1 hr incubation at RT, the wells were washed 6 times with 200 µL of PBS containing 0.1% v/v Tween 20 with rocking for 2 min per wash. The wells were treated with a solution of secondary antibody-HRP conjugate in 1% BSA/PBS (1: 3000 dilution) at RT for 1 hr. After incubation, the wells were washed 6 times with 200 µL of PBS containing 0.1% v/v Tween 20 with rocking for 2 min per wash. Then, a TMB solution (100 µL) was added and after 5 minutes, the peroxidase reaction was developed with 2N sulfuric acid and the absorbance at 450 nm was measured on a plate reader.

Evaluation of interactions of immobilized heparinoid-BSA conjugates with anti-HS antibody, 10E4: The wells of a 96 well plate coated with heparinoid-BSA conjugates as described above. After blocking with 2% BSA solution in PBS for one hour at RT, the solution was removed and a solution of 10E4 antibody in a 1% BSA/PBS (100.0 µL, 1:1000) was added. After incubation, the wells were washed 6 times (200.0 µL PBS, 0.1% v/v Tween 20) and rocked for 2 minutes per wash. The wells were treated with a solution of XMs-HRP (IgM) antibody in 1% BSA/PBS (100.0 µL,1:2000) for one hour at RT. After incubation, the wells were washed 6 times (200.0 µL PBS, 0.1% v/v Tween 20) and rocked for 2 minutes per wash. And a TMB solution (100.0 µL) was added. After 5 minutes, absorbance was measured at 655 nm. The peroxidase reaction was developed using 2 N sulfuric acid and absorbance at 450 nm was measured on a plate reader.

Determination of relative immobilization efficiency for biotinylated heparinoid-BSA conjugates via ELISA: The wells of a 96 well plate coated with heparinoid-BSA conjugates as described above. After the last wash solution was removed, the wells were treated with a 2% BSA solution in PBS for one hour at RT to minimize nonspecific binding interactions. The blocking solution was removed and the wells were treated with a solution of streptavidin-HRP conjugate in 1% BSA/PBS (1:3000) for 1 hour. After incubation, the wells were washed 6 times (200.0 µL PBS, 0.1% v/v Tween 20) and rocked for 2 minutes per wash. Then, TMB solution (100.0 µL) was added and after 5 minutes absorbance at 655 nm was measured. The peroxidase reaction was developed with 2N sulfuric acid and the absorbance at 450 nm was measured on a plate reader.

Determination of relative heparinoid density in immobilized heparinoid-BSA conjugates via heparinase digest and anti-HS stub antibody, 3G10: The wells of a 96 well plate coated with heparinoid-BSA conjugates as described above. After blocking with 2% BSA solution in PBS for one hour at RT, the blocking solution was removed and a solution of heparinase III (5 mU/mL, 200.0 µL) was added to each well, and allowed to digest immobilized heparinoids for one hour at RT. After incubation, the wells were washed 6 times (200.0 µL PBS, 0.1% v/v Tween 20) and rocked for 2 minutes per wash. Next, the wells were treated with a 2% BSA solution in PBS for 1 hour at RT to block nonspecific interactions. After the removal of the blocking solution, the wells were incubated with a solution of 3G10 antibody in 1% BSA/PBS (1:1000) for 1 hour at RT. After incubation, the wells were washed 6 times (200.0 µL PBS, 0.1% v/v Tween 20) and rocked for 2 minutes per wash. The wells are treated with a solution of XMs-HRP antibody in 1% BSA/PBS (1:3000) for one hour at RT. After incubation, the wells were washed 6 times with 200 µL PBS 0.1% v/v Tween 20 with rocking for 2 minutes per wash. After HRP-antibody incubation, a TMB solution (100.0 µL) was added and, after 5 minutes, absorbance was measured at 655nm. The peroxidase reaction was developed with 2 N sulfuric acid and the absorbance at 450 nm was measured on a plate reader.

4.3.8 Proliferation of hMSCs on heparinoid displays

General cell culture procedures. Bone marrow derived human mesenchymal stem cells (hMSCs) were maintained in MSC medium containing rh-FGF2 (5 ng/mL), rh-IGF1 (15 ng/mL), L-alanyl-L-glutamine, 7% FBS, and penicillin/streptomycin (1:100). The cells were grown in monolayer culture in tissue culture treated T25 flasks at 37 °C, 5% CO2.

Media was changed every 3 days of growth and the cells were passaged every 6 days at a ratio of 1:10 after dissociation with 0.05% trypsin-EDTA at 37 °C, 5%CO2, which was neutralized with an equal volume of growth medium. Cells were washed with PBS after the removal of old media. Cells were used for experiments when they reached passage 6. All cellular experiments took place in 24 well tissue culture plates. Statistical analysis was performed using Prism software. Error bars refer to standard deviation from the mean and p values were calculated using a one-way ANOVA, $p^* < 0.05$, $p^{***} < 0.001$.

Cell proliferation Assay. In a 24 well plate, hMSCs were seeded in MSC growth medium in wells coated with heparinoid-BSA conjugates at a seeding density of 2,500 cells/cm^2. The cells were allowed to adhere for 18 hrs, after which time the cells were washed once with PBS and then cultured in α-MEM medium supplemented with 10% FBS and penicillin/streptomycin (1:100) on Day 0. Control condition cells were seeded in wells coated with BSA alone and treated in the presence or absence of soluble heparin (100 µg/mL) or PD173074 (10 nM). On Day 2, [^{3}H]thymidine (0.5 µCi) was added to each well in a total volume of 10 µL in PBS and the cells were cultured for additional 24 hrs. On Day 3, the media were removed, cells were washed 3 times with PBS and lysed in a lysis buffer (400 µL, 0.1 M NaOH, 0.1% w/v sodium dodecyl sulfate). The radioactive lysate (300 µL) was transferred to a scintillation vial containing 5 mL of Ultima Gold liquid scintillation fluid and analyzed using a liquid Scintillation counter. For assessment of proliferation via cell counting, 3 random viewing frames per well were acquired using phase microscopy at 100x magnification and the cells were counted. Counting was repeated daily and on Day 3, the cells were live-stained with Calcein AM (1 µM in PBS)

to enhance the accuracy of counting, as the cells become more confluent and less easily distinguished from one another.

4.5 APPENDIX

Heparin and 6-O Desulphated Heparin disaccharide anaylsis

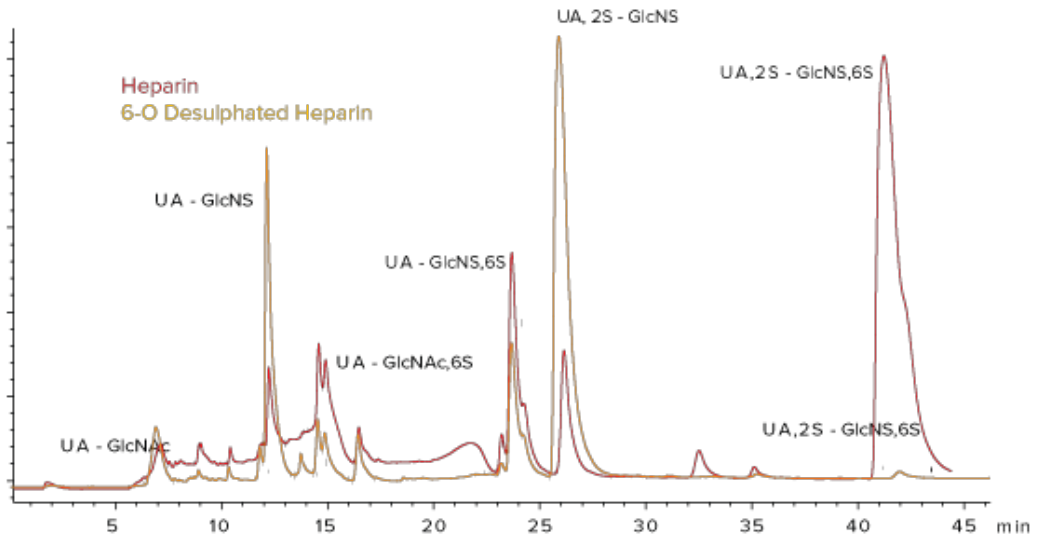

Heparin and 2-O Desulphated Heparin disaccharide anaylsis

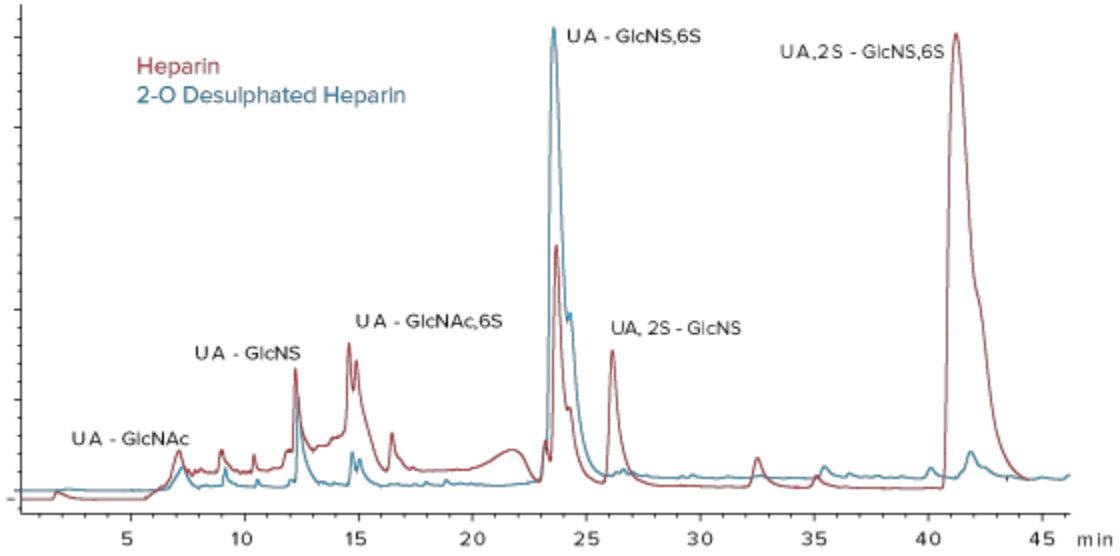

N-Desulphated Heparin (DSH003/N) disaccharide anaylsis

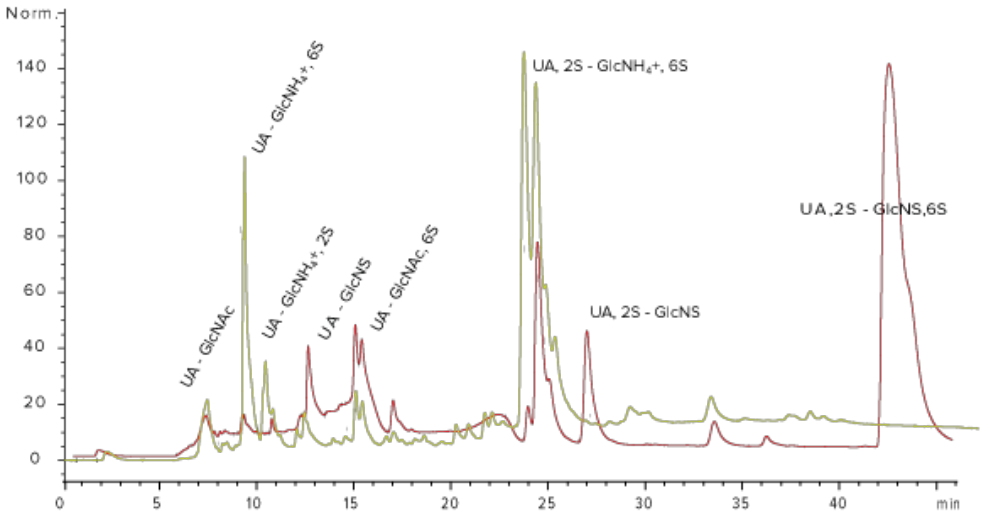

Heparin and N-Desulphated re-N-Acetylated Heparin disaccharide analysis

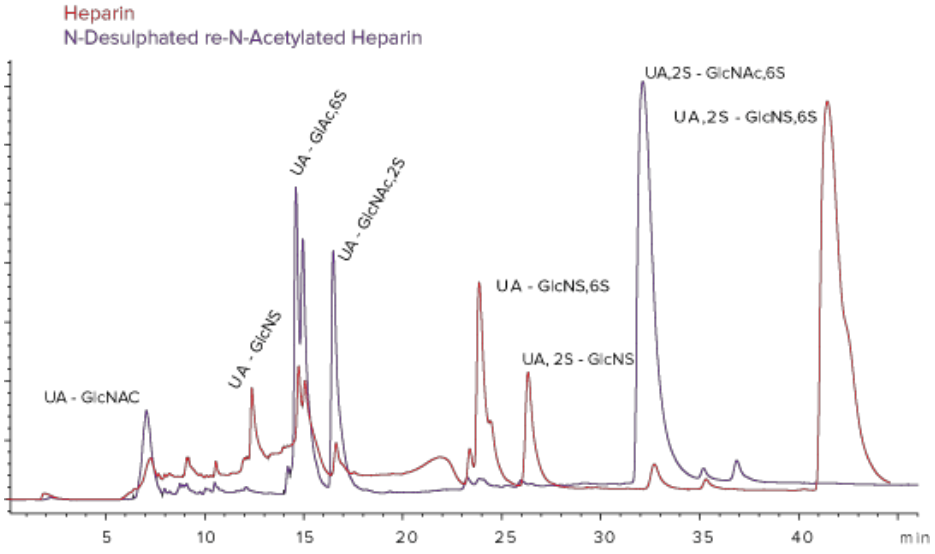

Heparin and 6-O Desulphated Heparin disaccharide anaylsis

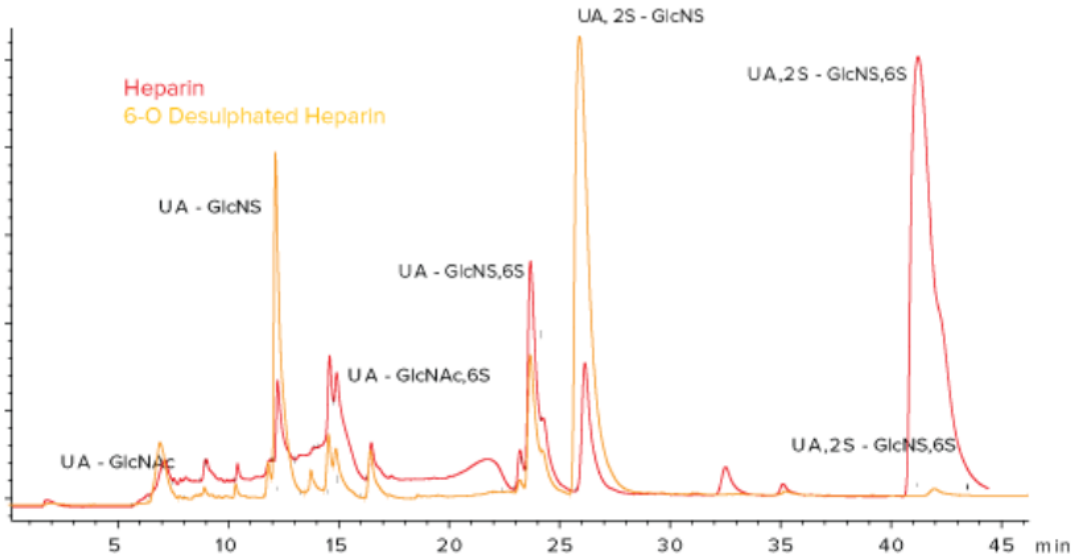

Heparin and 2-O Desulphated Heparin disaccharide anaylsis

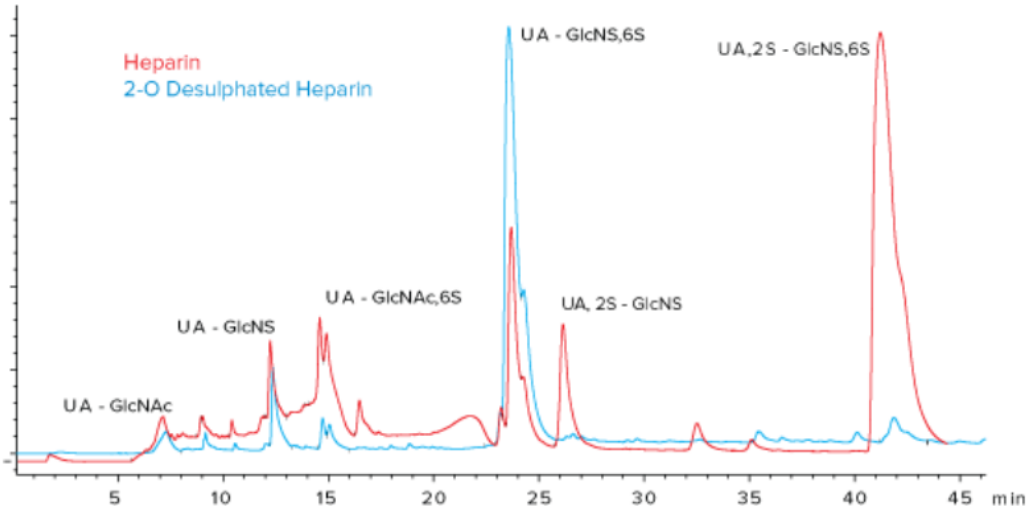

N-Desulphated Heparin (DSH003/N) disaccharide anaylsis

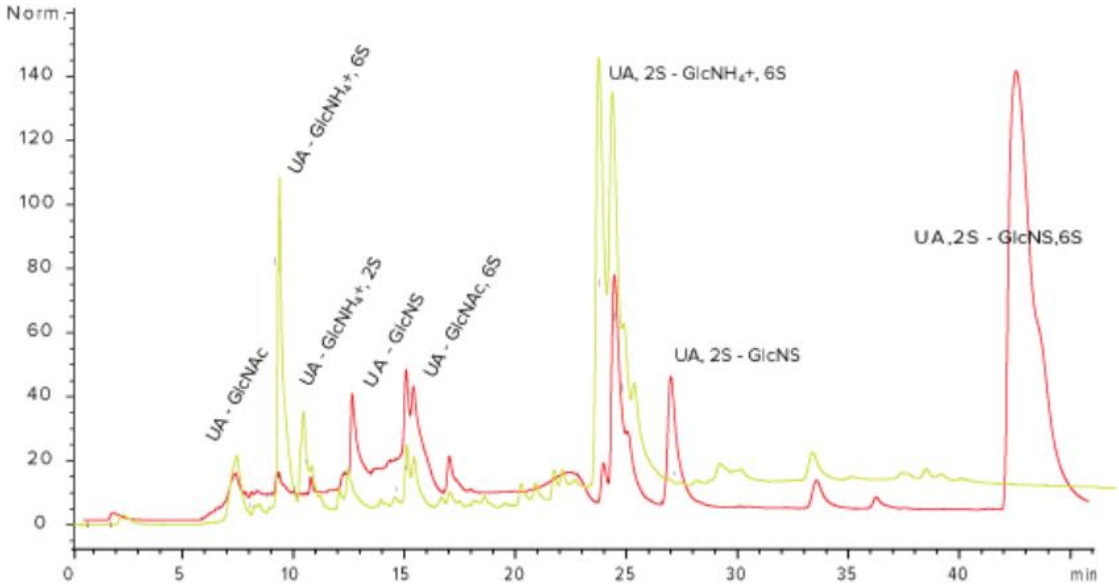

Heparin and N-Desulphated re-N-Acetylated Heparin disaccharide analysis

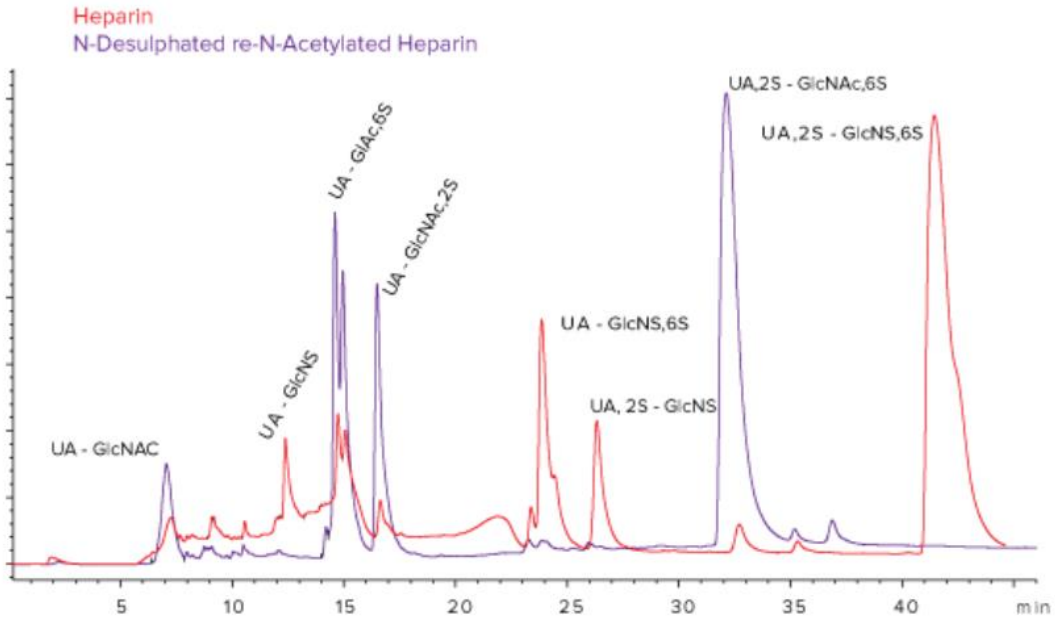

4.5 ACKNOWLEDGMENT

Chapter 4 is a modified reprint of the material as it appears in Bioconjugate Chemistry, 2019. Trieger G. W. VerespyIII S, Gordts P. L. S. M. Godula K. Efficient Synthesis of Heparinoid Bioconjugates for Tailoring FGF2 Activity at the Stem Cell–Matrix Interface. The dissertation author was the primary investigator and author of this paper

4.6 REFERENCES

[1]. Lutolf, M. P.; Hubbell, J. A. *Nat. Biotech*. **2008**, *23*, 47-55. Synthetic biomaterials as instructive extracellular microenvironments for morphogenesis in tissue engineering.

[2] Lee, K.; Silva E. A.; Moony D. J. *J. R. Soc. Interface* **2011**, *8*, 153-170. Growth factor delivery-based tissue engineering: general approaches and a review of recent developments.

[3] Xu, D.; Esko J. D. *Annu. Rev. Biochem.* **2014**, *83*, 129-157. Demystifying heparin sulfate-protein interactions.

[4] Vlodavsky, I.; Bar-Shavit, R.; Ishai-Michaeli, R.; Bashkin, P.; Fuks, Z. *Trends Biochem Sci.* **1991**, *7*, 268-271. Extracellular sequestration and release of fibroblast growth factor: a regulatory mechanism?

[5] Ayerst, B. I.; Merry, C. L. R.; Day, A. J. *Pharmaceuticals* **2017**, *10*, 54. The good the bad and the ugly of glycosaminoglycans in tissue engineering applications.

[6] Hudalla G. A., Murphy W. L. Adv. *Funct. Mater.* **2011**, *21*, 1754–1768. Biomaterials that regulate growth factor activity via bioinspired interactions.

[7] Huang M. L.; Smith R. A.A.; Trieger G., W.; Godula K. *J. Am. Chem. Soc.* **2014**, *136*, 10565-8. Glycocalyx remodeling with proteoglycan mimetics promotes neural specification in embryonic stem cells.

[8] Naticchia M. R.; Laubach L. L.; Tota E. M.; Lucas T. M.; Huang M. L.; Godula K. *ACS Chem. Bio.* **2018**, DOI: 10.1021/acschembio.8b00436. Embryonic stem cell engineering with a glycomimetic FGF2/BMP4 co-receptor drives mesodermal differentiation in a three-dimensional culture.

[9] Pulsipher A.; Griffin M. A.; Stone S. E.; Hsieh-Wilson L. C. *Angew Chem. Int. Ed.* **2015,** *54*, 1466–1470. Long-lived glycan engineering to direct stem cell fate.

[10] Lianga Y.; Kiick K. L. *Acta Biomater*. **2014**, *104*, 1588–1600. DOI: 10.1016/j.actbio.2013.07.031. Heparin-functionalized polymeric biomaterials in tissue engineering and drug delivery applications.

[11] Martinoa M. M.; Briqueza P. S.; Rangaa A.; Matthias L. P.; Hubbell J. A. *PNAS* 2013, *110*, 4563-4568. Heparin-binding domain of fibrin(ogen) binds growthfactors and promotes tissue repair when incorporated within a synthetic matrix.

[12] Hudalla G. A.; Koepsel J. T.; Murphy W. L. *Adv. Mater*. **2011**, *23*, 5415-5418. Surfaces that sequester serum-borne heparin amplify growth factor activity.

[13] Roy S.; Lai H.; Zouaoui R.; Duffner J.; Zhou H.; P Jayaraman L.; Zhao G.; Ganguly T.; Kishimoto T. K.; Venkataraman G. *Glycobiology* **2011**, *21*, 1194-205. Bioactivity screening of partially desulfated low-molecular-weight heparins: a structure/activity relationship study.

[14] Lundin L.; Larsson H.; Kreuger J.; Kanda S.; Lindahl U.; Salmivirta M.; Claesson-Welsh L. *J. Biol. Chem*. **2000**, *275*, 24653-24660. Selectively desulfated heparin inhibits fibroblast growth factor-induced mitogenicity and angiogenesis.

[15].Freudenberg U.; Zieris A.; Chwalek K.; Tsurkan M. V.; Maitz M. F.; Atallah P.; Levental K. R.; Eming S. A.; Werner C. *J. Control. Release* **2015**, *220*, 79-88. Heparin desulfation modulates VEGF release and angiogenesis in diabetic wounds.

[16] Xua X.; Jhaa A. K.; Duncan R. L.; Jia X. *Acta Biomater.* **2011**, *7*, 3050-3059. Heparin-decorated, hyaluronic acid-based hydrogel particles for the controlled release of bone morphogenetic protein 2.

[17] Benoit, D. S.; Anseth, K. S. *Acta Biomater*. **2015**, *1*, 461–470. Heparin functionalized PEG gels that modulate protein adsorption for hMSC adhesion and differentiation.

[18] Mathews S.; Mathew S. A.; Gupta P. K.; Bhonde R.; Totey S. J. *Tissue Eng. Regen. Med.* **2014,** *8*, 143–152. Glycosaminoglycans enhance osteoblast differentiation of bone marrow derived human mesenchymal stem cells.

[19] Zieris A.; Dockhorn R.; Röhrich A.; Zimmermann R.; Müller M.; Welzel P. B.; Tsurkan M. V.; Sommer J. U.; Freudenberg U.; Werner C. *Biomacromolecules*, **2014** *15*, 4439–4446. Biohybrid networks of selectively desulfated glycosaminoglycans for tunable growth factor delivery.

[20] Köwitsch A.; Zhou G.; Groth T. *J. Tissue Eng. Regen.* **2018**, *12*, e23-41 Medical application of glycosaminoglycans: a review.

[21] Zieris A.; Dockhorn R.; Röhrich A.; Zimmermann R.; Müller M.; Welzel P. B.; Tsurkan M. V.; Sommer J. U.; Freudenberg U.; Werner C. *Biomacromolecules*, **2014** *15*, 4439–4446. Biohybrid networks of selectively desulfated glycosaminoglycans for tunable growth factor delivery.

[22] Uygun B. E.; Stojsih S. E.; Matthew H. W. *Tissue Eng Part A.* **2009**, *15*, 3499-3512. Effects of immobilized glycosaminoglycans on the proliferation and differentiation of mesenchymal stem cells.

[23] Pulsipher A.; Griffin M. E.; Stone S. E.; Brown J. M.; Hsieh-Wilson L. C. *J. Am. Chem. Soc.* **2014**, *136*, 6794–6797. Directing neuronal signaling through cell-surface glycan engineering.

[24] Zhang F.; Fath M.; Marks R.; Linhardt R. *J. Anal. Biochem*. **2002**, *304*, 271–273. A highly stable covalent conjugated heparin biochip for heparin–protein interaction studies.

[25] Gildersleeve, J. C.; O. Oyelaran; J. T. Simpson; B Allred. *Bioconjug. Chem.* **2008**, *19*, 1485–1490. Improved procedure for direct coupling of carbohydrates to proteins via reductive amination.

[26] Kolb H. C.; Finn M. G.; Sharpless K. B. *Angew Chem Int Ed Engl.* **2001**, *40*, 2004-2021 Click chemistry: diverse chemical function from a few good reactions.

[27] Jewett J. C.; Bertozzi C. R. *Chem Soc Rev*. **2010**, *39*, 1272–1279. Cu-free click cycloaddition reactions in chemical biology.

[28] Spicer C. D.; Pashuck E. T.; Stevens M. M; *Chem Rev.* **2018**, *118*, 7702-7743. Achieving controlled biomolecule-biomaterial conjugation.

[29] He, X. P.; Zeng, Y. L.; Zang, Y.; Li, J.; Field, R. A.; Chen, G. R. *Carbohydr. Res*. **2016**, *429*, 1-22. Carbohydrate CuAAC click chemistry for therapy and diagnosis.

[30] Fajardo, A. R.; Guerry, A.; Britta, E. A.; Nakamura, C. V.; Muniz, E. C.; Borsali, R.; Halila, S. *Biomacromolecules* **2014**, 15, 2691-2700. Sulfated glycosaminoglycan-based block copolymer: preparation of biocompatible chondroitin sulfate b poly(lactic acid) micelles.

[31] Upadhyay K. K.; Le Meins J.-F.; Misra A.; Voisin P.; Bouchaud V.; Ibarboure E.; Schatz C.; Lecommandoux S. Biomacromole*cules* **2009**, *10*, 2802-2808. Biomimetic doxorubicin loaded polymersomes from hyaluronan-block-poly(γ-benzyl glutamate) copolymers.

[32] Yamaguchi, M.; Kojima, K.; Hayashi, N.; Kakizaki, I.; Kona, A.; Takagakia, K. *Tetrahedron. Lett*. **2006**, *47*, 7455-7458. Efficient and widely applicable method of constructing neo-proteoglycan utilizing copper(I) catalyzed 1,3-dipolar cycloaddition.

[33] van Kuppevelt T. H.; Oosterhof A.; Versteeg E. M. M.; Podhumljak E.; van de Westerlo E. M. A.; Daamen W. F. *Sci. Rep.* **2017**, *7*, 14785. Sequencing of glycosaminoglycans with potential to interrogate sequence-specific interactions.

[34] DeAngelis P. L.; Liu J.; Linhardt R. J. *Glycobiology* **2013**, *23*, 764–777. Chemoenzymatic synthesis of glycosaminoglycans: re-creating, re-modeling and re-designing nature's longest or most complex carbohydrate chains.

[35] Chen Y.; Narimatsu Y.; Clausen T. M.; Gomes C.; Karlsson R.; Steentoft C.; Spliid C. B.; Gustavsson T.; Salanti A.; Persson A. et al. *Nat. Methods.* **2018**, DOI: https://doi.org/10.1038/s41592-018-0086-z. The GAGOme: a cell-based library of displayed glycosaminoglycans.

[36] Qiu H.; Shi S.; Yue J.; Xin M.; Nairn A. V.; Lin L.; Liu X.; Li G.; Archer-Hartmann S. A.; Dela Rosa M.; Galizzi M.; Wang S.; Zhang F.; Azadi P.; van Kuppevelt T. H.; Cardoso W. V.; Kimata K.; Ai X.; Moremen K. W.; Esko J. D.; Linhardt R. J.; Wang L. *Nat. Methods*. **2018,** *15*, 889-899. A mutant-cell library for systematic analysis of heparan sulfate structure-function relationships.

[37] Baik J. Y.; Gasimli L.; Yang B.; Datta P.; Zhang F.; Glass C. A.; Esko J. D.; Linhardt R. J.; Sharfstein S. *T. Metab. Eng*. **2012**, *14*, 81-90. Metabolic engineering of Chinese hamster ovary cells: towards a bioengineered heparin.

[38] Smith J. M.; Vitali F.; Archer S. A.; Fasan R. *Angew. Chem., Int. Ed*. **2011**, *50*, 5075 – 5080. Modular assembly of macrocyclic organo–peptide hybrids using synthetic and genetically encoded precursors.

[39] Laaf D.; Bojarová P.; Pelantová H.; Křen V.; Elling L. *Bioconjug Chem.* **2017,** *28,* 2832-2840. Tailored multivalent neo-glycoproteins: synthesis, evaluation, and application of a library of galectin-3-binding glycan ligands.

[40] Prasanphanich N. S.; Song X.; Heimburg-Molinaro J.; Luyai A. E.; Lasanajak Y.; Cutler C. E.; Smith D. F.; Cummings R. D. *Bioconjug Chem.* **2015**, *26*, 559-571. Intact reducing glycan promotes the specific immune response to lacto-N-neotetraose-BSA neoglycoconjugates.

[41] Zhang Y.; Li Q.; Rodriguez L. G.; Gildersleeve J. C. *J. Am. Chem. Soc.* **2010**, *132*, 9653-9662. An array-based method to identify multivalent inhibitors.

[42] Hermanson, G. T. *Bioconjugate Techniques, Third Edition*, **2013**. Academic Press. Chapter 4.1 Zero length crosslinkers.

[43] Uchimura K.; Morimoto-Tomita M.; Bistrup A.; Li J., Lyon M.; Gallagher J.; Werb Z., Rosen S. D. *BMC Biochem.* **2006**, *7,* 2. HSulf-2, an extracellular endoglucosamine-6-sulfatase, selectively mobilizes heparin-bound growth factors and chemokines: effects on VEGF, FGF-1, and SDF-1.

[44] Hermanson, G. T. *Bioconjugate Techniques, Third Edition*, **2013**. Academic Press. Chapter 4.1 Zero length crosslinkers.

[45] Uchimura K.; Morimoto-Tomita M.; Bistrup A.; Li J., Lyon M.; Gallagher J.; Werb Z., Rosen S. D. BMC Biochem. 2006, 7, 2. HSulf-2, an extracellular endoglucosamine-6-sulfatase, selec-tively mobilizes heparin-bound growth factors and chemokines: effects on VEGF, FGF-1, and SDF-1.

[46] Cesaretti M.; Luppi E.; Maccari F.; Volpi N. *Carbohydr. Polym.* **2003**, *54*, 59-61. A 96-well assay for uronic acid carbazole reaction.

CHAPTER 5: Development and evaluation of a glycosaminoglycan microarray for the manipulation of stem cell differentiation

5.1 INTRODUCTION

The preceding chapters focused on the development and application of GAG-mimetic materials to engineer the cell surface (Chapters 2 and 3) and extracellular matrix (Chapter 4) glycan microenvironments of progenitor cells to tailor their interactions with morphogens and influence their proliferation and differentiation. This chapter describes efforts to integrate these materials with high-throughput microarray platforms to directly connect and rapidly survey changes in cellular functions in response to the composition of glycan microenvironments. Microarray-based approaches for the discovery of functional biomaterials based on DNA and proteins have contributed to the recent rapid advances in the fields of tissue engineering and cell-based therapies.[1] A technology incorporating glycans into the biomaterial discovery process would be similarly transformative in the context of biomedical research. However, the structural complexity of glycans, the challenging and time-consuming chemical synthesis of glycomaterials, and the often limited understanding of glycan functions in cellular processes, complicates the development of such technologies. Here, I describe my efforts to generate an array platform prototype, which would allow me to directly correlate changes in glycan microenvironment composition to cellular activity, specifically in the context of stem cell differentiation.

The microarray format reduces the requirement for large quantities of materials and offers high-throughput multiplexing in biological assays. The cell-based functional

readout streamlines the discovery process by linking material structure directly to cellular responses, which overcomes current limits on our understanding of the roles of glycans in cellular signaling and eliminates inefficiencies of approaches focused on analysis of individual glycan-protein interactions, which may not always be predictive of a successful biological outcome *in vivo*.

One difficulty in obtaining structure-activity relationships between GAGs and proteins of interest lies with the small amounts of the GAGs that can be obtained from biological samples and the structural heterogeneity in such samples. This problem is typically addressed through harvesting of a GAG from organs or large-scale cell culture combined with the application of advanced chromatography and mass spectroscopy methods for their purification and structural analysis.[3,4] As a result, there has been a significant amount of synthetic work focused on generating more complex, but structurally-well defined, HS oligosaccharides.[5,6] A recent impressive effort was published where 47 different HS tetrasaccharides were synthesized, arrayed, and profiled for growth factor binding with FGF2.[7] The best binders of FGF2, or "hits," were then evaluated in solution for their ability to impact proliferation. This is a typical workflow in most studies that aim to prepare a variety of HS oligosaccharides, where an initial binding assay is run, then the "hits" are scaled-up in preparation and evaluated in a biological context. The shortcoming of this approach is that short oligosaccharide sequences, which are more synthetically accessible and can produce a "hit" on a microarray, may not always be sufficient to induce biological activity in cells. At least a hexasaccharide motif with sulfation at the *N*- and 6 -*O*-position of the glucosamine and 2-*O*-sulfation on the iduronic acid have been identified as the minimal HS sequence needed to promote FGF2 signaling

and mitogenic response in swiss 3t3 fibroblasts. [8,9,10] Much larger oligosaccharide sequences may be required for signaling activity via other growth factors (e,g. BMP4).[11] GAG structures of such size and complexity pose a formidable synthetic challenge. While chemoenzymatic methods are being to emerge that provide access to such structures,[12] a parallel effort focuses on the development of nanoscale materials that integrate available GAG oligosaccharide fragments with synthetic macromolecular architectures to derive biologically active GAG mimetics (see chapters 1 and 2 for more detailed discussion).

To connect binding data obtained from glycan array screens with purified proteins of interest to the biological outcomes observed in *in vivo* assays, efforts have begun to emerge to develop arrays in which the structure of the arrayed glycan can be linked directly to cellular response. The most common approach to achieve this objective is to alter the surface chemistry of the array substrate to support cell growth while allowing for immobilization of glycans.[13] This strategy has been commonly applied with successful results to identify matrix compositions that provide desired cellular outcomes, often in stem cells, such as enhanced proliferation or altered differentiation.[14] For Instance, the Bhatia lab prepared a microarrays composed of combinations of matrix proteins (i.e., laminin, fibronectin and collagen I, III and IV) printed in spots at varying ratios to identify ECM compositions most effective for supporting hepatic differentiation.[16] In another study, the Lutolf lab developed a massively high-throughput 3D-cell-encapsulating hydrogel array to evaluate a variety of physical, chemical, and biochemical parameters of the stem cell niche environment on cell renewal and differentiation.[17] Unfortunately, GAGs and glycans in general are rarely included for analysis in these high throughput screens.

Nonetheless, a handful of early examples of GAG-focused cellular arrays have been reported in the literature. The Turnbul lab reported a 2D HS array generated by pipette spotting of oligosaccharides of increasing length purified after partial enzymatic hydrolysis of heparin on aminosilane-coated slides. They were able to successfully evaluate the effects of the immobilized oligosaccharides based on their length on MAPK signaling activity in response to FGF2 stimulation in 3T3 fibroblasts.[19] The Linhard lab reported a series of studies evaluating the effects of GAGs on stem cell proliferation in 3D arrays, where GAG polysaccharides and mouse embryonic stem cells were physically entrapped in hydrogel droplets and exposed to different members of the FGF growth factor family. It should be noted that the GAGs were not covalently linked to the degradable hydrogel network and likely functioned as a soluble, rather than matrix-associated, FGF co-receptors. The distinct biological effects of GAGs based on their different presentations in cellular context (i.e., soluble ligands vs. matrix- or cell surface-associate) poses a considerable challenge for predicting the biological activities of GAG-mimetic biomaterials.

This chapter describes my efforts to integrate GAG-mimetic biomaterials developed in Chapters 2 (synthetic GAG-mimetic polymers) and 4 (multivalent GAG polysaccharide-protein conjugates) into a microarray platform and directly asses their ability to influence FGF2-mediated MAPK signaling and neural differentiation in mESCs. If successful, such an array platform, in conjunction with the simple and efficient synthesis and structural diversification of the glycoconjugates, would allow for rapid identification of biologically active GAG-mimetic biomaterials for applications in tissue engineering.

5.2 RESULTS AND DISCUSSION

5.2.1 Generation of Microarray Substrates for Cell Culture

We envisioned designing a cellular microarray substrate for the immobilization of GAG-mimetic materials that could also support long-term mESC culture required for many differentiation protocols. We hypothesized that the GAG-materials immobilized in spots on the array would generate unique local cellular microenvironments with the capacity to bind and concentrate GFs from media and, possibly, engage cell surface receptors directly to activate GF signaling.

To generate a cell-adhesive pattern on the array substrate, we first spotted porcine gelatin on epoxide-functionalized glass. The protein was expected to react through its solvent exposed nucleophilic amino acid residues with the electrophilic surface and covalently attach to the glass. To prevent cell spreading and migration between spots on the array, we next evaluated several surface passivation methods. Taking advantage of the remaining epoxide groups between gelatin spots, we grafted a 10kDa bis-amino polyethylene glycol polymer (A-PEG) to the surface under cloud point conditions.[41] The term “cloud point” refers the cloudiness that can occur when non-ionic surfactants containing polyoxyethylene chains in aqueous solutions are heated in the presence of salts above a cloud-point temeperature, at which the dissolved substrate begins to slightly shed its hydration shell and partially come out of solution without fully precipitating. This simultaneous presence of two phases causes the observed cloudiness. This behavior is characteristic for poly(ethylene glycol) (PEG) polymers, which exhibit inverse relationship between solubility and temperature in water.[42] The temperature at which clouding occurs

can be tuned by salt concentrations in the solution. This method can be used to enhance the exposure and grafting of PEG molecules to a reactive surface, and increase the density of the resulting PEG-brushes on glass and their long-term stability under cell culture conditions.[41]

We treaded epoxy glass with a 10 mg/mL solution of 10kDa A-PEG in 0.1M PBS containing 0.62 M K_2SO_4 overnight at 37 °C. Although the cloud point for A-PEG under these conditions occurs at approx.. 20 °C, we chose the treatment at the slightly higher 37 °C temperature to ensure constant cloud point exposure, as the salts in solution had a tendency to precipitate out during overnight incubations with a loss of cloud point. Exceeding the cloud point temperature prevented this problem and the solution remained cloudy throughout the treatment. It was important that the temperature of the cloud point did not reach 50 °C, at which the gelatin began to melt and dissociate from the glass surface. In addition to the A-PEG cloud point method, we also evaluated the passivation with bovine serum albumin (BSA) in 5% aqueous solution, previously reported to be suitable for cell culture, or by opening all of the unreacted surface epoxides with ethanolamine, which has not be reported in the context of cell culture but is often employed in the processing of glycan arrays.

Cell seeding experiments on the resulting gelatin arrays revealed significant differences in the effectiveness of the different passivation methods method (**Fig. 575**). On Day 1 after seeding followed by a stringent wash, BSA had almost no effect and the cells grew rampantly over the entire slide surface, while the ethanol amine treatment gave a marginal improvement with some decrease in the number of cells populating areas between gelatin spots, and the formation of colonies is apparent. The cloud point

passivation method was the most effective yielding well-formed colonies at all seeding densities with the least amount of adherent cells in between spots.

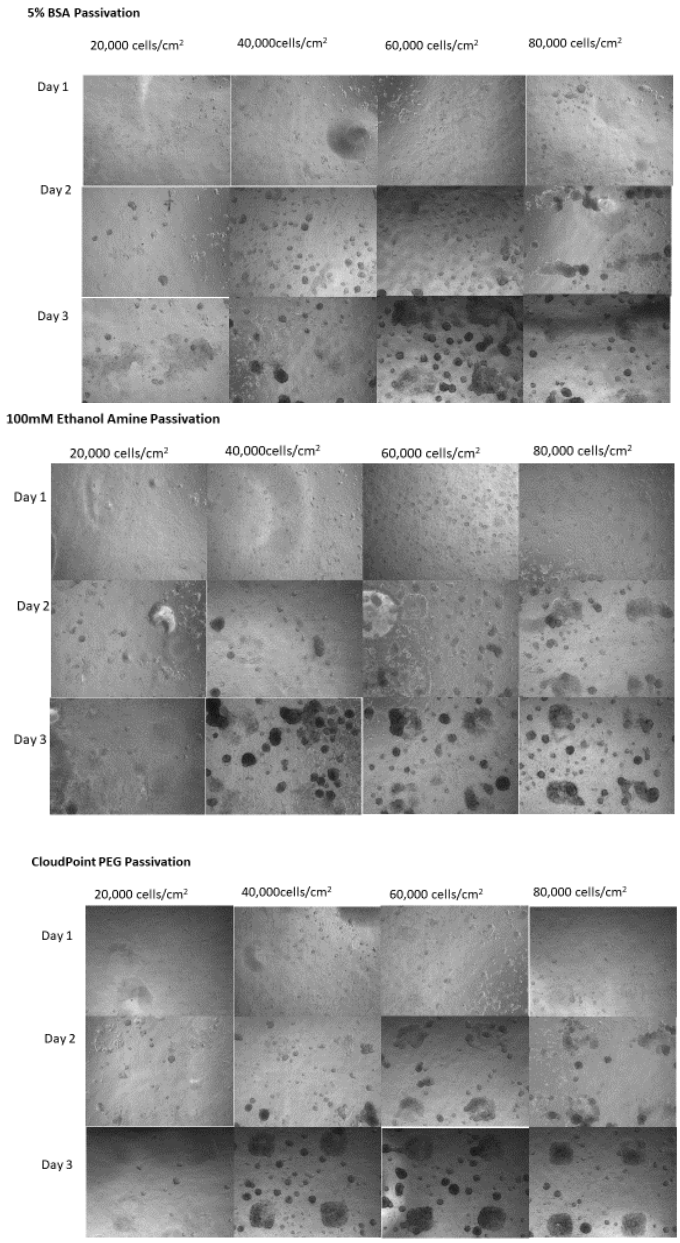

Figure 75. Validation of cloud point passivation with mESC. Cells seeded at a 20,000, 40,000, 60,000, and 80,000 cells/cm^2 onto gelatin arrays printed upon epoxide slides and observed for daily for growth for three days. Prior to seeding arrays with cells, arrays were passivated using the indicated method: *top pane*) 100mM ethanol amine in pH 8.5 borate buffer, 24 hr. *Middle Panel*: 5mg/mL BSA in PBS, 24 hr. B*ottom panel* cloud point PEG passivation: 10 mg/mL poly(ethylene glycol) bis(amine) Mw 10kDa, in 0.62 M K_2SO_4, 0.1M phosphate buffer, pH 6.5, 37 °C, 24 hr.

Unfortunately, none of the methods afforded complete passivation, with cells always growing to some extent between spots. This would become more problematic during long-term experiments (7 to 9 days), where cells would have more time to grow and deposit their own extracellular matrix onto the passivated glass surfaces to support their spreading and "bridging" from one spot to another.

Next, we turned our attention to an alternative strategy previously reported for generating cellular arrays based on surfaces coated with poly(acrylamide) hydrogels.[43] Preparation of the arrays was done according to the published procedure by first etching regular glass microscope slides under basic conditions followed by treatment with trimethoxysilane-methacrylate to facilitate grafting of the hydrogel to the glass surface. The functionalized slide was coated with an aqueous solution of acrylamide monomer and bisacrylamide crosslinker, and a redical UV initiator. Coverslip was then attached and the gels were cured using UV light to generate a poly(acrylamide) hydrogel layer about 40 μm thick covalently attached to the glass slide surface. These acrylamide slides were very affordable and could be made in bulk, which were two immediately attractive aspects of the method. After printing and physisorption of gelatin solutions onto dehydrated hydrogels films, we were observed that the cells were unable to grow on the poly(acrylamide) gels in the absence of the gelatin matrix (**Fig. 76**).

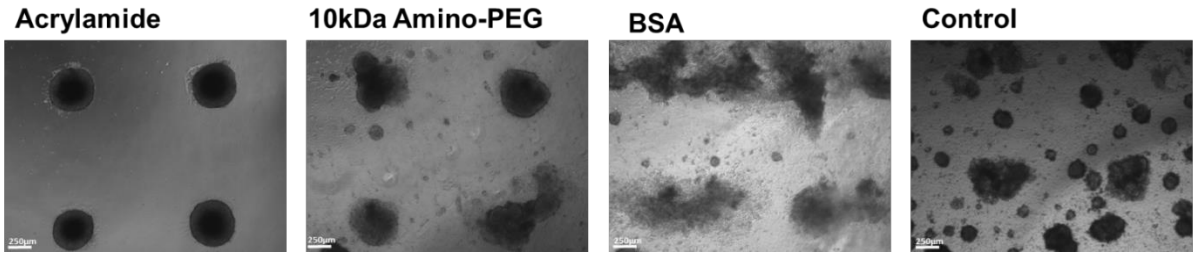

Figure 76. Comparison of passivation techniques. Glass microscope slides were passivated using the acrylamide hydrogel method, or remained unmodified glass (control) while epoxide slides were passivated with a 10mg/mL 10kDa amino-PEG cloud point solution, or 5% BSA. Incubation in passivation solution occurred over 24 hrs. Cells seeded at 20,000 cells/cm^2 grown for 6 days in mESC maintenance media.

Based on the ability of the poly(acrylamide) hydrogel substrates to maintain uniform stem cell colony growth for over 6 days in culture, we selected this method for further development toward the desired cellular glycan array.

5.2.2 Preparation and characterization of heparinoid displays on surfaces

Our next aim was to integrate our glycomaterials into the hydrogel network, evaluate the retention of the materials in the hydrogel matrix, and analyze their ability to bind to growth factors and antibodies (**Fig. 77**). To introduce reactive handles for the covalent immobilization of GAG-mimetics into the polymer network, we added allyl glycidyl ether (AGE) as a co-monomer during the hydrogel polymerization. This allowed us to introduce an epoxide group that was subsequently reacted with dibenzocycooctyne amine (ADIBO) for the conjugation of azide-carrying GAG-mimetic glycopolymers via the strain-promoted alkyne-azide cycloaddition (SPAAC) reaction (**Fig.** and Chapter 2). The resulting hydrogels were thus primed for array assembly by printing GAG-mimetics solutions

containing gelatin. While the gelatin becomes physically entrapped and intercalated within the hydrogel, the glycoconjugates can covalently graft to the polymer network.

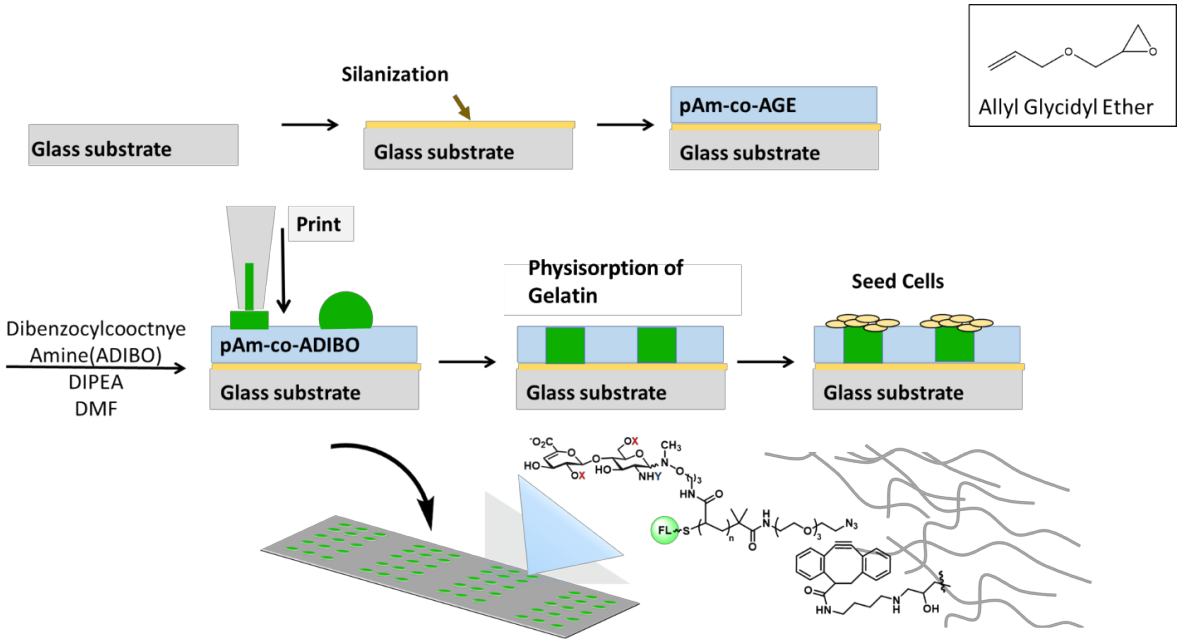

Figure 77. Fabrication of cellular microarrays. An untreated glass microscope slide is first etched and salinized with TMS-methacrylate. The methacrylate then participates in an acrylamide polymerization occurring on the surface of the slide, so that the hydrogel is covalently adhered to the plate. The acrylamide reaction can also proceed in the presence of allyl glycidyl ether, which when reacted with ADIBO, allows the hydrogel to bear a click handle. This surface can then be printed upon with gelatin which remains physically entrapped and/or azide presenting materials which will covalently incorporate into the hydrogel matrix. Cells can then be seeded upon the array.

To facilitate the optimization of GAG-mimetic array construction by “clicking” the azide functionalized glycopolymers to the cyclooctyne-functionalized hydrogels, we decided to generate a stable and affordable positive control with similar FGF2 binding as the GAG-mimetics to which we could benchmark our new materials. To do so, we conjugated heparin to gelatin in two steps. First, we converted the carboxylates in iduronic acids in heparin into activated *N*-hydroxy succinimidyl (NHS) esters in the presence of the

carbodiimide coupling reagent, 1-ethyl-3-(3-dimethylaminopropyl)carbodiimide (EDC). ^{1}H NMR analysis confirmed a successful ester activation with the four NHS methylene proton signals clearly detected as a singlet at 2.8 ppm (**Fig. 78**). Next, the NHS-heparin was coupled to gelatin through it solvent exposed amine groups in PBS buffer. The resulting BSA-heparin conjugate was printed on dehydrated hydrogel slides and physically entrapped in the gel network. Probing the array with FGF2 labeled with AlexaFluor 647 (AF647) indicated robust binding to the arrayed heparin-BSA conjugate (**Fig. 79**). Notably, covalent pre-conjugation of heparin to the BSA protein carrier greatly increased the retention of heparin the polymer network as non-conjugated heparin was rapidly lost from the array during washes (**Fig. 79**).

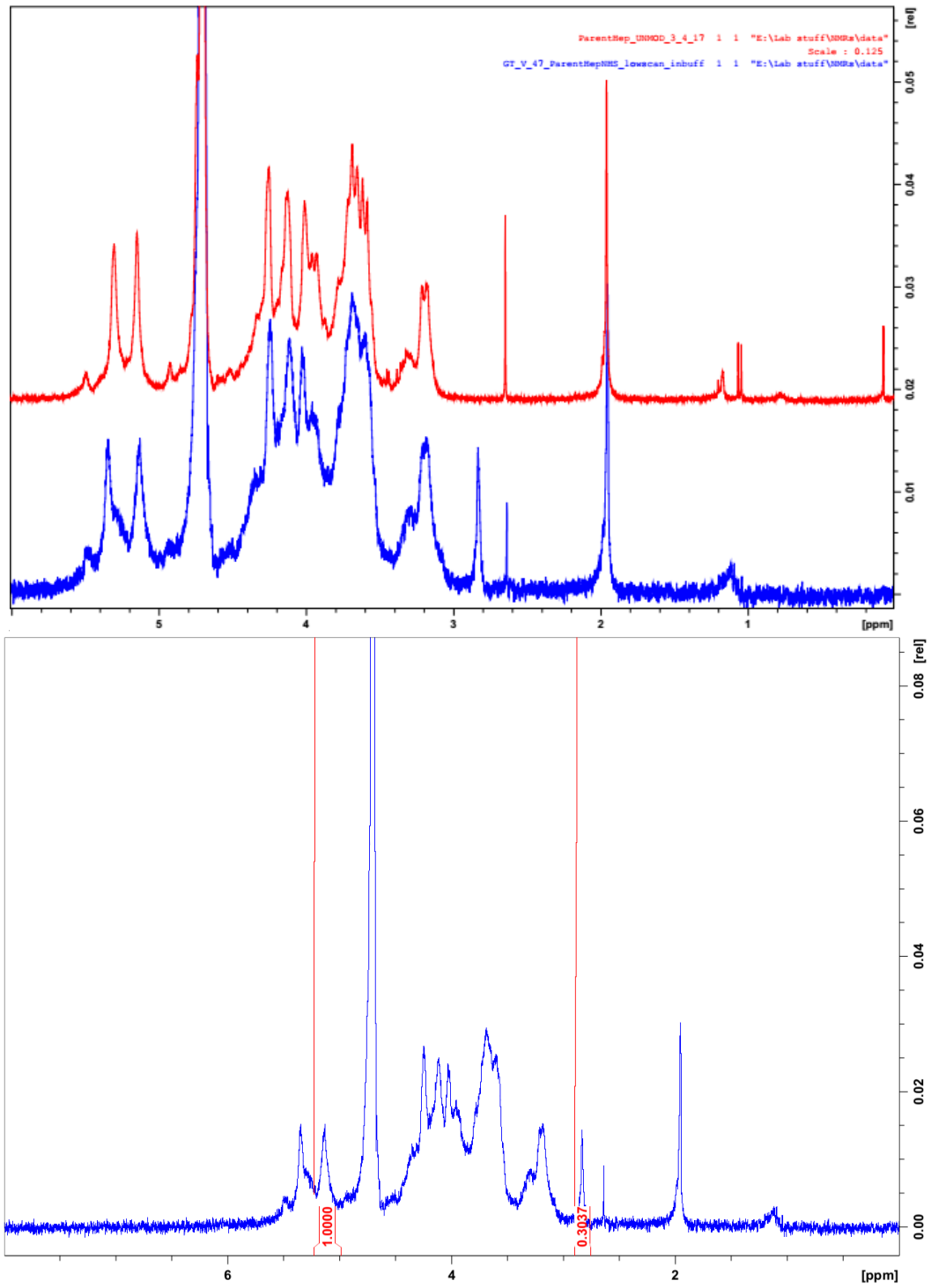

Figure 78 NMR Spectra of hep-NHS (blue spectra). *Top* NMR overlay of heparin (red) with hep-NHS, with the signature NHS peak at 2.8 ppm. *Bottom* NMR of hep-NHS.

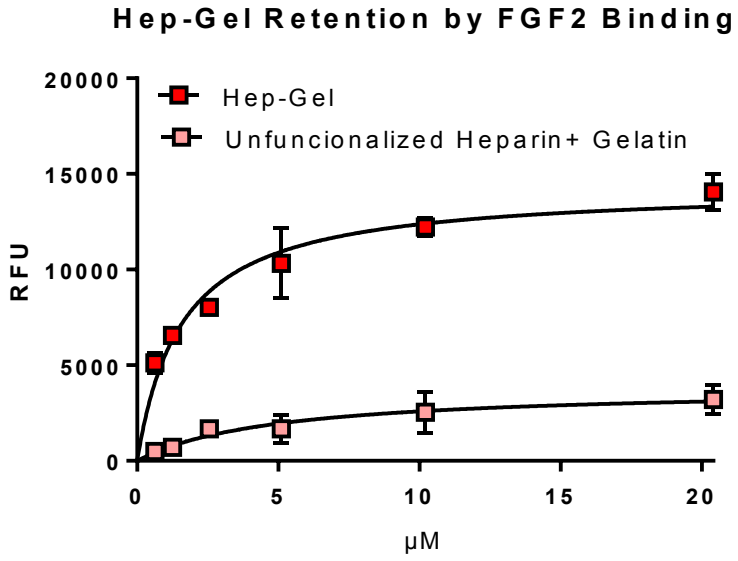

Figure 79. Heparin and hep-gel retention at different concentration after additional washing with 2X PBS 0.1% tween 3x15 min, 1x24 hr at 37 °C, as determined from relative AF647-FGF2 (10 nM) binding.

With a positive control established, we began evaluating GAG-mimetic glycopolymer printing conditions by assaying for FGF2 binding by the arrayed materials. We focused on FGF2 interactions in the array for its role in activating MAPK signaling and neural differentiation in mESCs and the ability of our GAG-mimetics to facilitate the process in the HS-defficient *EXT1*$^{-/-}$ mESCs (see Chapter 2).

To control the amount of GAG-mimetic polymer retained on the array, we titrated both the concentration of the polymer in the printing solution as well as the amount of AGE, and thus cyclooctyne, incorporated into the poly(acrylamide) supporting hydrogel network (**Fig. 80**). Increasing the concentration of AGE monomer fraction from 1% to 10% enhanced retention of glycopolymers as indicated by an increase in fluorescence associated with bound FGF2-AF647 (**Fig. 80**).Even at the highest level of ADIBO functionalization (10%), the FGF2 bindng to the D2A6 polymer did not reach that of our

heparin positive control. This is not surprising, as much more heparin is likely to be introduced through trapping of its conjugate with BSA compared to the amount of GAG-mimetic polymer that can be covalently grafted to the hydrogel. We found that the 5% and 10% functionalized acrylamide performed similarly in FGF2 binding assays. Therefore, we opted to use the 5% acrylamide to continue with the development of the cellular glycan array platform.

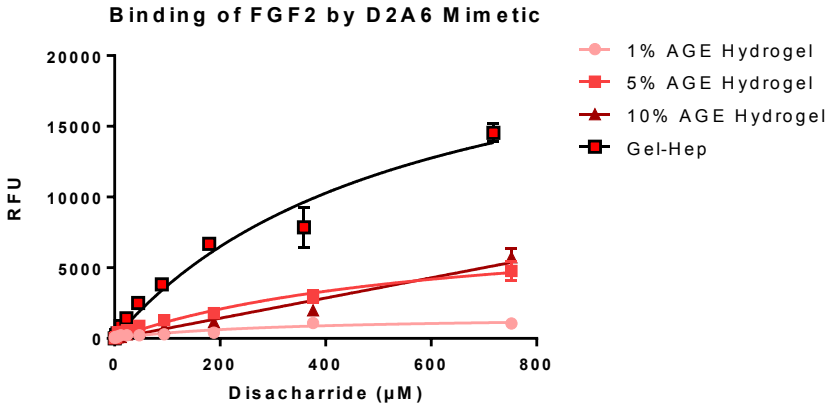

Figure 80. Grafting of D2A6-polymer at increasing ADIBO functionalization of poly(acrylamide) hydrogels (1%,5%, 10% based on AGE monomer fraction) as determined by the fluorescence of bound FGF2-AF647. Gelatin functionalized with heparin (Hep-Gel) was included as a positive control. Thorough washing (2X PBS, 0.1% tween 3x15 min, 1x24 hr at 37 °C) was performed prior to FGF2 binding to asses polymer retention.

Further investigation was done to evaluate if cyclooctyne pre-functionalization was required for retention of the azide-modified GAG-mimetic glycopolymers on the arrays. We reasoned that if other macromolecules, such as gelatin, were retained by the hydrogel network through physical trapping in the polymer mesh, there was a possibility the same could be true for the glycopolymers. We evaluated the retention and protein binding capacity of a set of GAG-mimetic glycopolymers containing either

an azide moiety (N_3) or terminated with carboxylic acid (CA) and carrying either the FGF2-binding D2A6 disaccharide motif, or the nonsulfated HS GAG disaccharide, D0A0, or the sulfate monosaccharide, GlcNAc6S, negative controls after printing on hydrogels either with or without ADIBO pre-functionalization. Prior to protein binding assays, extensive washing of the printed arrays in 2X PBS with 0.1% tween overnight at 37 °C was performed to remove any loosely bound glycopolymers (**Fig. 81**). We used FGF2 and the lectin wheat germ agglutinin (WGA) at various concentrations to detect the presence of the D2A6 and GlcNAc6S glycopolymers, respectively. ADIBO pre-functionalization proved to enhance the amount of protein retained and the reproducibility of the binding assays. It seems that although some polymer is retained in the absence of covalent immobilization, the lack of control over polymer retention introduces greater statistical errors due to spot heterogeneity and weak signal.

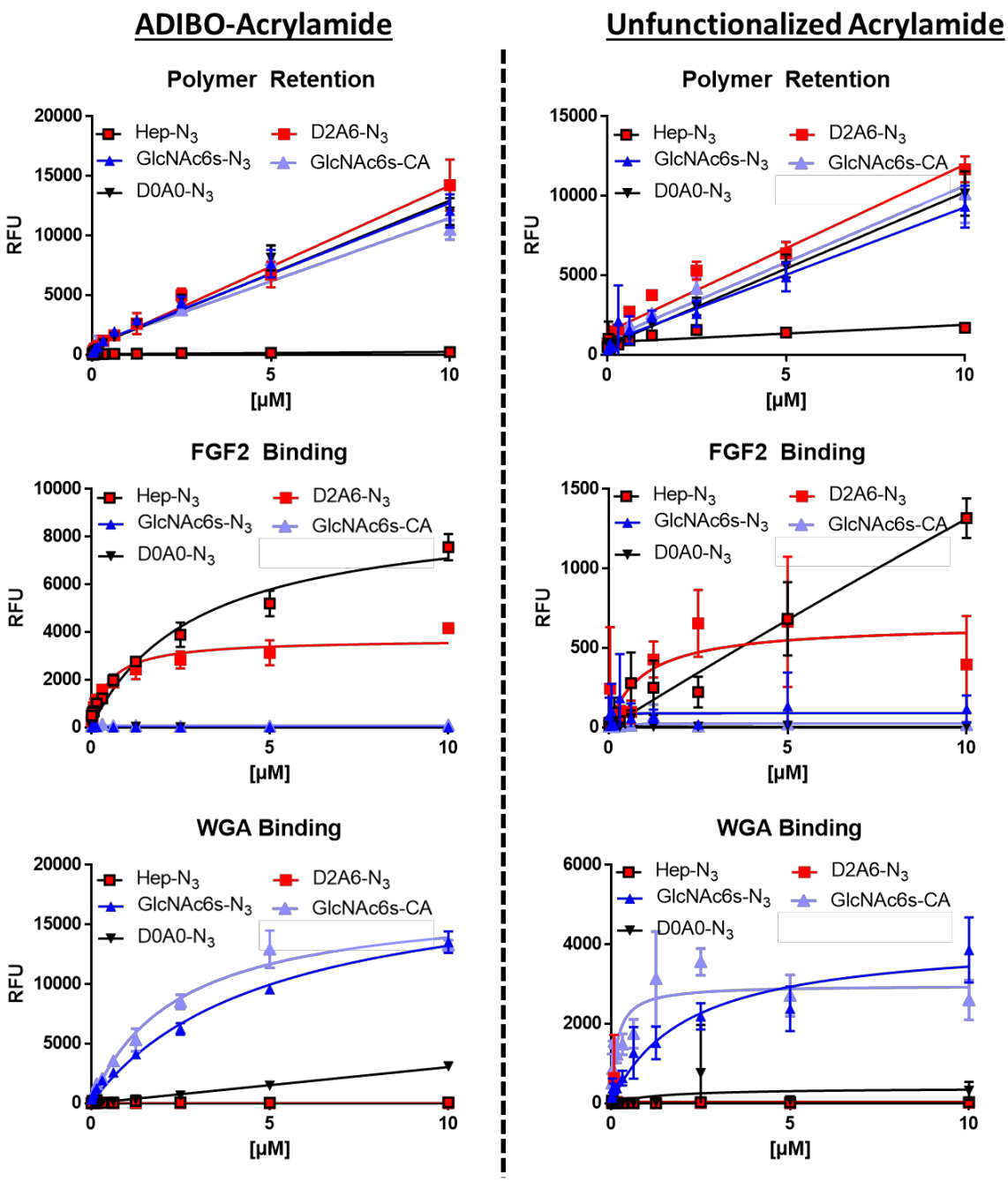

Figure 81 Comparison of ADIBO-functionalized acrylamide to unfunctionalized acrylamide hydrogel arrays when azide functionalized GAG-mimetics were printed upon the surface (excluding Hep-Gel, which serves as a FGF2 binding control.) Additional washing performed prior to fluorescent scan of polymer retention and FGF2 binding: 2X PBS, 0.1% tween 3x15 min, 1x24 hr at 37 °C *Top panel:* Retention of printed GAG-mimetic, which is labeled with TAMRA. *Middle panel*: FGF2 Binding of printed GAG-mimetics. *Bottom panel*: Wheat germ agglutinin binding of printed GAG-mimetics.

Realizing the high efficiency of direct trapping of the heparin-gelatin conjugate (**Fig. 80**), we decided to expand our array to include similar gelatin conjugates with other GAG polysaccharides (i.e., chondroitin sulfate (CS) and hyaluronic acid (HA)) as well as chemically modified heparinoids with distinct sulfation patterns and FGF2 binding activities. Accordingly, we converted a set of full-length heparinoids desulfated at the *N*-, 2-*O*-, or 6-*O*- position as well as an *N*-desulfated/*N*-acetylated analog in NHS derivatives (NDSH, 2ODSH, 6ODSH, NDSH-reacetylated, respectively) using the same carbodiimide chemistry described above. We used the detection of the NHS methylene proton NMR signal at 2.8 ppm to confirm the transformation (**Fig. 82- Fig. 84**). These reactive GAGs were then coupled with gelatin, printed on the hydrogel substrates and probed with GAG-binding protein. (**Fig. 82, Fig. 83**) We used FGF2, the anti-CS antibody (CS 56), and the hyaluronic acid binding protein (HABP) to detect heparionids, CS and HA, respectively. Gratifyingly, the array assay results confirmed the known protein binding activities for each GAG polysaccharide.

.

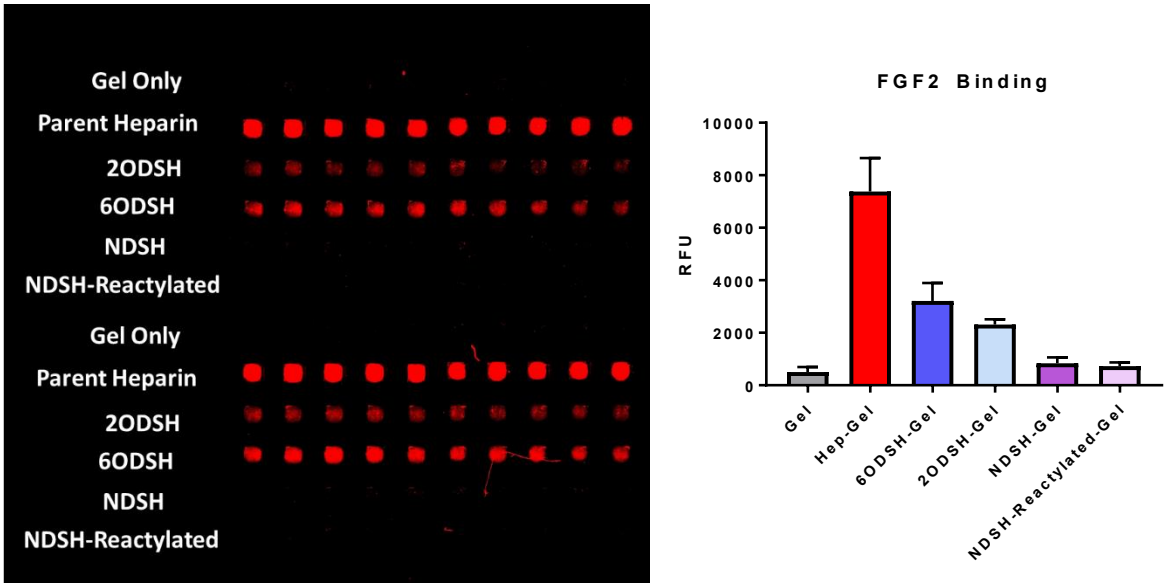

Figure 82 AF647-FGF2 (10nM) binding of selectively desulfated heparinoid panel.

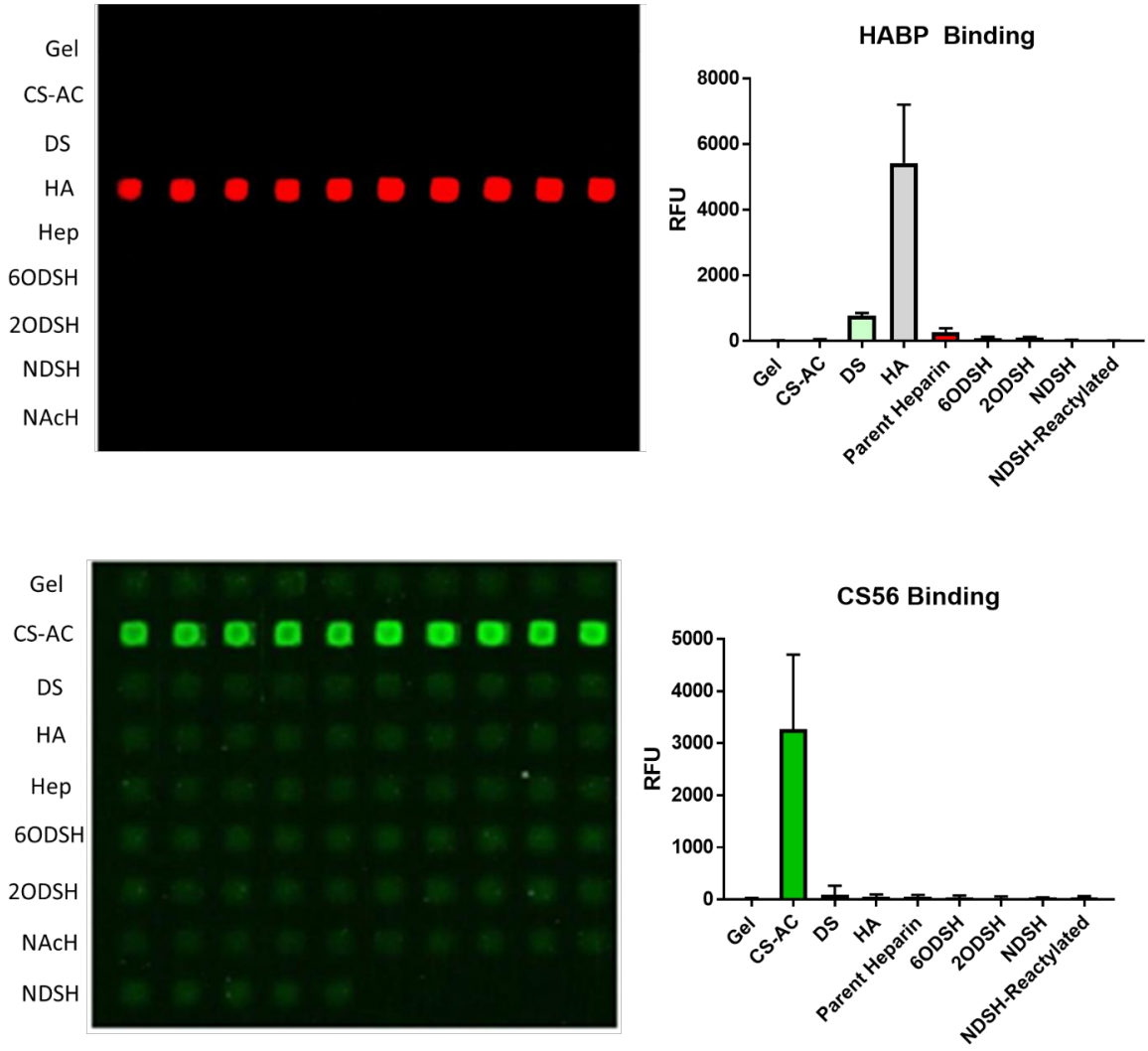

Figure 83. Binding targeted antibodies to non-heparin GAGs. *Top* hyaluronic acid binding protein binds to hyaluronic acid-gel. *Bottom* CS56 binds to chondroitin sulfate AC.

5.2.3 Establishing controls for microarray analysis

Having created a microarray substrates that could reliably support cell growth for six days and simultaneously present a variety of GAG-mimetic glycomaterials, we set to confirm that the cellular array design would support neural specification of mESCs and that differentiation outcomes could be easily and reliably monitored and quantified based

on fluorescence of differentiation markers using standard microarray scanner instruments. We utilized two mESC GFP reporter lines: one with a GFP fusion reporting on the expression of the pluripotency marker, Oct4, (Oct4-GFP mESC) and another with a GFP reporter for the early neural marker, Sox1, whose expression typically peaks at about Day 3 of differentiation (Sox1-GFP mESC) (obtained from PrimCells LLC).[44]

First, we performed a neural specification on a set of gelatin arrays with spots of about 500 μm diameter, and analyzed the outcome both by quantification of both GFP-fluorescence of adhered spots as well as by flow cytometry of cells lifted from arrays in a parallel experiment. This way, we could directly compare outcomes of the same experiment assessed two different assays. We had confidence that flow cytometry would be a reliable standard for comparison because it analyzes individual cells and is a robust and accepted method for fluorescence quantification. On the other hand, we had concerns about direct fluorescence imaging of adhered colonies, due to their tendency to become confluent and densely packed. Under such conditions, light may not effectively penetrate the colonies and scatter, thus reducing the accuracy of fluorescence signal magnitude. Another aspect of this investigation was to determine optimal cell seeding densities on the arrays to avoid overgrowth of cells during the differentiation experiments. When cells overgrow on the limited space of an array spot, the colonies begin to take on three-dimensional character and begin to “lift off” from the array, rending the colony unfit for analysis. As a negative control, we included a condition with a potent FGFR inhibitor, PD173074074. By inhibiting FGFR signaling, neural specification is unable to proceed, and the cell remain pluripotent (i.e., Oct4 positive), linking the differentiation process directly to the MAPK signaling pathway.

The arrays were seeded and allowed to adhere overnight. After this time, the neural induction medium, N2B27, was introduced (Day 0) to initiate differentiation. On the Day 6 of differentiation, the cells were analyzed for the expression of the embryonic Oct4 and neural Sox1 markers by fluorescence microscopy and by flow cytometry (**Fig. 84**). We were delighted to observe that the cells underwent differentiation as expected and the outcome of microscopy analysis closely matched that perormedf by flow cytometry. This indicated that the direct on-array fluorescent analysis of cells is valid. In addition, we identified optimal seeding density of 10,000 cells/cm^2 with minimal cell overgrowth and colony lifting. When lower seeding density was used, the colonies were all formed to different extents, with some completely confluent and others with barely any cells on the spots. At higher seeding densities, we observed denser (darker) colonies, which were prone to lift-off during washing and media changes. Thus, the lowest and the highest seeding density conditions suffered from a reduced total number of viable colonies at the end of the experiment, albeit for completely different reasons (**Fig. 85**).

Figure 84. Validation of fluorescence quantification by microscopy, and selection of optimal seeding density. Oct4-GFP and Sox1-GFP cells were separately differentiated at different seeding densities to day 6 in N2B27 and then analyzed by microscopy for GFP fluorescence relative to a nuclear stain (Syto59) to indicate pluripotency (Oct4) or neural commitment (Sox1). Parallel array experiment with the same cells and conditions was also performed but GFP fluorescence was assessed using flow cytometry (FACS) of cells collected from microarray. (A) Oct4-GFP expression by microscopy on day 6 of neural differentiation. (B) Sox1 GFP expression by microscopy on day 6 of neural differentiation. (C) Quantification of Oct4-GFP expression relative to Syto59 using ImageJ densitometry. (D) Quantification of Sox1 GFP expression relative to Syto59 using ImageJ densitometry. (E) Quantification of Oct4-GFP expression by flow cytometry. (F) Quantification of Sox1 GFP expression by flow cytometry

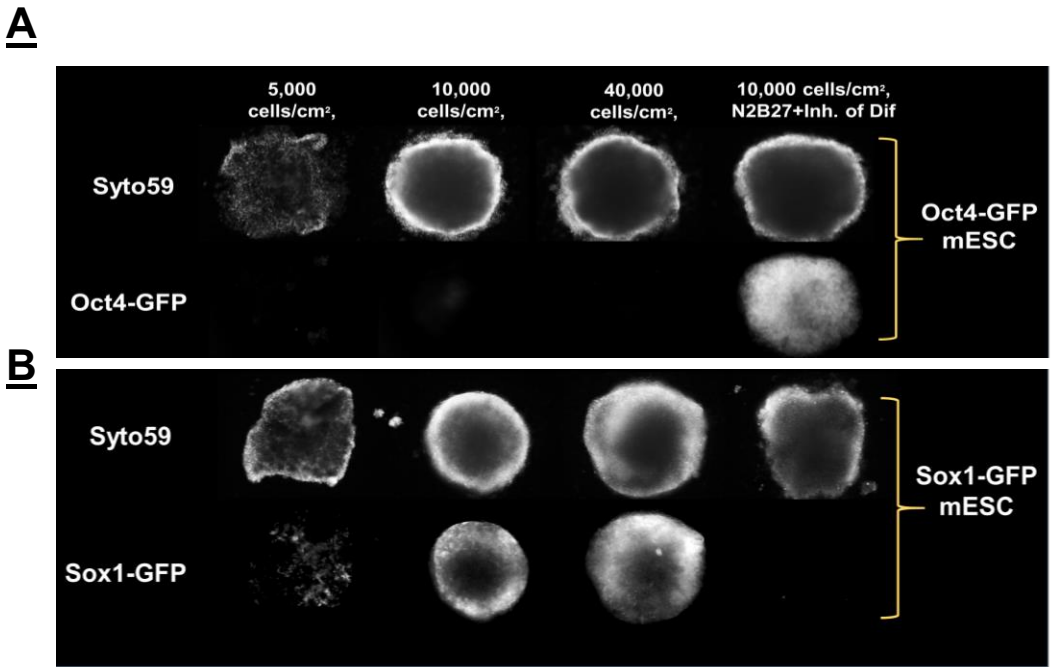
A
5,000 cells/cm²,
10,000 cells/cm²,
40,000 cells/cm²,
10,000 cells/cm², N2B27+Inh. of Dif
Syto59
Oct4-GFP
Oct4-GFP mESC
B
Syto59
Sox1-GFP
Sox1-GFP mESC

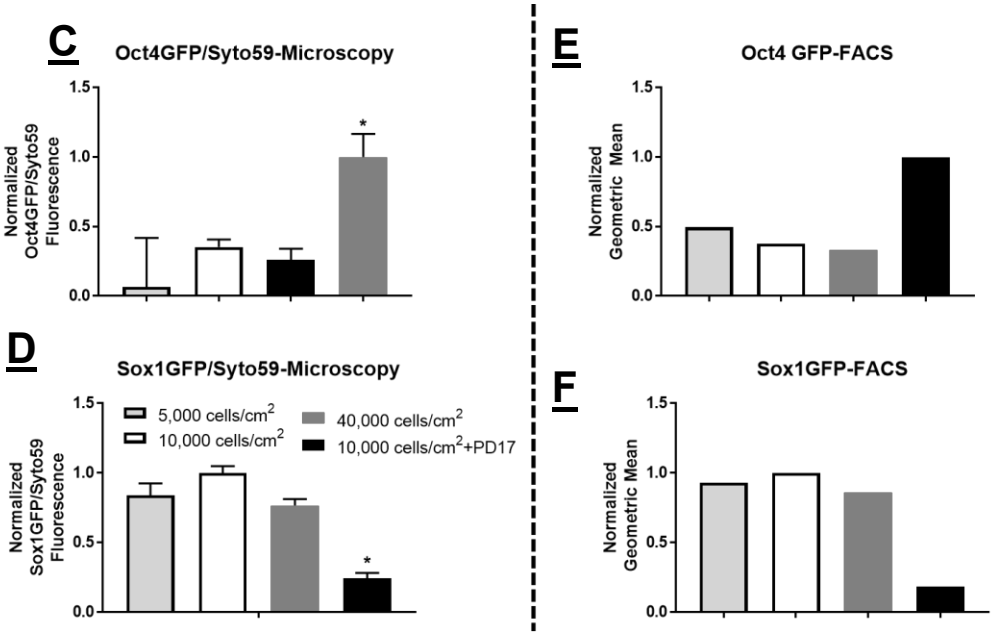
C
Oct4GFP/Syto59-Microscopy
Normalized Oct4GFP/Syto59 Fluorescence
1.5
1.0
0.5
0.0
*
D
Sox1GFP/Syto59-Microscopy
Normalized Sox1GFP/Syto59 Fluorescence
5,000 cells/cm2
10,000 cells/cm2
40,000 cells/cm2
10,000 cells/cm2+PD17
*
E
Oct4 GFP-FACS
Normalized Geometric Mean
F
Sox1GFP-FACS
Normalized Geometric Mean

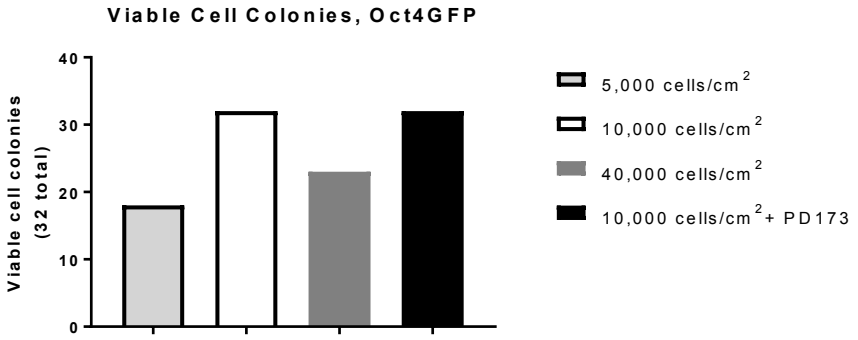

Figure 85. Evaluation of viable Oct4-GFP mESC colonies seeded at 5,000, 10,000 and 40,000 cells/cm^2 after 6 days of differentiation In N2B27 media. 5,000 cells/cm^2 seeding density led to incomplete formation of confluent spots, often leading to cell death. On the other hand, the 40,000 cells/cm^2 seeding density led to overgrown spots which lifted from the array, especially during day 5 and 6 of the experiment.

The main aim for this project was to evaluate whether neural differentiation in the HS GAG-deficient *EXT1*$^{-/-}$ mESCs can be restored in the presence of arrayed GAG-mimetic materials. However, the Oct4 and Sox1 GFP-reporters were not available in the mutant mESC line. Therefore, we also developed immunofluorescence-based assays to analyze the progress of mESC differentiation. It bears repeating that a truly high-throughput cellular array platform should be amenable to automated analysis using standard fluorescence microarray readers. Using the Oct4-GFP mESC line, we optimized an immunofluorescence assay for the detection of the neural markers, Nestin and βIII-tubulin, which was benchmarked to the expression of the Oct4-GFP reporter. Because the expression of the two neural markers coincides with the loss of Oct4, a successful immunostaining assay would show high Nestin or β-III-tubulin fluorescence in cells lacking the Oct4-GFP signal.

We differentiated Oct4-GFP mESCs to Day 6 and confirmed loss of pluripotency using the GFP signal. As expected, high levels of Oct4-GFP expression were maintained in cells subjected to differentiation in the presence of the FGFR inhibitor, PD173074. Cells from both conditions were fixed and stained with anti-nestin and anti-β-III-tubulin antibodies.

As we anticipated, we observed the predicted inverse trend for Oct4-GFP expression relative to the neural marker, Nestin (**Fig. 86**). Surprisingly, we discovered that β-III-tubulin, a neural marker associated with later stages of neural differentiation (~ Day 8), did not provide a reliable readout of neural committment based on total fluorescence quantification. While visual inspection of β-III-tubulin staining using fluorescence microscopy clearly distinguished between the positive and negative controls, this difference was not born out in the total amount of fluoreoscence detected in those colonies. β-III-tubulin is a cyctoskeletal protein associated with axonal structures and possibly suitable for visual inspection and analysis using tubule tracing software; however, the cells on the arrayed spots were too densely packed to be accurately traced. Nonetheless, the immunostaining for nestin successfully reported on the outcome of neural differentiation in the arrayed mESC colonies and should be suitable for the monitoring of differentiation in the mutant *EXT1*$^{-/-}$ mESCs line on microarrays.

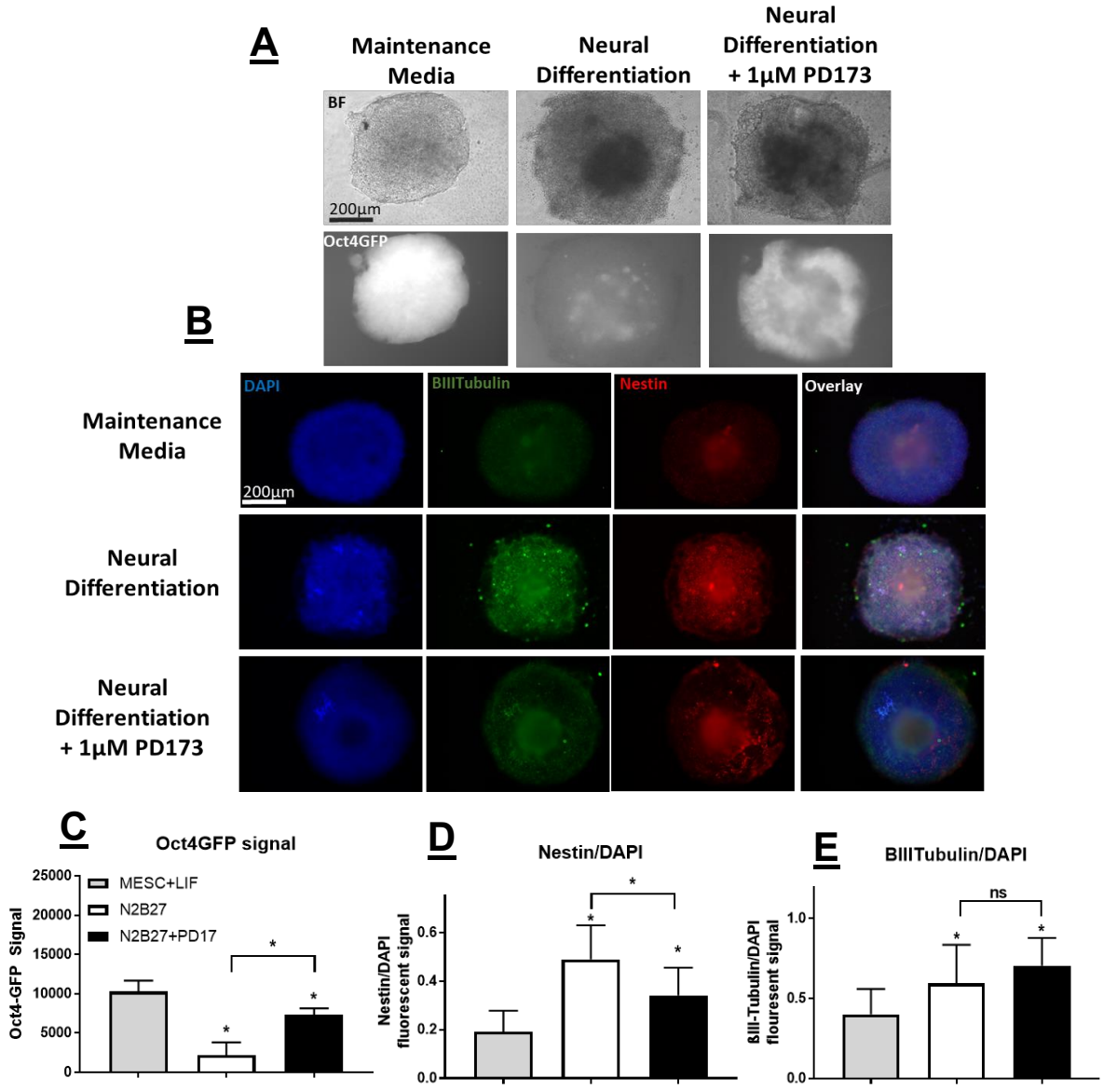

Figure 86 Oct4-GFP cells were used to validate neural differentiation and ICC in a cellular microarray format. (A) Oct4-GFP linked mESCs were differentiated to day 6 and the live cells were analyzed for Oct4 expression fluorescently. (B) Oct4-GFP linked mESCs were differentiated to day 6 and the fixed cells were stained neural differentiation markers Nestin and βIII-tubulin, as well as with the nuclear stain DAPI. (C) Fluorescent analysis of Oct4 expression day 6 live Oct4-GFP mESCs. (D) Nestin expression staining relative to DAPI to account for cell population. (E) βIII-tubulin expression staining relative to DAPI to account for cell population.

With confidence that the cellular microarray had been optimized to support neural specification, which could be reliably analyzed and quantified using immunofluorescnce, we moved forward on-array differentiation studies in the *EXT1*$^{-/-}$ mESC mutant cell line (**Fig 87**). The lack of HS on the surface of these cells prevents their differentiation under neural induction conditions. Neural differentiation can be restored by supplementing the differentiation media with heparin (5 µg/mL). Because these cells did not express the the Oct4-GFP reporter, we needed to monitor the pluripotency in these stem cells by immunostaining against Oct4, along with staining for the neural marker, nestin. As expected, nestin expression was upregulated during differentiation of *EXT1*$^{-/-}$ mESC on the arrays only in the presence of exogenously added heparin. Surprisingly, Oct4 expression was not reduced relative to cells grown under embryonic conditions or undifferentiated in the presence of the FGR inhibitor, PD173074. This result was inconsistent with the Oct4 expression profile observed in the Oct4-GFP mESC line but observed consistently despite our extensive efforts to optimize the Oct4 immunostaining conditions. Analysis of Oct4 expression under identical conditions using conventional culture showed regular expression profile, suggesting that the anomalous Oct4 signal was the result of the array format. We observed similar outcomes using Rex1 as an alternative pluripotency marker (**Fig. 89**). Again, while Nestin expression was enhanced in conditions supplemented with soluble heparin, the expression of Rex1 did not decrease. Despite great efforts, a functional antibody for pluripotency was never identified for use on the microarray.

One rationale is that the three-dimensional structure of the colonies interferes with the antibody staining. It is worth highlighting that neural specification is usually performed

at a very low cell density, which is difficult to achieve in the cellular microarray format where the cell rapidly fill the limited surface area of 500 μm^2 (spots containing 10 cells per spot reach 100% confluence by the third day of the experiment). The colony overgrowth into three-dimensional structures may cause difficulties with antibody penetration and marker detection. This three-dimensionality was observed by the Bhatia lab in similar cellular arrays, who found that cell colonies were over 70 μm tall.[37]Alternatively, in the case of the *EXT1*$^{-/-}$ mESC, increase in cell proliferation is expected in the presence of heparin, leading to a larger total number of cells (differentiated and undifferentiated), which may explain the increase of the embryonic markers compared to the negative control conditions.

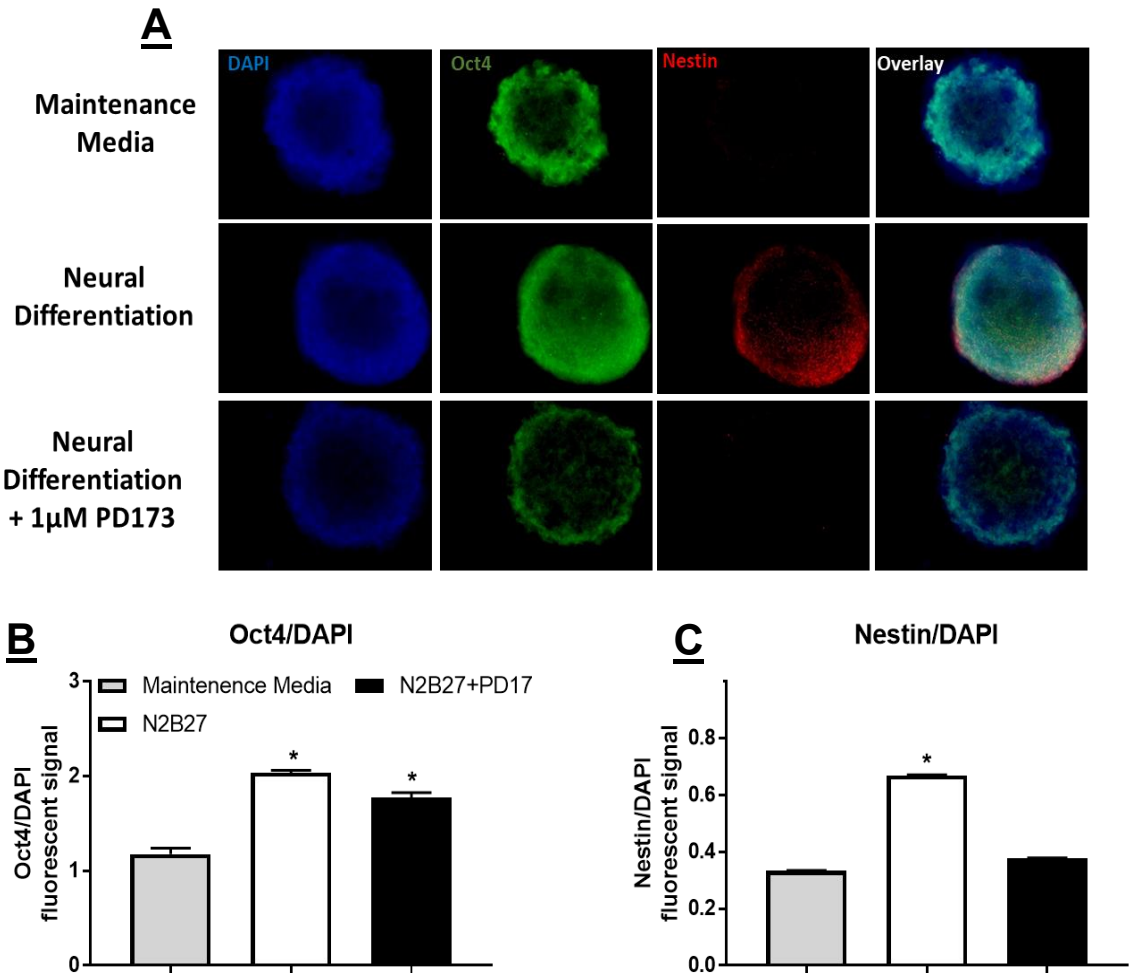

Figure 87. (A) *EXT1*$^{-/-}$ mESCs were differentiated to day 6 on a microarray and stained for markers of pluripotency (Oct4) and neural commitment (Nestin) as well as with the nuclear stain DAPI. (B) Oct4 stain relative to DAPI quantified by densitometry. (C) Nestin stain relative to DAPI quantified by densitometry.

5.2.4. Differentiation of mESC *on heparinoid displays*

Despite being unable to accurately characterize Oct4 expression in the *EXT1*$^{-/-}$ mESCs using immunostaining, we found the Nestin detection sufficiently convincing to continue our investigation into the impact of arrayed GAG-mimetics on the neural differentiation in these cells. Accordingly, we arrayed Hep-Gel, the most effective FGF2-ligand, onto the hydrogel substrates at increasing concentrations. *EXT1*$^{-/-}$ mESCs were then seeded on the resulting array and allowed to differentiate with soluble heparin condition included as a positive control. The expression of Oct4 and Nestin were assessed by immunostaining as described above (Fig 86). We observed that the soluble heparin induced higher Nestin expression than in any other condition, while the Oct4 staining failed to inversely correlate with Nestin expression as we would have expected(**Fig. 88, Fig. 89)**. Disappointingly, no neural differentiation was observed in stem cells grown on immobilized hep-gel conjugates.

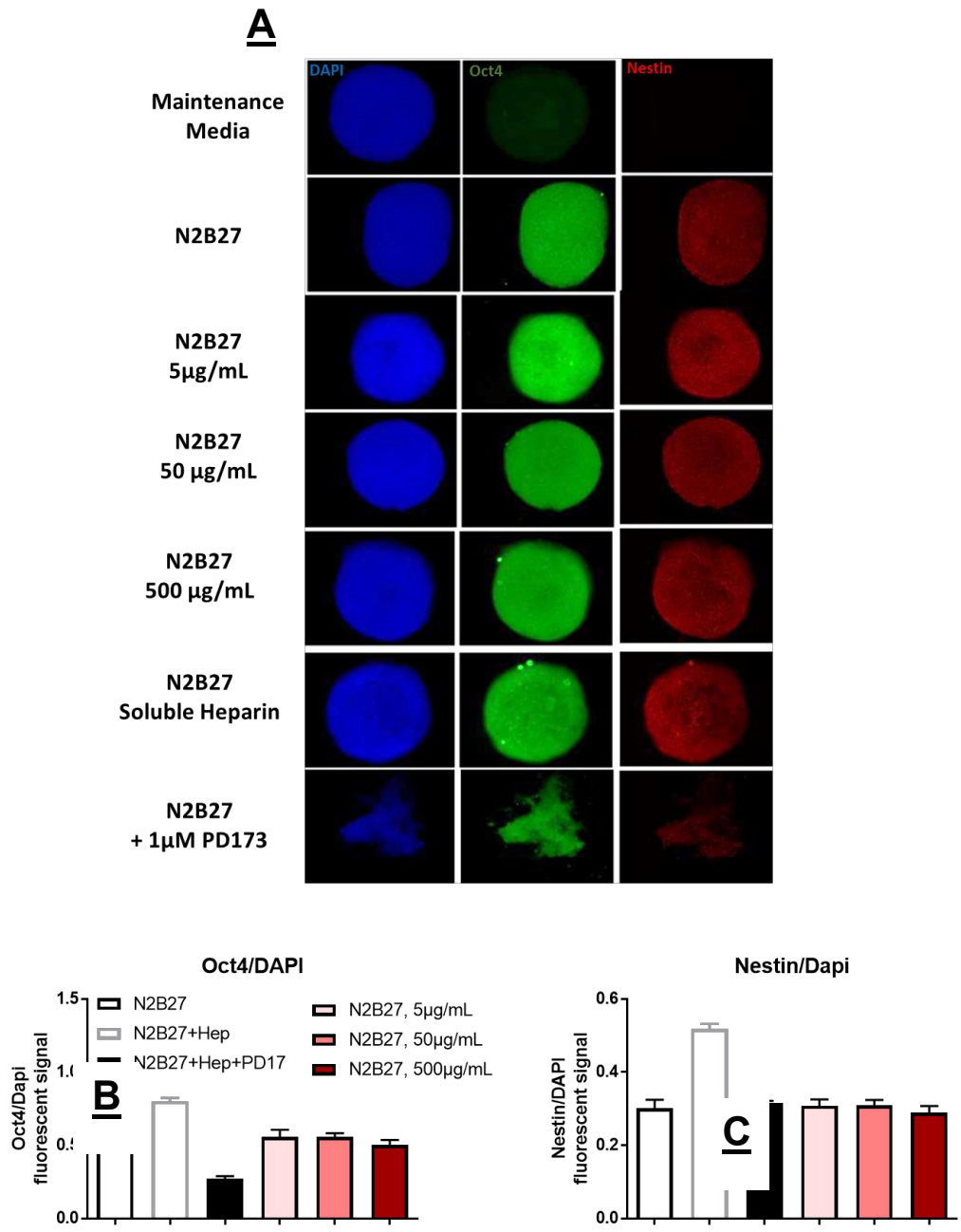

Figure 88 *EXT1*$^{-/-}$ mESC were differentiated in neural differentiation media to day 6 in a microarray consisting of hep-gel printed at different concentrations (5, 50, and 500 µg/mL). (A) Cells were stained for Oct4, Nestin, and DAPI and fluorescent signal was quantified relative to DAPI signal strength. (B) Oct4/DAPI signal. (C) Nestin/DAPI signal.

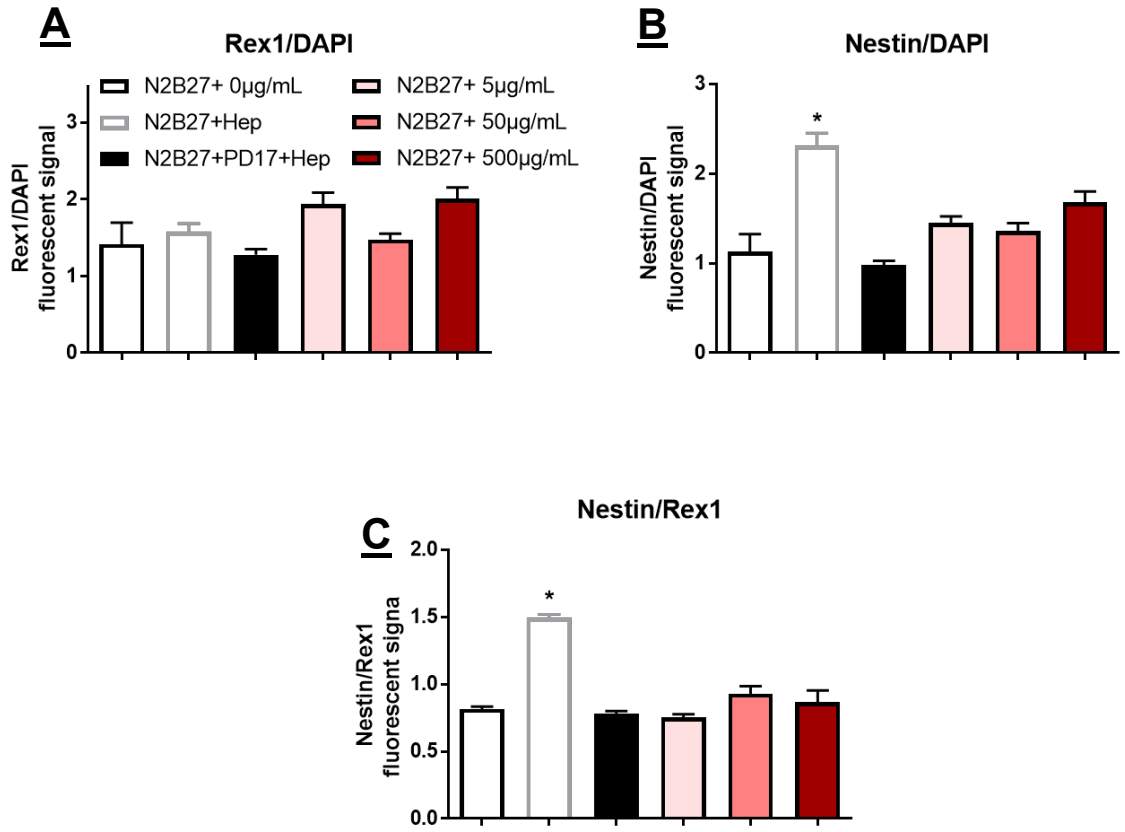

Figure 89. *EXT1*$^{-/-}$ mESC were differentiated in neural differentiation media to day 6 in a microarray consisting of hep-gel printed at different concentrations (5, 50, and 500µg/mL). Cells were stained for Rex1, Nestin, and DAPI and fluorescent signal was quantified relative to DAPI signal strength. (A) Rex1/DAPI (B) Nestin/DAPI signal. (C) Nestin/Rex1 signal.

Unable to enhance neural specification in *EXT1*$^{-/-}$ mESCs on immobilized heparin conjugates, we began to consider methods which could enhance signaling and differentiation. FGF2 is the major driver of MAPK signaling and neural differentiation in

mESCs. FGF4, also and HS-binding growth factor, has been demonstrated to further enhance this process. Thus, we reasoned that by supplementing FGF4 throughout the experiment, in addition to the endocrine expression of FGF2 by the stem cells, we could further drive differentiation. In addition, we extended the neural specification protocol to 8 days, in the case the differentiation proceeded slower on the surface-immobilized heparin conjugates (**Fig 90**).

FGF4 treatment had a noticeable effect on β-III-tubulin staining in the positive control (soluble heparin), with tubules becoming more distinct and potentially longer, however quantification software was unable to measure the overlapping tubules effectively because of the tight packing of the cells. We observed no difference in β-III-tubulin staining in cells differentiated in the presence or absence of immobilized hep-gel. On the other hand, the Nestin expression proved to be a poor marker for neural induction because at Day 8, as this marker begins to taper off in expression after Day 5. Thus the most differentiated cells (based on β-III-tubulin staining) had the least amount of Nestin expression, rendering this stain impractical for this length experiment.

We decided against pursuing differentiation experiments for more than 8 days because of the issues associated with cell overgrowth, (lifting of colonies, uneven staining, cell death) and a lack of a reliable assay for analyzing differentiation.

Concluding that the hep-gel conjugate trapped within the hydrogel network was ineffective in stimulating cell differentiation (presumably due to limited accessibility to the cell surface), we next tested the more surface exposed covalently grafted D2A6 glycopolymers after 6 days of differentiation (**Fig. 91**). Unfortunately, the D2A6

glycopolymer across a range of concentrations failed to promote differentiation based on nestin staining in the presence (Fig 91 A-D) or absence (Fig 5.91 E-F) of FGF4.

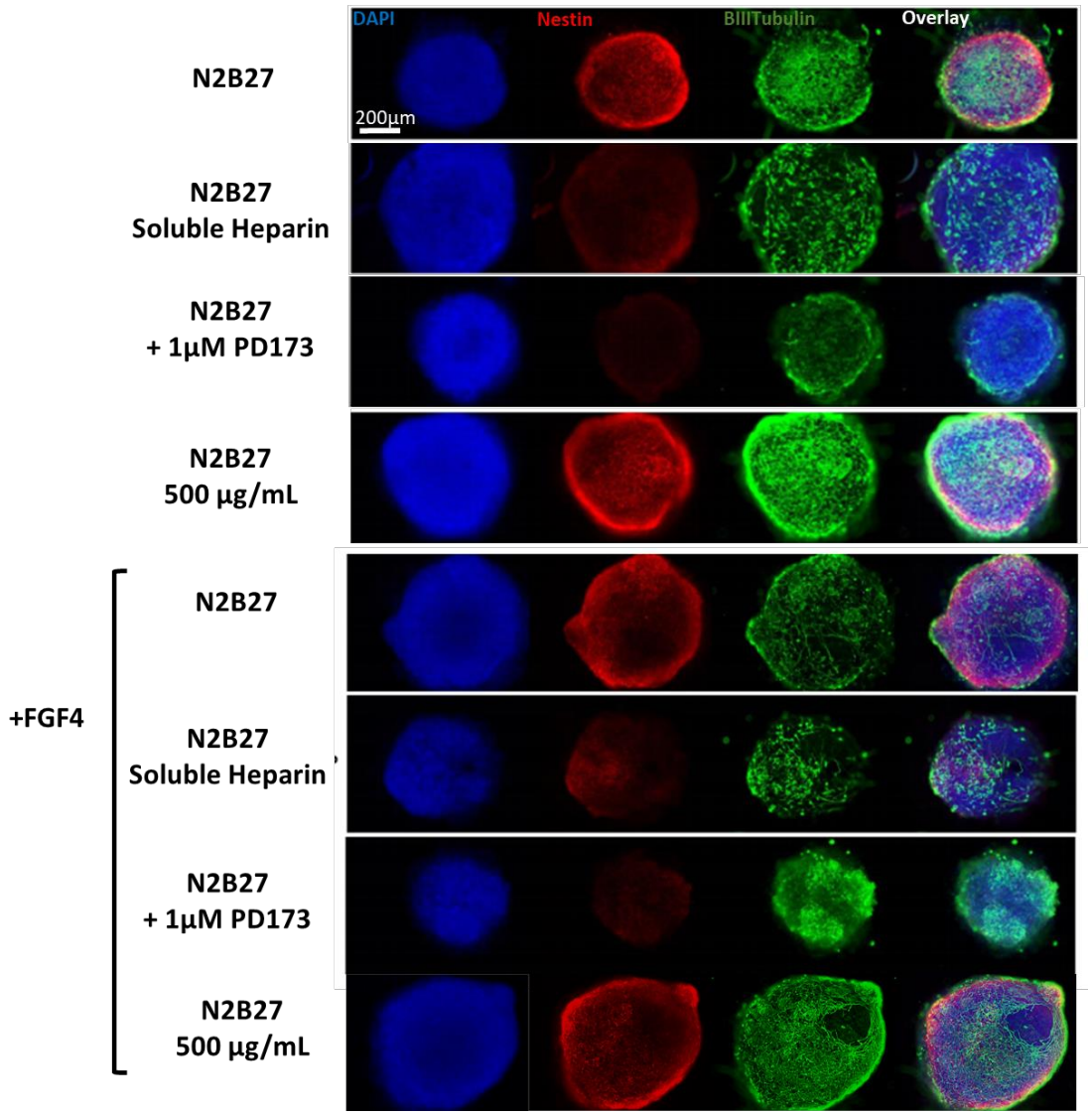

Figure 90 *EXT1*$^{-/-}$ mESC were seeded onto a gelatin array consisting of gelatin only, and Hep-Gel spots (500µg/mL). Cells were differentiated to day 8 in neural induction media with or without FGF4 (2ng/mL) as well as the additional supplements indicated. Cells were stained with βIII-tubulin, Nestin, and DAPI.

Figure 91 *EXT1*$^{-/-}$ mESC were seeded onto a gelatin array consisting of gelatin and D2A6 glycopolymer at 3 different concentrations (2.5, 0.5 0.05, and 0.00 μM) which is covalently attached to surface via CuAAC. Cells were differentiated to day 6 in neural induction media (N2B27) with (A-D) or without (E-H) 2ng/mL FGF4 as well as the additional supplements indicated.

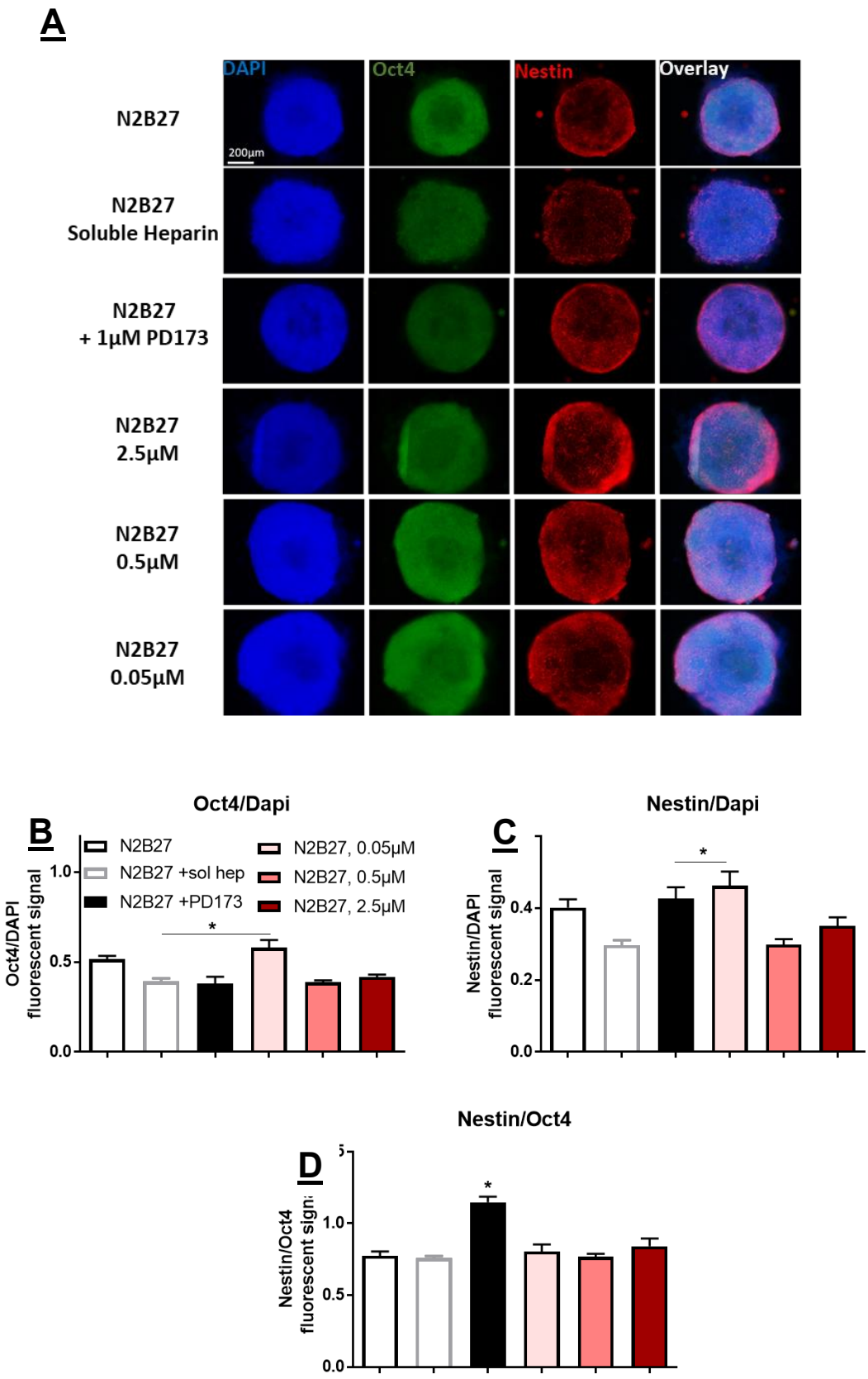
A
DAPI
Oct4
Nestin
Overlay
200µm
N2B27
N2B27
Soluble Heparin
N2B27
+ 1µM PD173
N2B27
2.5µM
N2B27
0.5µM
N2B27
0.05µM
B
Oct4/Dapi
N2B27
N2B27 +sol hep
N2B27 +PD173
N2B27, 0.05µM
N2B27, 0.5µM
N2B27, 2.5µM
Oct4/DAPI
fluorescent signal
1.0
0.5
0.0
*
C
Nestin/Dapi
Nestin/DAPI
fluorescent signal
0.4
0.2
0.0
*
Nestin/Oct4
D
Nestin/Oct4
1.0
0.5
0.0
*

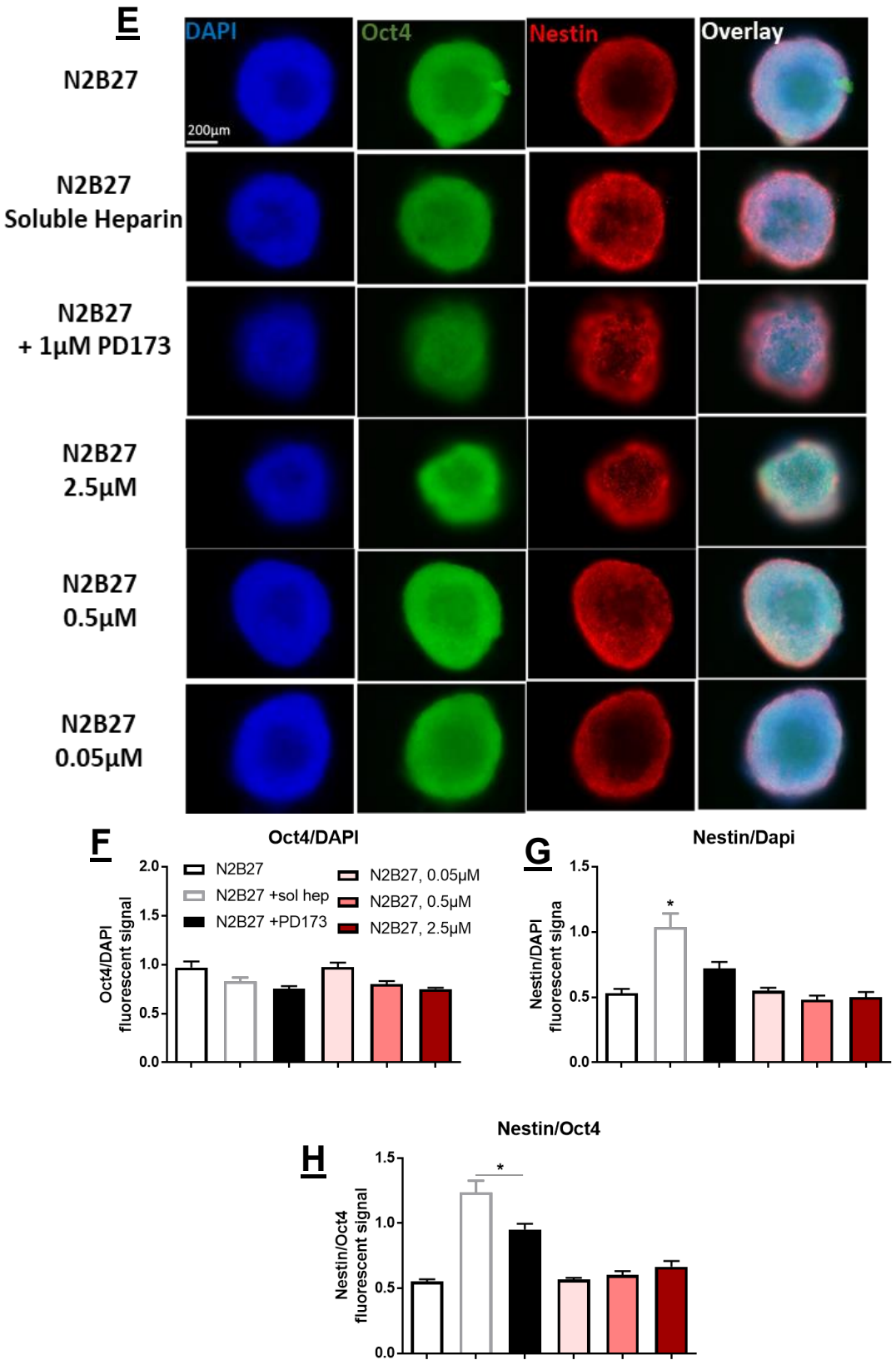

Figure 91 continued *EXT1*$^{-/-}$ mESC seeded onto a gelatin array and differentiated.

The conclusion to these studies was that the immobilized glycoconjugates, whether physically entrapped within or covalently linked to the hydrogel network, failed to promote FGF2 signaling and neural differentiation. The simplest explanation for this outcome is that these glycoconjugates, although capable of binding FGF2 (**Fig. 81, 82**), are not presented in a form accessible to the cell surface receptors required to activate signaling. This may be further compounded by the cells depositing their own extracellular matrix on the arrayed spots after seeding.

Cellular glycan arrays are not an unattainable technology, but a reevaluation of the current approach is required. Based on my observations, that the main future focus should be on utilizing these arrays to evaluate 1) the sequestration of GFs, such as FGF2, away from the cell surface and the corresponding effects on cell proliferation and differentiation and 2) to identify new hydrogel glycomaterials that can serve as depots for growth factors with tunable long-term release in engineered tissue scaffolds. The concept of using immobilized glycomaterials as growth factor reservoirs, is supported by my own work showing that the proliferation of hMSC can be tuned in conventional culture on heparinoid substrates (see Chapter 4). Additionally, it is likely that using 3D array culture conditions within functional degradable hydrogel networks may overcome some of the issues arising from limited exposure of the glycomaterials to cell surface receptors identified in this study.

5.3 MATERIALS AND METHODS

5.3.1 General Chemistry

All chemicals, unless stated otherwise, were purchased from Sigma Aldrich. Purchased starting materials were used as received unless otherwise noted. Heparin and desulfated heparinoids were purchased from Iduron (Manchester, UK). The selectively chemically desulfated heparinoids originated from the unmodified heparin used in this study. The distributors of the heparin reported the average molecular weight of the parent heparin approximately 12,000 g/mol, but stated the heparin they prepare has a wide range of molecular weights, and do not have a polydispersity data for the polymer. The disaccharide analysis of the heparin and desulfated heparins are depicted in the spectra (Figure found in chapter 4) Briefly, the major (greater than 75%) disaccharide unit of heparin is the trisulfated IdoA(2S)-GlcNS(6S). The extent of desulfation of the heparinoids are as follows: 6ODSH: approximately 90% reduction in 6-O-sulphates and 25% loss of 2-O-sulphates, 2ODSH: approximately 95% reduction in 2-O-sulphates, NDSH and NAcH: approximately 92% reduction in N-sulphates. The progress of reactions was monitored by analytical thin-layer chromatography (TLC, Merck silica gel 60 F-254 plates) using detection via UV illumination, or by staining with iodine or ninhydrin. Solvent compositions are reported on a volume/volume (v/v) basis unless otherwise noted.

5.3.2 General Instrumentation

Nuclear magnetic resonance (NMR) spectra were collected on a Bruker 300MHz NMR spectrometer. Spectra are reported in parts per million (ppm) on the δ scale relative to the residual solvent as an internal standard. Size exclusion chromatography (SEC) was performed on a Hitachi Chromaster system equipped with an RI detector and an 8μm, mixed bed, 300 x 7.5 mm cm PL aquagel-OH mixed medium column. Bright field and live cell fluorescence microscopy images were taken using ZEISS Axio Observer microscope. Fixed cells were fluorescently imaged using a Keyence BZX-700 fluorescent microscope. Microarray slides used for protein binding assays were assessed using an Axon GenePix 4000B microarray scanner (Molecular Devices). All microarray experiments, cellular and protein binding, we performed using ProPlate gaskets (Gracebiolabs, cat. No. 248864) which were attached to the array slide. (Note: when using these gaskets, be sure to use only the steel spring clips, not the plastic clips, which are rigid and typically break the glass slide.)

5.3.3 General Microarray Printing

Microarrays were printed using an Arrayit SpotBot Extreme microarrayer. Arrays were printed in 65% humidity using 500μm spot pins (SMP15). While the number of spots varies from array to array, spacing between spots was consistently 1400μm in cellular microarrays to reduce chance of cellular colonies bridging between spots. For protein

binding assays, this spacing was not needed and these spots were spaced 750μm apart. In order to get 4 well gaskets to fit on array slides, arrays must be centered correctly and printed using the correct program within the Arrayit software. For the arrays published here, the print parameter option MAUI4 was selected, and the lateral and vertical offset were 1 and 3 mm respectively. Arrays were always printed with 0.5 mg/mL porcine gelatin bloom 180 in PBS with 10% glycerol, .003% triton X-00. When concentration gradients we printed, the lowest concentration was always printed last. When including glycopolymer or GAG-Gelatin conjugate, the concentration of gelatin was also 0.5 mg/mL, and the buffer remain unchanged.

After printing, slides are placed into a slide holder and allowed to dry and/or react with the surface overnight at 4 °C. Prior to use, slides are washed in MQ H_2O for 2 minutes by loading slides into a steel rack and rapidly and repeatedly dipping slides into a crystallization dish full of MQ H_2O. After this, slides are washed three times in PBS, 15 minutes, and then "spin dried" by centrifuging slides at 500 rpm for 5 minutes. Then the slides are "snap dried" by placing the cells array-side-up onto a slide warmer heated to 50 °C for 10 minutes, or until slides are clearly dried. We typically heated a clean glass pane upon a metal 4mL vial multireactor plate heated to 50 °C on a hotplate for a slide warmer. At this point, slides could be stored or used for up to a month

5.3.4 Preparation of Cellular Microarrays

Cloud point passivation: An epoxide slide with an array printed upon it is placed into a coplin jar with a solution of 10mg/mL Poly(ethylene glycol) bis(amine) Mw 10kDa, in 0.62 M K_2SO_4, 0.1M phosphate buffer, pH 6.5, 37 °C. coplin jar is sealed and the slide is

allowed to incubate overnight. After overnight incubation, remaining epoxides are opened by a 4 hour incubation in 50mM borate buffer with 50mM ethanol amine, pH 8.5 (9.5g tetraborate decahydrate, 3g ethanol amine, 500mL MQ). After incubation, slide is rinsed in PBS and stored at 4 °C.

BSA passivation: An epoxide slide with an array printed upon it is placed into a coplin jar with a 5% BSA solution in PBS. coplin jar is sealed and the slide is allowed to incubate overnight at room temperature. After overnight incubation, remaining epoxides are opened by a 4 hour incubation in 50mM borate buffer with 50mM ethanol amine, pH 8.5 (9.5g tetraborate decahydrate, 3g ethanol amine, 500mL MQ). After incubation, slide is rinsed in PBS and stored at 4 °C.

Ethanol amine passivation An epoxide slide with an array printed upon it is placed into a coplin jar with a 50mM borate buffer with 50mM ethanol amine, pH 8.5 (9.5g tetraborate decahydrate, 3g ethanol amine, 500mL MQ) overnight. After incubation, slide is rinsed in PBS and stored at 4 °C.

Preparation of NaOH etched slides: Untreated, unfrosted glass microscope slides are loaded into a steel slide rack and submerged in a crystallization dish filled with MQ H_2O. the slide rack is washed five times with water, allowing the slides to remain in the last water wash for 30 minutes on a rocker. After 30 minutes, the water is removed and replaced with acetone. This solution rocks for 30 minutes, covered. The acetone is the removed and replaced with MeOH, which again rocks for 30 minutes, covered. The

MeOH is removed and replaced with a solution of 0.05 NaOH (1g NaOH, 500mL H_2O), and rocked for 2 hours. Slides are then rinsed three times in MQ H_2O and then spin dried (500 rpm, 5 min). The slides are then lightly blow-dried using 0.22μm filtered air. The slides can then be placed into a vacuum oven to dry at 70 °C, 20 PSI. However, for most preparations, a vacuum oven was not available and a normal oven set at 120 °C, or overnight dessication, worked fine. These slides can be stored for up to a month

Preparation of methacrylate slides: Dry, NaOH etched slides (in a steel rack) are placed into a solution of 2% 3-(trimethoxysilyl) propyl methacrylate 98% toluene v/v, and rocked for 1 hour. The solution is then removed and the slides are washed three times in fresh toluene to remove residual 3-(trimethoxysilyl) propyl methacrylate. The slides are spin dried (500 rpm, 5 min), blow-dried with 0.22μm filtered air, and placed in a desiccator overnight. The slides also can be dried in a vacuum oven to dry at 70 °C, 20 PSI for one hour. These slides can be stored for up to a month. The slides are then glutaraldehyde activated, by rocking the slides for 2 hours in a 0.05% solution of glutaraldehyde in MQ H_2O. The slides are spin dried (500 rpm, 5 min), blow-dried with 0.22μm filtered air, and placed in a desiccator overnight. The slides also can be dried in a vacuum oven to dry at 70 °C, 20 PSI for 15 minutes. These slides can be stored for up to a month.

Preparation of acrylamide slides: A 10mL H_2O solution of 2.85 g acrylamide, 0.150 g bisacrylamide is prepared (30% w/v acrylamides, 19:1 w/w). Then, a 10% w/v ammonium persulfate (APS) solution is prepared in MQ H_2O. The polymerization solution is then prepared by combining 985 μL MQ H_2O, 500 μL 30% 19:1 Acrylamide solution, 15 μL

10% APS , and 0.6 µL TEMED, in that order. The polymerization solution is then placed in the center of glutaraldehyde activated methacrylate slides in 110µL aliquots. Then, a cover slip is placed on each slide with a polymerization aliquot in such a way that no air bubble form (absolutely none). To do this, angle the coverslip at about 45 degrees over the glass slide so that the liquid drop makes contact with both the slide and the coverslip. Now, slightly lift the coverslip and widen the angle relative to the slide to pull the droplet back towards the edge of the slide (where the apex of the created angle is). When the droplet reaches the back edge of slide it will begin to widen and distribute along the length of the slide slightly, once this has occurred, gently place the coverlip on the slide, reducing the space and angle between the slide and coverslip until the coverslip can no longer be held without disturbing the slide, at which point it can be dropped. Be aware that once the TEMED has been added, the polymerization solution typically takes about 3-5 minutes to begin polymerization, so it is important to work quickly as the polymerization solution is used. The polymerization is then allowed to occur for 2 hours with the slides completely undisturbed. After 2 hours of polymerization, the slides are loaded into a steel slide rack with the coverslips still on, and allowed to sit in H_2O for 15 min, causing the coverslip to loosen on the slide as the gel pad is hydrated and expands. Slides are removed from water, and using a razorblade, the coverslips are gently removed, with great care not to disturb the hydrogel. Any disturbances on the slide lead to the acrylamide failing (lifting off, rippling, further tearing etc.). The hydrogel exposed slides are then carefully reloaded into the steel slide racks and submerged in a crystallization dish filled with MQ H_2O. The MQ H_2O is replaced every 24 hours for 48 hours as the slides are washed away of any remaining acrylamide, which is a cytotoxic chemical. After the 48 hour water wash, the

slides are spin dried and placed slides hydrogel-side-up onto a slide warmer heated to 50 °C for 10 minutes, or until slides are clearly dried. We typically heated a clean glass pane upon a metal 4mL vial multireactor plate heated to 50 °C on a hotplate.

Preparation of ADIBO functionalized acrylamide slides: A 10 mL H_2O solution of 2.70 g acrylamide, 0.150 g bisacrylamide, and 155.92 µL allyl glycidyl ether is prepared (30%, 1:1:18, 5% allyl glycidyl ether). Then, a 10% w/v ammonium persulfate (APS) solution is prepared in MQ H_2O. The polymerization solution is then prepared by combining 985 µL MQ H_2O, 500 µL 30% 19:1 acrylamide solution, 15 µL 10% APS , and 0.6 µL tetramethylethylenediamine, in that order. The polymerization solution is then placed in the center of glutaraldehyde activated methacrylcate slides in 110µL aliquots. Then, a cover slip is placed on each slide with a polymerization aliquot in such a way that no air bubble form (absolutely none). To do this, angle the coverslip at about 45° over the glass slide so that the liquid drop makes contact with both the slide and the coverslip. Now, slightly lift the coverslip and widen the angle relative to the slide to pull the droplet back towards the edge of the slide (where the apex of the created angle is). When the droplet reaches the back edge of slide it will begin to widen and distribute along the length of the slide slightly, once this has occurred, gently place the coverslip on the slide, reducing the space and angle between the slide and coverslip until the coverslip can no longer be held without disturbing the slide, at which point it can be dropped. Be aware that once the TEMED has been added, the polymerization solution typically takes about 3-5 minutes to begin polymerization, so it is important to work quickly as the polymerization solution is used. The polymerization is then allowed to occur for 2 hours with the slides completely

undisturbed. After 2 hours of polymerization, the slides are loaded into a steel slide rack with the coverslips still on, and allowed to sit in DMF for 15 min, causing the coverslip to loosen on the slide as the gel pad is hydrated and expands. Slides are removed from DMF, and using a razorblade, the coverslips are gently removed, with great care not to disturb the hydrogel (Safety Tip: DMF destroys gloves pretty quickly, I would typically wear 4 layers of gloves when removing the cover slips because the glass edges cut the DMF-weakened gloves). The hydrogel exposed slides are then carefully reloaded into the steel slide racks and submerged in a crystallization dish filled with an ADIBO functionalization solution consisting 1mM ADIBO and 10mM DIPEA in DMF (0.269 mL DIPEA and 46.38 mg into 150 mL DMF). The ADIBO functionalization solution is removed after 24 hours of reaction in the dark, the slides are loaded into a clean steel rack and repeatedly dunked into fresh DMF for 2 minutes. At this point, the slides are ADIBO functionalized and thus are light sensitive, so all incubations are done in containers covered in foil. The slides are then rocked in DMF for 45 minutes, replacing the DMF every 15 minutes with fresh DMF. After the final DMF wash, the DMF is removed and the slides are placed into MQ H_2O for 10 minutes to allow DMF to wash away from the hydrogels. Then, the slides are placed into a pH 8.5, 50 mM ethanolamine borate buffer (9.5 g tetraborate decahydrate, 3 g ethanol amine, 500 mL MQ H_2O) for four hours to open any remaining epoxides which may have not reacted during the ADIBO functionalization. After incubation in borate buffer, the sldies are washed for 48 hours in MQ H_2O, replacing the water every 24 hours. After the 48 hour water wash, the slides are spin dried (5oo rpm, 5 min) and placed slides hydrogel-side-up onto a slide warmer

heated to 50 °C for 10 minutes, or until slides are clearly dried. We typically heated a clean glass pane upon a metal 4mL vial multireactor plate heated to 50 °C on a hotplate.

5.3.5 Preparation of glycoconjugates and AF647-FGF2

Preparation and characterization of Hep-Gel and other GAG-Gel conjugates.[45] Following a previously published procedure, HEPES buffer (100 mM, 15.0 mL, pH 7.4) was first prepared. Then, heparin (2.0 mg, 0.3 μmol) was dissolved in 200.0 μL the stock solution and stirred overnight at 4 °C to afford heparin NHS-ester. The activated NHS ester solution was diluted to a total volume of 2.5 mL using in MQ water, loaded onto a PD-10 column, and eluted with 2.5 mL MQ water. The solution was lyophilized to afford intermediate heparin NHS-ester (2.0 mg, 100% mass recovery). This intermediate could be confirmed for NHS functionalization by proton NMR detection of the succinimide ring protons found at 2.89 ppm. The 2 mgs of hep-NHS product of which was dissolved in a PBS solution containing gelatin (10.0 mg/mL, 200.0 μL). The reaction was allowed to proceed overnight and the resulting heparin-Gelatin conjugate (Hep-Gel). The product solution was run through a PD-10 column (2.5mL load, 2.5 mL elute). The resulting solution was lyophilized to afford purified Hep-Gel as a white spongy solid (4.1mg, 100% mass recovery based on BSA). For the preparation of other GAG-NHS and GAG-Gel constructs, the same stoichiometry by mass was used.

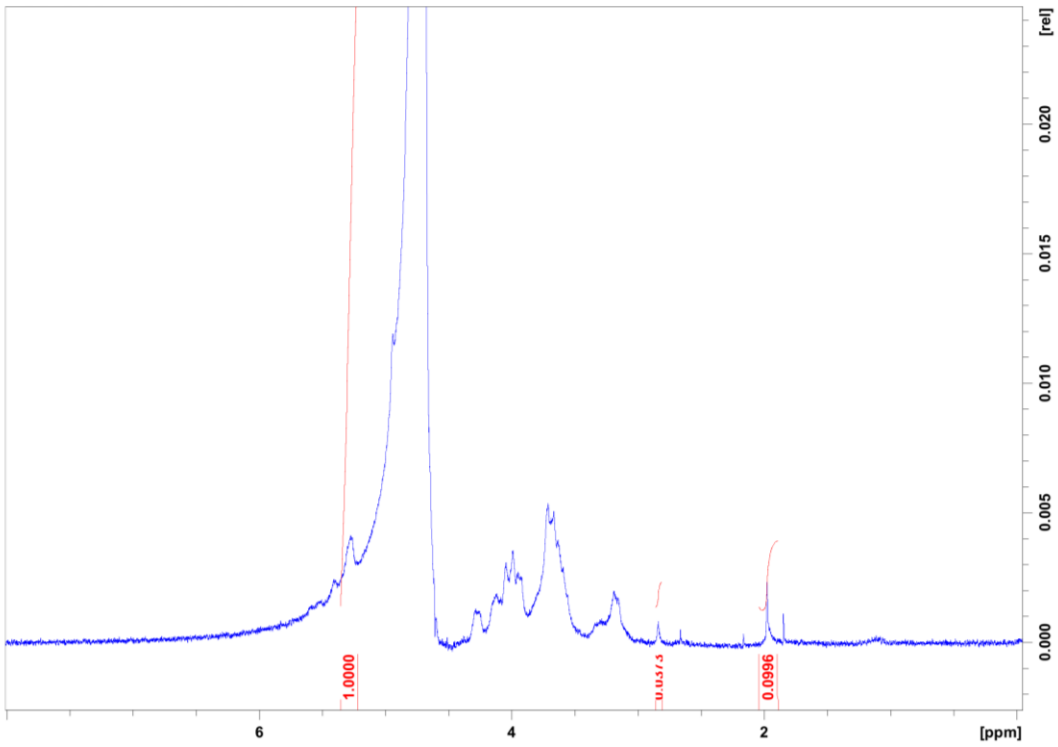

Figure 92 ^{1}H NMR of 2-O desulfated heparin-NHS

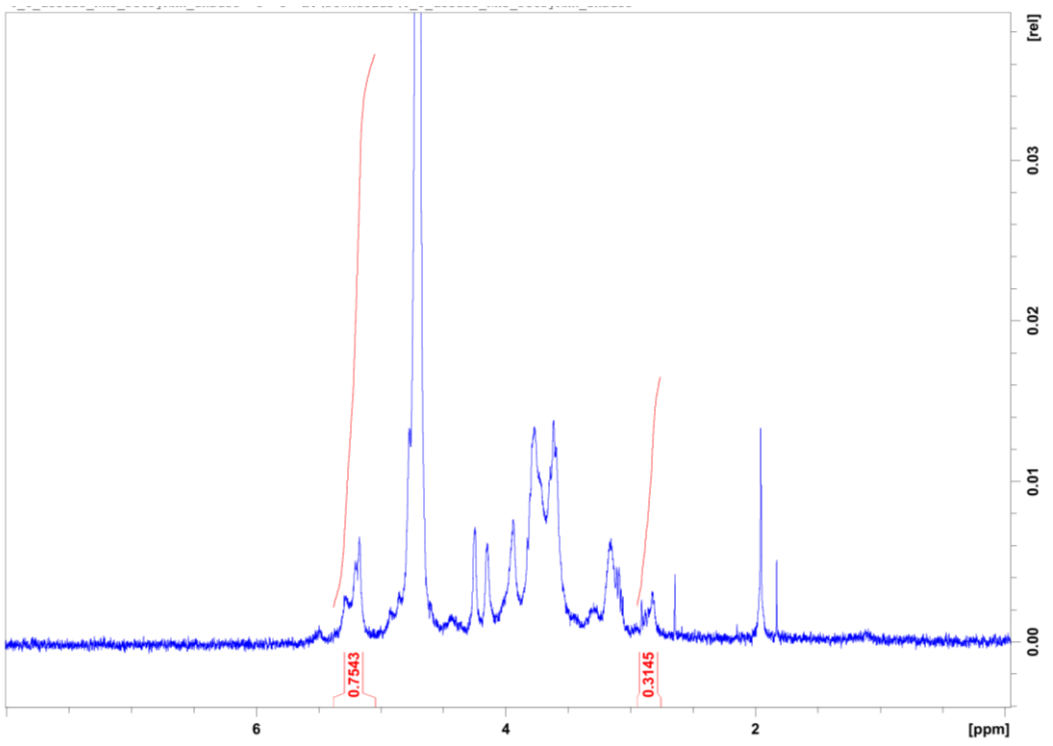

Figure 93 ^{1}H NMR of 6-O desulfated heparin-NHS.

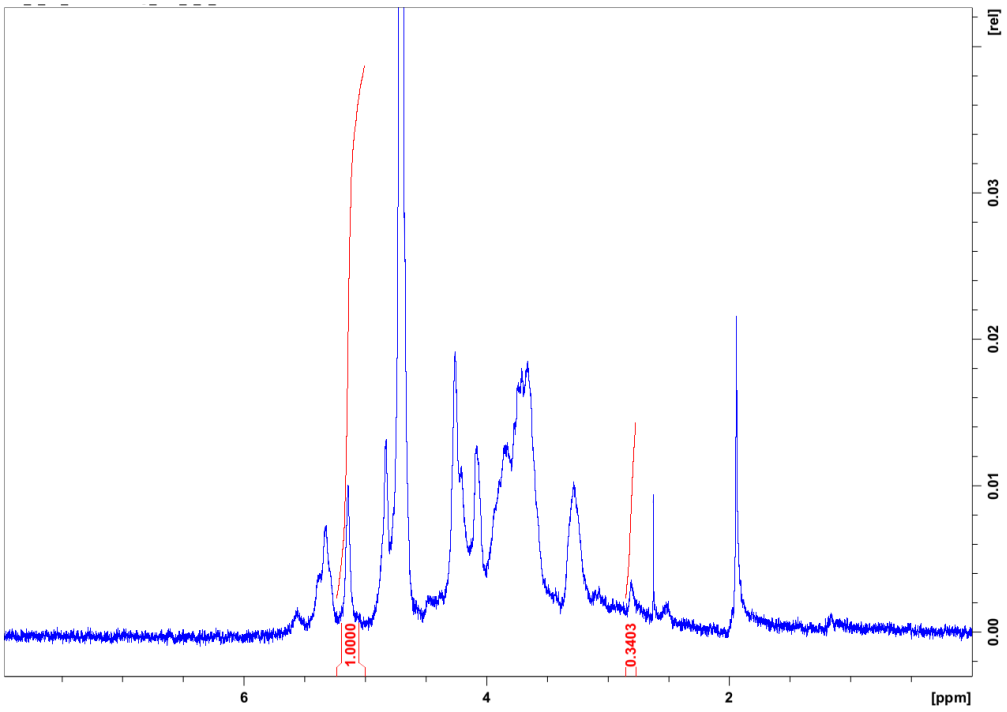

Figure 94 ^{1}H NMR of N-desulfated heparin-NHS.

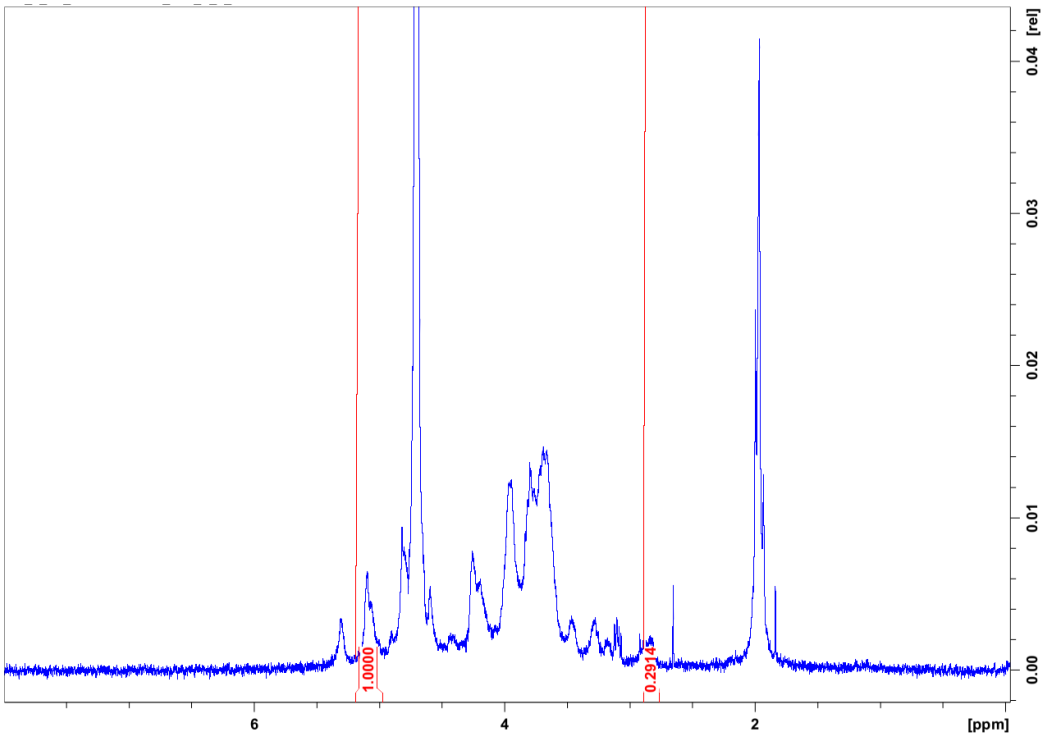

Figure 95 ^{1}H NMR of N-desulfated N-reacetylated heparin-NHS

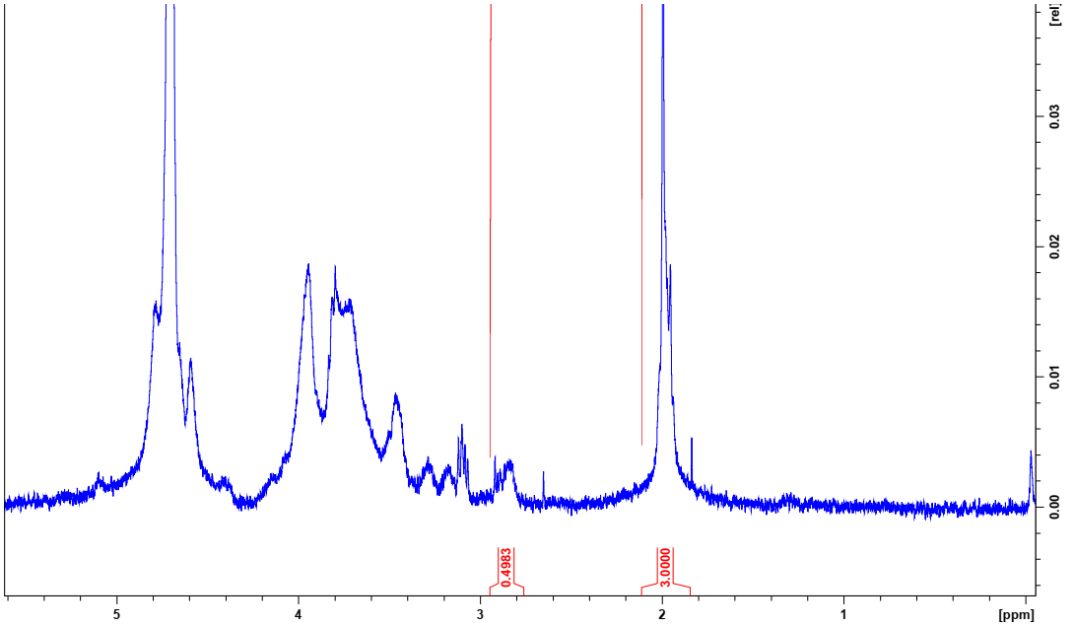

Figure 96 ^{1}H NMR of dermatan sulfate-NHS.

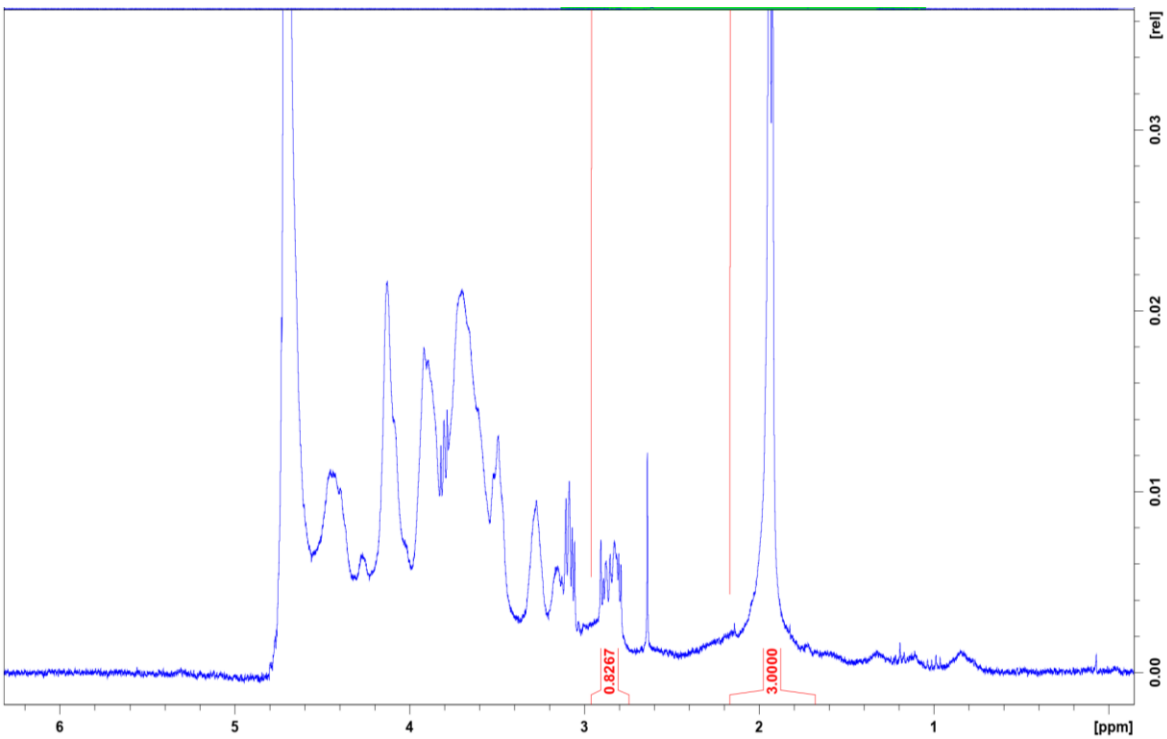

Figure 97 ^{1}H NMR of chondroitin sulfate AC.

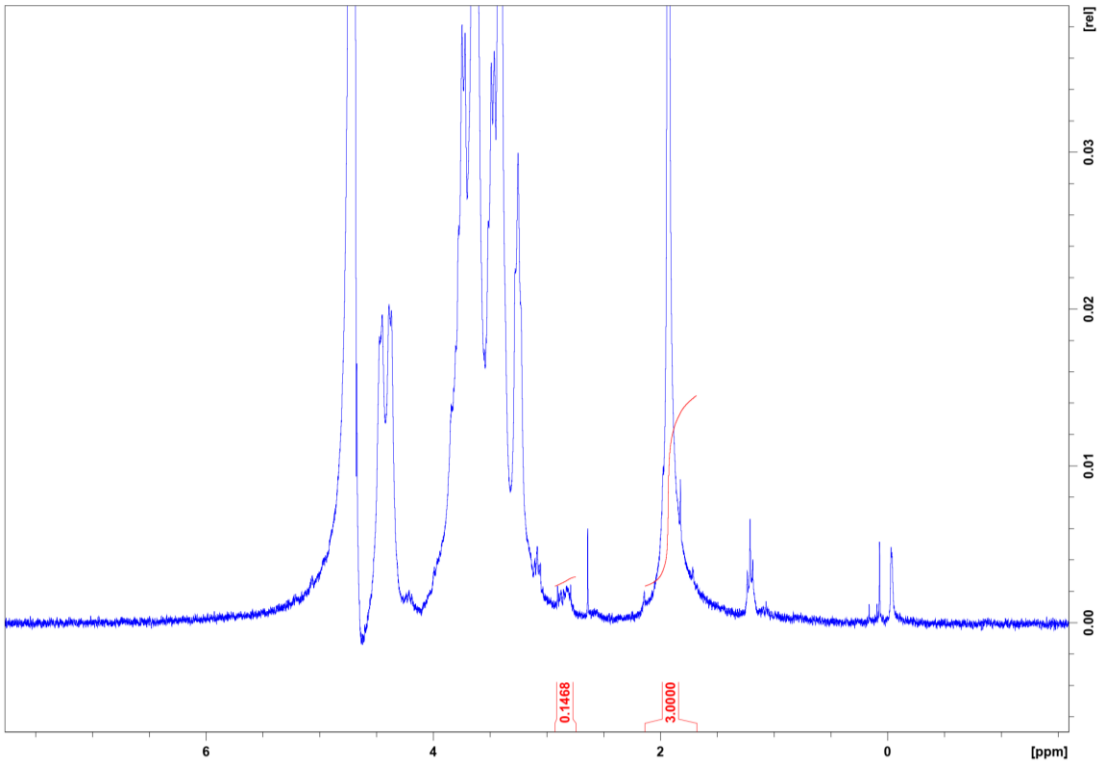

Figure 98 ^{1}H NMR of dermatan sulfate-NHS

Preparation of glycopolymers: preparation of glycopolymers is extensively covered in chapter 2 of this thesis.

Preparation of AF647-FGF2: 100µg Human FGF2 (100-18b-100UG) is dissolved in 200µL 0.2M HEPES buffer, pH 8.4. Then, 20 µL of a 20 mg/mL heparin solution in MQ H_2O is added to the FGF2 solution and 10 minutes are allowed to pass, at which point 2 µL of a 10 mg/mL NHS-AF647 solution in DMF is added to to the solution. The reaction is gently rocked for 3 hours, and is quenched by the addition of 80µL of a 20mg/mL glycine solution in MQ H_2O. To purify the reaction, a heparin sepharose column (1 mL) must be prepared and used. 500 µL of heparin sepharose is added to a column, which is then centrifuged at 1000 rpm for 15 seconds to remove the liquid from the heparin sepharose. Then, 500 µL of elution buffer (3M NaCl, .2% BSA, 20mM HEPEs, pH 7.4) run through

the column and removed by spinning 1000rpm for 15 min. This is repeated once, and then twice more using a wash buffer (0.5M NaCl, 0.2% BSA, 20 mM HEPES, pH 7.4). At this point, the quenched reaction can be loaded onto the column. Because this reaction is done with 100µg/mL, the product should be purified on two separate columns to avoid overloading. Half of the reaction mix was loaded onto a 1 mL column and the column was spun at 1000 rpm for 15 seconds. Then the eluted solution was reloaded onto the column and spun again at the same speed and duration. Then, 500 µL of the wash buffer was loaded and spun through at 1000 rpm for 15 seconds. This was repeated five times, and then 500 µL of elution buffer was loaded to elute the protein. The elution was repeated with fresh buffer and the two fractions were combined with eachother, as well as the elutions from the column done in parallel, to bring the final volume to 2 mL of FGF2 protein. We assume 100% return, and thus the solution is 2.9 µM.

5.3.6 Microarray studies- analysis of protein binding and printed polymer

Retention studies: Retention studies were performed on slides with both Hep-Gel as well as glycopolymers on slides which have completed the general printing procedure, including the typical washing. At this point, the slides were incubated in 2X PBS with 0.1% tween 3x15 min rocking, with a final overnight incubation at 37 °C. After this incubation, slides were rinsed in water three times and scanned and/or used in protein binding assay and assessed for binding and relative retention.

Binding assays on array, general: Slides used for protein binding assays are equipped with a gasket chamber and then blocked for 45 minutes. Using a filtered PBS solution

with 1% BSA and 0.1% tween 20. Typically, 16 or 4 well gaskets were used, and were incubated with 50 and 250µL solution volumes respectively. After blocking, protein binding incubations are performed at 4 °C for 90 minutes in blocking solution with the protein or antibody. Between protein incubations, wells are washed four times with blocking solution. After all incubations, a final series of three PBS washes for 15 minutes each are performed, the slide in spin dried, and scanned. The concentrations of the various protein stains are detailed in Table 2.

Table 2 Protein and Antibody concentrations used in microarrays.

Protein	Concentration
FGF2	**100nM**
AF647-FGF2	**10 nM**
Biotinylated WGA	**1:600**
CS56	**1:100**
HABP	**100 nM**
All secondary antibodies	**1:1000**
MsXFGF2	**1:1000**

5.3.7 Cellular microarray studies

General Biology (Cell counting, culture media, passage rate, etc): For embryonic culture, mESCs were grown on gelatin-coated plates in knockout (KO)-DMEM + 10% FBS in the presence of LIF. Cells were passaged every other day using 0.05% trypsin at a ratio of 1:10.

General Cellular Microarray Analysis: Fluorescent images obtained on a microscope were quantified in imageJ. Specifically, colonies were outlined and measured for their integrated density, mean, and area. These numbers are then used to calculate the

corrected total cell fluorescence (CTCF) in the following formula: CTCF= integrated density- (area x mean fluorescence of background readings).

Sterilization of arrays: Arrays were sterilized for cell culture in a laminar flow tissue culture hood by placing arrays and gaskets (previously autoclaved) in 100% EtOH for 5 minutes, followed by a sterile PBS wash. The is then assembled onto the slide, and the slide is washed with PBS and left under UV light for at least 15 minutes this is repeated twice, each time with fresh PBS.

Seeding arrays: Arrays were seeded after sterilization. At least 20 minutes before seeding, 500 µL of mESC maintenece media is added to each well of a 4 well gasket attached to an acrylamide slide with an array printed upon it. Cells are then seeded onto the array in a volume of 1 mL, bringing the final volume to 1.5 mL. 18 hours after seeding, the outlines of gelatin spots become noticeable due to cells growing upon the spots, and the slide is washed once with DMEM and the media appropriate for the desired experiment is added onto the plate in a 1 mL volume. Initially seeding in 1.5 mL helps seeding to occur more evenly because it prevents excessive interference from the meniscus of the solution in the well.

Staining with Syto59: To 10 mL of DMEM, 2 µL of a 5mM solution of syto59 is added. Cells are then incubated in this solution for 25 minutes at 37 °C, 5% CO2. After incubation, cells are washed three times with DPBS and imaged.

Neural Specification For neural differentiation, mESCs were plated into a 4 well gasket well (surface area = 2.56 cm^2) at a density of 10 x 104 cells per cm^2 in mESC growth medium. The following day (day 0), medium was replaced with N2B27 medium, a 1:1 mixture of DMEM/ Ham's F12 (Gibco, Cat. #11330-032) and Neurobasal medium (Gibco Cat. #21103-049), 0.5x N2 supplement (Gibco, Cat. #17502-048), 0.5x B27 supplement (Gibco, Cat. #17504-044), 50 µg/mL BSA fraction V, 500 µM L-glutamine, 55 µM 2-mercaptoethanol, 100 units/mL penicillin and 100 µg/mL streptomycin (Gibco). Additionally, heparin was added at 5 µg/mL to + heparin conditions. Medium was replaced every one to two days as required. Cells were fixed at day six with 4% (w/v) paraformaldehyde for ten minutes at room temperature for subsequent analysis via immunocytochemistry.

Staining with Antibodies Fixed cells were blocked and permeabilized for one hour at room temperature using block solution (2% (v/v) goat serum, 1 mg/mL BSA, 0.1% (v/v) Triton-X100 in PBS). Primary and secondary antibody incubations were performed for one hour at room temperature. Primary antibodies against Nestin (1:250, Millipore, cat #MAB353) and Oct3/4 (1:100, Santa Cruz Biotechnology, Cat. #sc-25401), Rex1, 1:250 BIII tubulin, 1:300 ProLong Gold antifade reagent with DAPI was added to stained cells to visualize nuclei and incubated for overnight at room temperature in the dark.

Table 3. Antibody concentrations used for ICC

Antibody	Concentration
Oct4	**1:100**
Nestin	**1:250**
BIII Tubulin	**1:300**
Rex1	**1:250**

FACs analysis of cellular arrays: For flow cytometry experiments, a BD FACS Calibur flow cytometer equipped with BD FACS Station was used, and data was analyzed using FlowJo (TreeStar) using 10, 000 events during collection. Cells were collected from array using 0.05% trypsinization of arrays, (3 min, 37 °C).

ABREVIATIONS

Abs = absorbance
ADIBO= dibenzocyclooctyne amine
BSA = bovine serum albumin
DMEM = Dublecco's modified eagle medium
DMSO = dimethyl sulfoxide
DPBS = Dulbecco's phosphate buffered saline
ELISA = enzyme-linked immunosorbent assay
EDTA = ethylenediaminetetraacetic acid
FBS = fetal bovine serum
FGF = fibroblast growth factor
GAG: glycosaminoglycan
HABP: hyaluronic acid binding protein
HEPES= 4-(2-hydroxyethyl)-1-piperazineethanesulfonic acid
Hep = heparin
hMSC = human mesenchymal stem cell
HSPG= heparan sulfate proteoglycan
mESC= mouse embryonic stem cell
MEM = modified eagle medium
MWCO= molecular weight cut-off
MQ= Milli-Q ultrapure water
NAcH = *N*-desulfated *N*-reacetylated heparin
NDSH = *N*-desulfated heparin
NHS = *N*-hydroxy succinimide
PBS = phosphate buffered saline
PD-10 = prepacked sephadex® G-25 medium disposable column
PD173074= PD173074074, FGFR inhibitor
RFU= random fluorescence units
SPAAC = strain promoted azide-alkyne cylocaddition
6ODSH = 6-*O*-desulfated heparin
2ODSH = 2-*O*-desulfated heparin

REFERENCES

[1] Hong H. J., Koom W. S., Won-Gun K. *Sensors*, **2017**, 17, 1293-1321. Cell microarray technologies for high-throughput cell-based biosensors.

[3] Warda M., Toida T., Zhang F., Sun P., Munoz E., Xie J., Linhardt R. J. *Glycoconj J.* **2006**, 23, 555-563. Isolation and characterization of heparan sulfate from various murine tissues.

[4] Saad O. M., EWbel H., Uchimara K., Rosen S. D., Bertozzi, C. R., Leary J. A. *Glycobiology*, **2005**, 15, 818-826. Compositional profiling of heparin/heparan sulfate using mass spectrometry: assay for specificity of a novel extracellular human endosulfatase.

[5] Yin J., Seeberger P.H. *Methods in Enzymology*, **2010**. Elsevier. Chapter nine-Applications of Heparin and Heparan Sulfate Microarrays.

[6] Xing Z., Vijayakanth P., Jester H. M., Lim A. M., Pham T. Q., Goulas A. M. P., Liu J., Linhardt, R. J. *Chemical Science*. **2017**. Chemoenzymatic synthesis of heparan sulfate and heparin oligosaccharides and NMR analysis: paving the way to a diverse library for glycobiologists.

[7] Zong C., Venot A., Li X., Lu W., Xia W., Wilkes J. L., Salanga C. L., Handel T. M., Wolfert M. A., Boons, GJ. *J. Am. Chem. Soc.* **2017**, 139, 9534-9543.

[8] Puvirajesinghe T. M., Turnbull, J. E. *Microarrays*. **2016**. 5, 3. Glycoarray Technologies: Deciphering Interactions from Proteins to Live Cell Responses.

[9] Guimond S., Maccarana M., Olwin B.B., Lindahl U., Rapraeger A.C. *J. Biol. Chem*. **1993.** 268, 23906-23914. Activating and inhibitory heparin sequences for FGF-2 (basic FGF). Distinct requirements for FGF-1, FGF-2, and FGF-4.

[10] Pye D.A., Vives R.R., Turnbull J.E., Hyde P., Gallagher J.T. *J. Biol. Chem*. **1998**, 273, 22936–22942. Heparan sulfate oligosaccharides require 6-O-sulfation for promotion of basic fibroblast growth factor mitogenic activity.

[11] Smith R. A. A., Murali S., Rai B., Lu X., Lim Z. X. H., Lee J. J. L., Nurcombe V., Cool S. M. *Biomaterials*. **2018**, 184, 41-55. Minimum structural requirements for BMP-2 binding of heparin oligosaccharides.

[12] DeAngelis P. L., Liu J., Lindhardt, R. J. **Glycobiology**. **2013**, 23, 764-777. Chemoenzymatic synthesis of glycosaminoglycans: Re-creating, re-modeling and re-designing nature's longest or most complex carbohydrate chains.

[13] Yarmush M. L., King K. R. *Annu Rev Biomed Eng.* **2009**, 11, 235-257. Living Cell Micorarrays.

[14] Fisher O. Z., Khademhosseini A., Langer R., Peppas N. A., *ACS Chem Res.* **2010**, 43, 419-428. Bioinspired materials for controlling stem cell fate.

[16] Flaim C. J., Chien S., Bhatia S. N. *Nat. Methods*, **2005,** 2, 119-125. An extracellular matrix microarray for probing cellular differentiation.

[17] Ranga A., Gobaa S., Okawa Y., Moseiwicz K., Negro A., Lutolf M. P. *Nat. Comm.* **2014.** 5, 4324. 3D niche microarrays for systems-level analyses of cell fate.

[19] Puvirajesinghe T. M., Ahmed Y. A., Powell A. K., Fernig D. G., Guimond S. E., Turnbull J. E. *Chem Biol*. **2012**, 19, 553-558. Array-based functional screening of heparin glycans.

[41] Ghaemi S. R., Harding F., Delalat B., Vasani R., Voelcker N. H. *Biomacromolecules,* **2013**, 14, 2675-2683 Surface Engineering for Long-Term Culturing of Mesenchymal Stem Cell Microarrays.

[42] Chen, J., Spear S. K., Huddleston J. G., Rogers R. D. *Green Chem.* **2005**, 7, 64-82. Polyethylene glycol and solutions of polyethylene glycol as green reaction media.

[43] Brafman D. A., Chien S., Willert K. *Nature Protocols*, **2012**, 7, 703-717. Arrayed cellular microenvironments for identifying culture and differentiation conditions for stem, primary and rare cell populations.

[44] Johnson, C. E., Crawford, B. E., Stavridis, M., ten Dam, G., Wat, A. L., Rushton, G., Ward, C. M., Wilson, V., van Kuppevelt, T. H., Esko, J. D., Smith, A., Gallagher, J. T., and Merry, C. L. R. *Stem Cells,* **2007**, 25, 1913−1923. Essential alterations of heparan sulfate during the differentiation of embryonic stem cells to sox1-enhanced green fluorescent protein expressing neural progenitor cells.

[45] Hermanson, G. T. *Bioconjugate Techniques, Third Edition*, **2013**. Academic Press. Chapter 4.1 Zero length crosslinkers.